2014

Investigations of Novel Mechanisms of Action for Anti-Bacterial and Anti-Cancer Agent Development

Jenson Verghese
Virginia Commonwealth University

INVESTIGATIONS OF NOVEL MECHANISMS OF ACTION FOR ANTI-BACTERIAL AND ANTI-CANCER AGENT DEVELOPMENT

A dissertation submitted in partial fulfillment of the requirements for the degree of Doctor of Philosophy at Virginia Commonwealth University.

by

JENSON VERGHESE

Masters in Science, Virginia Commonwealth University, Richmond, V.A, U.S.A, 2009

Director: KEITH C. ELLIS

ASSISTANT PROFESSOR, DEPARTMENT OF MEDICINAL CHEMISTRY

Virginia Commonwealth University

Richmond, Virginia

May 2014

Acknowledgement

First and foremost, I would like to thank my wife: Anu and my family for all the support they provided while I was preparing this work. The last few months in school was exhaustive and torturous and I would not have made it through, if it was not for their unending support and encouragement.

I would like to thank my advisor and mentor Dr. Keith C. Ellis for the support and knowledge he has given me throughout the past five years. I have learned a lot during this time specifically how to think as a synthetic chemist, which would not have been possible without his guidance.

Next, I would like to thank my committee members: Dr. Glen Kellogg, Dr. Rong Huang, Dr. Tony Wright and Dr. Frank Gupton for taking the time to patiently read through my dissertation and attend all the meetings, especially Dr. Kellogg who fastidiously went through every page in this work including the experimentals!

Special thanks goes to Dr. Thuy Nguyen and Robert Coover for performing the AKT assays for this work and to the other Ellis lab members: Sudha Korwar and Lauren Gaskell, who were a constant encouragement during the past five years.

Finally I would like to thank all my friends who were in Richmond during this period: Ashwin Belle, Reethi Iyengar, Sudhir Nagaraja, Preeti Sastry, Phong Nguyen, Orgil Elbegdorj and Rami Alhorani.

Table of Contents

List of Tables

Page

List of Figures

Page

List of Figures

Page

List of Figures

Page

List of Figures

Page

List of Figures

Page

Abstract

INVESTIGATIONS OF NOVEL MECHANISMS OF ACTION FOR ANTI-BACTERIAL AND ANTI-CANCER AGENT DEVELOPMENT

By Jenson Verghese, Ph.D.

A dissertation submitted in partial fulfillment of the requirements for the degree of Doctor of Philosophy at Virginia Commonwealth University.

Virginia Commonwealth University, 2014.

Major Director: Keith C. Ellis

Assistant Professor, Department of Medicinal Chemistry

The development of drugs and therapeutic agents for combating infections and human malignancies continues to be a forefront area in both academic and industrial research. This is driven by the rapid emergence of multi-drug resistant bacterial strains and accumulating mutations in cancer targets that is quickly rendering our current arsenal of drugs ineffective for these therapies. Unless new drugs with novel mechanisms of action

are identified and developed at a faster pace, we face a losing battle in managing these diseases.

The first part of this work concerns with the natural product Simocyclinone D8 (SD8). Simocyclinone D8 is an angucyclinone antibiotic that inhibits DNA gyrase with a novel mechanism of action that has been termed competitive inhibition. Simocyclinone D8 was found to inhibit the growth of both Gram-(+ve) and Gram-(–ve) organisms and also inhibit a fluoroquinolone resistant mutant of DNA gyrase. Inspired by the structure and novel mechanism of action that SD8 displays, we synthesized analogues based on the co-crystal structure of SD8 with DNA gyrase. These compounds were found to inhibit DNA gyrase, albeit by a different mechanism of action than that of SD8. We also conducted studies towards the total chemical synthesis of SD8 and made three out of the four fragments in SD8 in decent yields.

The second part of this work is focused on the development of a substrate-competitive covalent inhibitor for protein kinase B (AKT). AKT is a valid target for cancer research with two compounds currently in late stage clinical trials. Developing substrate-competitive inhibitors for kinases is a novel approach in targeting them, with very few examples in the literature. This mechanism has been postulated to overcome common resistance mutations that cancer targets harbor. A major drawback in this approach is the low binding affinity for peptide substrates by kinases. We circumvented this problem of affinity by utilizing a covalent mode of binding and synthesized a potent non-peptide active-site directed irreversible compound that inhibits AKT. Further studies on this compound are underway and are expected to yield a compound that can be used as a therapeutic agent or as a probe for AKT.

List of Abbreviations

A- angstrom

Ac- acetyl

ADP- adenosine diphosphate

Atm- atmospheres

ATP- adenosine triphosphate

Bn- Benzyl

Boc- *tert*-butoxycarbonyl

°C- degrees Celcius

d- doublet

dd- doublet of doublets

DNA- deoxyribose nucleic acid

DCM- dichloromethane

DMAP- dimethylaminopyridine

DMF- dimethylformamide

E. coli- Escherichia coli

EDCI- 1-ethyl-3-(3-dimethy

laminopropyl)carbodiimide

Et- ethyl

Fig- figure

g- gram

H_2- hydrogen

HCl- hydrochloric acid

H_2O- water

K_2CO_3- potassium carbona

kDa- kilodalton

M- molar

mL- milliliter

mM- millimolar

nM- nanomolar

THF- tetrahydrofuran

CHAPTER 1: FLAVONE BASED ANALOGUES INSPIRED BY SIMOCYCLINONE D8 (SD8)

1.1: Critical need for New Anti-Bacterial agents

The discovery of anti-bacterial agents has been one of the most significant scientific achievements of the past century. Their influence has not only revolutionized the treatment of infectious diseases, but also many advanced surgical procedures would not have been possible without them. However, bacterial resistance has evolved to every anti-bacterial that has been commercially introduced and most pharmaceutical companies have already exited this area of drug discovery[1].

The introduction and discovery of anti-bacterials is the most prototypical incident in the archives of medicinal chemistry research. It could be argued that the discovery of the first synthetic anti-bacterial agent, Salvarsan (Arsphenamine), by Paul Ehrlich in 1909 was the first documented instance of lead optimization by systematic chemical modifications for biological activity. In fact, the term “magic bullet” was first introduced in drug discovery. Salvarsan was discovered form the lead Atoxyl (Arsanilic acid) and was used for the treatment of syphilis and was the world’s first blockbuster drug until the discovery of penicillin and sulfonamides. These compounds heralded a new era in medicine, where the concept of the “magic bullet” came closer to reality[2].

Currently there are many anti-bacterial agents that have been introduced to the market. Broadly they can be classified into synthetic and natural scaffolds. The synthetic scaffolds consist of the sulfonamides, diaminopyridines, quinolones and oxazaolidinones and the natural scaffolds consist of β-lactams, tetracyclines, macrolides, aminoglycosides and glyco and lipo peptides. However, these compounds target a very limited number of clinically relevant targets: DNA gyrase and topoisomerase IV, ribosomal function inhibition and inhibition of cell wall biosynthesis. Most compounds currently in the pipeline of pharmaceutical companies are derivatives of the above mentioned chemical scaffolds, but there already exists microbes with underlying resistance mechanisms in clinical settings that have built resistance to all these chemical classes. Derivatizing these already existing chemical scaffolds might temporarily improve efficacy of the drug, but the binding interaction with the target remains unchanged; hence, development of resistance to the scaffold is just a matter of time[3].

Drug resistance is mostly seen in gram-positive and gram-negative organisms, both in hospital and community based settings. The majority of these organisms that cause infections and are effectively resistant to most of the current drugs have been collectively termed as the "ESKAPE" pathogens (*Enterococcus faecium, Staphylococcus aureus, Klebsiella pneumonia, Acinetobacter baumanii, Pseudomonas aeruginosa and Enterobacter* species). In addition to these, there are reports of increasing infection and death rates in hospitals due to methicillin-resistant *S. aureus* (MRSA), vancomycin-resistant *E. faecium* (VRE) and fluoroquinolone-resistant *P. aeruginosa*. Due to the increasing immunocompromised patient population consisting of geriatrics, patients undergoing surgery, chemotherapy and neonatal units, infections due to these antibiotic

resistant pathogens are rising rapidly and are of significant concern in the medical community[4].

There are various factors that lead to the slow development of anti-bacterials. The overall time line, success rate and investment required to launch a novel broad-spectrum antibacterial is staggering as compared to other therapeutic areas. Scientifically, it is also an exhaustive challenge considering that bacterial cells are quite different from human cells, so the general rules used in drug discovery for e.g. Lipinsky's "rule of 5" does not translate into antibiotics.

The advent of the genomic era in the 1990's followed by the complete sequencing of the *Haemophilus influenza* genome changed the focus of drug discovery from chemical modification of already existing molecules to discovery of newer targets and molecules in the pharmaceutical industry. High throughput screens (HTS) were run with isolated enzyme or protein targets and whole cells, but these did not translate well into lead molecules. Most molecules that progressed into the lead optimization stage did not make it through Phase 1 testing. The difficulties were attributed to less diversity in compound libraries screened, multiple pathogens that have to be inhibited by a broad-spectrum compound, both Gram-positive and Gram-negative species with different molecular targets, membrane permeabilities, metabolic pathways and an acceptable and convenient pharmacokinetic and dynamic profile. After the failure of this earlier genomic based approach for anti-bacterial drug discovery, the current approach in industry has been shifting to a renewed focus on novel chemical scaffolds, concentrating on already validated targets, exploring new binding modes and including more diversity in chemical screens[5].

There is a critical and unmet need for the development of newer anti-bacterials. This is driven by the emergence of bacterial strains that have the capacity to mutate over a time period of hours compared to the years required to develop antibiotics, rendering our current arsenal of antibiotics ineffective. The discovery of anti-bacterials was one of the biggest discoveries in medicine, but unless newer anti-bacterials are developed at a faster pace, we face a losing battle.

1.2: DNA-Gyrase as a drug target.

DNA Topoisomerases are enzymes that change the topology of DNA in both prokaryotic and eukaryotic cells. They catalyze changes in the topology of DNA at various steps in the replication cycle. The helical intertwined nature of DNA presents a problem during replication and transcription, where DNA gets overwound ahead of the replication fork. To overcome this tension, topoisomerases either bind to one strand or both strands of DNA and nick the phosphate backbone. This process removes supercoils of DNA and after the process, the DNA strand is resealed, so these enzymes remove catenanes and knots in DNA. Topoisomerases are classified into type I and type II based on whether they catalyze the transient breakage of one strand or both strands of DNA[6].

DNA gyrase is a type II topoisomerase that can also introduce negative supercoils in DNA. It is the only known topoisomerase enzyme that can generate negative supercoils as well as relax positive and negative DNA supercoils; however, generating negative supercoils appears to be the primary function of gyrase in the cell. The enzyme uses the hydrolysis of ATP to carry out this process. Prokaryotic DNA gyrase consists of two subunits A and B. In the active enzyme, these associate to form an A_2B_2 complex. The *E. coli* gyrase has a molecular weight of 97 and 90 KDa for its A and B subunits,

respectively. The A subunit interacts with DNA and has the active site tyrosine that catalyzes the DNA cleavage. The B subunit consists of the ATP binding site and catalyzes the ATPase activity.

DNA gyrase is an important anti-bacterial drug target due to its important function in the cell. The mechanism by which the enzyme supercoils DNA is complex and multistep and this offers an avenue for its inhibition at various steps in the process. A model called the "two – gate mechanism" has been proposed for how gyrase supercoils DNA and is supported by structural and biochemical data[7, 8]. DNA gyrase consists of three interfaces that interact with DNA, and they can either exist in an open or closed conformations (**Figure 1**). The "N–gate" is the N–terminal domain of GyrB, "DNA gate" is the GyrA–GyrB–DNA interface that cleaves DNA and the "C–gate" is the C–terminal area of coils where DNA exits the enzyme. The supercoiling reaction progresses in the following fashion: the first step (step 1, **Figure 1**) involves DNA (named as the G-segment) association with the unliganded enzyme at the GyrA and GyrB interface that is between the TOPRIM domain of GyrB and the N–terminal domain of GyrA dimer. This leads to conformational changes and the formation of the DNA gate (step 2, **Figure 1**), following which about 130 base pairs of DNA wrap around the enzyme in a right handed supercoil. Wrapping of DNA around the C–terminal domain of gyrase facilitates the T–segment of DNA (the segment that will be passed through the cleaved DNA) to reach the N gate and is placed over the G segment (the segment that forms the DNA gate, step 3, **Figure 1**). ATP binding dimerizes GyrB allowing the trapping of the T segment and cleaving the G segment at the DNA gate (step 4, **Figure 1**). The cleavage site in double stranded DNA occurs 4 base pairs apart and results in the G segment covalently attaching itself to the

GyrA subunit of DNA gyrase. The T segment is passed through the DNA gate and the cleaved G segment and finally through the exit gate. The translocation of the T segment is allowed by the rotation of GyrB, due to the hydrolysis of one molecule of ATP. The next step is the religation of the G segment, which introduces two negative supercoils in DNA (step 5, **Figure 1**). The hydrolysis of a second molecule of ATP opens the N-gate and the enzyme is ready for the next supercoiling cycle and resets to step 2. One gyrase cycle introduces two negative supercoils into DNA at the expense of two ATP molecules. The supercoiling reaction is a complex cycle and the exact order and mechanism of the steps are not unambiguously known, however due to the multiple number of steps, there exists enough opportunity for disruption of this cycle with inhibitors.

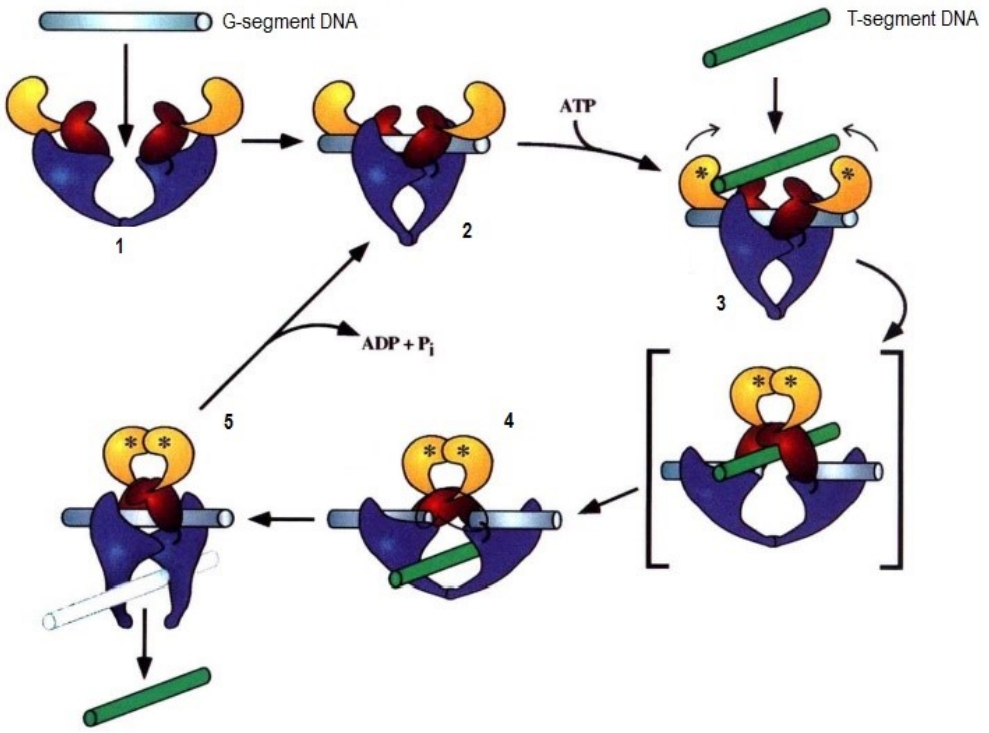

Figure 1: Model for the catalytic reaction of topoisomerase II. ATPase domain is shown in yellow, domain in red forms the DNA gate and the domain in blue has the catalytic tyrosines[9].

There are multiple points of intervention in the supercoiling cycle that inhibitors act on i.e. DNA binding, DNA cleavage, strand passage and ATP hydrolysis. There are two main mechanisms by which inhibitors act on DNA gyrase. The first one involves the inhibition of the enzymatic activity of gyrase and the second is the stabilization of the covalent enzyme DNA adduct or otherwise known as gyrase poisoning.

1.3: Quinolones

The origin of Quinolones can be traced to the discovery of nalidixic acid, a by–product formed during the preparation of chloroquine (an anti–malarial). Systematic chemical modifications lead to the discovery of the fluoroquinolones: norfloxacin, ciprofloxacin,

levofloxacin and gemifloxacin (**Figure 2**). These compounds have been significantly used as broad spectrum antibiotics in the treatment of both Gram positive and Gram negative infections[10].

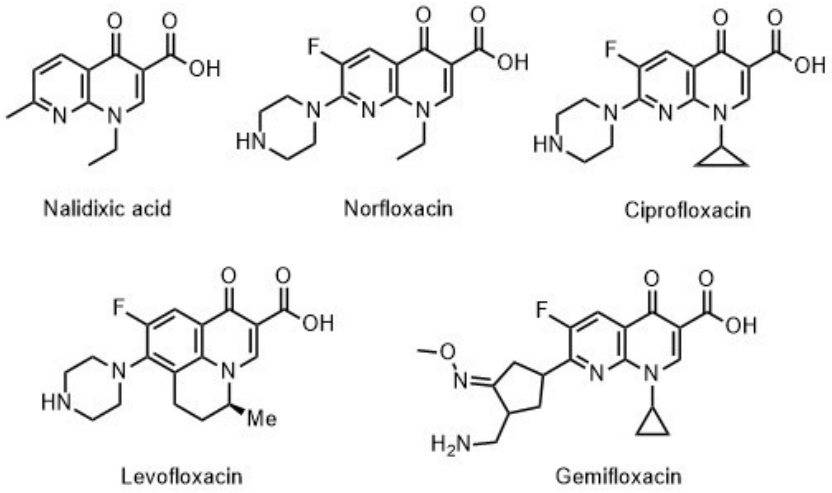

Figure 2: Structure of Quinolones

Based on the type of organism and the quinolone, topo IV has also been indicated as a target in addition to gyrase. Bacteria harbor resistance genes to fluoroquinolones and the site of point mutations that give quinolone resistance is called the quinolone resistance–determining regions or QRDR. Fluoroquinolone resistance has been reported in pneumonia, influenza, MDR/XDR tuberculosis and respiratory tract diseases.

Quinolones stabilize the covalent gyrase DNA complex, where DNA gyrase is covalently bound to the 5' ends of the cleaved DNA. Crystal structures of the fusion protein involving C–terminal of GyrB with the N–terminal of GyrA, show that the DNA gate is in the closed conformation, suggesting that opening of this gate is not required for quinolone binding. The aromatic rings of the quinolone are found to be stacked against the DNA bases at

the site of cleavage. This interaction can cause a misalignment of DNA on either side of where cleavage happens and difficulty in joining the broken DNA[11].

Quinolones *in vivo* display both bacteriostatic and bactericidal activities. The quinolone–gyrase (or quinolone–topo IV) complex formed can stall the replication fork and lead to a bacteriostatic effect. The bactericidal effect mechanistically happens through two distinct pathways; first one dependent on protein synthesis and the second on in its absence, which depends on the particular type of quinolone. The ultimate consequence of a quinolone–stabilized gyrase (or topo IV) complex with DNA is cell death that occurs through chromosome fragmentation, induction of SOS response and eventually cell fragmentation that could involve reactive oxygen species.

It has been hypothesized that the mode of action that the quinolones employ for gyrase (or topo IV) inhibition is the most effective. Relatively only a low occupancy of inhibitor bound to the target is required to cause enough chromosome fragmentation for cell death to occur.

1.4 Aminocoumarins

The aminocoumarins are characterized by their 3-amino–4,7-dihydroxycoumarin ring. Further substitutions on the ring or groups attached to the amine or phenol make up the diversity in this class of compounds. The prototypical aminocoumarins: novobiocin and clorobiocin (**Figure 3**) were extracted from *Streptomyces* species. These compounds were used once to treat methicillin resistant *S. aureus* (MRSA), but they have been withdrawn from clinical use because of their toxicity and poor pharmacokinetic parameters[12].

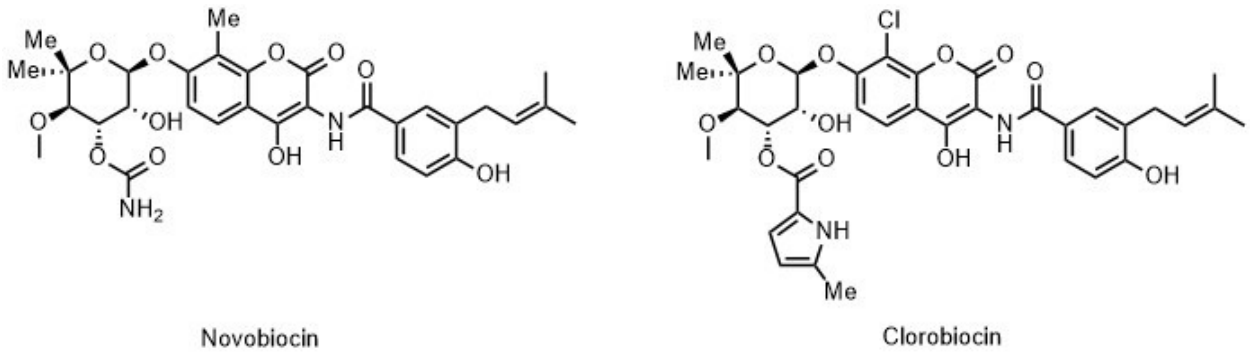

Figure 3: Structure of Novobiocin and Clorobiocin

Aminocoumarins bind tightly to the B subunit of DNA gyrase and they work mechanistically by inhibiting the catalytic activity of DNA gyrase. They compete with ATP for binding to the GyrB domain; hence, the ATPase reaction of gyrase is inhibited. Their binding site overlaps the ATP binding site in GyrB that is a 24–KDa amino–terminal subdomain in GyrB and is named as the aminocoumarin binding site. This binding prevents ATP binding to the site and thus inhibits the supercoiling reaction from proceeding[13].

Naturally occurring resistance to the aminocoumarins has been observed in DNA gyrase and these involve mutations in the aminocoumarin binding site (Arg136 and Gly164, *E. coli* numbering). However, due to the proximity of this site to the ATP binding site, these mutants show a loss in enzymatic activity due to impaired ATPase activity.

In vitro aminocoumarins are potent inhibitors of DNA gyrase, but they display poor activity against Gram negative bacteria. Additionally, their mammalian toxicity and poor bioavailability have precluded their use clinically and they have been most commonly used to study the ATP–binding site of DNA gyrase.

1.5: New Bacterial Topoisomerase Inhibitors (NBTIs)

NBTIs are a new class of synthetic anti-bacterials, which have a non-quinolone scaffold but bind to topoisomerase II class of enzymes in a similar fashion as that of the quinolones. They have a mechanism of action distinct from that of the quinolones and currently are being pursued by the pharmaceutical industry because they are not affected by mutations that affect fluoroquinolone binding[14].

One of the most studied compounds is the quinolone based drug candidate NXL101, licensed by Novexel (**Figure 4**). NXL101 displayed a preference for inhibition of topo IV over DNA gyrase in *E. coli* and displayed the opposite trend when it came to *S. aureus*. This preference in targets was the opposite to that displayed by fluoroquinolones. NXL101 displays the ability to inhibit mutant forms of gyrase that are resistant to fluoroquinolones and the mutations that render the drug ineffective were found to be outside the QRDR domain region in DNA gyrase. One of the mutations that confers fluoroquinolone resistance is Ser84 in GyrA (*S. aureus* numbering), whereas for NXL101 was Asp83 (*S. aureus* numbering), which highlight the differences in binding of NXL101 as compared to fluoroquinolones. Nonetheless, the lack of co–crystal structures of DNA gyrase with NBTIs has made determination of the precise binding site impossible. However, in 2009, the development of NXL101 was discontinued due to QT prolongation in Phase I studies[15].

In 2010, GSK reported the crystal structure of the compound GSK299423 (**Figure 4**) with DNA and *S. aureus* gyrase. They isolated the precleaved complex of mutant *S. aureus* gyrase (Tyr123 to Phe) and observed that the cyano–quinoline region of the compound intercalates DNA, midway between the two gyrase active sites and arrests the complex before the double strand is cleaved. The compound does not directly inhibit the DNA

cleavage and religation process like quinolones do, but it stabilizes the pre-cleavage complex and prevents strand separation. This binding site is distinct from the fluoroquinolone binding site and the compound was active against MRSA and fluoroquinolone resistant strains. But no further studies on this compound have been reported[16].

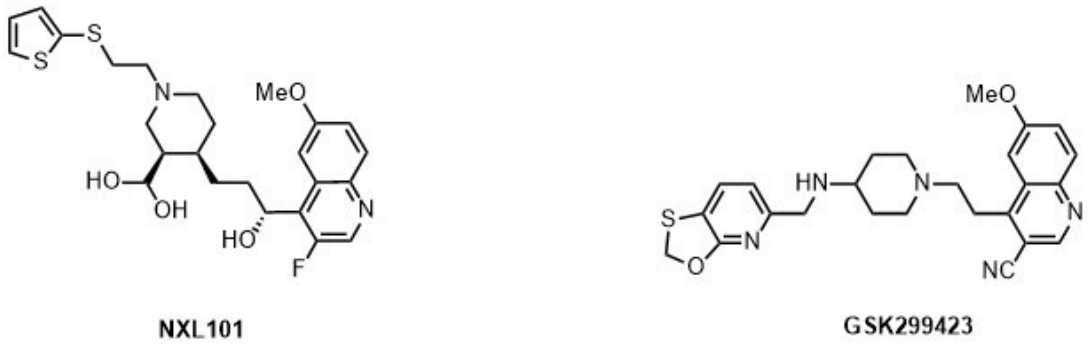

Figure 4: Structures of NXL101 and GSK299423

1.6 Simocyclinone D8 (SD8)

Simocyclinone D8 is an antibiotic that belongs to the family of angucyclinones. It was first reported in 2000 by Fiedler *et al.* after they isolated it from *Streptomyces antibioticus* Tu 6040[17]. Screening of metabolites from the novel *Streptomyces* strain that was isolated from a soil sample in Argentina, lead to the discovery of SD8. Simocyclinone D8 was found to have antibiotic activity against Gram positive bacteria (*S. aureus, Bacillus brevis, Bacillus subtilis* and *Streptomyces viridochromogenes*) and cytostatic effect on tumor cells lines, but no significant activity against Gram negative organisms (*E. coli*). The authors also optimized the fermentation conditions and reported that various partially substituted analogues of SD8 can be obtained by varying the carbohydrate source in the medium[18]. The SD8 molecule consists of three subunits: an aminocoumarin similar to

that present in novobiocin and clorobiocin, a tetraene linker that is present in the veterinary antibiotic fumagillin and an angucyclinone, which is comprised of an olivose sugar bound by a C–glycosidic bond to a highly substituted benz[*a*]anthracene system **(Figure 5)**[19]. This angucyclinone system is very similar to that present in the natural product aquayamycin. The biosynthetic gene cluster of SD8 was cloned by Heide *et al.* in 2002[20]. The authors reported that the gene cluster consists of several genes with high similarity to that of the aminocoumarin class of antiobitics, however in contrast with the aminocoumarins, the SD8 gene cluster doesn't have an obvious resistance gene, hindering the identification of a possible target. They also proposed a biosynthetic pathway of how SD8 is synthesized in the microorganism[21].

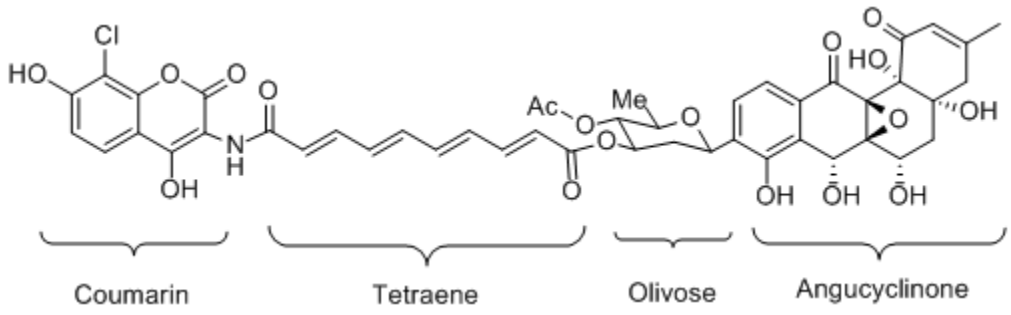

Figure 5: Structure of SD8

The first report that garnered attention for SD8 in the scientific community was published by Maxwell *et al.* in 2005[19]. The authors test the compound for inhibition of DNA gyrase because of its chemical similarity to the aminocoumarin antibiotics. They found that SD8 inhibits gyrase supercoiling reaction with an IC_{50} of 0.1 μM as compared to novobiocin with an IC_{50} of 0.25 μM and 0.7 μM for ciprofloxacin. SD8 also inhibited the DNA relaxation activity of gyrase with an IC_{50} of 0.5 to 1.0 μM. To determine the possible mode of binding, they tested whether the observed inhibition was dependent on ATP and report that SD8

does not compete with ATP unlike novobiocin. Assaying SD8 with a ciprofloxacin resistant DNA gyrase (Ser83 to Trp) for supercoiling activity increased the IC_{50} 10-fold, whereas for ciprofloxacin increased 30-fold. This established that SD8 does not share the same binding site on DNA gyrase as novobiocin and there might be an overlap of binding regions with quinolones. SD8 also did not form linear DNA from supercoiled DNA in the presence of gyrase and it also abolished DNA–DNA gyrase cleavage complex formation in the presence of ciprofloxacin, suggesting that it had a distinct mechanism of action from the quinolones by inhibiting the enzyme prior to DNA cleavage.

Binding studies by SPR indicated that SD8 prevented DNA from binding to gyrase, while isothermal calorimetric studies showed that SD8 bound to the GyrA subunit in a ratio of 1:1. This mechanism of inhibition has been termed as catalytic and SD8 is the first and only molecule reported to date as a catalytic inhibitor of DNA gyrase.

In 2009 the first co-crystal structure of SD8 was reported with the N-terminal domain of GyrA (GyrA59) at 2.6 Å resolution (**Figure 6**)[22]. This crystal structure also assigned the absolute stereochemistry of SD8. The crystal structure reveals a homotetramer of two A59 dimers cross-linked by four molecules of SD8. Each GyrA subunit has two distinct pockets for the aminocoumarin and the polyketide moieties. The tetraene subunit, about 10 Å long, displays no interaction with the enzyme and holds the two binding moiety's apart. The stoichiometry remain consistent (1:1), as reported earlier by the ITC studies.

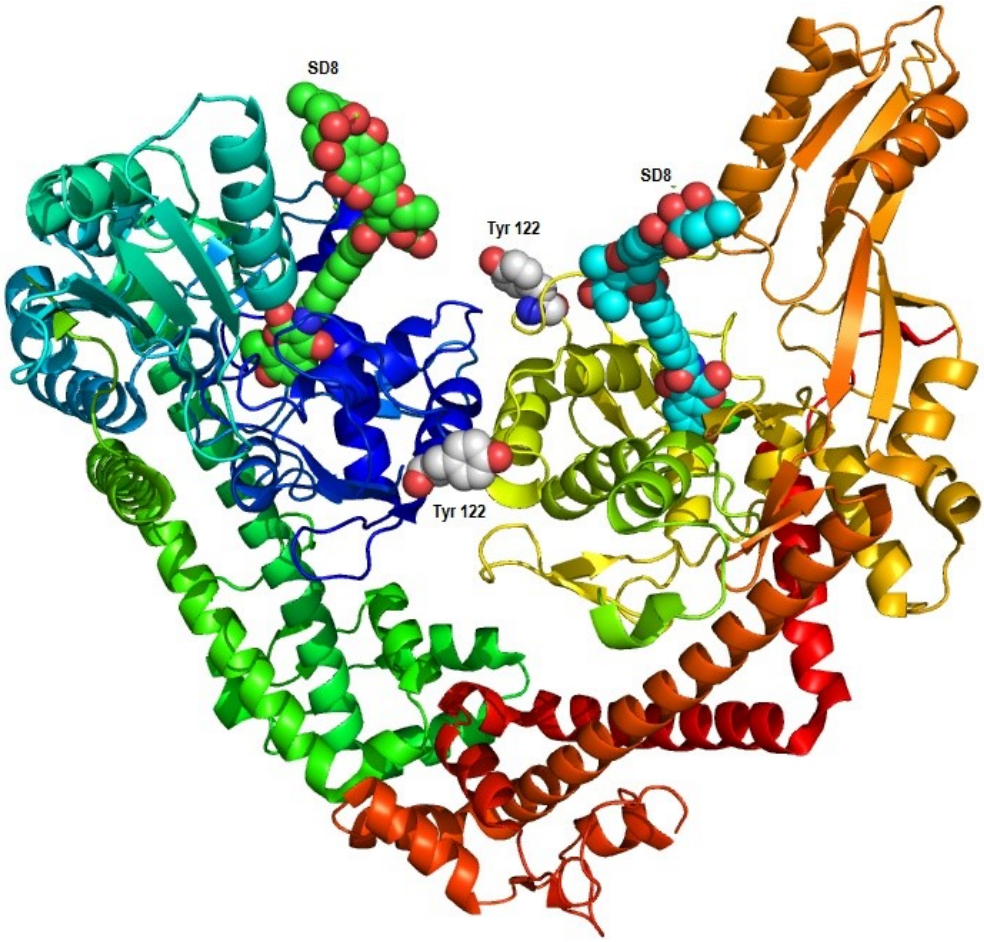

Figure 6: GyrA59 dimer with two molecules of SD8. The catalytic Tyr122 on both subunits are labeled (PDB ID: 2Y3P).

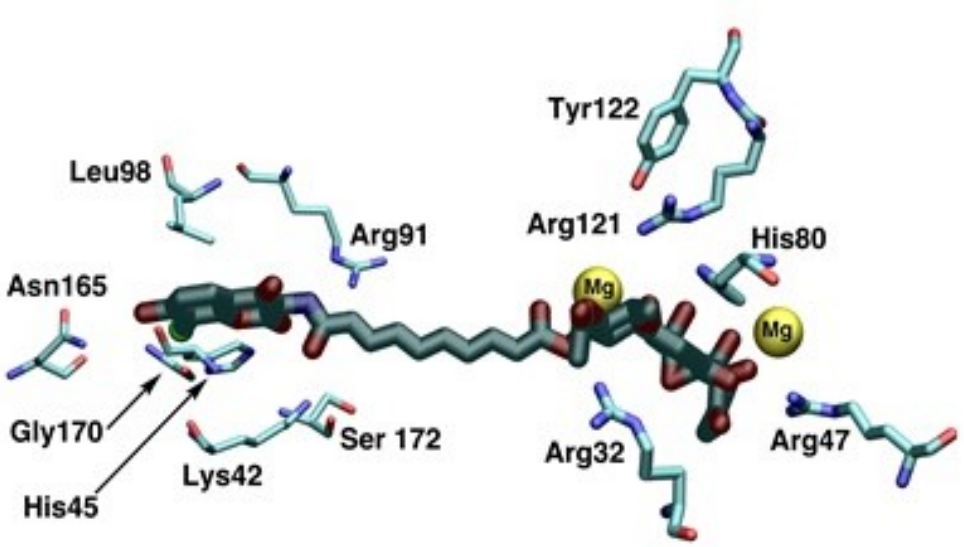

Figure 7: Residues interacting with SD8 in GyrA59 structure (PDB ID: 2Y3P).

Also, the SD8 molecule can be modeled in a bent conformation that bridges between the aminocoumarin and polyketide binding pockets within the same subunit. This could place the tetraene linker possibly interacting with the α-helix 4 of GyrA. Nanoelectrospray ionization mass spectrometry experiments reveal that the most probable binding conformation is a single SD8 molecule bound to the aminocoumarin and polyketide pockets within the same subunit. SD8 at high concentration causes tetramerization of GyrA by bridging the homodimers, but at pharmaceutically relevant concentrations, the dimeric form of GyrA exist bound to one or two SD8 molecules.

Analysis of the crystal structure reveals some interesting observations for both the pockets. The aminocoumarin and polyketide both bind in separate pockets and the tetraene linker and olivose sugar are not seen interacting with any residues. In the aminocoumarin pocket there is a halogen bond between the 8-position chlorine on the

coumarin ring with the carbonyl oxygen of Gly170. In the polyketide pocket, Arg121 and Tyr122 in the active site interact via water molecules to a Mg^{2+} that is bound to the diols on the polyketide fragment. On a similar basis His80 makes a water-mediated interaction with the second Mg^{2+} ion that coordinates to the angular diols on the polyketide ring. His80 also π stacks with the phenol on the angucyclinone. The tetra-substituted epoxide on the angucyclinone ring interacts with the guanidine group on the side chain of Arg32 (**Figure 7**).

Mutations in the aminocoumarin and polyketide pockets result in significant abrogation of supercoiling activity. Also, QRDR mutations in the α-helix 4 region of GyrA result in resistance to SD8, despite none of these amino acids making direct contact with SD8. It might be possible that mutating the residues in the α-helix 4 might impede the conformation of the linker and affect bridging of the aminocoumarin and polyketide binding sites.

Further mass spectrometry studies with GyrA and SD8 reveal that the binding is a function of both aminocoumarin and polyketide groups on SD8, and comparison with free aminocoumarin and polyketide groups reveal that the polyketide fragment binds with five times more affinity than the aminocoumarin fragment, but these individual fragment interactions are much weaker than bifunctional SD8[23]. Furthermore, binding of SD8 induces a strong allosteric cooperativity between the two binding sites, where occupancy in the first pocket strongly promotes binding in the second pocket. A >20-fold increase in affinity of binding the aminocoumarin subunit is seen after binding of the first polyketide unit. Edwards *et al.* report that the only binding mode supported by this data is that where both binding sites on a single monomer are bound by a single molecule of SD8. Based

on the binding constants of aminocoumarin and polyketide fragments, they hypothesize that: polyketide fragment binds first, increasing the local concentration of the aminocoumarin fragment followed by its binding. This bent over conformation of SD8 induces a strain in the tetraene linker that results in small structural changes in GyrA, which then results in the positive cooperativity upon binding of SD8.

In 2010, protein melting studies were reported to characterize the interaction of SD8 with DNA gyrase[24]. The circular dichorism profile of DNA gyrase indicates that both the A_2B_2 heterodimer and individual subunits (GyrA and GyrB) were established in presence of SD8 at various temperatures. For the GyrA subunit, as expected, a compound mediated shift of T_m was recorded and by plotting T_m vs SD8 concentrations, a cooperative conformational change was noticed. Unexpectedly, however binding of SD8 with the GyrB47 domain induced a change in T_m. The GyrB47 domain is also involved in DNA binding and the GyrA site displays much higher affinity than that of the GyrB domain. SD8 also changed the proteolytic pattern of GyrB digestion by trypsin, which also indicates a binding site on GyrB.

In 2014, a new crystal structure of SD8 was published with GyrA55 at 2.05 Å resolution (**Figure 8**)[25]. This 55 kDa fragment lacks the crucial residues that stabilize the tetrameric state of GyrA, hence obtaining a better picture of SD8 binding in physiological concentrations. The conformation of bound SD8 in this structure is different from that in the earlier reported crystal structure. The polyketide moiety binds at the interface of the two GyrA monomers, displaying interactions with 5 residues, out of which Asp87 and Met120 are from the adjacent monomer. The aminocoumarin pocket is the same as earlier, but the orientation of the AC moiety in the pocket is different. The tetraene in this

structure is distant from the α-helix and does not interact with it, although it is seen to have hydrophobic interactions with Val44 and His78. No Mg^{2+} ions were found in the polyketide pocket (**Figure 9**).

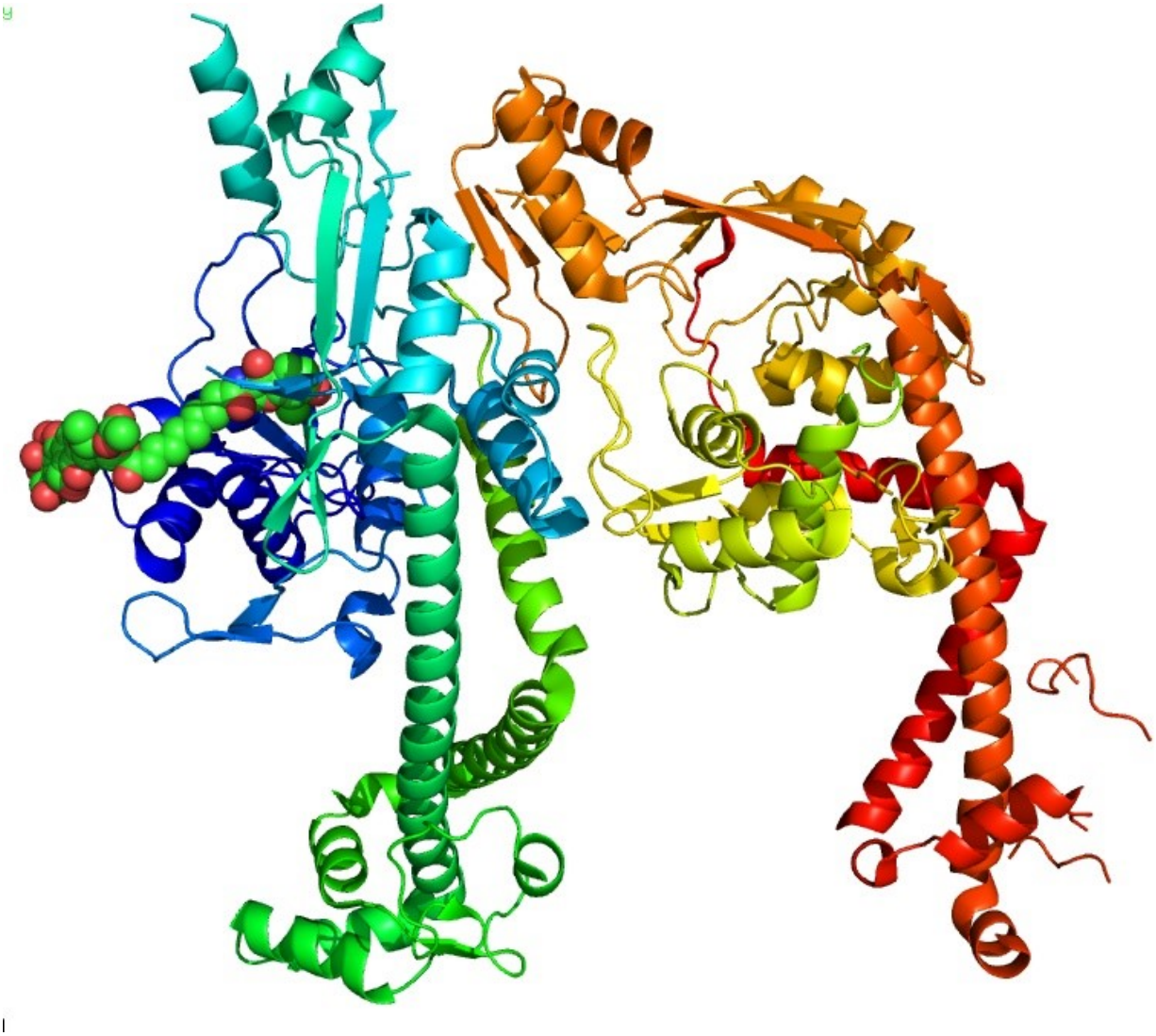

Figure 8: GyrA55 dimer with SD8 (displayed as spheres) bound in "bent-over" conformation (PDB ID: 4CKL).

The report also reevaluates the mutation data that was published in the original GyrA59-SD8 paper and the crystal structure explains all the observed data for GyrA mutants. Also to validate the intra-dimer binding mode of SD8 in the GyrA55-SD8 complex, three mutants were made: Met120 to Pro (PK pocket), Lys42 to Ala (AC pocket) and Ala84 to Arg (α-helix 4). The first two resulted in 60- and 50-fold increases in resistance to SD8, but the Ala84 to Arg mutant showed very little increase in resistance to SD8. The authors explain this by asserting that the Arg84 side chain adopting a conformation that does not impinge on the SD8 binding site. Based on this recent crystal structure, they also hypothesize a mechanism by which SD8 blocks DNA binding to gyrase: SD8 positions itself on the dimer interface and “staples” the dimer closed and preventing the DNA gate from opening for strand passage and also interfering with the conformational changes required in the DNA gate for DNA binding. The interaction of Asp87 and Gly81 with SD8 will prevent movement of α-helix 4, interaction of Met120 and SD8 will prevent the loop having the catalytic tyrosine (Tyr122) from orienting itself with DNA, and binding of Arg91 on α-helix 4 with the AC will prevent it from stabilizing the GyrA-DNA complex.

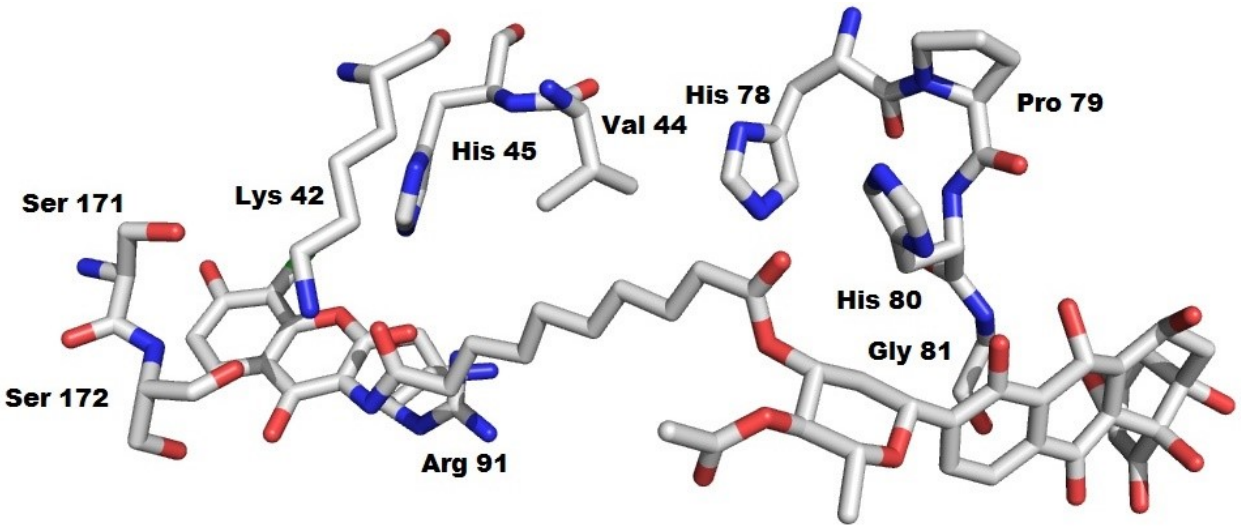

Figure 9: Residues interacting with SD8 in GyrA55 structure (PDB ID: 4CKL).

ITC studies of SD8 with GyrA and GyrB43 (N-terminal GyrB) and GyrB47 (C-terminal GyrB), yielded a substantially higher affinity of SD8 for GyrA over GyrB (1000 fold). The authors conclude that GyrA is the primary target for SD8 and the interaction with GyrB is an *in vitro* artifact manifested in the absence of GyrA.

Because most gyrase inhibitors also inhibit topo IV, SD8 was tested for its *in vitro* and *in vivo* profiles of enzyme inhibition[26]. The *in vitro* activity was accessed by determining the sensitivity of *E. coli* and *S. aureus* type II topoisomerases to SD8 and *in vivo* activity was studied using microarray analysis for cellular responses. The IC_{50} (supercoiling assay) for *E. coli* gyrase (Gram -ve) and *S. aureus* gyrase (Gram +ve) were 0.41 μM and 1.45 μM, respectively, whereas for *E. coli* topo IV and *S. aureus* topo IV they were 270 μM and 14.5 μM respectively. These results show that SD8 is much more selective for DNA gyrase as compared to topo IV. Transcriptional responses of *E. coli* to SD8 treatment are similar to the profile of gyrase inhibition; i.e., upregulation of gyrase genes and downregulation of the topo I gene. SD8 treatment does not induce an SOS response, unlike the response to quinolones. The compound also displayed an enhanced activity against *E. coli* cells that lacked the AcrB multidrug efflux pump, thus explaining why, in spite of SD8 being a potent inhibitor for DNA gyrase, it displays no activity against Gram negative bacterium. Because SD8 was initially reported as possessing cytostatic activity against tumor cells, it was tested against malignant mesothelioma (MM) and non-small cell cancer (NSCLC) cell lines and displayed an IC_{50} ranging from 75-125 μM[27]. Further assays revealed that the target in human cancer cells was human topo II with an IC_{50} of 100 μM. Later, it was found that SD8 can also inhibit human topo I with an IC_{50} of 60 ± 15

μM. Hence, SD8 is a dual catalytic inhibitor of human topo I and II[28]. Although the affinity of SD8 for these enzymes is low and the concentrations required for growth inhibition are not feasible *in vivo*, further structural modification might allow for analogues that display better anti-cancer activity.

A recent publication also demonstrated that SD8 was highly active against *E. coli* clinical isolates and also moderately effective against *K. Pneumoniae.* The authors explain this unexpected result because earlier laboratory *E. coli* isolates were used for testing, and these lab strains have reduced cellular uptake of the antibiotic in comparison to clinically present strains[29].

1.7: Rationale for the work

DNA gyrase is a validated drug target for developing anti-bacterials. Currently, the only drugs in the market that target DNA gyrase are the quinolones. The quinolones have enjoyed widespread success since their introduction and are widely used in the clinic because of their broad-spectrum activity. However, due to the prevalent use of quinolone antibiotics, resistance to them has already emerged in community and clinical settings[30-33]. To counter the threat of these fluoroquinolone-resistant infections, compounds that inhibit DNA gyrase by a mechanism of action other than the quinolones is required.

The natural product simocyclinone D8 is one such compound that potently inhibits DNA gyrase (IC_{50} = 0.4 μM, supercoiling activity) by a different mechanism of action than the quinolones. Unlike quinolones, which stabilize the cleavage complex formation of DNA gyrase with DNA, SD8 acts as a competitive inhibitor for DNA, by binding to the GyrA domain of DNA gyrase and effectively blocking the catalytic apparatus. The mode of

inhibition of DNA gyrase by SD8 has been termed catalytic inhibition and SD8 is the only reported compound to exhibit such a mechanism. Also, SD8 inhibits a ciprofloxacin resistant mutant, demonstrating that this novel mechanism can be used to combat fluoroquinolone resistance[19]. SD8 was also been shown to be active against Gram positive and Gram negative bacteria in clinically relevant concentrations. Taken together, all of this data show that the competitive inhibition mechanism of SD8 is a valid mode of action that can be used to develop new anti-bacterials and SD8 can be used as an ideal lead for further compound development.

The SD8 molecule has three subunits: an aminocoumarin, a tetraene linker and an olivose sugar bound to a highly substituted benz[*a*]anthracene system by a C-glycosidic linkage (**Figure 5**).

The GyrA59-SD8 crystal structure reveal that GyrA has 2 separate binding pockets that can accommodate the AC and the PK moieties. The tetraene linker and the olivose sugar do not make any contacts with the enzyme. Based on the report published by Maxwell *et al.*[22], the only known structure activity relationships for SD8 and reported analogues are as follows: Simocyclinone D8 (SD8, compound **1**) has an IC_{50} of 0.4 μM, Simocyclinone D4 (SD4, compound **2**), which is a biosynthetic intermediate of SD8 and does not have the chlorine on the coumarin ring, has an IC_{50} of 1.6 μM. Simocyclinone C4 (SC4, compound **3**); an intermediate from the biosynthesis of SD8 that lacks the aminocoumarin and the tetraene linker has an IC_{50} of 70 μM and MGD8N2A (compound **4**), a semisynthetic intermediate obtained from the hydrolysis of SD8 and lacks the angucyclic polyketide fragment, has an IC_{50} of 50 μM (**Figure 10**). This data underscores the importance that both the fragments of SD8 are required for optimal activity.

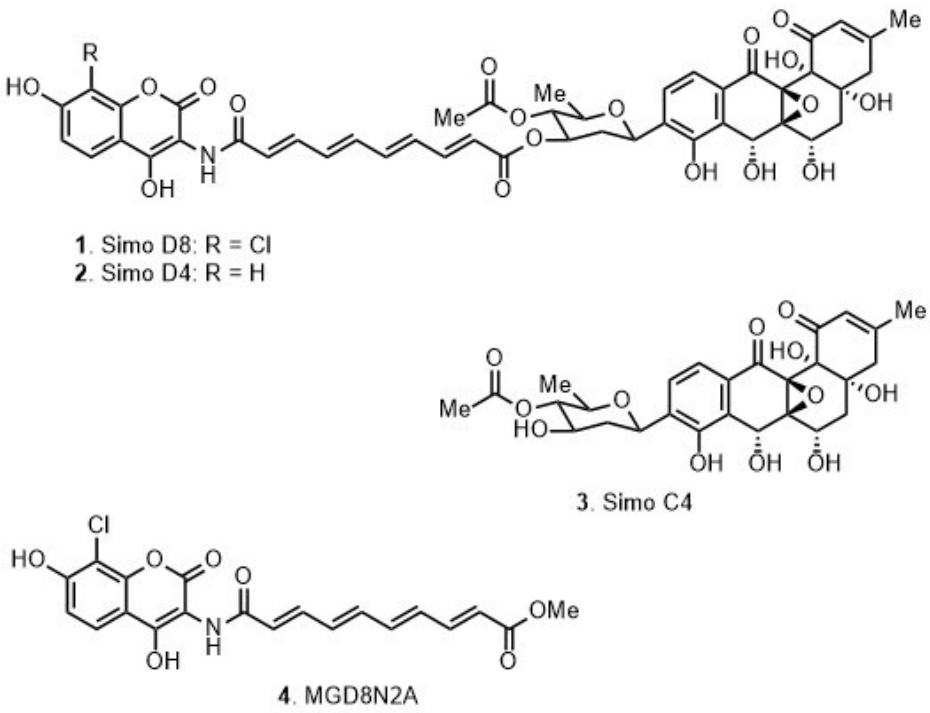

Figure 10: Structures of SD8, SD4, SC4 and MGD8N2A

The goal is to design simplified analogues of SD8 as antibacterial agents where in the simplest pharmacophore (extracted from the GyrA59-SD8) would be two binding elements separated by a linker (**Figure 11**). In the crystal structure, the tetraene linker and the olivose sugar do not seem to make any potential interactions with the enzyme, merely serving as a bridge to place the AC and PK moieties in their respective pockets.

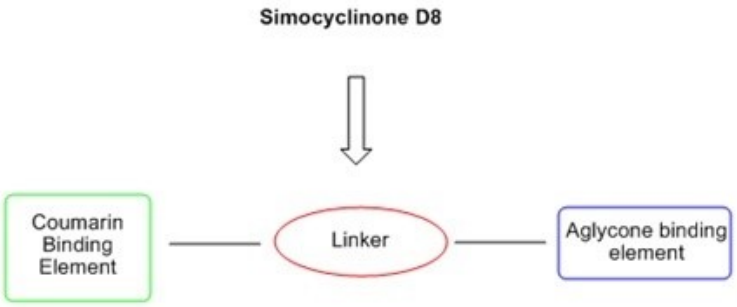

Figure 11: Simplest pharmacophore extracted from GyrA59-SD8

We decided to use a flavone moiety as a suitable replacement for the aminocoumarin. Flavones have previously been used as isosteric replacements for coumarins in Hsp90 inhibitors[34]. The 2-phenyl ring of the flavone could potentially occupy a hydrophobic cleft formed by Leu98, Gly170 and Tyr266 that lie beside the AC binding site and potentially create more hydrophobic interactions (**Figure 12**).

For the flavone, we chose to use quercetin because of its commercial availability, and for the ease of synthesis of the linker, we chose a flexible linker comprised of pimelic acid and glycine. The linker length of 15 Å was chosen based on the modeled binding geometry of SD8 in the GyrA59 crystal structure. Also in the recent GyrA55-SD8 crystal, where SD8 was crystallized in its "bent over conformation", the distance from the residue that interacts with the carbonyl oxygen of the amide (His45, AC fragment) to the residue that interacts with the phenol (His80, PK fragment) is ~15 Å (**Figure 13**).

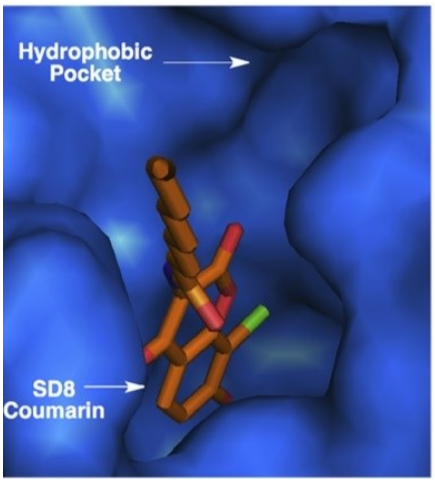

Figure 12: Binding pocket for the SD8 coumarin on GyrA59 (PDB ID: 2Y3P). The angucyclinone aglycone has been omitted for clarity[22].

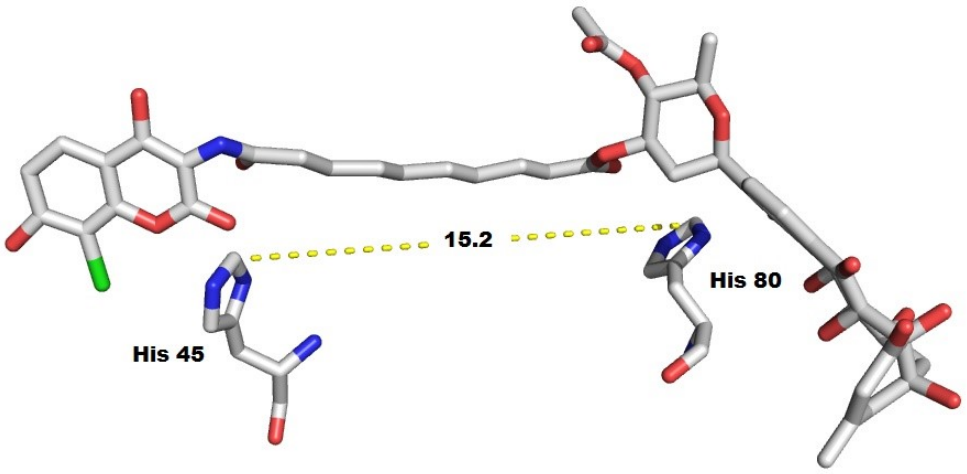

Figure 13: Distance for the linker chosen (PDB ID: 4CKL)[25].

To potentially create interactions in the PK binding site, we chose to couple substituted anilines to the linker. We envisioned that the aromatic ring of the anilines can π-stack with the His80, located 15 Å away. This has been proved to be a critical residue by crystallography and mutation studies. Based on the interactions of the highlighted diol with Tyr122 and Arg121 through a Mg^{2+} ion and water, we decided to substitute the meta- and para- positions of the aniline. Because the hydrogen bond distances are long in the GyrA59-SD8 structure, we decided to extend the diol and use a more acidic substituent (carboxylic acid). To probe the space available at the para- position of the aniline, we decided to use a range of substituents from hydrogen to isopropyl group. To probe the electronics of the aromatic ring, we used a para chloro and a para methoxy substituent (**Figure 14**).

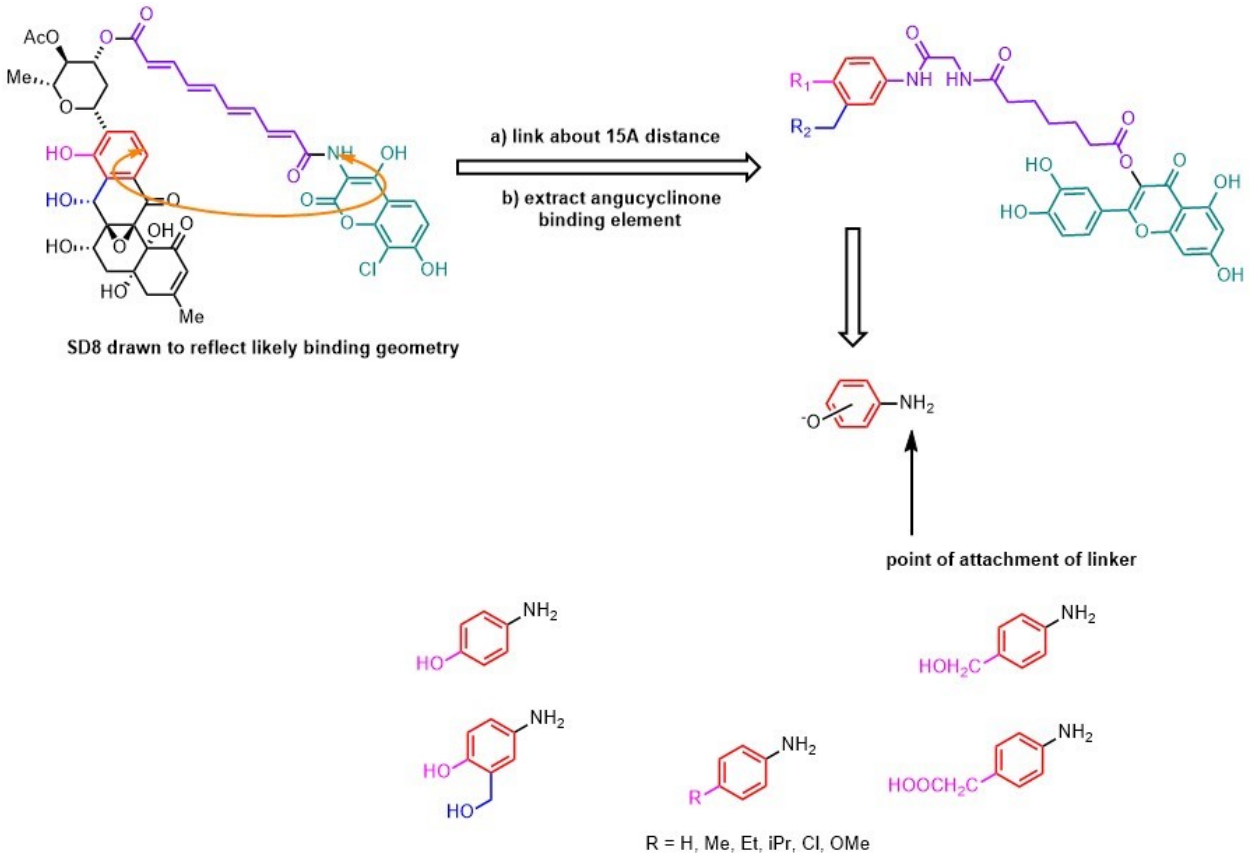

Figure 14: Design of quercetin-pimelic acid-glycine linked aniline analogues

Our aims in designing these analogues were to find simpler compounds that could bind to the AC and PK pockets of GyrA and also to determine a synthetically accessible scaffold that could potentially bind to the PK pocket, thus obviating the need to make structurally complex analogues of the SD8 angucyclinone.

1.8: Synthesis of flavone-based analogues of SD8

To begin our work, we protected commercially available quercetin **5** with benzyl bromide in DMF, using potassium carbonate as a base to give tribenzyl quercetin **6** in 50% yield. Pimelic acid **7** was selectively protected as the mono-tertbutyl ester by a standard peptide coupling protocol using *tert*-butanol, *N*-(3-dimethylaminopropyl)-*N'*-(ethylcarbodiimide)

hydrochloride (EDCI) and 4-(dimethylamino)pyridine (DMAP) as the base in chloroform to obtain the mono protected *tert*-butyl ester of pimelic acid **8** in 44% yield (**Figure 15**).

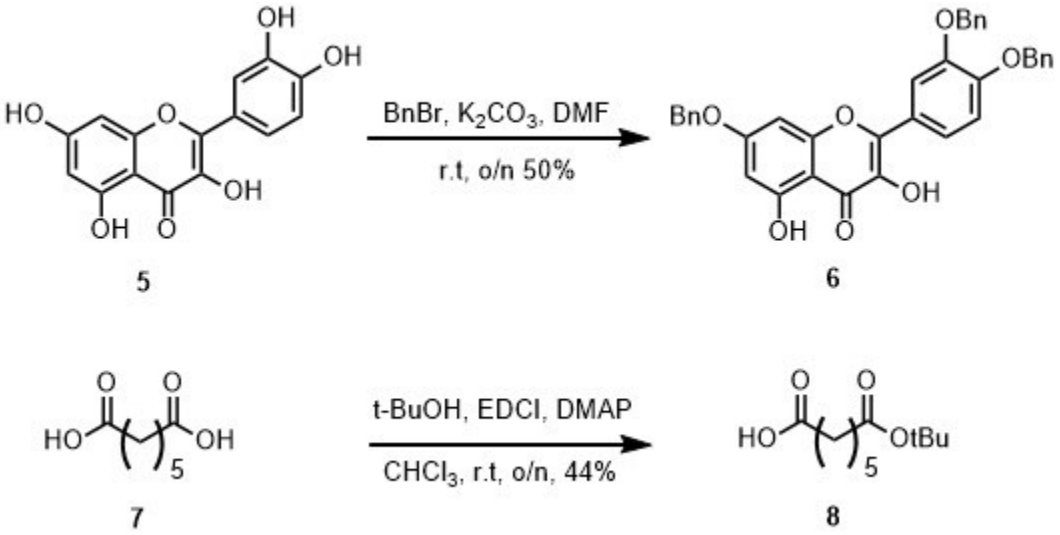

Figure 15: Synthesis of **6** and **8**

Tribenzyl quercetin **6** was esterified using the acid **8** and the peptide coupling reagent EDCI in THF, with stoichiometric amounts of Hunig's base and catalytic DMAP in THF to obtain the ester **9** in quantitative yield. The *tert*-butyl ester was removed using trifluoroacetic acid (TFA) in DCM with triethylsilane as a cation scavenger to afford the compound **10** in 76% yield (**Figure 16**).

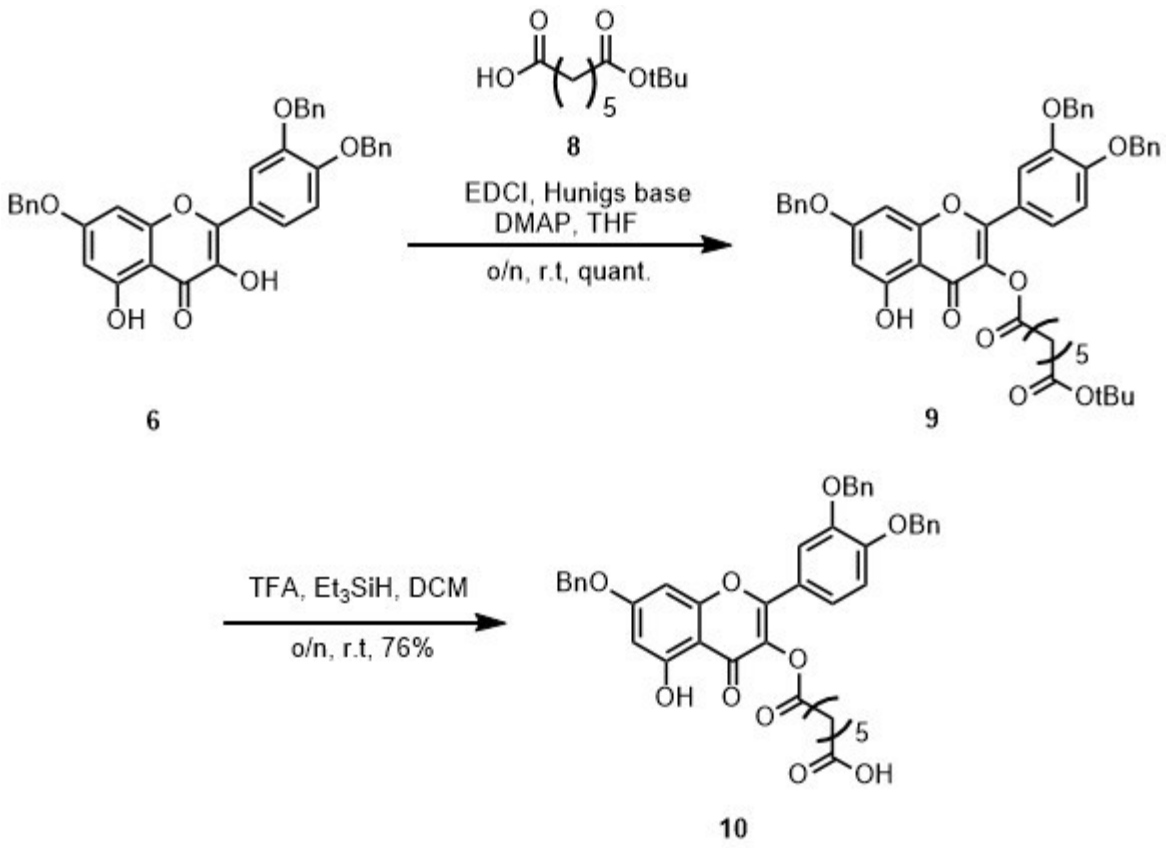

Figure 16: Synthesis of compound **10**

Suitably protected anilines **11a** – **11j** were coupled to N-phthaloyl-glycine acid chloride in THF with triethylamine as the base under reflux conditions. The obtained aniline-glycine-phthalimide compounds were sufficiently pure to be used for the next step. The phthalimide protecting groups were removed using hydrazine hydrate in ethanol under reflux conditions. The deprotected primary amines **12a** – **12j** were purified on silica and were obtained in 60-80% overall yields (**Figure 17**).

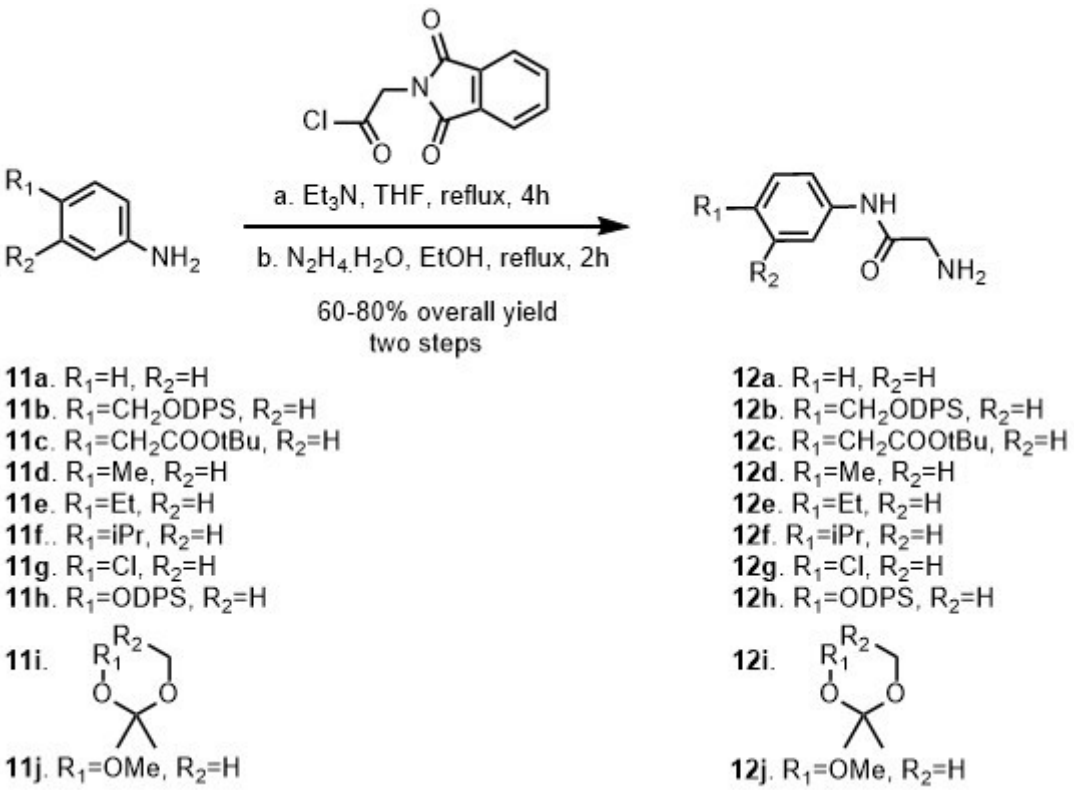

Figure 17: Synthesis of compounds **12a** to **12j**

These obtained compounds **12a** – **12j** were coupled to the acid **10** using standard peptide coupling procedures with EDCI as the coupling reagent, 1-hydroxybenzotriazole as the promoter and *N*-methyl morpholine as the base in DMF to offer the amides **13a** – **13j** in 77 to 95% yield (**Figure 18**).

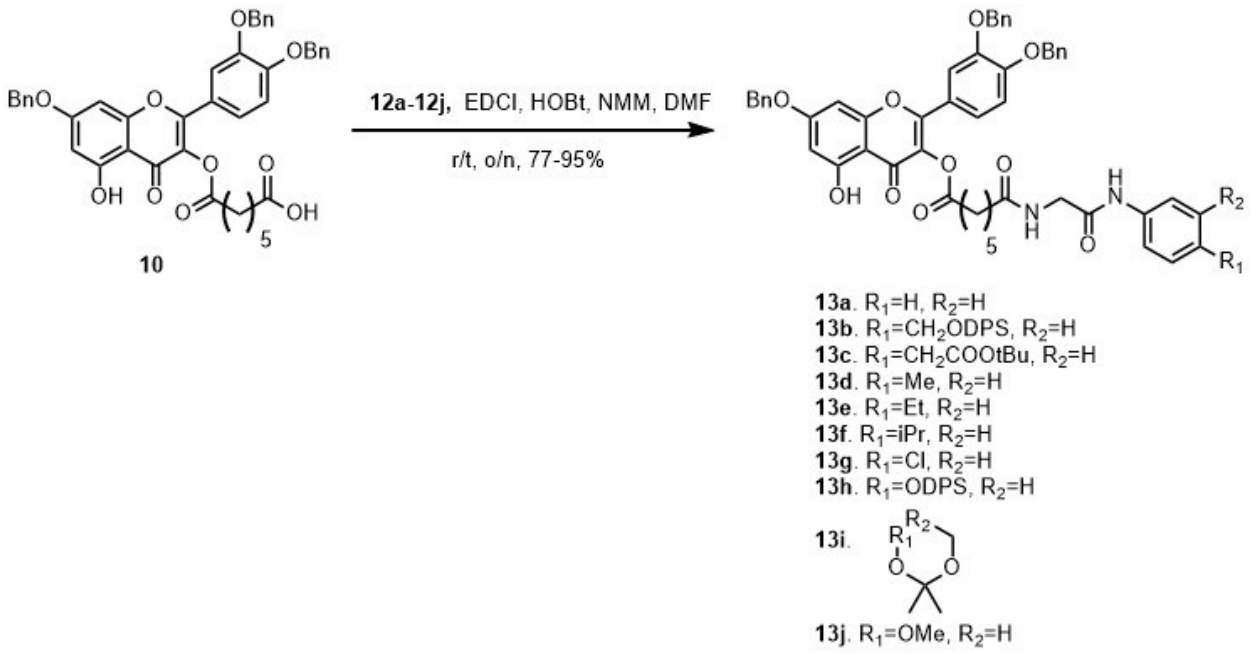

Figure 18: Preparation of compounds **13a** to **13-j**

From the obtained amides, the aniline protecting groups were initially removed, followed by removal of the benzyl ethers. The silyl protecting groups were removed using tetrabutylammonium fluoride in THF, which gave the alcohols in moderate yields (69% for compound **14b** and 65% for compound **14h**, **Figure 19**). *Tert*-butyl ester was removed using TFA and the cation scavenger triethylsilane in DCM to give the carboxylic acid **15c** in quantitative yield (**Figure 20**). The acetonide protecting group was removed using HCl in THF, obtaining the diol **14i** (**Figure 21**) in 36% yield. The benzyl ethers were removed by hydrogenation using hydrogen at 1 psi (balloon pressure) and palladium on charcoal as the catalyst to obtain the benzyl deprotected quercetin derivatives **15a** – **15j** in yields ranging from 33% - 57% (**Figure 19 – Figure 22**).

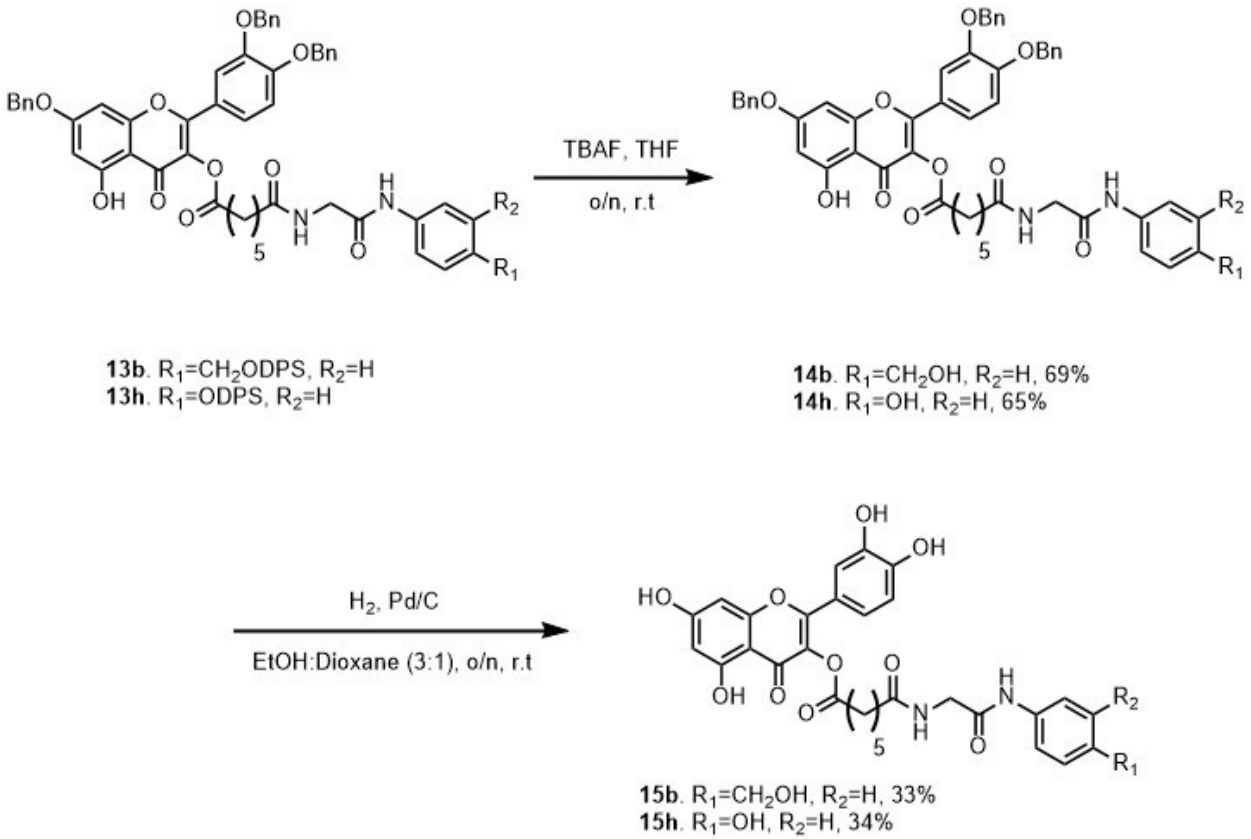

13b. R_1=CH_2ODPS, R_2=H
13h. R_1=ODPS, R_2=H

14b. R_1=CH_2OH, R_2=H, 69%
14h. R_1=OH, R_2=H, 65%

15b. R_1=CH_2OH, R_2=H, 33%
15h. R_1=OH, R_2=H, 34%

Figure 19: Synthesis of compounds **15b** and **15h**

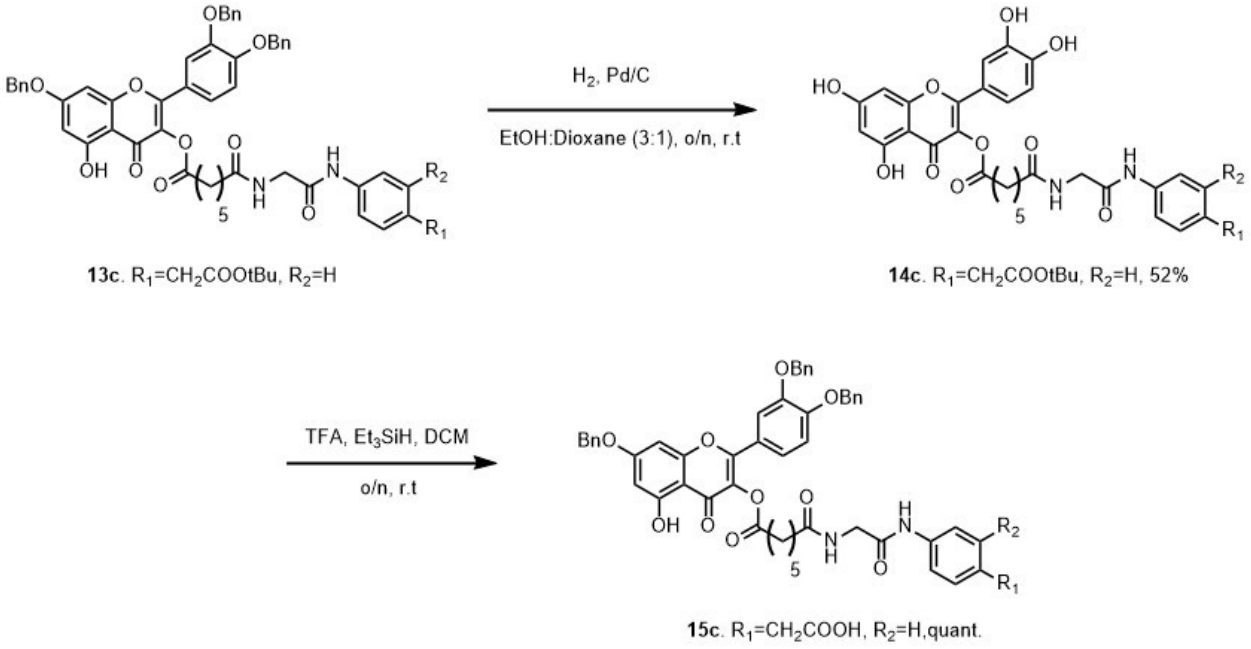

13c. R_1=$CH_2COOtBu$, R_2=H

14c. R_1=$CH_2COOtBu$, R_2=H, 52%

15c. R_1=CH_2COOH, R_2=H,quant.

Figure 20: Synthesis of compound **15c**

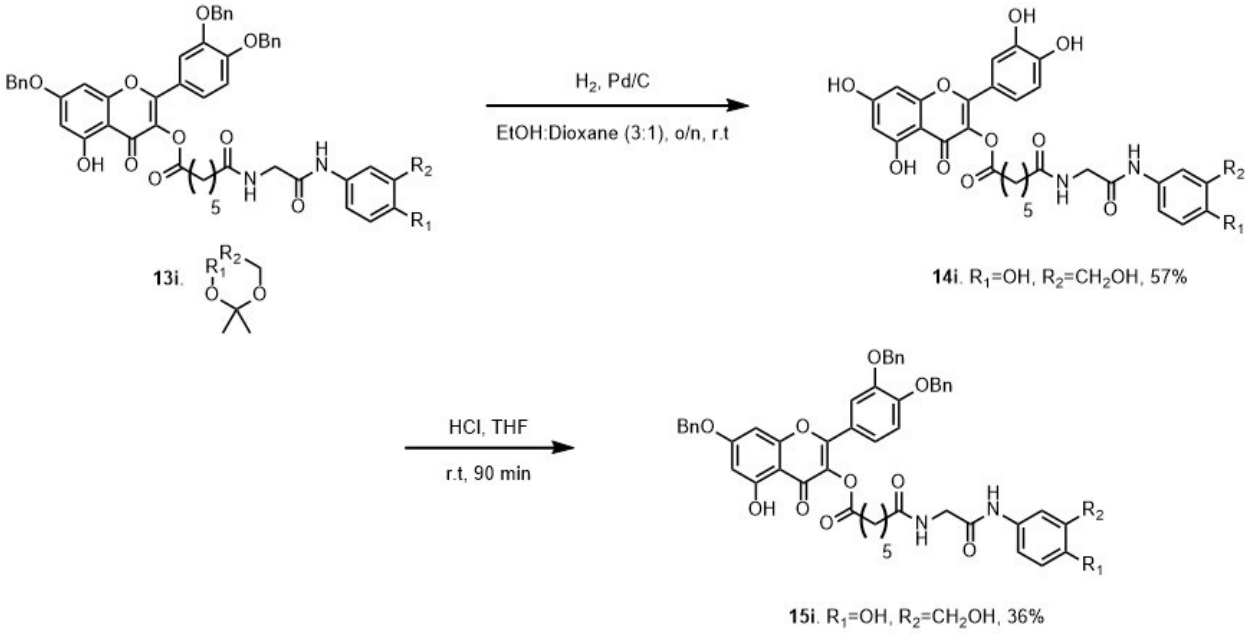

Figure 21: Synthesis of compound **15i**

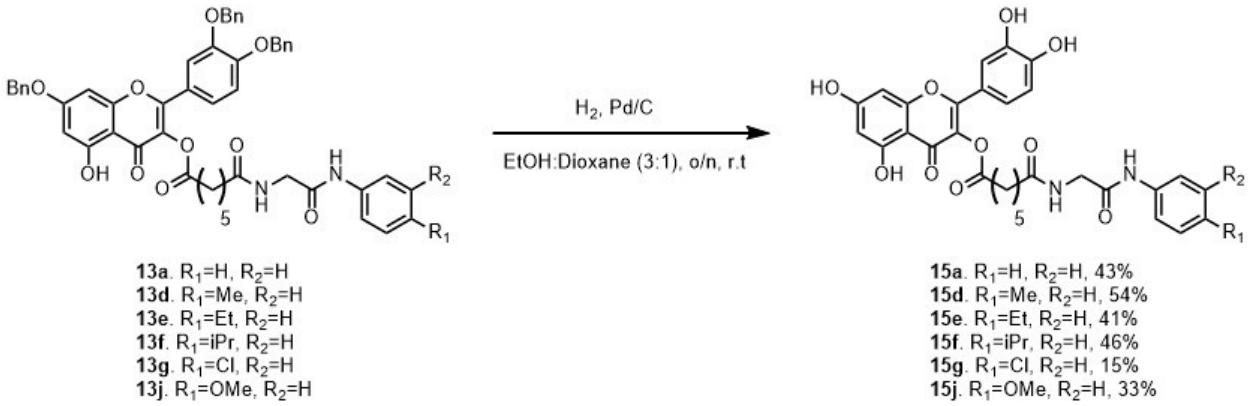

Figure 22: Preparation of compounds **15a, 15d-g, 15j**

As a control compound, we prepared a flavone based analog **15k** without the aniline fragment. Tribenzyl-quercetin **6** was esterified with mono-methyl sebacic acid, to give the ester **14k**. The ester was hydrogenated to obtain quercetin-sebacic acid methyl ester

analog **15k** (**Figure 23**). This compound lacks the aromatic ring that would bind to the PK pocket.

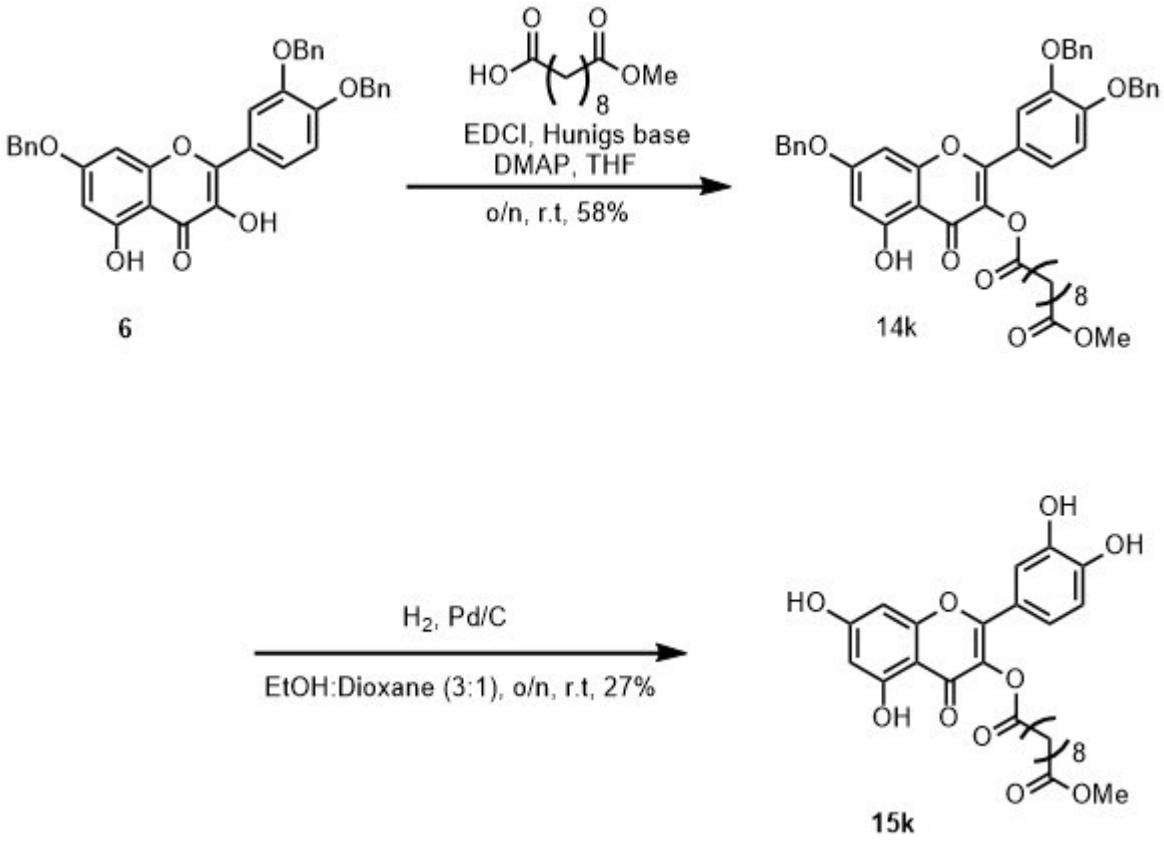

Figure 23: Synthesis of compound **15k**

1.9: Biological activity of flavone-based analogues

To assess the ability of the flavone analogues to inhibit *E*. coli DNA gyrase we performed a supercoiling activity assay[26]. Briefly, the assay uses the relaxed plasmid PBR 322 and *E.* coli gyrase. The DNA gyrase supercoils the plasmid DNA, which is shown as a band of topoisomers into the supercoiled form that moves faster on the gel. Upon addition of the compound, if gyrase is inhibited, the amount of supercoiled plasmid is reduced. The

assay was performed in the presence of varying concentrations of these flavone analogues and the 50% inhibitory concentration (IC_{50}) was determined (**Table 1**). Compounds **15d – 15g** and **15j** were not soluble in the assay medium, so we could not determine any further data from these compounds.

Table 1: Activity of compounds against *E*. coli DNA gyrase

Compound	**Supercoiling assay IC_{50} (μM)**
15a	48.6 ± 0.8
15h	84.7 ± 5.5
15b	>200
15c	>200
15i	>200
15k	>200
SD8	0.41

Next, to determine whether these compounds inhibit *E.* coli DNA gyrase by a catalytic mechanism similar to SD8, they were tested for their ability to disrupt binding of DNA gyrase to DNA by surface Plasmon resonance (SPR)[19]. Neither compounds was active in this assay nor was disruption of the DNA –enzyme interaction observed (**Figure 24**).

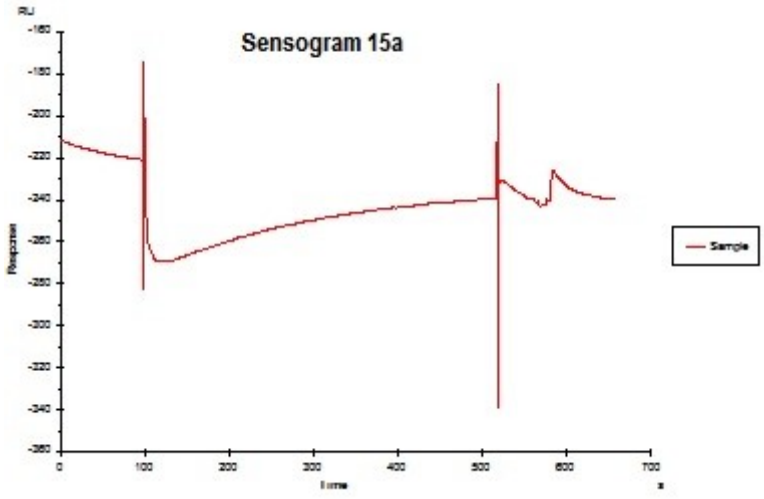

Figure 24: Sensogram of compound **15a**

To further investigate the mechanism of how these compounds inhibited DNA gyrase, we tested the effect of these compounds on the DNA cleavage activity of *E.* coli DNA gyrase (**Table 2**)[26]. Topoisomerases cause changes in DNA topology by cleaving and religating strands. When quinolones inhibit this religation process, they form linear DNA that makes covalent complexes with the enzyme. Formation of linear DNA is quantified to determine whether the compound works as a topoisomerase poison.

Table 2: DNA cleavage assay for compounds

Compound	DNA cleavage (Fold – stimulation)
15a	7.8
15h	5.0
15b	3.0
15c	1.8
15i	1.9
15k	>1
SD8	>1

So, determining that these compounds inhibit DNA gyrase, but with a mechanism different than that of SD8, we tested them against human Topo II[27, 28]. We first evaluated the effect of these compounds on the decatenation activity of human Topo II and also on the DNA cleavage activity of Human Topo II (**Table 3**).

Table 3: Effect of flavone analogues on Human topo II

Compound	Decatenation assay IC_{50} (μM)	DNA Cleavage (Fold – Stimulation)
15a	149 ± 3.2	2.7
15h	>200	2.4
15b	>200	2.1
15c	>200	<1
15i	78.9 ± 1.4	<1
15k	>200	<1
SD8	100	

Since quercetin can intercalate into DNA[35, 36] and the compounds **15a**, **15h** and **15b** have the quercetin moiety in them, we decided to examine if these compounds can intercalate into DNA by using a DNA unwinding assay. We also used quercetin as a control, to compare the level of intercalation that occurs (**Figure 25**). If the compound intercalated into DNA (in this case plasmid PBR 322), after treatment with gyrase, it forms relaxed or underwound DNA that converts into supercoiled DNA. The presence of supercoiled DNA indicates DNA intercalation has happened. The extent of intercalation of a compound can be measured as the level of negative supercoils introduced into the covalently closed, relaxed circular substrate DNA[37].

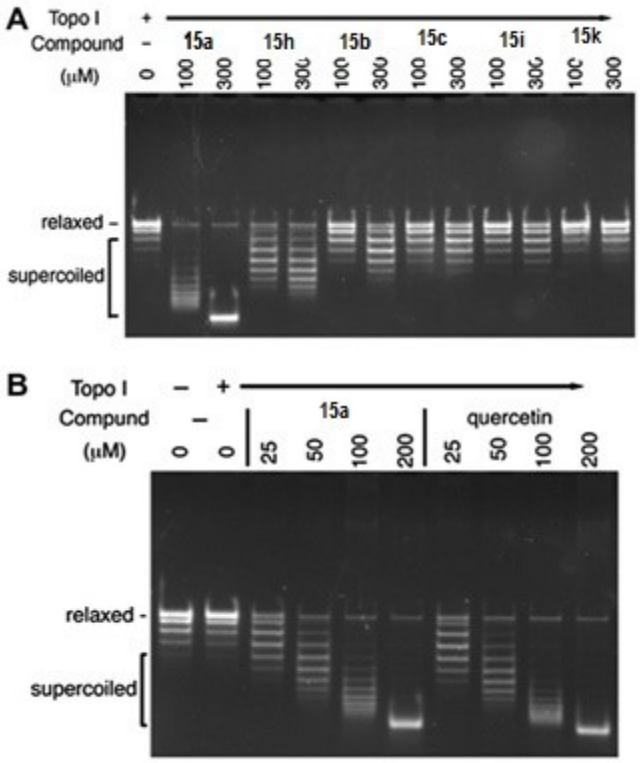

Figure 25: (A) Intercalation of compounds **15a** – **15k**. **(B)** Intercalation of compound **15a** as compared to intercalation by quercetin

1.10: Conclusions and Discussion

Based on the structure and competitive mechanism of action of SD8 against DNA gyrase[19], we designed and synthesized ten flavone based analogues. We prepared compounds using the flavone quercetin as the AC binding element and various substituted anilines to bind to the PK pocket of DNA gyrase linked by a flexible glycine-pimelic acid linker in modest yields.

Initially, we tested the ability of these flavone-based compounds to inhibit *E.* coli DNA gyrase supercoiling by a supercoiling activity assay. Compounds **15a** and **15h** displayed

modest inhibitory effects on the supercoiling activity of gyrase with IC_{50} values of 48.6 ± 0.8 μM and 84.7 ± 5.5 μM, respectively, but the other compounds were not active (i.e., IC_{50} values greater than 200 μM). The activities of these compounds for DNA gyrase were significantly lower than that of SD8 (IC_{50} = 0.41 μM) and quercetin alone (IC_{50} value of 0.14 μM), but similar to that of the coumarin-linker subunit of SD8 (MGD8N2A, IC_{50} = 50 μM). Compound **15k**, the flavone-based analog most similar to MGD8N2A was inactive, suggesting that the aniline fragment is required for activity against DNA gyrase.

To determine the mechanism of DNA gyrase inhibition by these compounds we performed an SPR assay. SD8 binds to DNA gyrase and inhibits the catalytic activity of the enzyme by preventing DNA from binding to the enzyme and this mechanism has been termed catalytic inhibition. SPR has been used to analyze this disruption of DNA binding to the enzyme by SD8[19]. Neither compound **15a** nor **15h** was active in this assay and no disruption of DNA-enzyme interaction was observed. This data suggested that the observed inhibition of DNA gyrase by the flavone analogues **15a** and **15h** were by a different mechanism than that of SD8.

Quinolones inhibit DNA gyrase by stabilizing the enzyme-DNA cleavage complex, thereby preventing religation and exit of DNA from the enzyme[11]. To investigate whether the flavone analogues inhibited *E*. coli DNA gyrase by a similar mechanism, we carried out a DNA cleavage assay. All compounds except **15k** modestly stimulated gyrase-catalyzed cleavage, with compounds **15a** and **15h** displaying the highest levels of stimulation (7.8-fold and 5.0-fold stimulation in generation of linear DNA at 200 μM, respectively). The extent of generation of linear DNA by compounds **15a** and **15h** tallies up with their

inhibition of supercoiling activity for *E. coli* gyrase. This suggests that compounds **15a** and **15h** inhibit the activity of DNA gyrase by poisoning it.

SD8 was found to be a dual inhibitor of human topo II and topo I[28]. Human topoisomerase inhibitors are used for cancer chemotherapy. To determine the potential toxicity of these compounds, we screened them against human topo II. Initially, the effect of these compounds on the decatenation activity of human topo II was assessed and it was found that compounds **15a** and **15i** exhibited modest activities with IC_{50} values of 149 ± 3.2 μM and 78.9 ± 1.4 μM. It is interesting to note that compound **15a** inhibited both *E. coli* DNA gyrase and human Topo II, whereas compound **15i** inhibited only human topo II and compound **15h** inhibited only *E*. coli DNA gyrase. To determine the mechanism of action of these compounds on human topo II, we assessed their activity on DNA cleavage by human topo II. Similar to the results obtained for *E. coli* DNA gyrase, compounds **15a** and **15h** displayed the highest level of poisoning activity against human Topo II, although the extent of DNA cleavage stimulation for Topo II were lower than that of *E. coli* DNA gyrase. Hence, the compounds **15a** and **15h** appear to inhibit the activity of topoisomerases by poisoning, as quercetin does. But, interestingly, compound **15i** exhibited modest inhibition of human topo II without poisoning it, suggesting a different mode of action for compound **15i**.

Since quercetin[35, 36] and also quinolones[38] can intercalate into DNA, we tested the DNA intercalation ability of these flavone based analogues by a DNA unwinding assay. Some of these compounds were found to intercalate into DNA and their levels of intercalation varied. Compound **15a** displayed the highest level of intercalation and the level of intercalation was similar to that of quercetin. Compound **15h** displayed a modest level of

intercalation but the level of intercalation of other compounds were limited. Compounds **15a** and **15h** displayed the highest level of poisoning activity among these compounds against both *E.* coli gyrase and human Topo II, indicating that these compounds might inhibit topoisomerases by their ability to intercalate into DNA.

In conclusion, we prepared flavone-based analogues inspired by the natural product simocyclinone D8. While two of these compounds do inhibit DNA gyrase, they do not act as catalytic inhibitors as SD8 does. The flavone based analogues **15a** and **15h** were determined to be topoisomerase poisons and DNA intercalators.

CHAPTER 2: SYNTHETIC STUDIES TOWARDS THE TOTAL SYNTHESIS OF SIMOCYCLINONE D8 (SD8)

2.1 Introduction

Natural products have long been a source for antibiotics and it is reasonable to expect new natural products to serve as promising leads for new antibiotic drug discovery. An overwhelming majority (69%) of antibacterial drugs FDA approved between 1981 and 2006 were either natural products or developed from natural products[39]. Antibacterial drug discovery from natural products has been more fruitful as compared from small molecule libraries because of the chemical diversity natural products afford and also due to their different physiochemical properties as compared to small molecules[40].

The fluoroquinolones are broad spectrum antibiotics that are able to treat both Gram-(+) and Gram-(-) infections[6]. They are the only class of drugs used clinically that inhibit DNA gyrase. However, mutations in DNA gyrase that confer resistance to the fluoroquinolone drugs like ciprofloxacin have emerged both in clinic and community settings. Fluoroquinolone resistance has been reported in pneumonia, influenza, MDR/XDR tuberculosis and pseudomonas respiratory infections. To counter this threat from fluoroquinolone-resistant bacterial strains, compounds that can inhibit drug-resistant DNA gyrase mutants must be developed[30-32]. One potential source of compounds that can inhibit fluoroquinolone-resistant mutants are compounds that can inhibit DNA gyrase by a novel mechanism.

SD8 is one such natural compound that inhibits DNA gyrase by a novel mechanism of action as compared to the fluoroquinolones. SD8 inhibits DNA binding to the enzyme and

has been termed competitive inhibition compared to fluoroquinolones that trap the DNA-DNA gyrase complex. SD8 was shown to inhibit both wild-type and a ciprofloxacin-resistant mutant in a supercoiling assay proving that the competitive mechanism of action can be exploited to overcome fluoroquinolone resistant mutants[19, 22].

The structure of SD8 is highly modular, consisting of three subunits: an aminocoumarin, tetraene linker and an angucyclinone aglycone comprised of an olivose sugar bound to a highly substituted benz[*a*]anthracene system by a C-glycosidic bond. SD8 belongs to the angucyclinone family of natural products, which are characterized by the benz[*a*]anthracene ring system and its angular A ring. Angucyclines are categorized along with tetracyclines and anthracyclines as antibiotics with a carbotetracyclic skeleton. SD8 is further categorized as belonging to the aquayamycin sub-type of angucyclinones. This sub-type is defined by molecules that incorporate both a C-glycoside and angular, tertiary diols at C4a and C12b in the aglycone (**Figure 26**)[41-43]. The structure is highly modular and this will be exploited while designing synthetic routes towards its total synthesis.

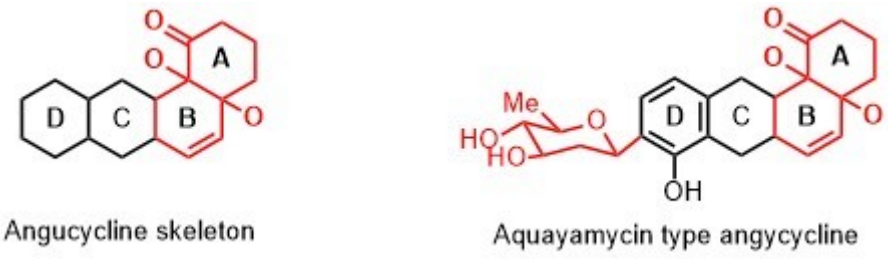

Figure 26: Structure of Angucycline antibiotics and Aquayamycin subtype Angucyclines

2.2: Review of literature

2.2.1: Prior synthetic efforts towards the Angucyclinone fragment

Various synthetic strategies have been reported for the synthesis of angucyclinone antibiotics, that either form the B, C or D rings as the key step. Most commonly reported methodologies for the key ring formation include Hauser cycloaddition, radical cyclization, Friedel-Craft cyclization, Michael addition and biomimetic reactions[41, 42].

The only reported total synthesis of an aquayamycin-type angucyclinone is of aquayamycin itself[44]. The study reported in 2000, uses a Hauser annulation between the 3-(phenylsulfonyl) phthalide fragment **16** and the optically active cyclohexanone fragment **17** to construct the BCD ring fragment (**Figure 27**). This synthesis uses a Lewis acid catalyzed C-glycosidation to install the olivose sugar in fragment **16**. The stereochemistry of the angular C4a alcohol was derived using enzymatic resolution by *Candida antartica* lipase of a racemic tertiary alcohol in the preparation of the fragment **17**. The stereochemistry at C4a is used to control the stereochemistry of the C12b alcohol during construction of the A ring by pinacol coupling[44-46]. This report provides precedent for construction of the A ring and control of stereochemistry while installing the angular diols.

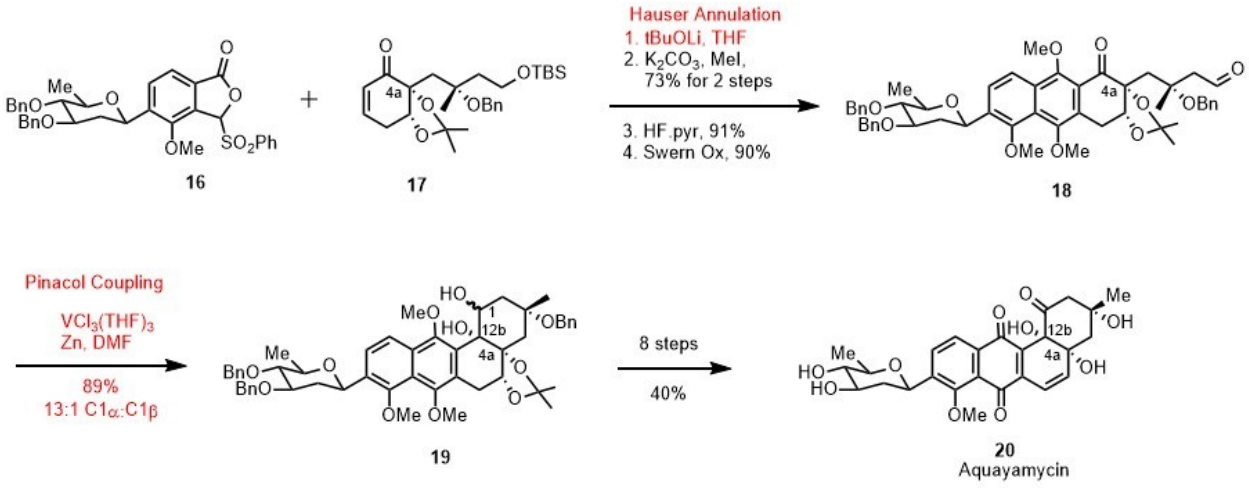

Figure 27: Total synthesis of Aquayamycin

Little synthetic work has been done on angucyclinones having epoxides. Sulikowski has reported an epoxidation on a benz[*a*]anthracene ring system in work towards the synthesis of angucycline SF 2315B (**Figure 28**)[47]. The epoxide of compound **22** was installed using radical oxidation by oxygenating a solution of the quinone **21** in THF in the presence of tetrabutylammonium fluoride and it was reported that only the α-epoxide is formed due to steric hindrance on the β-face by the A ring. This breaks the conjugated quinone system, and Sulikowski then performs a chelation-controlled *syn*-reduction of the C12 quinone ketone of **23** using tetramethylammonium triacetoxyborohydride to get **24**. These conditions are chemoselective and the β-hydroxyketone can be reduced in presence of an epoxide and a ketone. This report offers the precedent of achieving chelation-controlled *syn*-reduction of a β-hydroxyketone in the presence of an epoxide and a ketone.

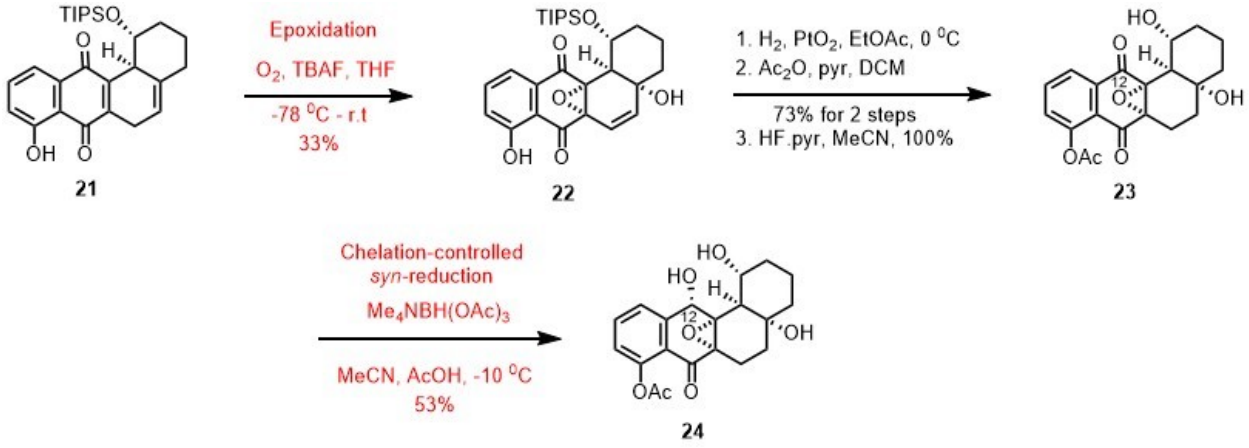

Figure 28: Sulikowsky synthesis of SF 2315B

Suzuki *et al.* report the selective substitution of the C3' alcohol of olivose over the C4' in the total synthesis of the antibiotic C104 (**Figure 29**)[48, 49]. TBS protection of the less hindered C3' alcohol **25** occurs more readily and is followed by the installation of the

dienone ester at C4' by Yamaguchi esterification to give **26**. This report provides the precedent of selective reactivity of the C3' alcohol over the C4' alcohol in olivose.

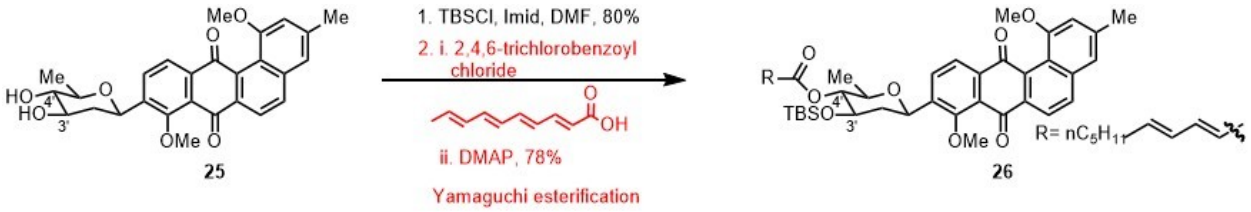

Figure 29: Selective reactivity of the C3'-OH over C4'-OH in the olivose sugar

2.2.2: Retrosynthetic Analysis of SD8

The structure of SD8 is highly modular, which we plan to exploit in our total synthesis. Our first disconnection is at the olivose-tetraene bond (**Figure 30**). We plan to install the coumarin-tetraene subunit **27** selectively at the C3' of the olivose sugar of the aglycone **28** by a Yamaguchi esterification following the precedent of Suzuki[48, 49].

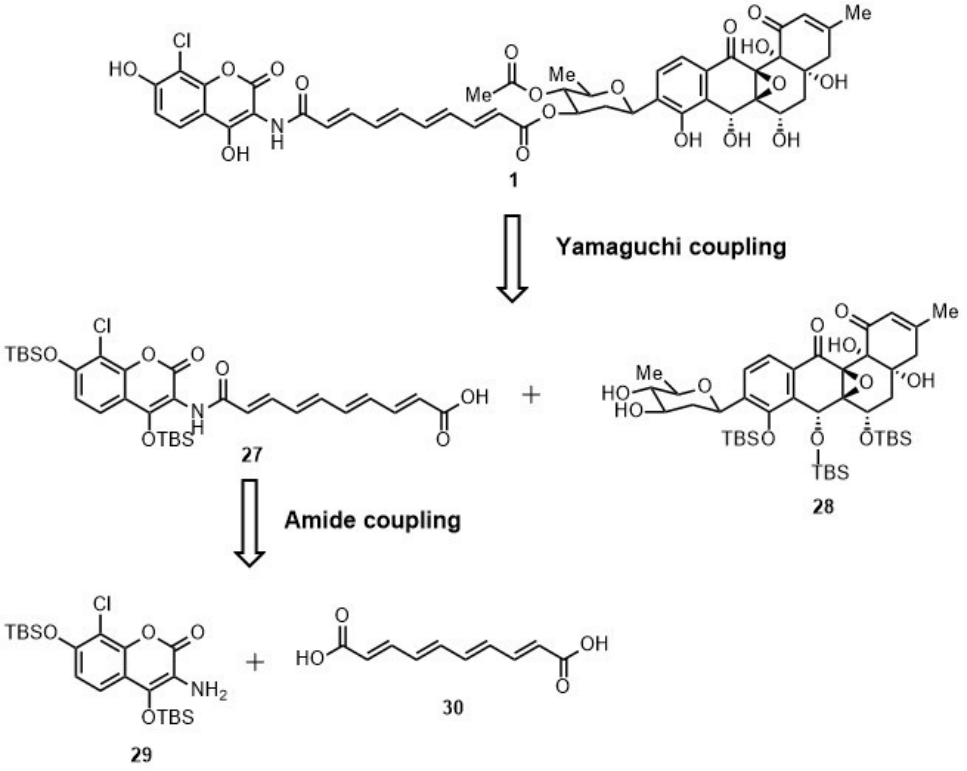

Figure 30: Retrosynthesis of SD8

The aglycone **28** will be prepared from the quinone **31** by a stereoselective epoxidation, chelation-controlled reduction of the C7 ketone, Suzuki coupling to install the A ring side chain and pinacol coupling to install the A ring. The BCD ring system **31** will be assembled by a Hauser annulation of the isobenzofuranone **33** and the α,β-unsaturated ketone **32** will be prepared by stereoselective Rubottom-type α-hydroxylation (**Figure 31**).

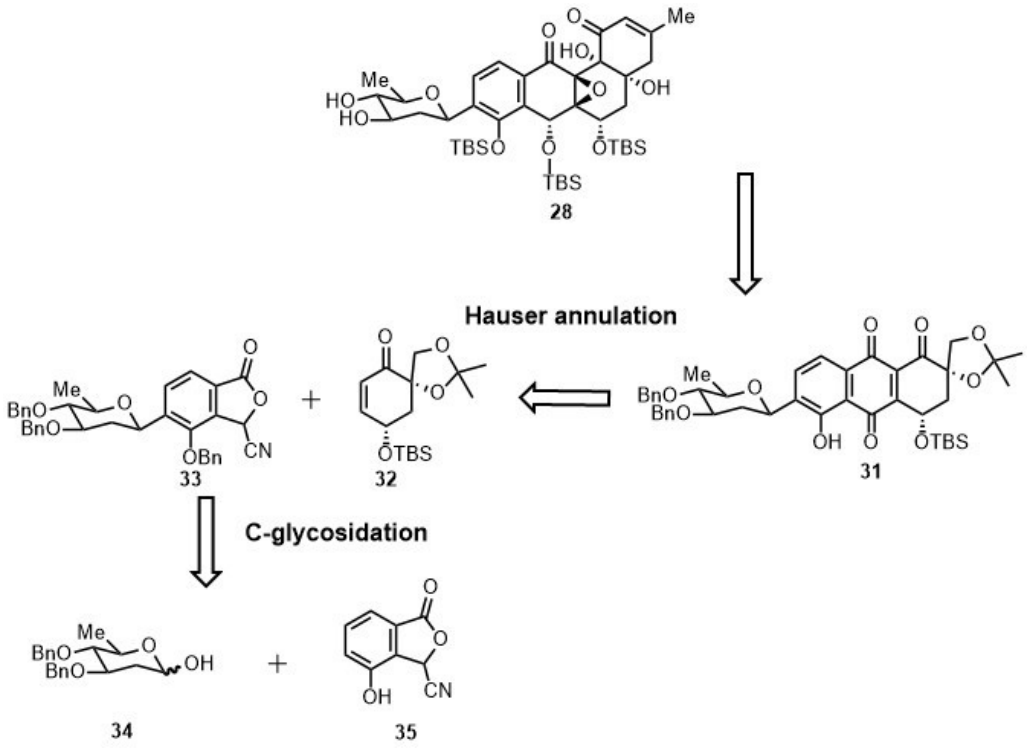

Figure 31: Retrosynthesis of the aglycone fragment **28**

Our proposed synthesis begins with the glycosidation of the sugar **34** and the isobenzofuranone **35** (**Figure 32**). The sugar can be installed using a well-precedented Lewis acid or protic acid catalyzed C-glycosylation reaction[50, 51]. Protection of the triol as the tri-benzyl ether completes the synthesis of the isobenzofuranone **33**.

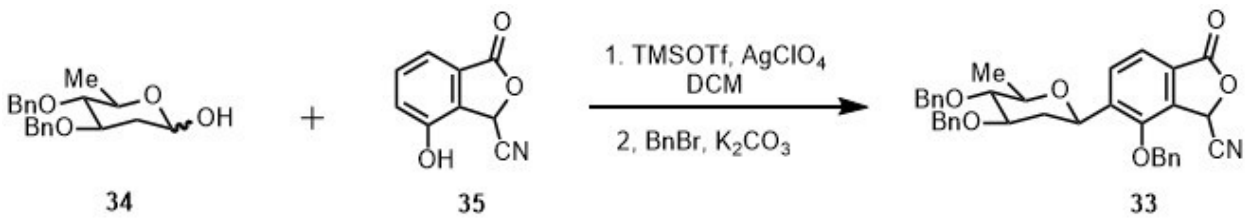

Figure 32: Synthesis of fragment **33**

We plan to synthesize the α,β-unsaturated ketone **32** as described in **Figure 33**. Using 4-OTBS-cyclohex-2-en-1-one **36**, which can be prepared on a large scale by multiple chemical or enzymatic routes as reported[52-55], we plan to install the hydroxymethyl at Cα' in a non-stereoselective manner to afford **37**. On this substrate, we plan to carry out an asymmetric α-hydroxylation using Rubottom-type conditions[56], which is well-precedented in the literature using Davis' chiral oxaziridine[57], Shi epoxide catalyst/Oxone[58], Mn(salen) complexes/NaOCl[59] and Sharpless Asymmetric Epoxidation (SAE)[60, 61]. The silyl enol ether is more electron rich than the olefin of the α,β-unsaturated ketone **37** and will react preferentially under these conditions[62]. We expect to isolate the triol **38** after a global deprotection using TBAF and reprotect the primary and tertiary alcohols as the acetonide and the secondary alcohol as the TBS ether to afford the compound **32**.

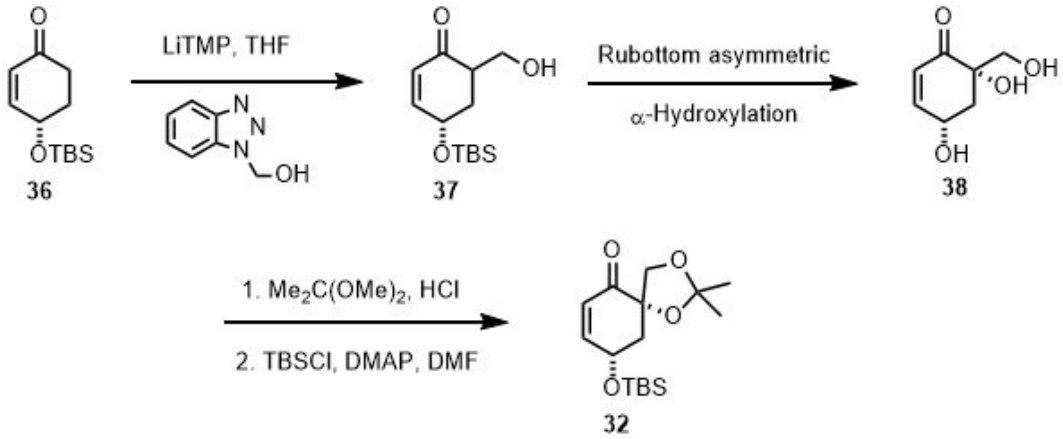

Figure 33: Synthesis of the cyclohexanone fragment **32**

Hauser cycloaddition of **33** and **32** under basic conditions (LiHMDS) followed by acidic neutralization using the procedure of Hauser[63] will afford the quinone **31** (**Figure 34**). We plan to install the epoxide in the next step. The timing of epoxide installation (early vs. late) was made after consideration of the stereochemical outcome of epoxidation of the early-stage and late-stage substrates (**Figure 35**). We predict that epoxidation on the early-stage substrate **31** will afford the desired β-epoxide **31''**. The protected C4a-OH and C6-OTBS groups in this intermediate will sit in the axial positions in the half-chair conformation, blocking the α-face and leaving the β-face sterically accessible for the approach of mCPBA. Epoxidation of the late-stage substrate **43**, wherein the A ring is already formed, might lead to poor facial selectivity and yield because both the α- and β-faces are sterically hindered. Thus, we will install the epoxide at this earlier point in the route. Treatment of the epoxide with TBAF will remove the C6-OTBS protecting group and will set the stage for the next chelation-controlled *syn*-reduction on the substrate **39**.

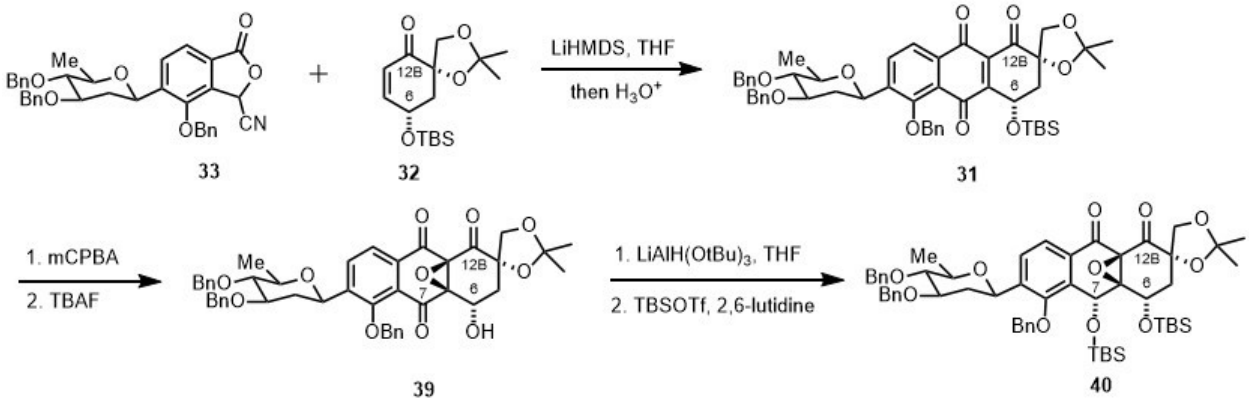

Figure 34: Preparation of fragment **40**

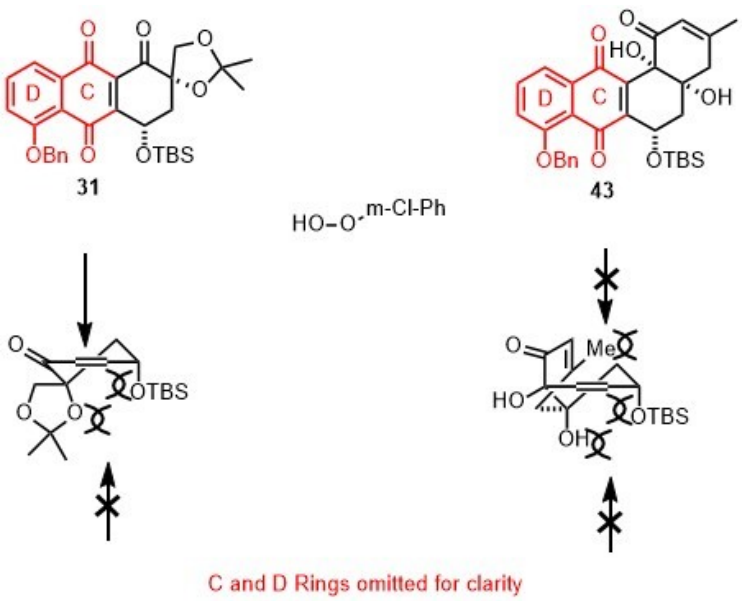

Figure 35: Epoxidation on early vs. late substrate

The C6-OH in **39** will provide the directing group for the stereoselective *syn*-1,3-chelation-controlled reduction of the C7 ketone[64]. Several reagents have been reported to offer high diastereoselectivity in similar systems including $LiAlH(OtBu)_3$, DIBAL-H, $LiBH_4$ and Luche reduction conditions[65-68]. Under chelation with the metal, the β-hydroxyketone **39** will adopt a half-chair conformation due to the stereochemistry of the C6 alcohol (**Figure 36**). The hydride will be delivered axially on the β-face to afford the C7-α-alcohol. The β-hydroxyketone can be reduced preferentially in the presence of the ketones at C11 and C12b and the epoxide. Both the newly formed alcohols will be protected as the O-TBS ethers **40** for the next step (**Figure 34**).

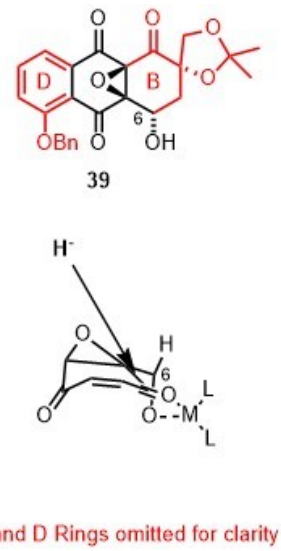

Figure 36: Chelation-assisted syn-reduction

Acetonide **40** will be deprotected using dilute acid to afford the diol and this will be treated with triphenylphosphine and DIAD to obtain the epoxide (**Figure 37**). The epoxide will be opened with iodide to give the alkyl iodide **41**. We plan to use this alkyl iodide in a Suzuki coupling reaction using the conditions reported by Fu and Zhou[69] with the vinyl boronate **42** to obtain the extended alkyl chain in compound **43**. Vinyl boronate **42** can be prepared by hydrozirconation/methylation of a 1-alkynylboronate according to literature procedures[70]. Alternatively, we can swap the coupling partners for the Suzuki reaction by using vinyl halide and an alkyltrifluoroboronate instead. Conditions for Suzuki coupling using alkyltrifluoroboronates and aryl halides have been reported by Molander *et al.*[71, 72]. The alkyltrifluoroboronate can be prepared by alkylation of the enolate by iodomethyl pinacolboronate and hydrolyzing the pinacol ester to the potassium trifluoroboronate by using KHF_2. We will prepare the vinyl iodide required for the Suzuki coupling as reported by literature procedures[73].

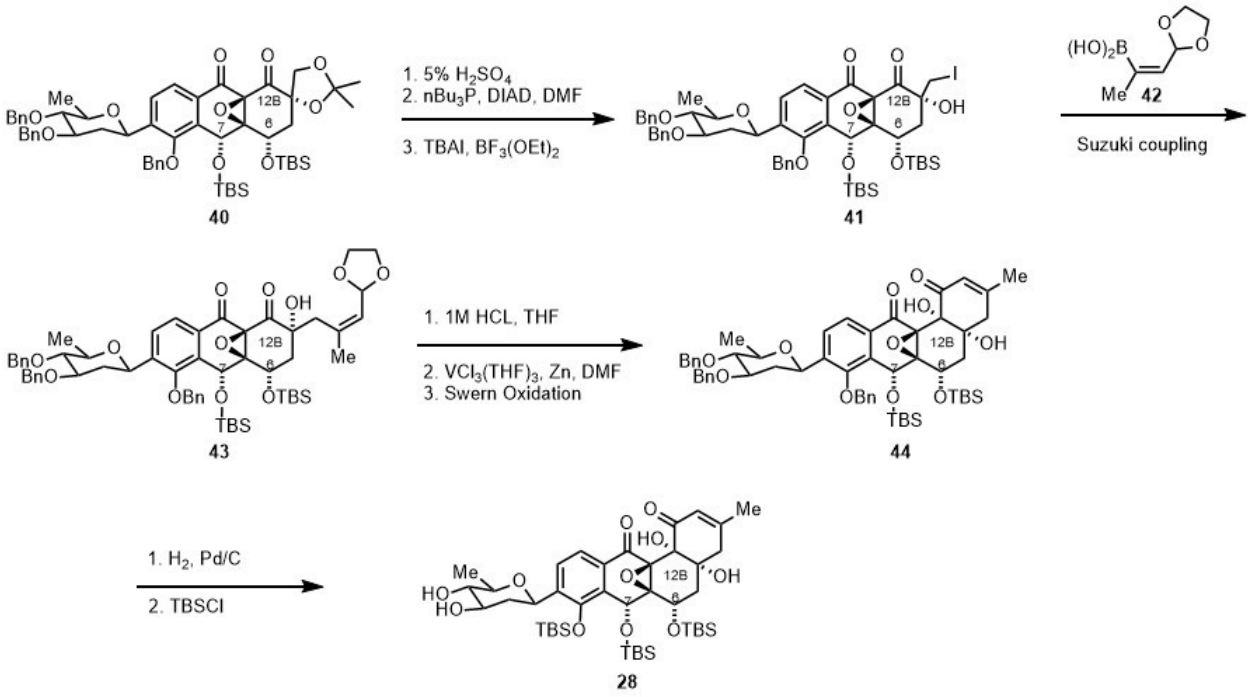

Figure 37: Synthesis of compound **28**

Following the extension of the side chain by Suzuki coupling, we will install the A ring using an intramolecular pinacol coupling similar to the one used for the preparation of aquayamycin. Hydrolysis of the ketal **43** with dilute acid will generate the aldehyde, which will be subjected to Pedersen conditions ($VCl_3(THF)_3$ and Zn in DMF) in a chelation-controlled pinacol coupling[74]. The stereochemistry of the C4a quaternary carbon will force approach of the aldehyde from the top β-face of the C12b ketone in the chelation complex with the metal (**Figure 38**). Similar to the aquayamycin total synthesis, we expect to obtain a mixture of epimers at C1. Oxidation of the C1 alcohol will result in the desired single diastereomer **44**. Synthesis of the aglycone will be completed by removal of the three benzyl protecting groups by catalytic hydrogenation and selective protection of the phenol as the O-TBS ether giving **28**, which will complete the synthesis of the aglycone.

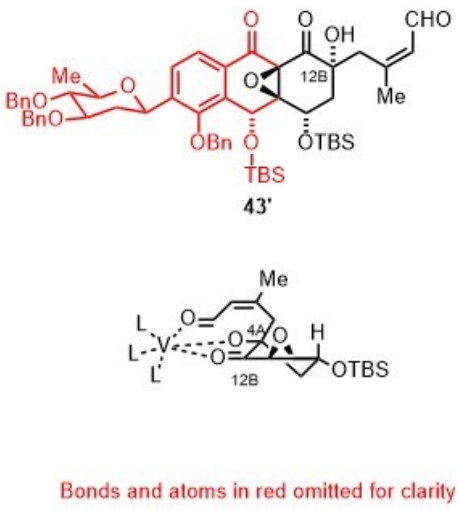

Figure 38: Pinacol coupling to form the A ring

We will make the coumarin-tetraene fragment **27** by an EDCI coupling (**Figure 39**). The amide coupling with aminocoumarins using EDCI is well precedented by the work of Blagg *et al.*[75]. The coumarin-tetraene fragment **27** will be unified with the C3' alcohol of olivose **28** by an ester bond using Yamaguchi coupling as described earlier. This will be followed by a global silyl-ether deprotection using either TBAF or HF/pyridine to give SD8.

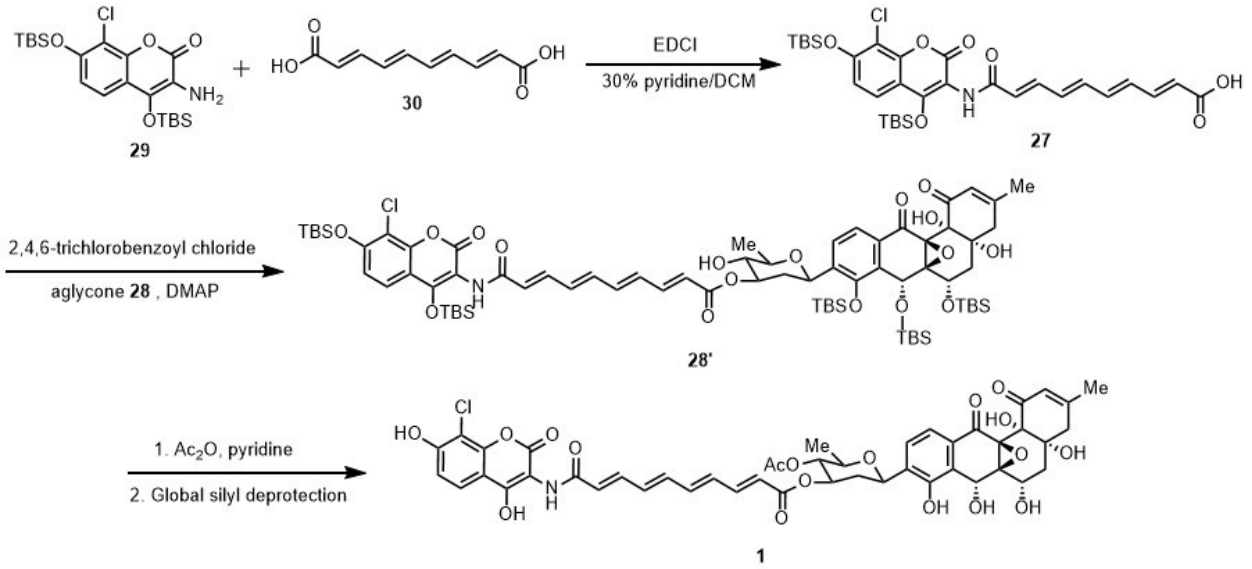

Figure 39: Final steps toward SD8

2.3: Progress towards the total synthesis of SD8

2.3.1: Synthesis of the tetraene linker

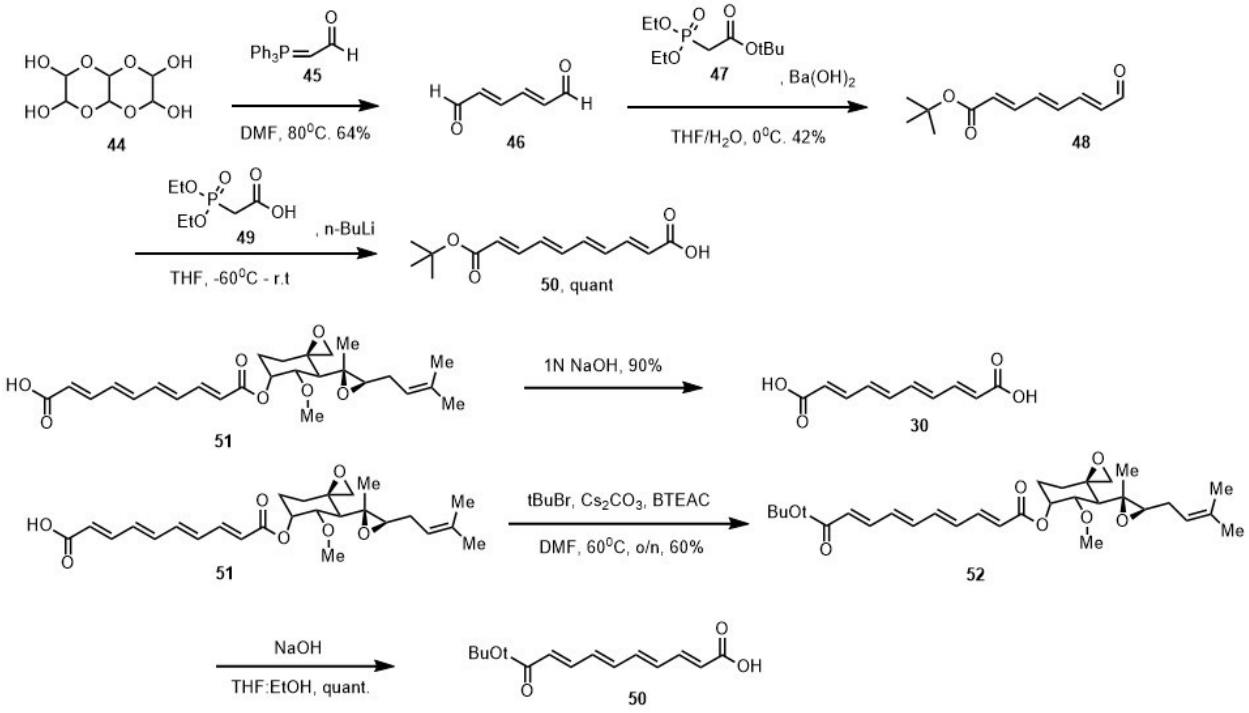

Figure 40: Synthesis of the tetraene linker

We prepared the mono-tert butyl protected tetraene linker through multiple synthetic routes (**Figure 40**). Initially, we synthesized mucodialdehyde **46** by a double Wittig[76] reaction of glyoxal trimer dihydrate **44** and the Wittig reagent (triphenylphospharanylidene) acetaldehyde **45** to give the compound **46** in 64% yield. This di-aldehyde was subjected to a mono Horner-Wardsworth-Emmons reaction with the HWE reagent *tert*-Butyl diethylphosphonoacetate **47** using barium hydroxide as the base to obtain the compound **48** in 42% yield. The yield of this reaction was unoptimized. The mono-aldehyde **48** was subjected to an HWE reaction with diethylphosphonoacetic acid

49 using n-BuLi as the base to obtain the tetraene-mono *tert*-buyl ester **50** in quantitative yield.

The tetraene di-carboxylic acid **30** is a component of the veterinary antibiotic fumagillin B **51** that is commercially available in gram quantities as a beekeeping antibiotic. We obtained the diacid **30** in 90% yield by base hydrolysis[77] of fumagillin **51** obtained after removal of excipients for the formulation by sodium bicarbonate wash.

We also prepared the mono-*tert*-butyl ester of fumagillin **52** in 60% yield using *tert*-butyl bromide and caesium carbonate as the base in DMF. The fumagillol fragment was removed using base hydrolysis to afford the compound **50** in quantitative yield.

2.3.2: Synthesis of the olivose sugar

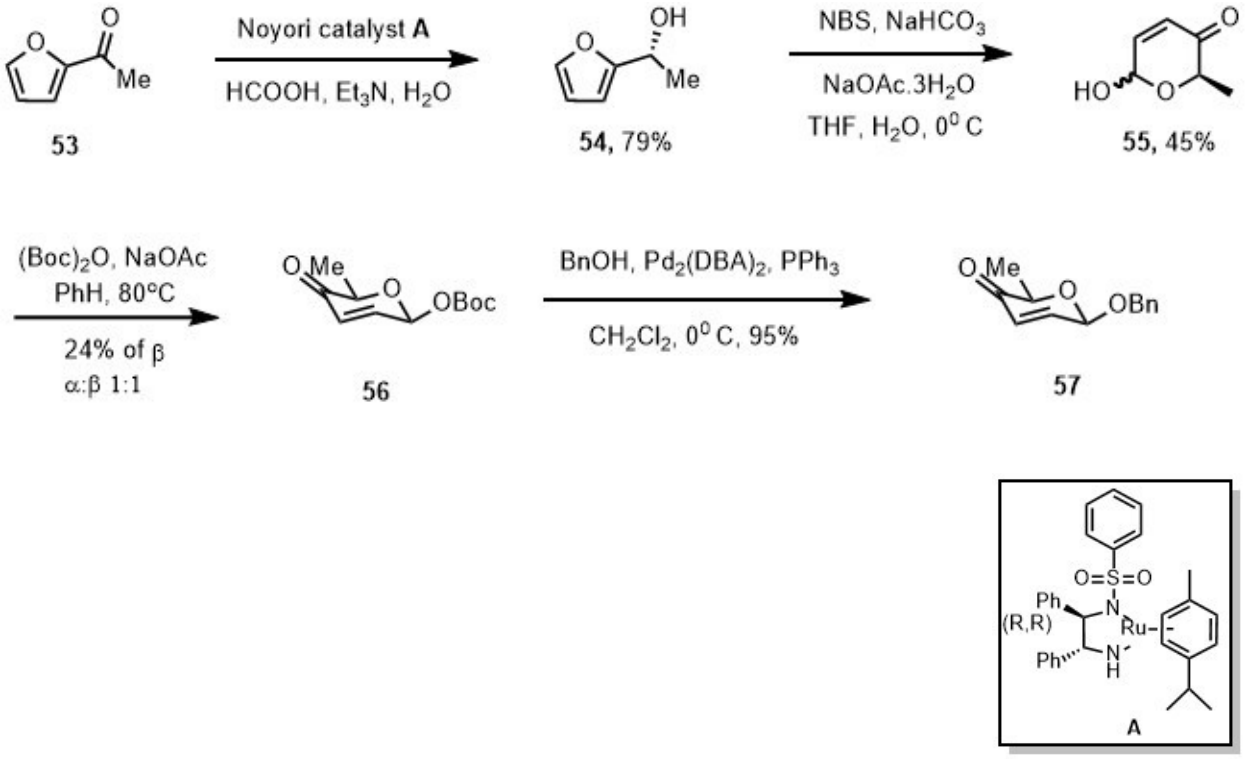

Figure 41: Synthesis of compound **57**

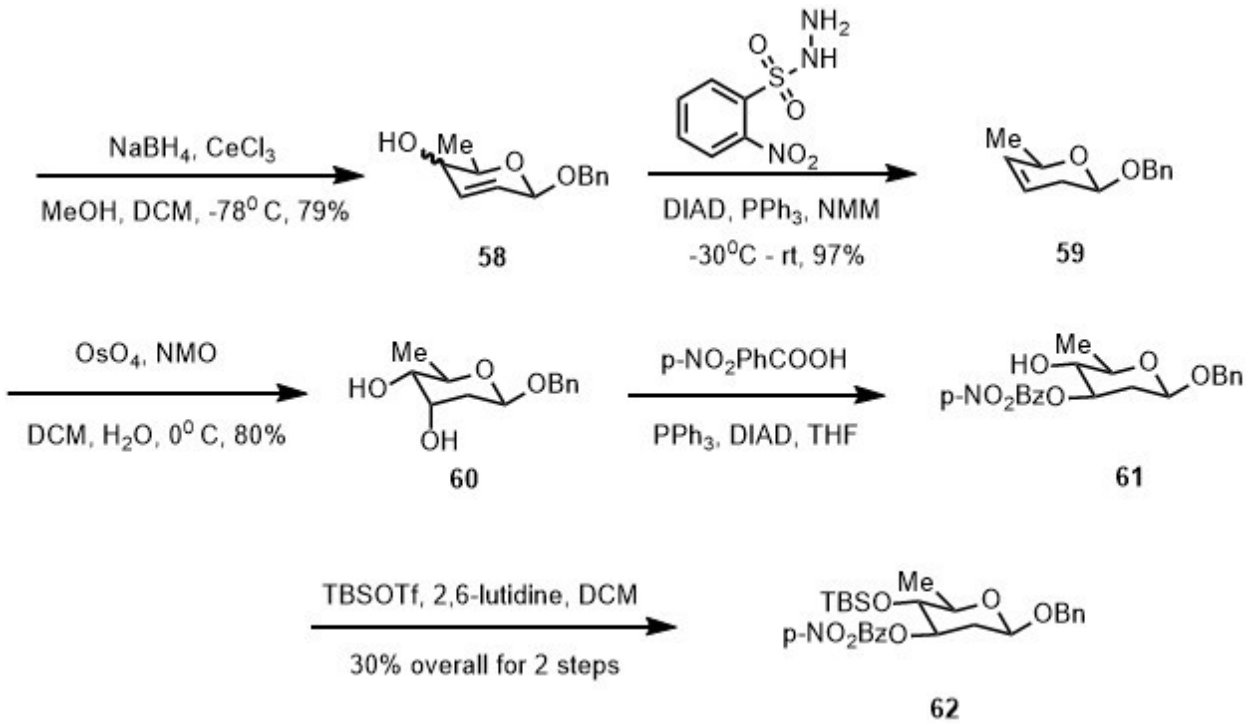

Figure 42: Synthesis of compound **62**

6-Deoxysugars such as D-olivose are commonly found in antibiotics produced by the *Streptomyces* bacteria. The classic route reported in literature towards 2-deoxysugars involve hydration of glycals under acidic conditions[78]. We chose to use the method of O'Doherty and co-workers to prepare the olivose sugar[79-81]. The first step involves a transfer hydrogenation from formic acid and triethylamine under Noyori reduction conditions using the catalyst (*R*)-Ru(η^6-mesitylene)-(*R, R*)-TsDPEN **A** of **53** to **54** (**Figure 41**). To prepare the pyran scaffold of olivose, an Achmatowicz reaction was carried out on the furan **54** to give the dihydropyranone **55** in 45% yield. We attribute this low yield in the initial two steps to the use of the commercially available ligand in preparation of **A** as compared to the recrystallized ligand used by O'Doherty, leading to unconverted starting material in the initial reduction. The separation of this unreacted material **53** was difficult leading to the reduced yield in the Achmatowicz reaction.

To separate the epimers on silica formed by the Achmatowicz reaction, the epimeric alcohol was protected as a Boc ether, and the β-epimer was purified (1:1, α:β, 24% of β, **56**). This was followed by a protecting group swap for the Boc to a benzyl using Bis(dibenzylideneacetone)palladium(0) in 95% yield to give **57**. Luche reduction on the pyranone **57** gives a mixture of the diasteromeric alcohols **58** in 79% yield (**Figure 42**). This mixture was not separated and was subjected to an allylic transposition reaction using 2-nitrobenzenesulfonyl hydrazide (NBSH) as the nucleophile, affording the olefin **59** in 97% yield. Mechanistically, this is a Mitsonobu reaction on the allylic alcohol using NBSH as the nucleophile, which forms the *N*-allylic sulfonylhydrazine derivative that at room temperature forms the allylic diazene intermediate. The diazene intermediate is unstable and results in the sigmatropic elimination of dinitrogen followed by the transposition of the olefin[82].

This olefin was dihydroxylated using OsO_4 to give the diol **60** in 80% yield. However, the stereochemistry of the C4'-OH obtained is opposite of what is desired (3S vs. 3R), hence this was inverted using a Mitsonobu reaction using para-nitrobenzoic acid to afford the compound **61**. The reaction had significant amount of impurities, which could not be removed entirely to obtain the pure product. Hence, a partially purified reaction mixture was subjected to TBSOTf and 2,6-lutidine as the base in DCM to give the 4-OTBS ether of D-olivose **62** in 30% yield (2 steps).

2.3.3: Synthesis of the coumarin

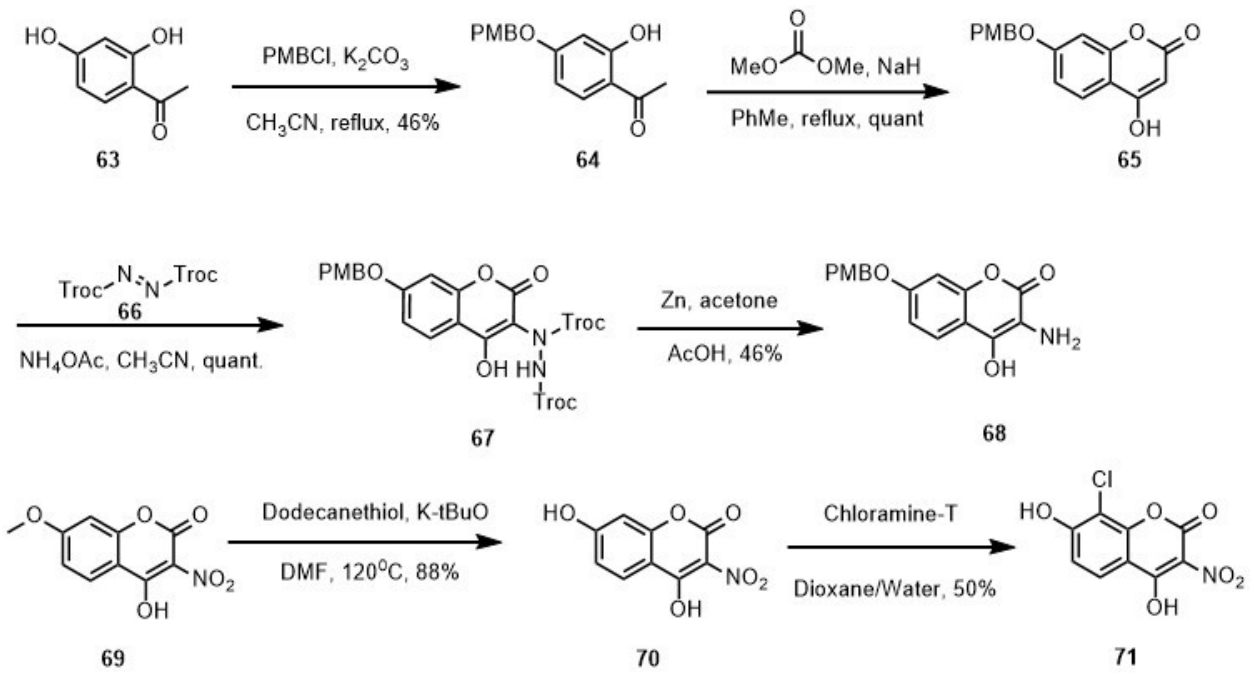

Figure 43: Synthesis of the compound **68** and **71**

The synthesis of 3-amino-8-chloro-4,7-dihydroxy-coumarin has not been reported in the literature. Generally, there are two common synthetic approaches to coumarins: Friedel-Crafts reaction of substituted phenols and cyclization of substituted 2-hydroxy-acetophenone with base and diethylcarbonate. We used the acetophenone route to synthesize 3-amino-4,7-dihydroxy-coumarin and explored a late stage chlorination approach to install the 8-chloro on the ring.

Starting from 2,4-dihydroxyacetophenone **63**, the 4-OH group was protected using para-methoxybenzyl chloride to afford the 4-PMB protected acetophenone **64** in 46% yield (**Figure 43**). This compound was cyclized into the coumarin using sodium hydride as the base in toluene and dimethyl carbonate as the electrophile to afford the coumarin **65** in quantitative yield. The most commonly reported method for introducing the nitrogen at the C3 position of the coumarin involves using concentrated nitric acid as the electrophile.

However, we decided to install the nitrogen using the electrophilic nitrogen source bis(Troc) azodicarboxylate[83] **66** to afford the compound **67** in quantitative yield. The decision to use this reagent was taken based on the high yielding electrophilic amination using this reagent and the ease in reaction workup and purification. Reduction of the hydrazide to the amine was carried out using zinc and acetone in acetic acid to afford the coumarin **68** in 46% yield. Acetone in this reaction forms the hydrazone from the hydrazide that is reduced readily by metallic zinc under these conditions[83]. We see a complete conversion of the starting material to the product by TLC and HPLC however; recovery of the polar amino alcohol **68** is difficult. Optimization of the workup conditions of this reaction will allow better recovery of the product.

We explored conditions for the late-stage installation of the chlorine on 4,7-dihydroxy-3-nitro-coumarin **70**. This compound was prepared in one step from commercially available 4-hydroxy,7-methoxy-3-nitro-coumarin **69** using dodecane thiol, KOtBu in DMF in 88% yield. Treatment of compound **70** with chloramine-T in refluxing dioxane/water affords a 1:1 mixture of the product **71** and the starting material **70** in quantitative yield. Reduction of the nitro group[84] and TBS protection will afford the desired coumarin **29**.

2.3.4: Suzuki coupling and model system

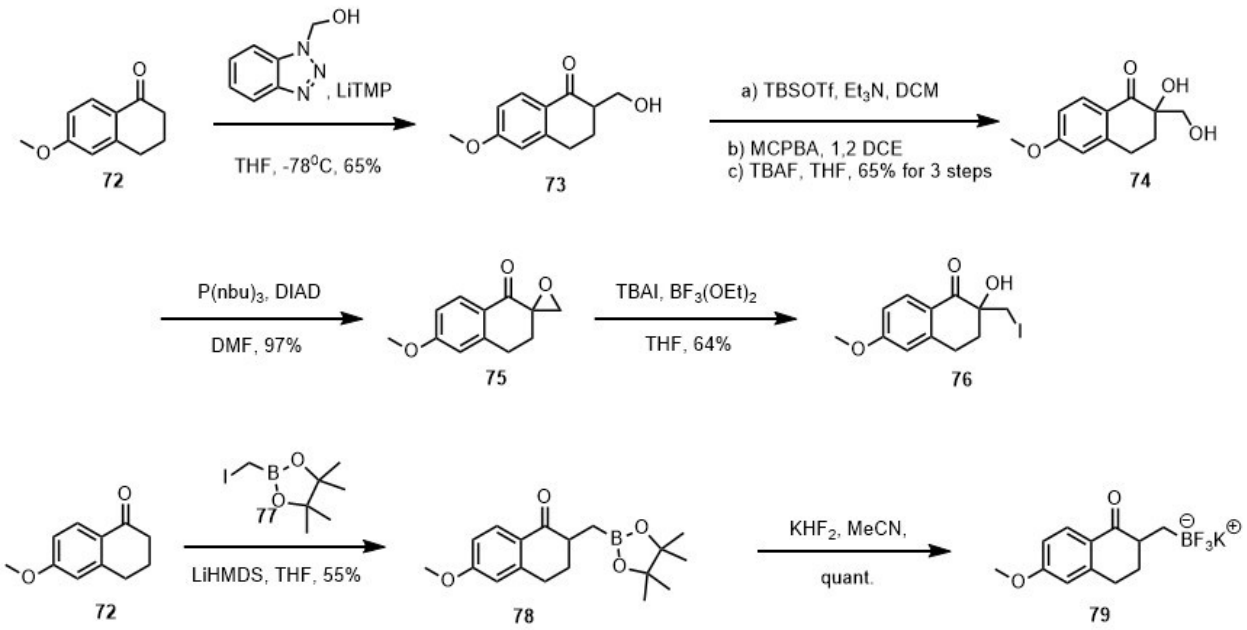

Figure 44: Synthesis of compound **76** and **79**

To prepare the A ring of the aglycone **43**, we plan to install the side chain required for formation of the A ring by Suzuki coupling of an alkyl iodide and a vinyl boronate. To develop and optimize reaction conditions for the coupling, we decided to use the model system having a tetralone scaffold. 6-methoxy tetralone **72** was hydroxymethylated at its Cα position using 1H-benzotriazole-methanol under basic conditions (LiTMP) to give the α-hydroxymethyl- derivative[85] **73** in 65% yield (**Figure 44**). This compound was hydroxylated at its alpha position under Rubottom conditions using m-CPBA as the oxidant. Briefly, the di-OTBS ether derivative was made using TBSOTf and, after reaction workup, the silanol-ether was oxidized using m-CPBA and 1,2-dichloroethane as the solvent. Use of 1,2 DCE simplifies the workup as after oxidation the 3-chlorobenzoic acid byproduct precipitates out of solution and after filtration the di-OTBS ether is obtained[86]. The compound was stirred with TBAF in THF to get racemic (±)-**74** in 65% overall yield. To prepare the alkyl iodide, compound **74** was subjected to intramolecular Mitsonobu

reaction conditions with tributylphosphine and DIAD to obtain the epoxide **75** in 97 yield. The epoxide was opened with iodine and $BF_3(OEt)_2$ as the Lewis acid[87] to obtain the iodide (±)-**76** in 64% yield.

We decided to swap the Suzuki coupling partners in case the reaction did not work with the alkyl iodide. Compound **78** was prepared by a procedure reported by Molander *et al.*. Alkylation of 6-methoxy tetralone **72** with iodomethylpinacol boronate **77** using LiHMDS as the base gave compound **78** in 55% yield. The potassium trifluoroboronate was prepared by using a saturated solution of KHF_2. After continuous Soxhlet extraction overnight using acetone, compound **79** was obtained in quantitative yield[71, 72].

2.3.5: Synthesis of the isobenzofuranone

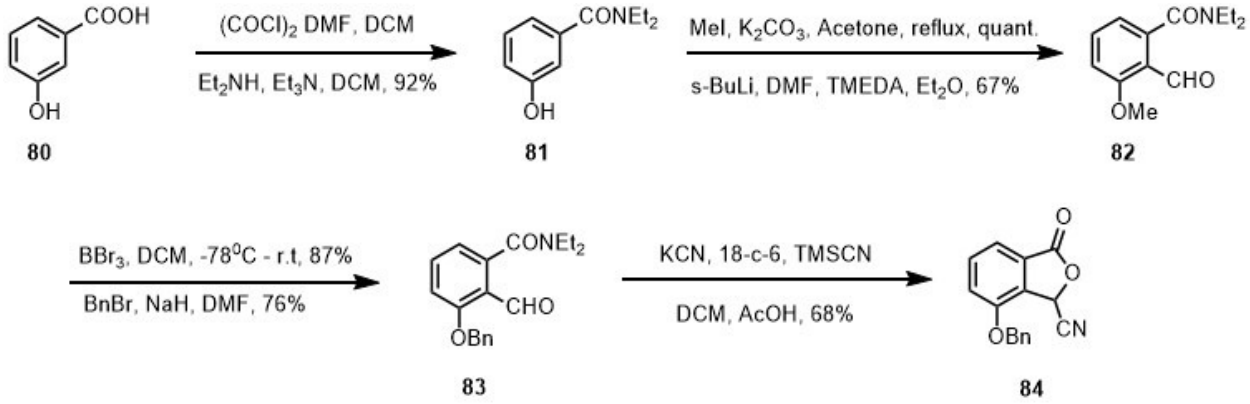

Figure 45: Synthesis of the Isobenzofuranone **84**

The Isobenzofuranone coupling partner for the Hauser reaction was prepared in 6 steps from 3-hydroxybenzoic acid **80** (**Figure 45**). Commercially available 3-hydroxybenzoic acid was converted to *N,N*-diethyl-3-methoxybenzamide **81** via the acid chloride in an overall yield of 92% for two steps. The *N,N*-diethylamide was synthesized in order to direct lithiation using *s*-BuLi at the ortho position. The lithium anion formed using *s*-BuLi

was quenched using DMF to give the compound **82** in 67% yield. This was followed by a protecting group swap from 3-*O*-methyl to 3-*O*-benzyl, initially deprotecting the methoxy group using the Lewis acid BBr_3 to give the phenol **82'** in 87% yield and alkylating the phenol with benzyl bromide, using sodium hydride as the base to give the compound **83** in 76% yield. The compound was cyclized to the furan using TMSCN and catalytic KCN and quenching with acetic acid to provide the product **84** in 68% yield.

2.3.6: Model reactions for the Olivose Sugar-Aglycone coupling (C-glycosidation)

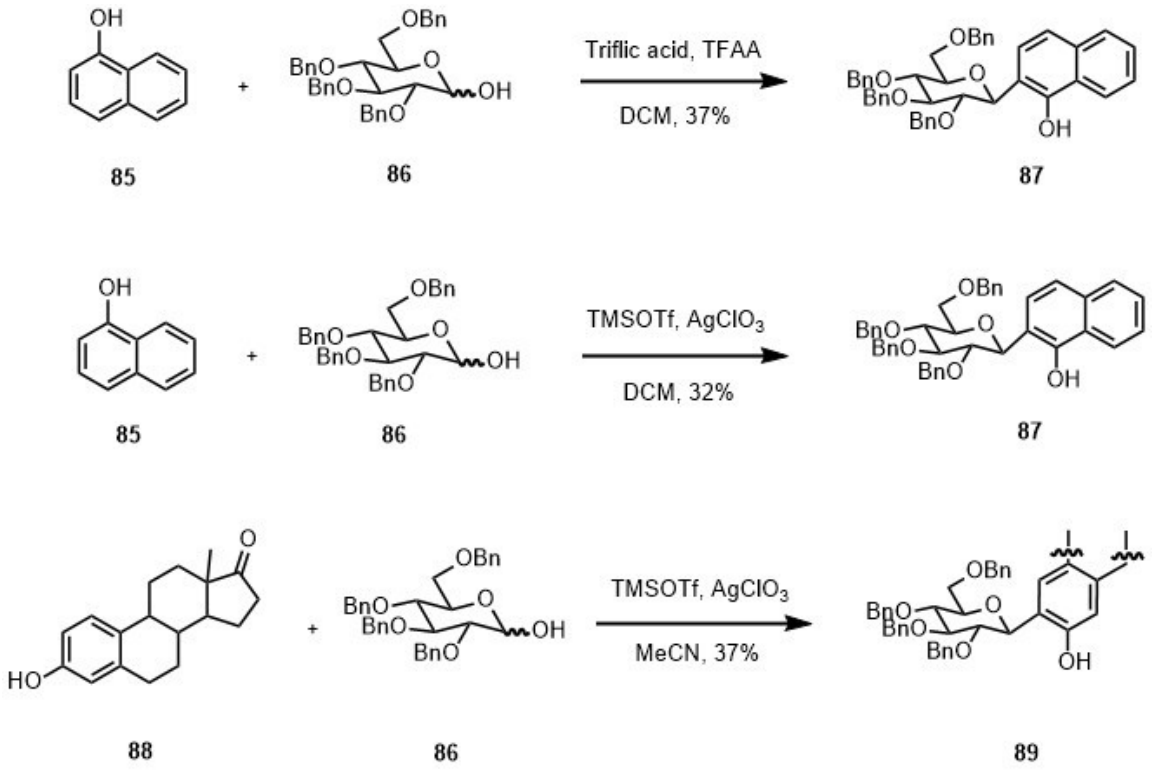

Figure 46: Model reactions for C-glycosidation

To demonstrate the feasibility of acid catalyzed C-glycosidation, we ran the reaction using two different conditions using 2,3,4,6-Tetra-*O*-benzyl-D-glucopyranose **86** as the glycosyl donor and 1-naphthol **85** and estrone **88** as the glycosyl acceptor (**Figure 46**). These

reactions were run only once and the yields were not optimized. Under these reaction conditions, first the phenolic oxygen attacks the anomeric carbon on the glycosyl donor forming an O-glycoside bond that rearranges to form the more stable C-glycoside. The first reaction between **85** and **86** involved protic acid conditions, using trifluoromethane sulfonic acid as the protic acid in DCM giving the C-glycoside **87** in 37% yield[51]. The second set of conditions involved the Lewis acid TMSOTf and silver perchlorate[50] as the promoter with 2,3,4,6-Tetra-*O*-benzyl-D-glucopyranose **86** as the glycosyl donor and 1-naphthol **85** and estrone **88** as the glycosyl acceptor. 1-Naphthol glycoside **87** was obtained in 32% yield and estrone glycoside **89** was obtained in 37% yield.

2.3.7: Model reactions for Coumarin-Tetraene and Tetraene-Olivose Sugar coupling

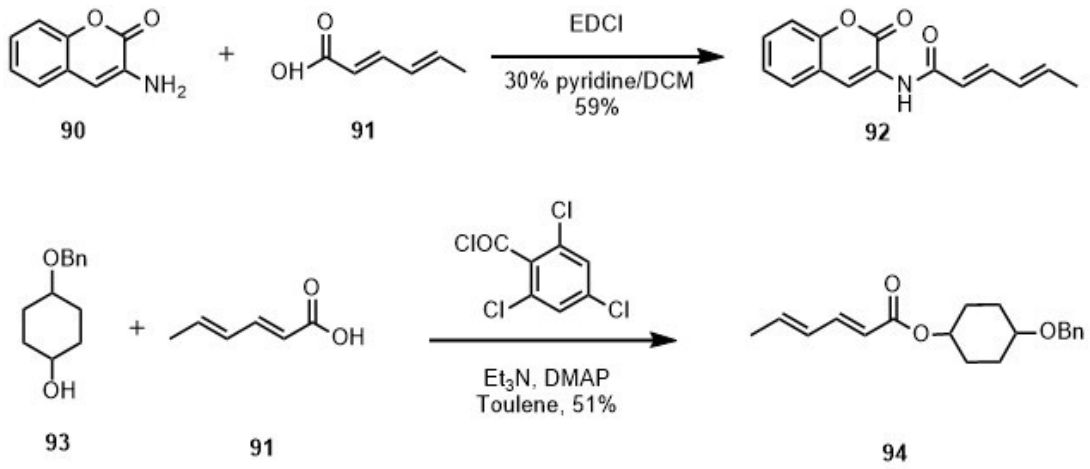

Figure 47: Model reactions for EDCI amidation and Yamaguchi reactions

To demonstrate the feasibility of the planned coupling of tetraene with the coumarin (EDCI amidation)[75] and with the Olivose sugar (Yamaguchi esterification), we have performed the reaction on a model system with the commercially available coumarin **90**, alcohol **93** and sorbic acid **91** (**Figure 47**).

The amidation was done on commercially available 3-aminocoumarin **90** and sorbic acid **91** using the conditions reported by Blagg[75] and coworkers to give the amide **92** in 59% yield. Once the target aminocoumarin **29** is available, this reaction condition can be used to synthesize the aminocoumarin-tetraene amide **27**.

To demonstrate that the Yamaguchi esterification[48, 49] will work on a similar substrate, we used the alcohol **93** as a surrogate for the sugar Olivose. Yamaguchi coupling proceeds through a mixed-anhydride intermediate. 2,4,6-trichlorobenzoyl chloride forms the mixed anhydride with sorbic acid **91** in the presence of triethylamine. This intermediate mixed-anhydride is treated with the alcohol and DMAP to form the ester. Compound **94** was isolated in 51% yield.

2.4: Conclusion

The structure of SD8 is highly modular, consisting of four distinct fragments – aminocoumarin, tetraene, olivose and the angucyclinone. We have proposed a synthetic route to the highly substituted and complex angucyclinone fragment in SD8. We also have identified and worked out synthetic routes to the aminocoumarin, tetraene and the olivose sugar. Although none of these reactions were optimized, we have prepared these fragments in a minimal number of steps and obtained modest overall synthetic yields (**Table 4**). We have identified and worked out various fragment-linking chemistries on model substrates like EDCI amidation for the Coumarin-tetraene fragment and Yamaguchi esterification for the Tetraene-Olivose fragment. We have also prepared the substrates for the Suzuki reaction for forging the A ring on model systems. Completion of synthetic work towards the angucyclinone fragment will help identify and synthesize

various analogues of SD8 that potentially will have better activity towards DNA gyrase and other fluoroquinolone resistant DNA gyrase mutants.

Table 4: Fragments of SD8 prepared and overall yield

Fragment synthesized	Total Synthetic Steps	Overall yield (%)
8-chloro-4,7-dihydroxy-3-nitrocoumarin	2	69
(2*E*,4*E*,6*E*,8*E*)-10-(*tert*-butoxy)-10-oxadeca-2,4,6,8-tetraenoic acid	2	80
D-Olivose	9	59
7-(benzyloxy)-3-oxo-1,33-dihydroisobenzofuran-1-carbonitrile (Isobenzofuranone)	6	82

CHAPTER 3: DESIGN AND SYNTHESIS OF A SUBSTRATE-COMPETITIVE COVALENT INHIBITOR FOR PROTEIN KINASE B (AKT)

3.1: Introduction

3.1.1: AGC Kinases

Phosphorylation is an important reversible covalent modification that regulates the function of proteins in cells. Enzymes that carry out phosphorylation in cells are called protein kinases. They transfer a phosphate group from ATP to their substrates by mostly attaching them to Serine (76-90%), Threonine (10-20%) or Tyrosine (0.05-4%) residues. Other residues found to be less frequently phosphorylated are histidine, aspartic acid and glutamic acid[88]. Protein kinases are classified into 8 major groups: AGC (PK**A**, PK**G**, PK**C**), CAMK (**Ca**-Cal**m**odulin dependent protein **k**inases), CMGC (**C**DK, **M**APK, **G**SK3, **C**LK), TK (**T**yrosine **K**inases), TKL (**T**yrosine **K**inase **L**ike **K**inases), STE (homologs of yeast kinases), RGC (**R**eceptor **G**uanylate **C**ylases) and CK1 (**C**asein **K**inase **1**)[89].

AGC kinases belong to the subgroup of Ser/Thr protein kinases that by sequence alignments were found to have a similar catalytic kinase domain as cAMP-dependant protein kinase 1. The AGC family has 60 out of the 518 protein kinases identified. Structurally, most of them consist of the kinase core and other functional domains that mediate membrane or substrate interaction[90].

A common structural feature seen in AGC kinases is a bilobal kinase fold that consists of an amino-terminal small lobe (N-lobe) and a carboxy-terminal large lobe (C-lobe) sandwiching one molecule of ATP. Activation in many AGC kinases requires phosphorylation of two highly conserved regulatory motifs: the activation segment (T-loop) and the hydrophobic motif. The activation segment is found in the C-lobe, beside the ATP binding site, and is connected to the N-lobe by an αC helix. Phosphorylation in this activation segment leads to conformational changes in the αC helix that are required for the catalytic activity of the enzyme. The αC helix also forms a part of the hydrophobic pocket in the N-lobe and is necessary for regulatory interactions of the N-lobe with the hydrophobic motif. The hydrophobic motif extends from the tail of the C-lobe, wraps around the N-lobe, and inserts into the hydrophobic motif pocket, thus stabilizing the active conformation of the αC helix. The turn motif is located at the C-terminal end, before the hydrophobic motif, and consists of a phosphorylation site required for full kinase activity. A groove near the active site of the kinase is involved in substrate binding and the sequence specificity is determined by residues forming this site. The structures of activated AGC kinases are quite similar, but those of inactive AGC kinases have revealed a range of conformations indicating that the domains are highly flexible and disordered. Phosphorylation locks the kinase in an ordered conformation required for its activity (**Figure 48**)[90].

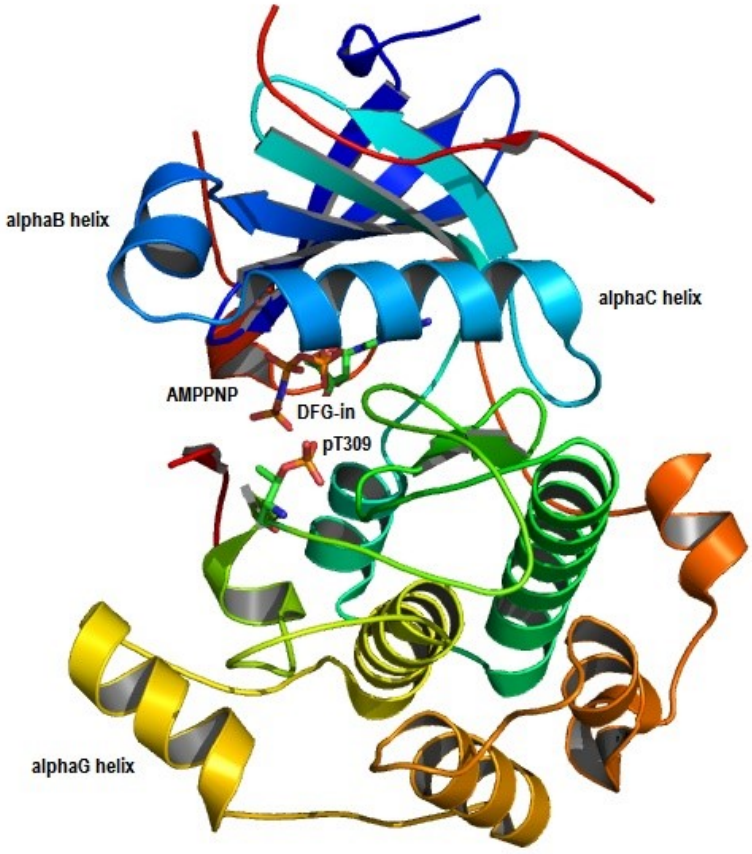

Figure 48: AKT2 in its active conformation (PDB ID:1O6K). pThr309 and the ATP analog are shown in stick representation. DFG-in denotes the active conformation of the DFG motif that is ordered in the activated kinase.

3.1.2: Protein Kinase B (AKT)

AKT serine/threonine kinase (protein kinase B) is a member of the AGC kinase family and is an important signaling molecule in eukaryotic cells. The *AKT* gene is the cellular homolog of the oncogene *v-AKT* and was first identified in 1977 by Staal *et al.* and named *c-AKT*[91]. In 1991, the AKT kinases were cloned and identified by three independent research groups[92-94]. There are 3 isoforms of AKT: AKT1 (PKBα), AKT2 (PKBβ) and AKT3 (PKBγ), all encoded by different genes. AKT1 is expressed ubiquitously throughout

all tissues, AKT2 is expressed in insulin sensitive tissues that include the liver, skeletal muscle and adipose tissue and AKT3 is mostly expressed in the brain and testes[95].

The three isoforms of AKT share similar structures: a N-terminal regulatory domain that includes a pleckstrin homology (PH) domain, a hinge region that connects the PH domain to the kinase domain and a C-terminal region required for kinase activity. The catalytic domain of AKT is quite similar to other PKA and PKC members (**Table 5**).

Table 5: Sequence Similarity (in %) between AKT isoforms[96]

PAIR	PH domain	LINK region	Catalytic domain	C-terminal extension
AKT1/AKT2	80%	46%	90%	66%
AKT1/AKT3	84%	40%	88%	76%
AKT2/AKT3	76%	17%	87%	70%

3.1.3: Regulation of AKT

3.1.3.1: Regulation by phosphorylation

One of the ways AKT can be activated is by the receptor PDGFR (Platelet Derived Growth Factor Receptor β) through the enzyme PI3 kinase[97]. The tyrosine kinase receptor PDGFR undergoes dimerization on activation and leads to auto-phosphorylation of its tyrosine residues: Tyr740 and Tyr751. This recruits PI3 kinase to the plasma membrane through the Src homology 2 (SH2) domains in their regulatory subunit and the phospho-tyrosine residues on the receptor. PI3 kinase then generates D3 phosphorylated lipids by the phosphorylation of phosphoinositides at the plasma membrane. This forms PIP2 and

PIP3. PIP3 binds to AKT at its PH domain, which results in the translocation of AKT to the plasma membrane. In addition to this PIP3 binding, phosphorylation of Thr308 in the T-loop and Ser473 within the hydrophobic motif are required to fully activate the enzyme. AKT is maintained in its inactive state by the interaction of the PH domain with the kinase domain. Once phosphoinositides bind to the PH domain, the conformation is changed and this allows subsequent phosphorylation events to occur[90].

PDK1, a serine/threonine kinase, also contains a PH domain and a kinase domain[97]. The PH domain binds to PIP3 at a higher affinity than that of AKT. Under physiological conditions, PDK1 is present as constitutively active at the plasma membrane of non-stimulated cells. Once the concentration of PIP3 at the cell membrane increases by the stimulation of PI3K, AKT is shuttled from the cytoplasm to the plasma membrane. Following binding of the PH domain of AKT to PIP3, PDK1 phosphorylates Thr308 at the kinase domain in AKT. The enzyme that phosphorylates Ser473 within the hydrophobic motif had been elusive for a long time; in 2005 this was identified as the mTOR complex-2 (mTORC2). mTORC2[98] directly phosphorylates Ser473 *in vivo* and also enhances the phosphorylation of AKT by PDK1. Other kinases such as DNA-PK and ILK1, are also capable of phosphorylating Ser473, but this may happen in a cell or context-dependent manner. The mTORC2 complex consists of the kinase mTOR bound to: the mTOR-interacting proteins rapamycin insensitive companion of TOR (RICTOR), SAPK-interacting protein (SIN1), mammalian lethal with SEC13 protein 8 (mLST8), protein observed with RICTOR1 (PROTOR1) and PROTOR2. In addition to this AKT is constitutively phosphorylated at Thr450 in its turn motif, which stabilizes it and protects

the hydrophobic motif from dephosphorylation. Phosphorylation at the turn motif happens soon after AKT is synthesized, but it is unclear which kinase participates in it.

Other miscellaneous ways in which AKT gets activated though PI3 kinase include Integrin-mediated[99] and B cell antigen receptor (BCR)[100] mediated stimulation. When cells get attached to fibronectin receptors in the extracellular matrix through integrin receptors on the cell surface Focal Adhesion Kinase (FAK), a tyrosine kinase in the cytoplasm gets activated and results in the phosphorylation of PI3 kinase. This activates PI3 kinase and activates AKT signaling through phosphoinositides. BCRs also play a role in activation of AKT though PI3 kinase.

AKT must be phosphorylated on both the hydrophobic motif (Ser473) and at the activation loop (Thr308) to be fully active. Phosphorylation of only the hydrophobic motif or the activation loop results in an enzyme with just 10% of kinase activity compared to the doubly phosphorylated enzyme. Phosphorylation of the activation loop orders the catalytic domain and forms the substrate and ATP binding site[101].

AKT is mainly negatively regulated by dephosphorylation aided by the activity of various phosphatases. Protein phosphatase 2A (PP2A)[102] is a serine/threonine heterotrimeric phosphatase that is present in the cytosol. It dephosphorylates Thr308 and returns AKT to its inactive conformation in the cytosol. Dephosphorylation of Ser473 is carried out by the PH domain leucine-rich repeat protein phosphatase (PHLPP), which belongs to a class of protein phosphatases 2C (PP2C) family[103].

PTEN (Phosphatase and Tensin Homologue deleted on chromosome 10) is a tumor suppressor gene, also referred to as MMAC1 (Mutated in Multiple Advanced Cancer 1)

and its mutation leading to loss of function has been implicated in many forms of cancers such as glioblastomas, prostate cancer and melanomas. The PTEN protein consists of a tensin-like domain and a catalytic domain similar to that of protein tyrosine phosphatases. PTEN has been found to have lipid phosphatase activity that preferentially dephosphorylates phosphoinositide substrates. It dephosphorylates PI(3,4,5)P3 to PI(4,5)P2; hence, PTEN negatively regulates levels of PIP3 in cells and regulates the AKT pathway. In addition to dephosphorylation of phosphoinositides, several reports demonstrate dephosphorylation of FAK by PTEN, leading to inhibition of cell migration and focal adhesion. PTEN only inhibits basal PKB activity, not affecting the pathway when stimulated by growth factors (**Figure 49**)[104].

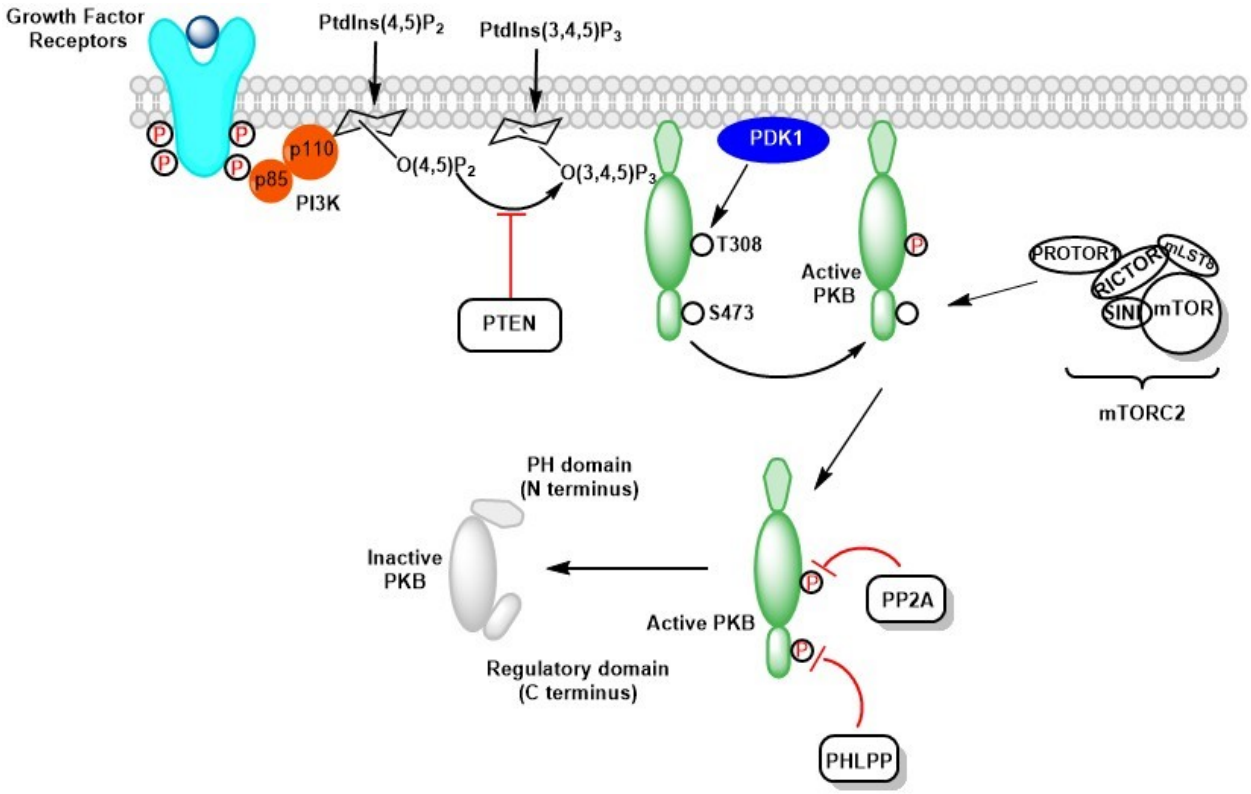

Figure 49: Model of AKT regulation

The SHIP (SH (Src homology)-2 containing Inositol 5' Phosphatase) phosphatases are lipid phosphatases with specific 5' phosphatase activity[105, 106]. They break down PI(3,4,5)P3 to PI(3,4)P2, removing phosphates form the 5-position rather than the 3-position. SHIP1 is present in haematopoietic cells and SHIP2 in non-haematopoietic cells. SHIP inhibits the AKT pathway when stimulated by growth factors. Activated PI3-kinase phosphorylates SHIP and it then translocates to the plasma membrane, leading to its phosphatase activity. Although both PTEN and SHIP regulate the level of PIP3 in cells, PTEN has the primary responsibility of controlling the mitogenic ability of these phosphoinositides because it dephosphorylates at the 3' position and this has been demonstrated in knockout mice[107, 108]. Phosphorylation at the 3' position is a necessity for binding to the PH domain of AKT.

3.1.3.2: Redox Regulation

AKT displays an intramolecular redox sensitive disulfide bond between Cys296 and Cys310 in its activation loop. Formation of this disulfide bond inactivates the enzyme that has been doubly phosphorylated at Thr308 and Ser473, suggesting that AKT is a redox-regulated protein. A crystal structure of inactive AKT2 with this disulfide bond has been reported. Formation of this disulfide bond changes the conformation of the activation loop and sterically hinders both substrate and ATP binding. It also promotes the dephosphorylation of Thr308 by PP2A. Under conditions of oxidative stress, AKT forms the disulfide bond and targets the protein for inactivation by PP2A. Also this intramolecular disulfide bond can be reduced by glutaredoxin *in vitro,* restoring AKT to its active, functional conformation[109].

3.1.4: Downstream substrates of AKT

The minimal substrate sequence for AKT has been found to be R-X-R-X-X-S/T-B, where X represents any amino acid and B represents bulky hydrophobic residues[110]. A representation of the most common downstream substrates is shown in **Figure 50**. These substrates are phosphorylated by AKT leading to either their activation or inhibition. Regulation of these substrates by AKT-mediated phosphorylation leads to the control of various cellular processes[111].

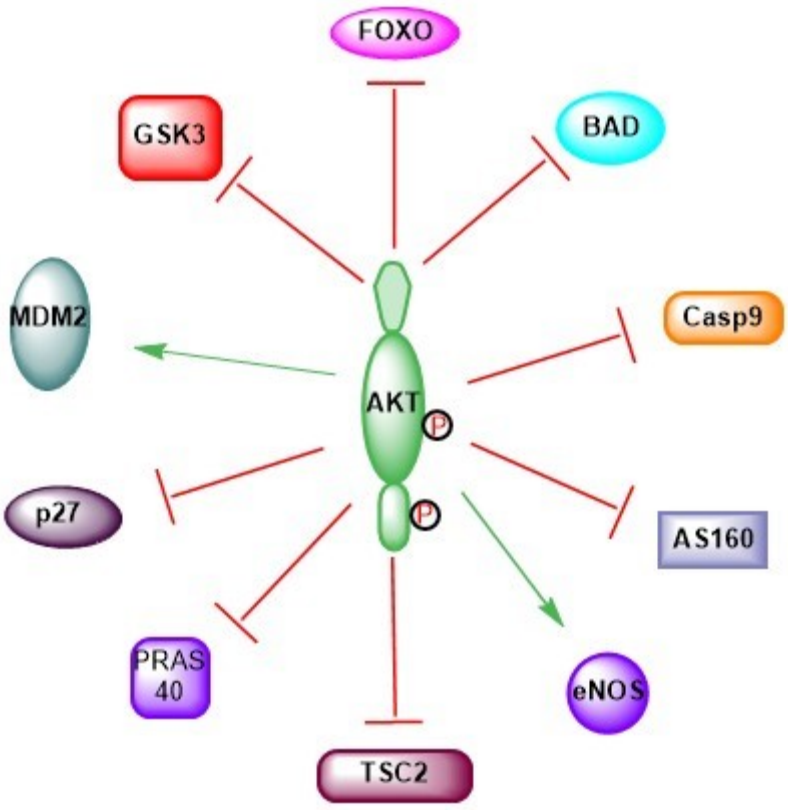

Figure 50: Substrates of AKT in the cell. AKT mediated phosphorylation of these substrates lead to their activation (green arrow) or inhibition (red blocking arrow)

3.1.4.1: Cell survival

AKT enhances cell survival by inhibiting the function of various proteins that participate in apoptosis: e.g. AKT phosphorylates the pro-apoptotic BH3-only protein BAD[112], which is

a member of the Bcl-2 gene family and inhibits it. When BAD is phosphorylated by AKT, it forms a homodimer and releases Bcl-2 to inhibit cytochrome *c*-mediated apoptosis. AKT also phosphorylates the transcription factors FOXO[113] and p53[114]. Phosphorylation of FOXO by AKT results in its exclusion from the nucleus thereby prevents transcription of its target genes that mediate apoptosis, cell-cycle arrest and metabolic processes. AKT promotes cell survival by phosphorylating MDM2[115], an E3 ubiquitin ligase that is responsible for degradation of p53, resulting in its translocation into the nucleus. Two important transcriptional targets of p53 are the BH3-only proteins Puma and Noxa that are important in p53 mediated apoptosis. AKT also phosphorylates GSK3, inhibiting the enzyme. An important target for GSK3 is the Bcl-2 family member MCL-1, which is found to enhance cell survival. Human pro-caspase-9 has been found to be phosphorylated by AKT and this correlates with the decrease in protease activity of caspase-9 *in vitro*[116].

3.1.4.2: Cell Growth

AKT plays a significant role in promoting cell growth (i.e. increase in cell mass) through activation of mTOR complex 1 (mTORC1 or the mTOR-raptor complex)[117]. This complex is regulated by both nutrients and growth factor signaling. AKT-mediated phosphorylation inhibits TSC2 (tuberous sclerosis complex 2) function and TSC2 is a negative regulator of mTORC1 signaling. This allows RHEb-GTP to activate mTORC1 signaling, which initiates translation and ribosome biogenesis.

The AKT substrate PRAS40[118] has also been found to be involved in mTORC1 regulation. PRAS40 associates with mTORC1 and negatively regulates mTORC1 signaling. Phosphorylation of PRAS40 by AKT results in its dissociation from mTORC1.

3.1.4.3: Cell Proliferation

Phosphorylation of p27 cyclin-dependent kinase inhibitor by AKT leads to its cytosolic sequestration and thus prevents its localization to the nucleus[119]. This negates its cell-cycle inhibitory effects. AKT also phosphorylates the cyclin dependent kinase p21, thereby inhibiting it[120].

GSK3 phosphorylates the G1 cyclins cyclin D and cyclin E and the transcription factors *c-jun* and *c-myc,* thus marking them for proteosomal degradation. These proteins play a critical role in the G1-to S- phase cell-cycle transition, and their enhanced stability by the inhibition of GSK3 by AKT increases the rate of cell proliferation. mTORC1 is a critical regulator of cell proliferation and the phosphorylation of TSC2 and PRAS40 by AKT regulates cell proliferation.

3.1.4.4: Angiogenesis

AKT signaling plays an important role in angiogenesis in both endothelial cells and tumor cells. In endothelial cells the pathway is activated by vascular endothelial growth factor (VEGF)[121]. The phosphorylation of the above-mentioned targets contributes to endothelial cell survival, growth and proliferation. In addition to this, AKT phosphorylates endothelial nitric oxide (NO) synthase (eNOS). The activated eNOS releases nitric oxide and this results in stimulation of vasodilation, vascular remodeling and angiogenesis[122].

Also through mTORC1 dependent translation, AKT leads to the increased production of hypoxia inducible factor α (HIF1α and HIF2α)[123]. This leads to expression and secretion of VEGF and other angiogenic factors[124]. Also, AKT1 in endothelial cells is required for proper endothelial cell migration.

3.1.4.5: Cellular Metabolism

AKT signaling regulates nutrient uptake and metabolism by its action on a variety of downstream targets. AKT acutely stimulates glucose uptake in response to insulin by associating with glucose transporter 4 (Glut4)-containing vesicles on insulin stimulation of adipocytes, and this leads to Glut4 translocation to the plasma membrane[125]. The protein Rab-GAP AS160[126] also known as TBC1 domain family member 4 (TBC1D4) is an important target that is phosphorylated by AKT in response to insulin. Phosphorylation of AS160 inhibits its GAP activity, allowing Glut4 vesicle translocation. Glut1 is the main glucose transporter in most cell types and AKT mediated activation of the mTORC1 pathway leads to increased transcription of the Glut1 gene, through HIFα-mediated transcription.

AKT activation also alters glucose and lipid metabolism in cells. It stimulates the association of hexokinase isoforms with the mitochondria where they more readily phosphorylate glucose to glucose-6-phosphate. Inhibition of GSK3 by AKT activates glycogen synthase leading to increased glycogen synthesis. AKT activation also increases the rate of glycolysis due to its ability to promote expression of glycolytic enzymes through HIFα. FOXO1 promotes glucose production in hepatocytes and regulates the differentiation of cells involved in metabolic control. AKT-mediated inhibition of FOXO1 also contributes to glucose homeostasis[127].

GSK3 promotes the degradation of sterol regulatory element-binding proteins (SREBPs) that are transcription factors, which turn on the genes involved in cholesterol and fatty acid biosynthesis. AKT-mediated inhibition of GSK3 increases SREBP stability and increases lipid production[128].

3.1.5: Rationale for inhibiting AKT

The hyperactivation of AKT is commonly seen in many cancers and through multiple cellular mechanisms results in tumor cell survival and enhanced resistance to apoptosis. The most frequent mechanism by which AKT is hyperactivated involves loss or downregulation of the PTEN tumor suppressor[104, 107, 108, 129]. Various reasons for targeting AKT for anti-cancer therapeutics are as follows;

1. Expression of PTEN in Jurkat T cells inhibited AKT activation and increased apoptosis[130]. Introduction of *wt*-PTEN into tumor cell lines (glioblastoma, renal cell carcinoma, breast and prostate cell) that are mutant for PTEN resulted in either cell cycle arrest or apoptosis[131, 132]. Expression of AKT protected cells from apoptosis mediated by PTEN[130].
2. Antisense AKT2 RNA expression in PANC-1 cells reduced their tumorigenicity in nude mice[133].
3. Expressing a kinase-dead (KD) AKT mutant in tumor cells expressing activated AKT induced apoptosis. This did not affect normal cells or tumor cells with low levels of activated AKT. On a similar note, expression of PTEN induced apoptosis in several tumor cells that lack PTEN expression, but not in cells having *wt*-PTEN or normal cells. These results suggest that inhibition of AKT signaling would not be toxic to normal cells[134].
4. In neural cells, expression of constitutively-active AKT enhances IGF-1-mediated survival, but expression of a dominant-negative allele of AKT increased apoptosis[135].

5. Introduction of anti-AKT-1 single chain antibodies into tumor cells resulted in reduced phosphorylation of GSK3α/β, leading to apoptosis in three cell lines with constitutive AKT activity, and inhibited tumor growth in a transgenic mouse model[136].
6. A peptide that binds to AKT, "AKT-in", inhibited cellular proliferation and anti-apoptosis *in vitro* and also tumor growth *in vivo*[137].
7. Reintroduction of a phosphatase PHLPP (PH domain/leucine-rich repeat protein phosphatase) that directly dephosphorylates AKT into a glioblastoma cell line caused suppression of cell growth[138].
8. Lung and breast cancer cell lines displayed inhibition of AKT signaling on treatment with the PI-3 kinase inhibitors Wortmannin and LY 294002[139, 140].
9. Studies indicate that blocking AKT activation is the key reason for the therapeutic efficacy seen with the drugs Gleevec[141], Trastuzumab[142], Gefitinib[104] and Tarceva.

Frequent alterations seen with the AKT pathway in human cancer include the activation of growth factor receptors (GFRs) by ligand stimulation, or by overexpression/mutation of the receptor, leading to upregulation of AKT signaling. Activation of oncoproteins in the pathway like AKT itself, RAS, PI3-K, EIF4E by overexpression or activating mutations are seen in many cancers. Loss or inactivation of tumor suppressors such as NF1, VHL, PTEN, TSC2/1, LKB1 also contribute to deregulation of the pathway and subsequent tumor formation. Multiple human cancers that include carcinomas, glioblastomas and various hematological malignancies all display aberrant AKT activation[97, 129, 143, 144] (**Table 6**)

Table 6: AKT activation in human cancers[129]

Tumor type	% Tumors with active AKT
Glioma	~55
Thyroid carcinoma	80-100
Breast carcinoma	20-55
Small-cell lung carcinoma	~60
NSCLC	30-75
Gastric carcinoma	~80
Gastrointestinal stromal tumors	~30
Pancreatic carcinoma	30-70
Bile duct carcinoma	~85
Ovarian carcinoma	40-70
Endometrial carcinoma	>35
Prostate carcinoma	45-55
Renal cell carcinoma	~40
Anaplastic large-cell lymphoma	100
Acute myeloid leukemia	~70
Multiple myeloma	~90
Malignant mesothelioma	~65
Malignant melanoma	43-67

3.1.6: Inhibitors of AKT

Based on the strong rationale for targeting AKT, development of inhibitors for AKT is an active field of research in both the pharmaceutical industry and academia. Currently, there are multiple compounds that inhibit AKT in clinical trials, with two of them in phase-2 studies (MK2206 and GSK2141795). This underscores the importance of developing inhibitors for targeting AKT[145].

AKT has multiple binding pockets where binding of inhibitors would block its downstream effects. One of the most studied pockets is the PI(3,4,5)P_3 pocket on the PH domain. The PH domain binds to PI(3,4,5)P_3 and PI(3,4)P_2. The interactions are mostly charge-driven through the D3 and D4 phosphates, with lysines and arginines in the pocket. Compounds that block the binding of phosphoinsositides with the PH domain have been shown to inhibit the growth of transformed cells. Their mode of inhibition will prevent AKT translocation to the plasma membrane and subsequent activation, but compounds in this class have problems with solubility, pharmacokinetics and potency and remain largely as probe compounds to study kinase activity. In the kinase domain, the most studied is the ATP binding pocket. However, given the high homology of the ATP pocket with other kinases, it is quite difficult to design compounds that bind selectively to the ATP pocket in AKT.

3.1.6.1: Phosphatidylinosotol Analogues

The lead compound in this class was DPI (**Figure 51**), which has an IC_{50} of 35 μM in the HT-29 colon cancer cells[146]. This compound is an analogue of phosphatidyl-myo-inositol, while members of the class lack the 3-position hydroxyl group, which was removed so that it cannot be phosphorylated by PI-3 Kinase. Further analogues of this compound led

to removal of the two labile ester groups to ether linkages resulting in DPIEL that has an IC_{50} of 2.1 μM in the HT-29 colon cancer cell line[147].

The analog PIA5 was found to have an IC_{50} of 4.13 μM in the H1603 cell line. Analogues of this class of compounds inhibited phosphorylation targets downstream of AKT. They also increased apoptosis in cells with higher levels of constitutive AKT activity[148].

The compound Perifosine, KRK-0401 (licensed to Aeterna Zentaris) has an IC_{50} = 4.7 μM against AKT and a GI_{50} = 5 μM in the PC-3 prostate carcinoma cell line. It was shown to be active in phase-2 trials as a combination therapy in colorectal cancer and multiple myeloma. But it has been withdrawn from phase-3 trials[145, 149, 150].

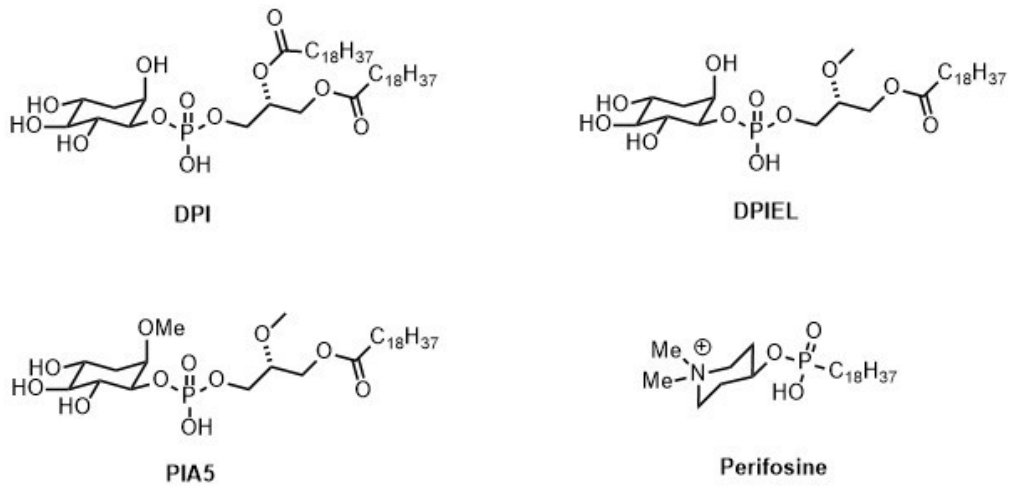

Figure 51: Structures of Phosphatidylinositol analogues

3.1.6.2: ATP-Competitive Inhibitors

There is a high degree of homology in the ATP binding pocket among AKT, PKA and PKC. Hence, compounds that bind to the ATP binding site in AKT have to be tested for PKA and PKC binding as a measure of selectivity.

High-throughput screening of the Abbott compound collection led to the identification of 3,5-disubstituted pyridine analogues that bind to the ATP binding pocket of AKT and these compounds have been classified as ATP-competitive, reversible pan-AKT kinase inhibitors that inhibit AKT activity *in vitro* and *in vivo* (**Figure 52**)[151]. Compound **95** has an Ki of 5 μM against AKT1. The chlorine atom was removed, the pyridine was replaced with an indazole and the methyl group was substituted with a 3-indole to give compound **96** that had a potency of 0.00016 μM and was 40-fold selective over PKA. Compound **96** displayed a dose dependent decrease in cell growth and lowered AKT mediated phosphorylation of downstream targets. It displayed an IC_{50} = 0.1 μM in MiaPaCa-2 human pancreatic cancer cells and decreased tumor growth in mouse xenograft models, however this compound displayed poor pharmacokinetic properties and displayed QT prolongation and hypotension[152]. Compound **96** was further modified to give **97**, which displayed a Ki = 0.0006 μM but with a lowered selectivity profile towards PKA. Despite a lowered potency and selectivity towards AKT, compound **97** exhibited no statistically significant hypotension when dosed orally in mice[153].

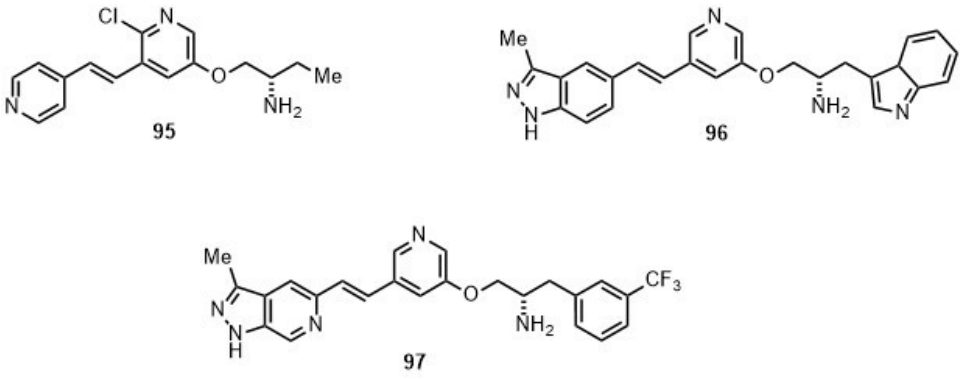

Figure 52: Structures of Abbott's 3,5-disubstituted pyridine analogues

In 2008 GSK described a series of AKT inhibitors analogued from the oxadiazole leads **98** and **99**[154]. Using molecular modeling and co-crystalization the preclinical candidate **100** (GSK690693) was identified (AKT1 IC_{50} = 0.002 μM, AKT2 IC_{50} = 0.013 μM, AKT3 IC_{50} = 0.009 μM, **Figure 53**). The compound **100** inhibited GSK3β phosphorylation in cells and displayed a dose dependent reduction in tumor volume in BT474 breast carcinoma xenograft mice[155]. The compound was withdrawn from phase-1 clinical trials while testing an IV formulation of the agent for undisclosed reasons[145].

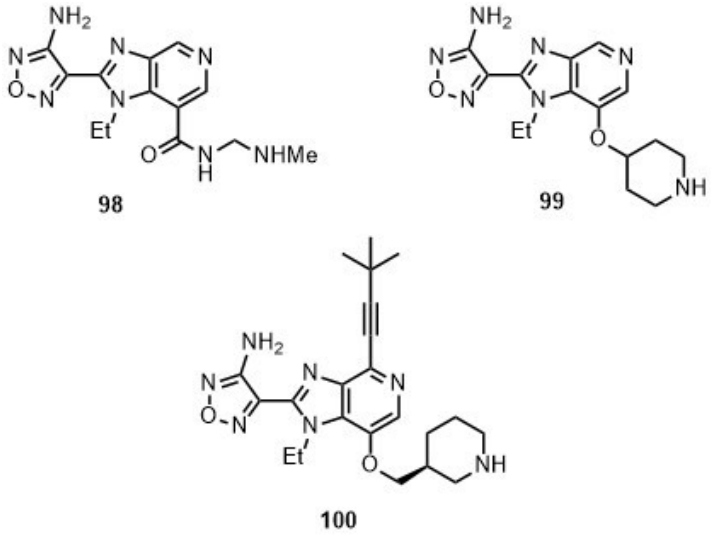

Figure 53: Structures of ATP competitive inhibitors from GSK

3.1.6.3: Allosteric inhibitors

Compounds **101** and **102** were identified from high throughput screening (**Figure 54**). Kinetic analyses indicated that neither compound competed with ATP nor the peptide substrate, also they were not active against AKT3, mutants lacking the PH domain or other closely related AGC kinases[156].

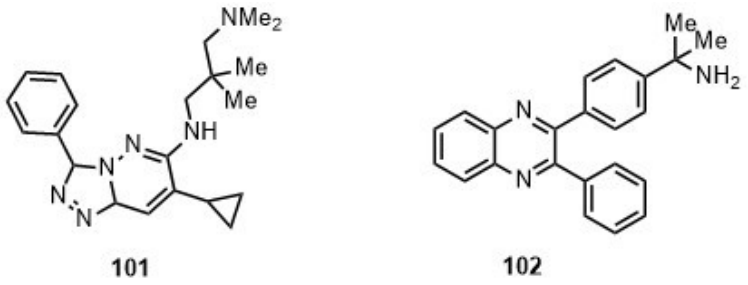

Figure 54: Allosteric inhibitors of AKT

Further work showed that these inhibitors prevented phosphorylation of Thr308[157] by PDK1. This led to a description of a model for this novel mode of inhibition wherein the inhibitors only bind to a site that exists in presence of the PH domain, and stabilize AKT in a closed conformation that is not capable of being activated by PDK1. This has been proved by further studies that show the residue Trp80 in the PH domain forms a cavity in AKT1, but is absent in AKT3. Also *in vivo* FRET data shows that compound **102** locks AKT into its inactive conformation preventing its activation by phosphorylation.

Merck, in 2005, identified the compound **103** (**Figure 55**), a dual AKT1/2 allosteric inhibitor from the lead **102**[158]. Compound **103** displayed PH-domain dependent inhibition and it inhibited AKT and AKT dependent phosphorylation in a mouse pharmacodynamics assay. Due to the poor physical properties of compound **102**, further work consisted of replacing the 2,3-diphenyl-quinoxaline core with a quinoline core to give compound **104**[158]. This analog displayed better physical properties, but to reduce molecular weight and increase basicity, the quinoline core was truncated to a pyridine to give compound **105,** a potent AKT1/AKT2 inhibitor with excellent aqueous solubility at pH 4.5[159]. Furthermore, chemical manipulation of the scaffold followed trying to improve aqueous

solubility, balancing biochemical and cell based activity and removing hERG liabilities, leading to the compound [1,2,4]triazolo[3,4-f][1,6]napthypyridine **106**[160].

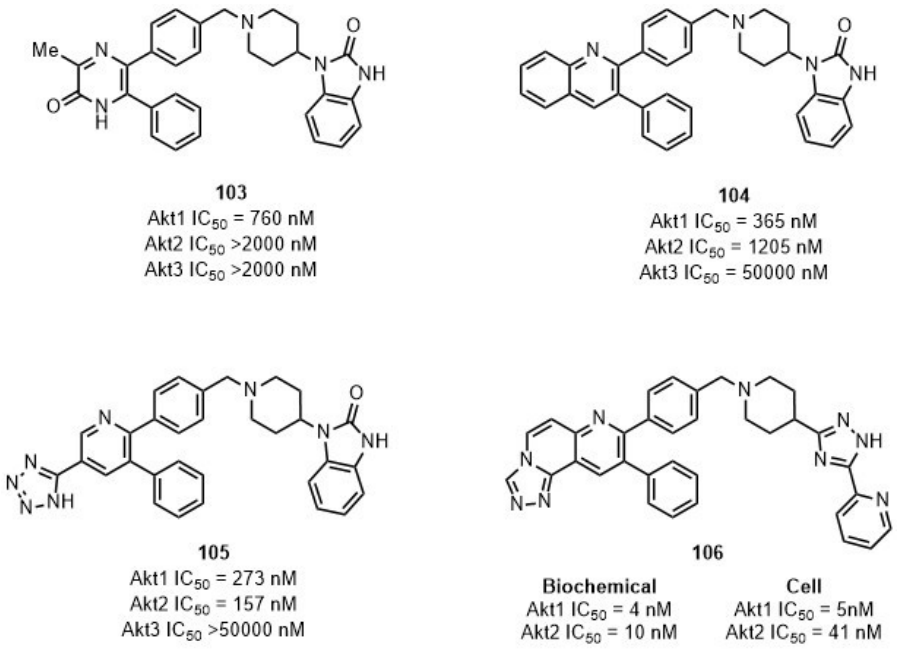

Figure 55: Allosteric inhibitors of AKT from Merck

Merck also disclosed their recent allosteric AKT inhibitor MK-2206 (**Figure 56**), which is based on the triazolone-napthypyridine core. It also has an allosteric mode of action and currently is in phase-2 studies[161].

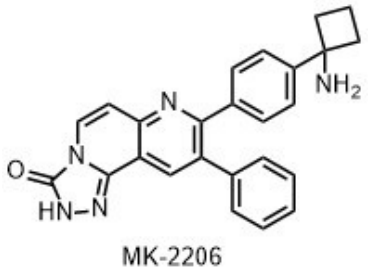

Figure 56: Structure of MK-2206

3.1.6.4: Covalent inhibitors

A high-throughput screening effort in 2007 led to the discovery of the pyanonaphthquinone lactones **107** and **108** (**Figure 57**). These compounds were found to be highly potent and selective inhibitors of AKT[162].

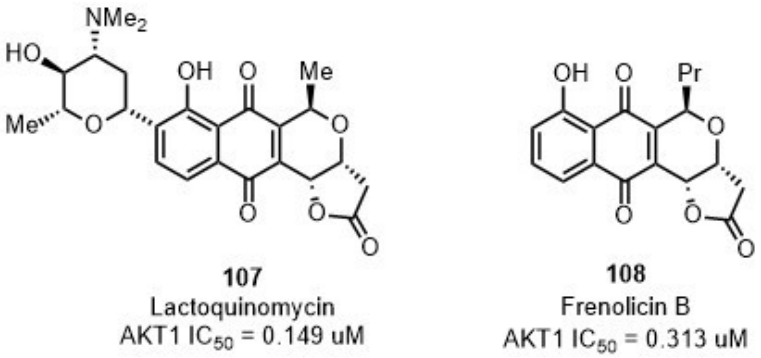

107
Lactoquinomycin
AKT1 IC_{50} = 0.149 uM

108
Frenolicin B
AKT1 IC_{50} = 0.313 uM

Figure 57: Structure of PNQ lactones

The mechanism of inhibition was found to be irreversible, with an adduct being formed with the pyanonaphthquinone and Cys310 and or Cys296 present in the T-loop of AKT1. A bioreductive alkylation mechanism was proposed wherein the quinone gets reduced under *in vitro* and *in vivo* conditions and forms a quinone methide **109'** that acts as a Michael acceptor. This reacts with the nucleophilic cysteine 310 in the T-loop of AKT and forms the adduct **110**. The formation of this activated quinone methide **109'** by reduction is essential for the activity of these compounds (**Figure 58**). Analogues that lack this lactone ring are inactive as AKT inhibitors up to concentrations of 20 μM[163].

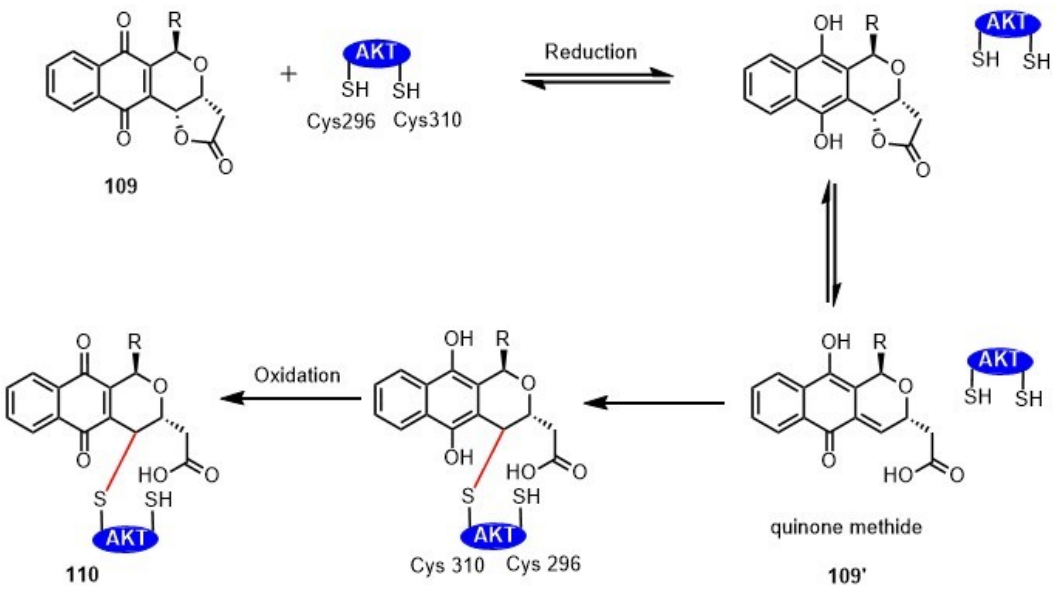

Figure 58: Bioreductive alkylation mechanism postulated for PNQ lactones

3.1.6.5: Substrate-Mimetic Inhibitors

These compounds are more selective than all the earlier mentioned classes of inhibitors due to the natural selectivity filter of the kinase substrate binding pocket to recognize only a limited number of substrates. The substrate binding site offers potential for a large number of interactions for small molecules that can mimic a peptide.

Activated AKT2 has been crystallized with the GSK3β 10 residue substrate sequence (^{3}GRPRTTSFAE^{12}) and a non-hydrolysable ATP analog (AMP-PMP)[164]. A similar shortened sequence **111** (GRPRTSSF), was reported by Alessi *et al.* to have a Km of 8 μM[110]. This shortened sequence was used by Hamilton *et al.* to develop substrate-mimetic inhibitors of AKT[165].

Initially, they substituted the serine, which can be phosphorylated, for a valine to give compound **112**. More rigidity was introduced into the sequence by substituting Thr-Thr with para-aminobenzoic acid and a hydrophobic group; benzyl was added to the C-

terminal Phe to get compound **113 (Figure 59**). This was followed by removal of the N-terminal GRP- sequence to obtain the compound **114**. Compound **114** displayed a 3-fold decrease in affinity compared to **113**, but Hamilton *et al*. were able to shorten the chain by 3 residues. Further optimization led to the extension of the linker between the para-aminobenzoic acid and the guanidine group and addition of an N-benzyl acetamide group to fill the pocket that was occupied by threonine side chain to get compound **115**.

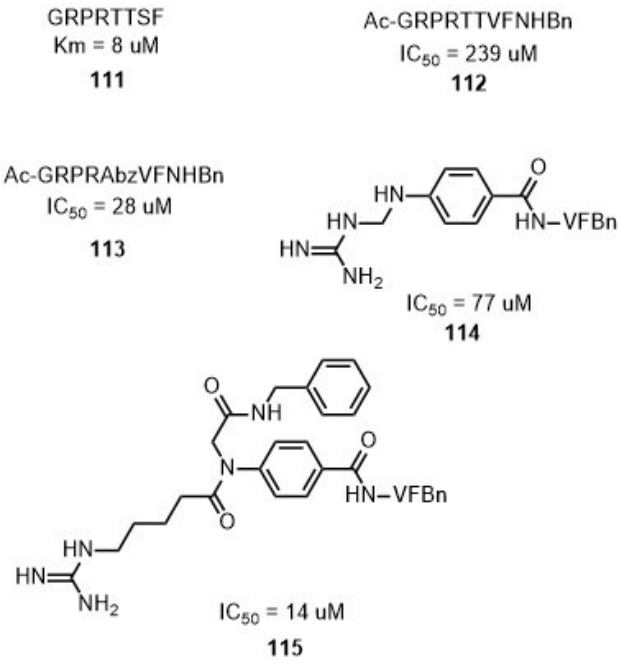

Figure 59: Peptidomimetic analogues

Livnah *et al.* prepared the novel heptapeptide inhibitor **116** (**Figure 60**), which was found to have more than 50-fold selectivity for AKT over PKA[166]. Peptide **116** selectivly killed prostate cancer cells where in AKT was upregulated but not normal cells or cancer cells in which AKT was not activated. Also, the compound was effective in two prostate cancer mouse models.

Arg-Pro-Arg-NVal-Tyr-Ser(Me)-Abu

IC_{50} = 0.2 uM

116

Figure 60: Livnah Heptapeptide inhibitor

Based on the structure of compound **115** and the 10 residue GSK3β peptide sequence (^{3}GRPRTTSFAE^{12}), Hamilton *et al.* designed compound **117** using the docking software GOLD (**Figure 61**)[167]. The compound was designed based on their observation that the N-terminal Gly3, Arg4 and Pro5 are not needed, the Thr7 and Thr8 are replaced with a *p*-aminobenzoic acid scaffold, and addition of a benzyl to the C-terminal Phe10 moiety increased affinity. The C-terminal dibenzyl group mimics Phe10 and the benzyl group from compound **115**. Addition of a phenyl substituent to the 3-position of the *p*-aminobenzoic acid scaffold gave **118** with an IC_{50} = 84 μM. Further rounds of analoguing led to the substitution of the C-terminal dibenzyl with a di-*p*-cyanobenzyl group, and gave the compound **119** that displayed a fourfold increase in inhibition. Substitution of a naphthyl group on the 3-position of the *p*-aminobenzoic acid gave compound **120,** and replacement of the ethylamine-linker with a glycine linker led to the compound **121** with about an eightfold increase in inhibition as compared with the computationally designed lead **117**. This work provides the example that the substrate binding site of AKT can be targeted with small molecule peptide mimetics.

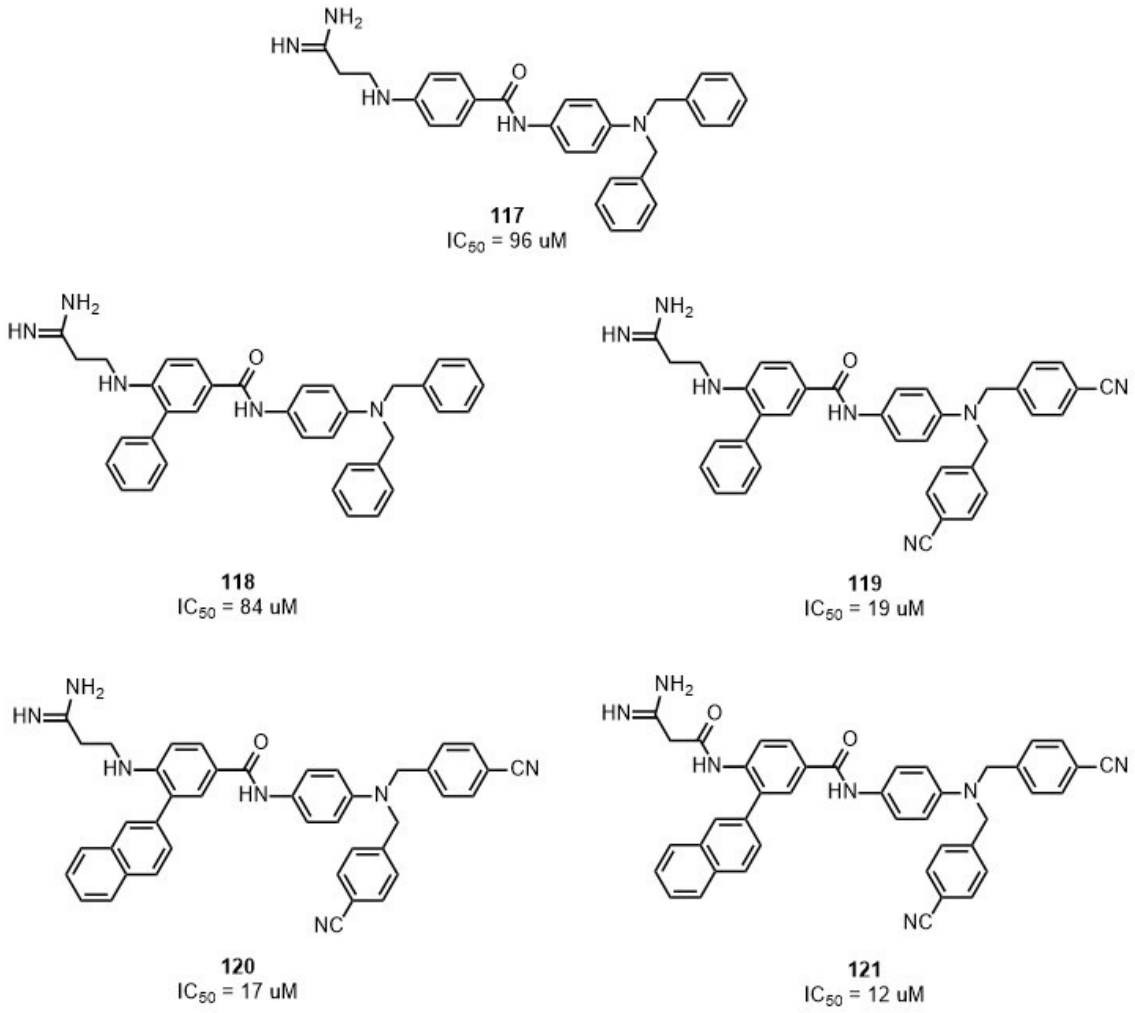

Figure 61: Structures of substrate-competitive peptidomimetics

Following the above mentioned work, Valle *et al.* reported synthesis of GSK3β peptide small molecule mimetics[168]. They used the lead GSK3β peptide (^{3}GRPRTTSFAE^{12}) as a lead and replaced the Thr7-Thr8 residues with a bicyclic-carbamate scaffold consisting of a proline, a 6-membered carbamate ring as a dipeptide surrogate and removed the N-terminus ^{3}GPR^{5} segment (**Figure 62**). Also they introduced the Val-Phe-NHBn fragment at the C-terminus as reported earlier by Hamilton *et al.* Further optimization led to the compound **122**, which is ~5 fold more potent than compound **121**.

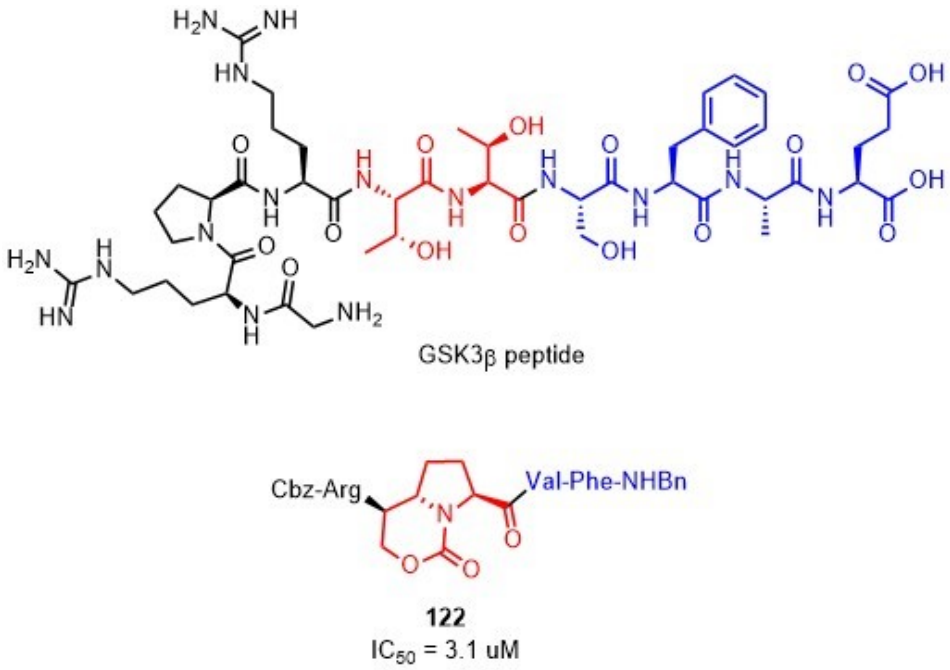

Figure 62: Peptidomimetic reported by Valle *et al.*[168].

3.2 Rationale for the work

3.2.1 Utilizing the Substrate Binding Pocket of AKT

AKT is a widely expressed Ser/Thr kinase that phosphorylates various substrates in the cell that are involved in regulation of cellular functions such as cell proliferation, transcription, migration, apoptosis, cellular differentiation and metabolism. Persistent activation of the AKT pathway leads to human oncogenesis. Disregulation of AKT kinase activity is seen in many human cancers such as ovarian, breast, thyroid and colon cancers[129, 143]. Suppression of this aberrant AKT signaling by using small molecules that target AKT kinase has been shown to increase apoptosis and reduce cell proliferation in tumor cells that in particular express high levels of activated AKT. The development of small molecules that target AKT kinase is currently a highly active area of research with many such compounds currently in clinical trials[169].

The majority of the small molecule AKT kinase inhibitors use the ATP binding site for binding to the kinase. The problem with such an approach is achieving selectivity with other homologous members in the AGC kinase family such as PKA and PKC. Selective binding in the ATP pocket of kinases is challenging, as this pocket is highly conserved among other kinases, and achieving specificity requires utilizing the subtle differences in residues lining these pockets. Hence, these inhibitors tend to compete with other enzymes that utilize ATP having similar binding regions and also with high cellular concentrations of ATP. This competition with millimolar concentrations of ATP in the cell explains why ATP mimetics require much higher concentrations for tumor growth inhibition compared to recombinant enzyme assays[170].

One significant problem with using kinase inhibitors that target the ATP pocket is the development of drug resistance. This is because the mutations that accumulate in the ATP binding site of the kinase, as was observed in patients with CML undergoing treatment with Imitinib. The mutated residues found in the ATP binding site were highly conserved among kinases, so use of the substrate binding pocket potentially may obviate that problem. Such a strategy has already been used sucessfully for targeting Extracellular signal Regulated Kinase (ERK), Polo-like Kinase 1, Abl kinase, Insulin-like growth factor-receptor 1 (IGF-RI) and AKT[170-172].

Substrate-mimetic inhibitors offer a new paradigm in the targeting of protein kinases by blocking phosphorylation, and thus not competing with ATP. The enzyme substrate binding site has evolved to recognize specific substrate sequences in contrast to the ATP binding site. These sites are adapted individually for each kinase to recognize a particular substrate sequence in the cell. Therefore, they offer a large number of specific potential

interactions that could be used for designing a small molecule to target these sites, compared to the corresponding ATP pocket. Hence, exploiting the substrate specificity of these sites will allow the design of a more specific inhibitor for AKT kinase[170].

3.2.2: Utilizing a Covalent Mode of Inhibition

The problem with using the substrate binding site is the large binding pocket and the extended binding conformation that many of the substrates use. This creates a problem where a large binding space has to be targeted for the design of an effective and specific inhibitor. Although the substrate peptides possess high selectivity and specificity in binding to the kinase, these sequences are poor inhibitors due to their lack in potency. The usual approaches used to increase potency with these peptides involve screening combinatorial libraries of peptides[173], incorporation of unnatural amino acids[166, 174] and bisubstrate approaches that link the peptide to an ATP pocket binder[175]. We chose to develop a covalent substrate competitive binding approach to increase potency.

Covalent mechanisms of binding to proteins has been traditionally shunned in drug development because these compounds were thought to form highly reactive metabolites and cause drug allergies. But, about 30% of the drugs on the market that target an enzyme do act through a covalent mechanism[176]. The risk of toxicity by covalent inhibitors can be minimized by optimization of the non-covalent binding interactions and by modulation of the reactivity of the electrophile. This would lead to more target specificity and mitigate unwanted side reactions with nucleophiles *in vivo*[177].

The advantages of a covalent mechanism of action include an improved biochemical efficiency due to irreversible binding, less frequency of dosing due to longer duration of

action, increased efficacy due to the lower concentrations required, and the potential to avoid drug resistance due to continuous suppression of the target. Also, targets with shallow binding sites could be inhibited. There has been a recent surge in the identification of covalent inhibitors with compounds from the programs targeting EGFR, BTK, FAAH and MetAP2 progressing to phase II and III clinical trials[172, 176, 178].

3.2.3: Identification of a Nucleophilic Residue in AKT

The pyranonaphthoquinone (PNQ) lactone class of natural products potently and selectively inhibits AKT by alkylating Cys310 in the activation loop. The PNQ lactones have been shown to form a covalent adduct with Cys311 in AKT2 (**Figure 59**)[162, 163].

Other non-selective cysteine alkylating electrophiles like *N*-ethylmaleimide[179], iodoacetic acid[180] and 4-hydroxynonenal[181] (4-HNE, a Michael acceptor) have been shown to alkylate Cys310 in AKT. An iodoacetamidate activity-based probe has been shown to alkylate Cys310 in AKT by Cravatt *et al.* by mass spectrometry[182].

3.2.4: Identification of an appropriate Substrate Mimetic for AKT

The X-ray crystal structure of activated AKT2 with the GSK3β 10 residue substrate sequence (^{3}GRPRTTSFAE^{12}) and a non-hydrolysable ATP analog (AMP-PMP) was reported in 2002[164]. The peptide is phosphorylated by AKT on Ser9 and includes the consensus sequence for AKT (RXRXXSF). The crystal structure shows the GSK3β peptide to be bound in an extended conformation, with discrete sections of the β-strand on either side of Ser9. According to the crystal structure, Phe10 of the GSK3β peptide aligns adjacent to AKT Cys310 (**Figure 63**). The distance measure from the peptide backbone of GSK3β to Cys310 is ~6.0 Å.

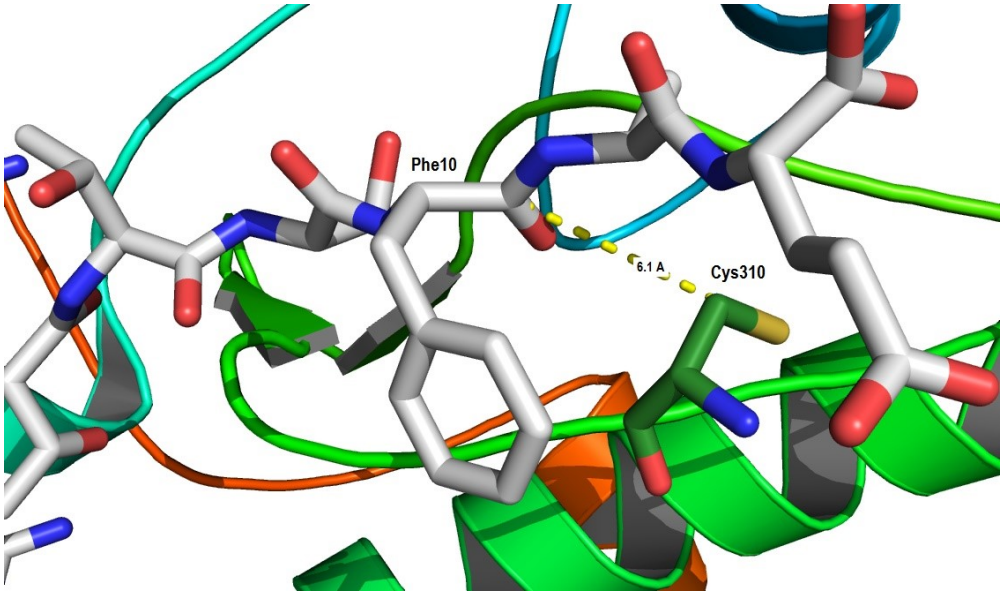

Figure 63: Distance between Cys310 and peptide backbone of GSK3β peptide

Hamilton and coworkers identified the small molecule peptidomimetic **121** of AKT by analoguing from the GSK3β peptide. In order to understand the spatial relationships of compound **121** binding to AKT, we docked this compound using GOLD into the substrate binding pocket of the AKT co-crystal structure (**Figure 64**)[167]. The docking pose we obtained closely matches that reported by Hamilton. The docking model predicts that one of the two *p*-cyanobenzyl rings on the C-terminal end of the molecule is located ~5.5 Å from the thiol of Cys311 (AKT311 numbering).

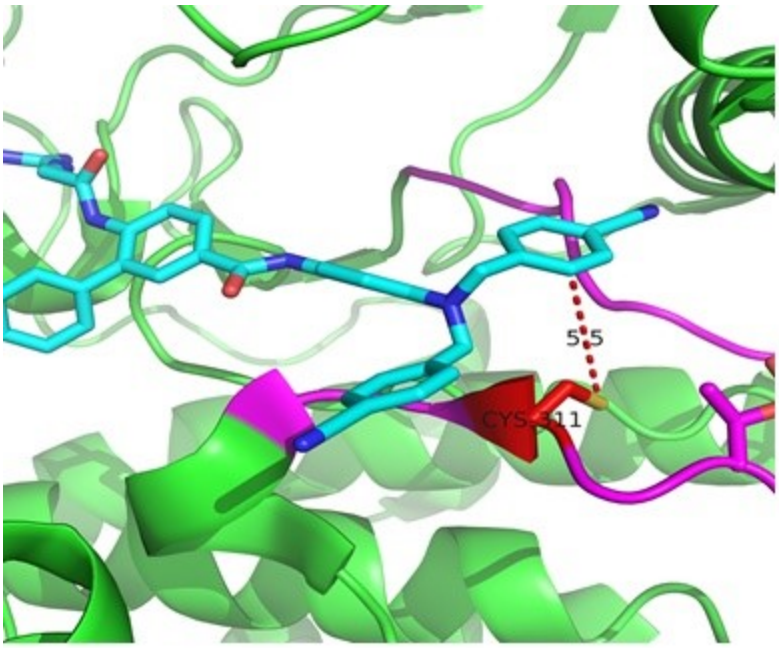

Figure 64: Docked Structure of compound **121**

3.2.5: Initial Design of Compounds and Selection of the Electrophile

Based on our docking model that predicts the distance of ~5.5 Å from the nucleophile of Cys310 in AKT to the *p*-cyanobenzyl group, we reasoned that we could replace this C-terminal moiety in **121** (**Figure 65**) with appropriate electrophiles that would react with the sulphur of Cys310. To synthesize covalent inhibitors of this type, we needed to identify electrophiles that can be installed on the aniline nitrogen and that could inhibit AKT. As our initial screen we decided to screen α-haloacetamides, maleimides, epoxides, acrylamides and vinyl ketones. These electrophiles have been reported to alkylate cysteines, when used in various kinase inhibitors[176-178]. For the ease of synthesis and quick screening for inhibition of AKT activity, we initially decided to use only the C-terminal end or the right hand fragment of compound **121** to install the electrophiles. We reasoned that from the most potent compound obtained from this set, we will elaborate by adding

the N-terminal end of the Hamilton fragment to result in a potent and selective substrate mimetic covalent inhibitor for AKT.

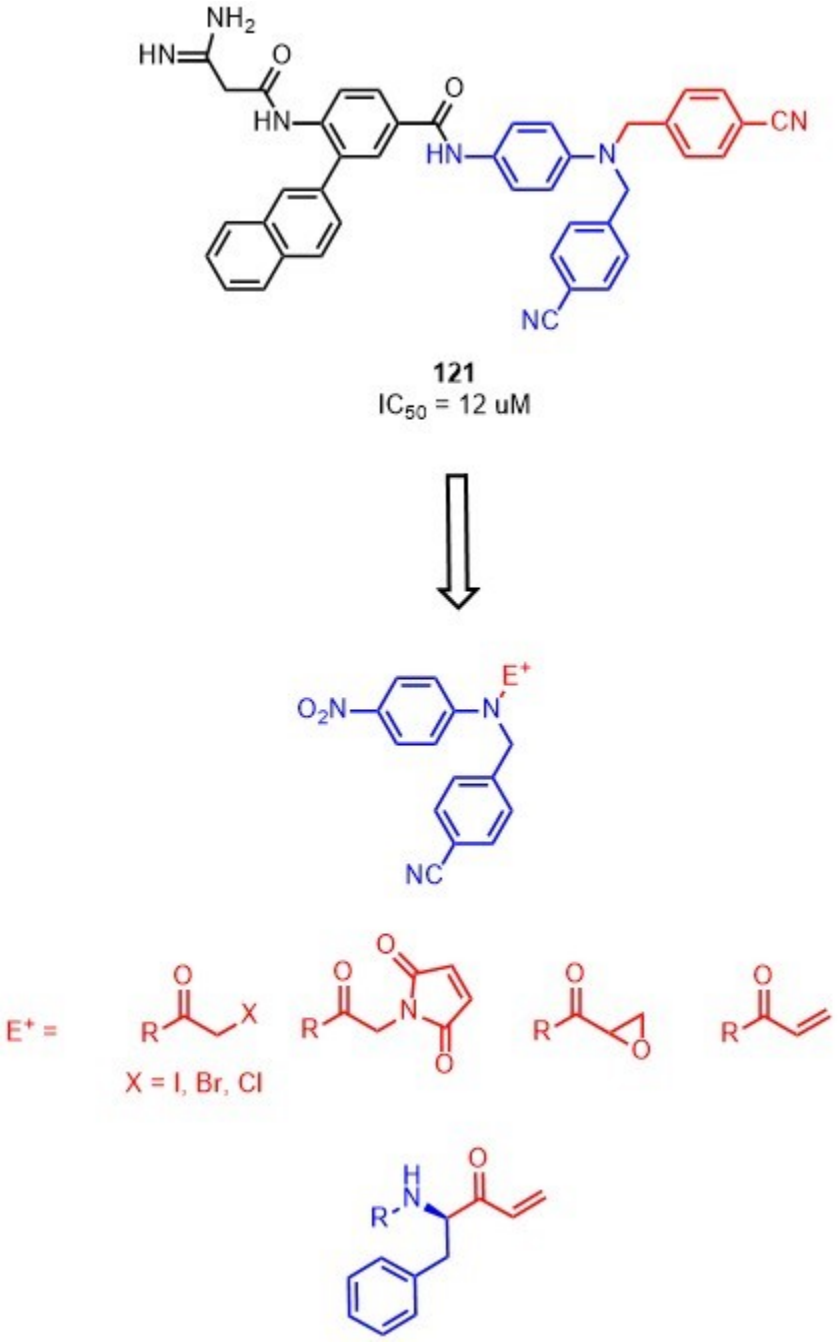

Figure 65: Design of the first set of compounds

3.3: Synthesis and Biological evaluation of the First Set of Compounds

3.3.1: Synthesis of α-haloacetamides

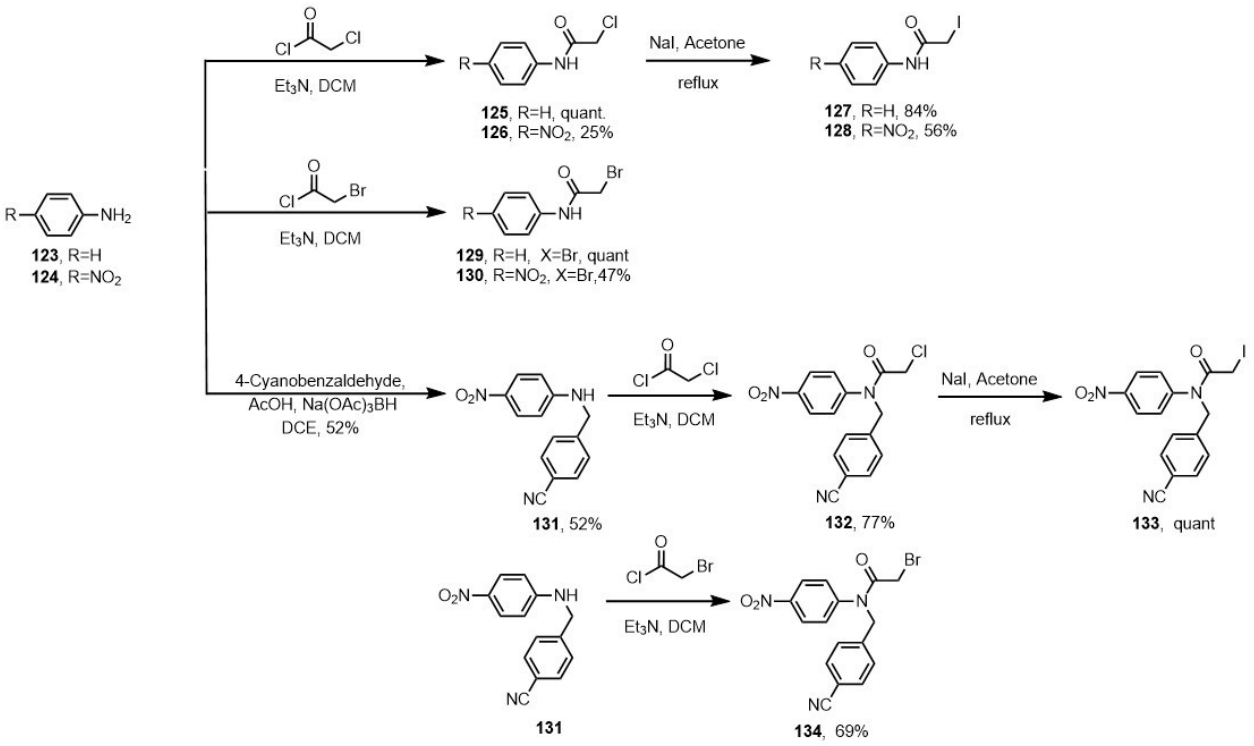

Figure 66: Synthesis of α-haloacetamides

The α-haloacetamides were synthesized either starting from aniline **123** or from 4-nitroaniline **124** as shown in Figure **66**. The electrophiles were installed using either chloroacetyl chloride or bromoacetyl chloride using standard acid chloride coupling conditions with triethylamine as the acid-trap. Compound **131** was prepared by reductive amination from 4-nitroanilline and 4-cyanobenzaldehyde using the acid stable sodium triacetoxborohydride as the reductant. The iodo-acetamides **127**, **128** and **133** were prepared using a Finkelstein reaction by refluxing the chloro-acetamides **125**, **126** and **132** with excess sodium iodide in acetone.

3.3.2: Synthesis of acrylamides

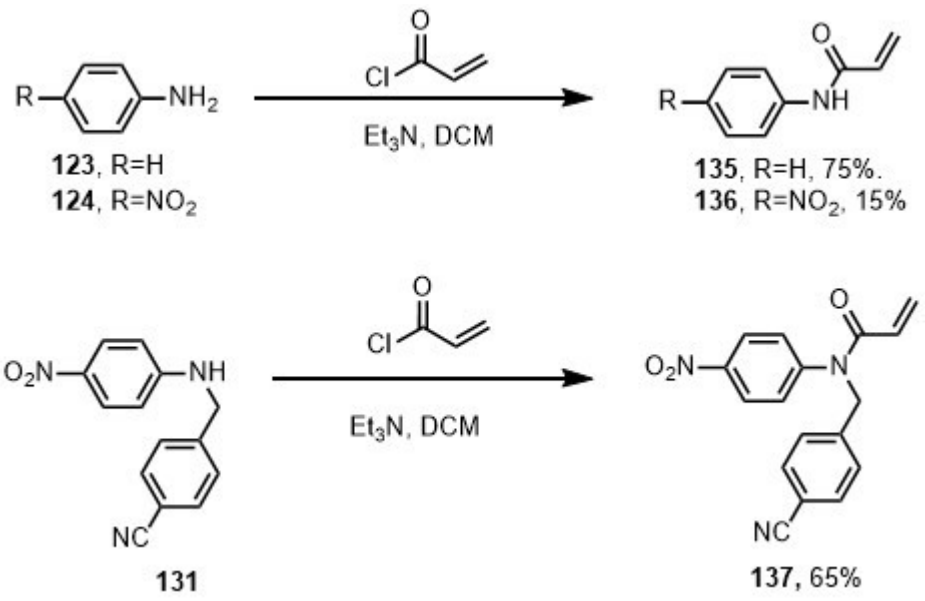

Figure 67: Synthesis of the acrylamides

The acrylamides **135**, **136** and **137** were prepared form aniline **123**, 4-nitroaniline **124** and compound **131** using acryloyl chloride by acid coupling conditions using triethylamine as the base (**Figure 67**). Acrolyl chloride was added at 0 ^{0}C to the reaction and they were allowed to react overnight at room temperature.

3.3.3: Synthesis of Epoxide

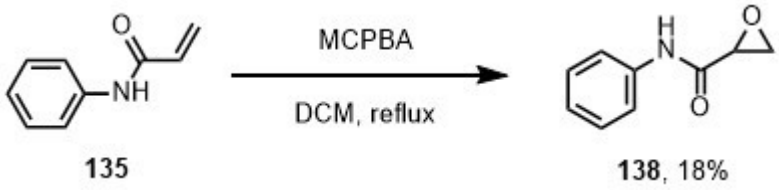

Figure 68: Synthesis of compound **138**

The compound **138** was synthesized from the acrylamide **135** by refluxing it with the oxidant m-CPBA in dichloromethane (**Figure 68**).

3.3.4: Synthesis of Maleimides

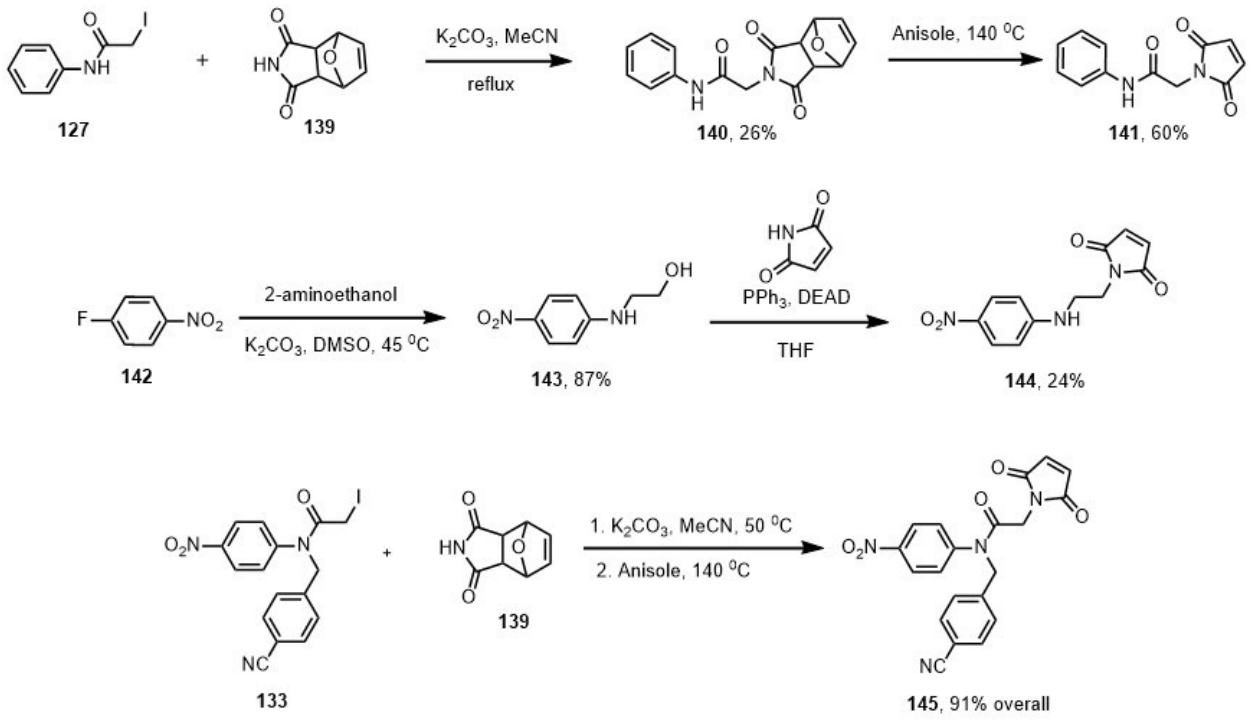

Figure 69: Synthesis of the maleimides **141**, **144** and **145**

The maleimides **141** and **145** were synthesized from the iodo-acetamides **127** and **133** according to **Figure 69**. Maleimide itself cannot be used in a base catalyzed reaction because of its reactive Michael-acceptors. Hence it was protected using furan in a hetero-Diels Alder cyclization to give compound **139**. This compound was then reacted with compounds **127** and **133** in an S_N2 reaction with potassium carbonate as the base to obtain the intermediates **140** and **145'**. The furan protecting group was removed using a retro Diels-Alder reaction by heating the compounds **140** and **145'** in anisole at 160 ^{0}C for four hours to give the maleimides **141** and **145**.

Compound **143** was prepared by a S_NAr reaction using 2-aminoethanol as the nucleophile and **142** as the electrophile. The primary alcohol was substituted with maleimide in a

Mitsonobu reaction to give the compound **144**. Mitsonobu reactions use much milder conditions and allow the use of unprotected maleimide itself as the nucleophile.

3.3.5: Synthesis of Vinyl ketones

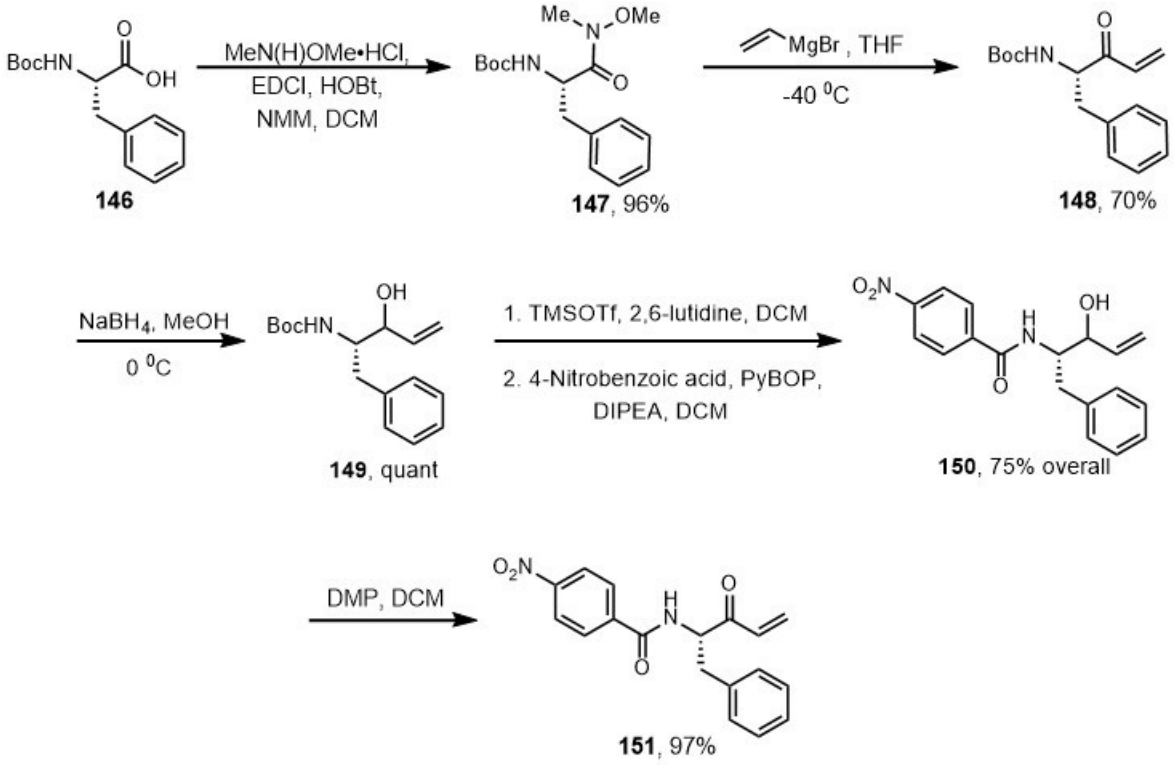

Figure 70: Synthesis of Vinyl ketones **148** and **151**

The vinyl ketone **148** was prepared starting from Boc-Phe-OH **146**, which was converted to the Weinreb amide **147** using EDCI as the coupling reagent and HOBt to prevent racemization (**Figure 70**). The Weinreb amide was reacted with the Grignard reagent vinyl magnesium bromide to obtain the vinyl ketone **148**. The vinyl ketone was found to be both acid and base labile, hence the *N*-Boc protecting group was removed by first reducing the ketone using sodium borohydride in methanol to obtain a diastereomeric mixture of alcohols **149**. From this compound **149**, the *N*-Boc group was removed using

a mixture of TMSOTf and 2,6-lutidine. The primary amine was coupled to *p*-nitrobenzoic acid to give a diasteromeric mixture of alcohols **150**. The secondary alcohol was oxidized using Dess Martin reagent in dichloromethane to give the vinyl ketone **151**.

3.3.6: Biochemical evaluation of the compounds

We evaluated the first set of compounds in a biochemical fluorescence assay (Z'-LYTE kinase assay, Ser/Thr kit 6, Invitrogen) using commercially available recombinant AKT1 (Invitrogen, P2999). This assay uses a proprietary peptide substrate that contains the AKT1 consensus sequence and is labeled with a coumarin on one end and fluorescein at the other. During the kinase reaction, the peptide substrate is phosphorylated by AKT1. After the reaction is stopped, the FRET signal between the coumarin and fluorescein is detected only on the phosphorylated peptide. Unphosphorylated peptide is cleaved by a site-specific protease when the reaction is developed, disrupting the FRET signal from the unphosphorylated substrate. Addition of compounds to the assay that inhibit phosphorylation of the substrate by AKT1 results in a decrease of the FRET signal. This assay detects functional inhibitors of AKT1 independent of mechanism of action.

Compounds **125** to **151** were evaluated by this assay in triplicate over a concentration range of 8 nM to 100 μM. The data we obtained is shown in **Table 7**.

Table 7: Evaluation of compounds against AKT1

Compound	AKT1 IC_{50} (μM)	Compound	AKT1 IC_{50} (μM)
125	>100	141	1.55

129	10.59	144	1.79
127	3.25	145	1.97
128	2.33	138	>100
133	1.11	148	0.58
135	>100	151	0.32

Based on the above IC_{50} data, the epoxide **138**, acrylamide **135** and the α-chloro acetamide **125** were inactive as AKT1 inhibitors with IC_{50} > 100 μM. The α-bromo **129** and α-iodo acetamides **127**, **128, 133** and the maleimides **141**, **144** and **145** were all active in the low-micromolar range of concentrations. However, the vinyl ketones **148** and **151** inhibited AKT in the submicromolar range of concentration, with an IC_{50} of 0.58 μM and 0.32 μM.

Among the α-haloacetamides, the inhibition was dependent on the reactivity of the electrophile. The α-chloro acetamides **125** were inactive, and the iodo-acetamides **127**, **128**, **133** were ~4 fold active, as compared to the bromo-acetamide **129**. Among the iodo-acetamides, compound **133** was twice as active as compared to **127** and **128**. This can be explained by the additional interactions made by the *p*-cyanobenzyl moiety.

Among the maleimides **141**, **144** and **145**, there were no differences in IC_{50}s among the compounds with these variations in structure. This suggests that the interactions were mostly covalent binding and the addition of more binding elements did not make any difference in the IC_{50}.

The most potent compounds in this series were the vinyl ketones **148** and **151**. The most potent compound **151** has the *p*-nitrobenzyl group instead of the *N*-Boc group. This is the fragment present in the Hamilton compound **121**, which can be elaborated on to add the N-terminal end of the compound.

3.3.7: Synthesis and biochemical evaluation of the reduced analogues and with the alkyne handle

Having identified the most potent compound in the series, we decided to confirm that the mechanism of inhibition was covalent. We inactivated the vinyl ketone electrophile by reducing it to the ethyl ketone using catalytic hydrogenation over palladium on charcoal to give the compounds **152** and **153** (**Figure 71**).

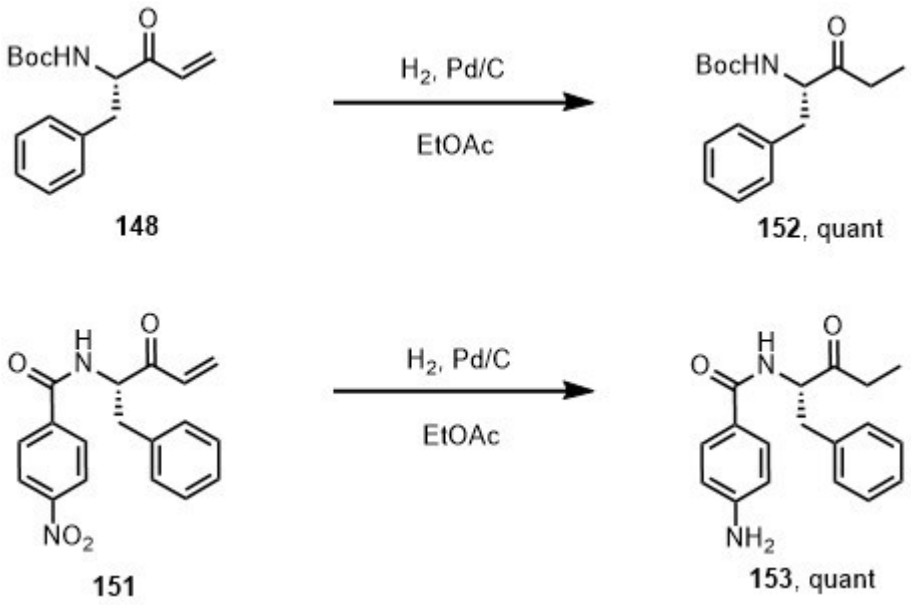

Figure 71: Synthesis of **152** and **153**

To determine the selectivity of the compounds in a cellular context, as compared with the purified recombinant enzyme, we made the vinyl ketones with an alkyne handle attached

to the N-terminal: **156** and **161** (**Figure: 72** and **Figure: 73**). The alkyne handle can be used to attach detection or purification tags to the compound in a biological sample. This will allow the identification of the compound-protein adduct in the sample.

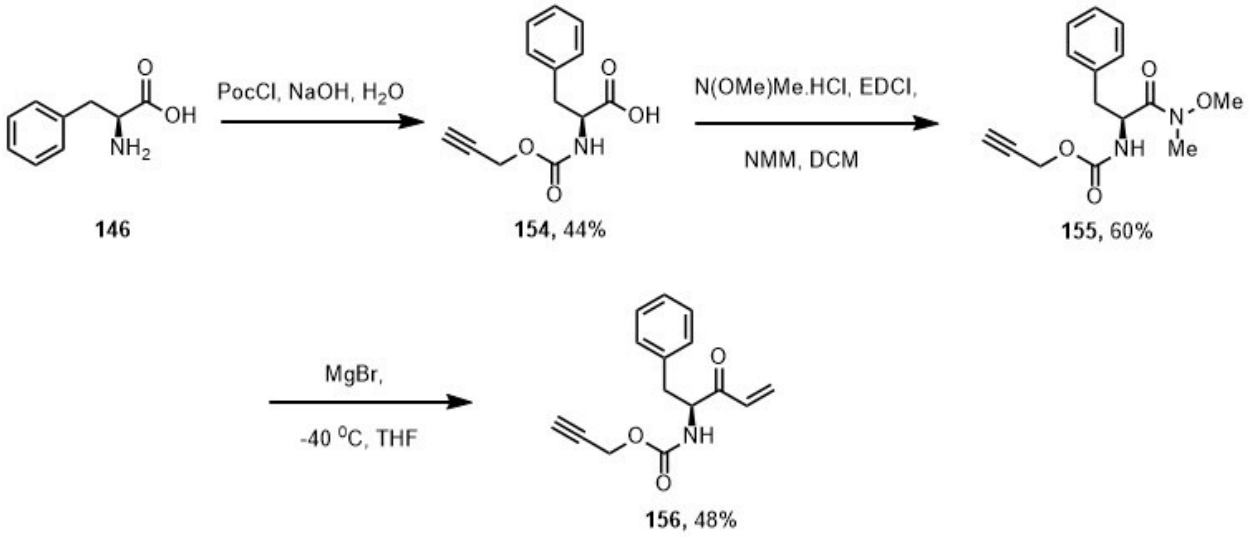

Figure 72: Synthesis of compound **156**

The compound **156** was synthesized starting from phenylalanine **146**, to which the propargyl carbamate group was installed using propargyl chloroformate and sodium hydroxide as the base. This compound was converted to the Weinreb amide using the coupling reagent EDCI to give compound **155**. This was reacted with the Grignard reagent vinyl magnesium bromide in THF to give the compound **156**.

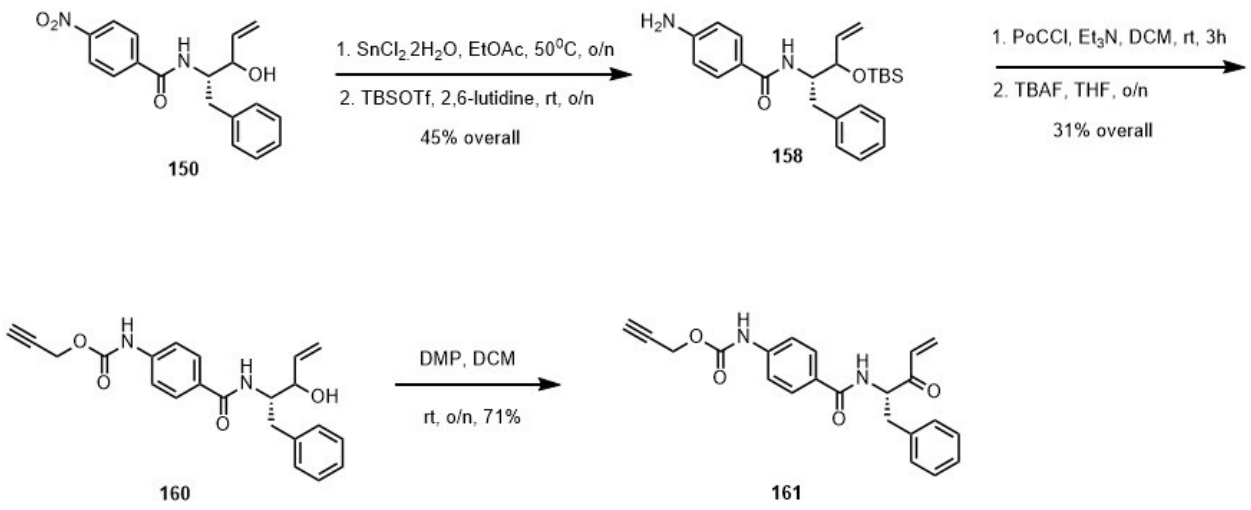

Figure 73: Synthesis of compound **161**

Compound **161** was synthesized starting from the mixture of the diastereomeric alcohols **150**. The nitro group was reduced to the amine using tin chloride dihydrate in refluxing ethylacetate to give compound **157**. The secondary alcohol was then protected as the TBS ether using TBSOTf and 2,6-lutidine as the base to give **158**. The propargyl group was then installed onto the amine using propargyl chloroformate and triethylamine as the base, followed by removal of the TBS ether using TBAF to give compound **160**. The secondary alcohol was oxidized using Dess-Martin periodane to give compound **161.**

To confirm the covalent mechanism of action of compounds, the inactivated analogues **152** and **153** were screened for inhibition of AKT phosphorylation using the Z-LYTE assay as described before. Also, to determine the selectivity of the compounds for AKT, we screened the alkyne analogues **156** and **161** against c-AMP-dependent protein kinase A (PKAα) (**Table 8**). PKAα is a member of the AGC kinases and is most identical to AKT, sharing 43% sequence identity in its kinase catalytic domain[183]. Hence, the fold selectivity

obtained for AKT over PKA is a probable measure of how selective the compound will be in a cellular context.

Table 8: IC_{50} of compounds against AKT1 and PKAα

Compound	AKT1 IC_{50} (μM)	PKAα IC_{50} (μM)
152	>100	nd
153	>100	nd
148	0.58	52.6
151	0.32	>100
156	2.44	
161	0.82	13.47

To confirm that the vinyl ketones **148** and **151** inhibit AKT by a covalent mechanism of action, we tested the inhibition of AKT by the inactivated analogues **152** and **153**. These compounds have their electrophilic moiety removed by reduction of the vinyl ketone to the ethyl ketone. As shown in **Table 8**, compounds **152** and **153** are inactive towards AKT with IC_{50}s > 100 μM. This confirms that the mechanism of action of these compounds is by covalent inactivation of AKT.

The first step in determining the selectivity of these compounds towards AKT is by screening them against c-AMP-dependent protein kinase A (PKAα), which is a member of the AGC kinase family. As shown in **Table 8**, the Boc-Phe-vinyl ketone **148** inhibits PKAα with an IC_{50} of 52.6 μM, hence is ~90 fold more selective for AKT1 than PKAα,

whereas the *p*-nitrobenzoyl-Phe-vinyl ketone **151** was essentially inactive towards PKAα (IC_{50} > 100 μM) displaying a selectivity of more than ~310 fold for AKT1.

To determine the selectivity of the compounds in a cellular context, we made the alkyne-tagged analogues **156** and **161**. These compounds were selectively and potently active towards AKT with **161** displaying a ~16 fold selectivity towards AKT1.

Now that we determined the mechanism of inhibition of these compounds to be covalent, we wanted to determine the residue in AKT1 that is covalently modified by the vinyl ketones. Hence, we made the fluorescein-labeled analog of **156** by azide-alkyne cycloaddition as shown in **Figure 74** to give the compound **165**.

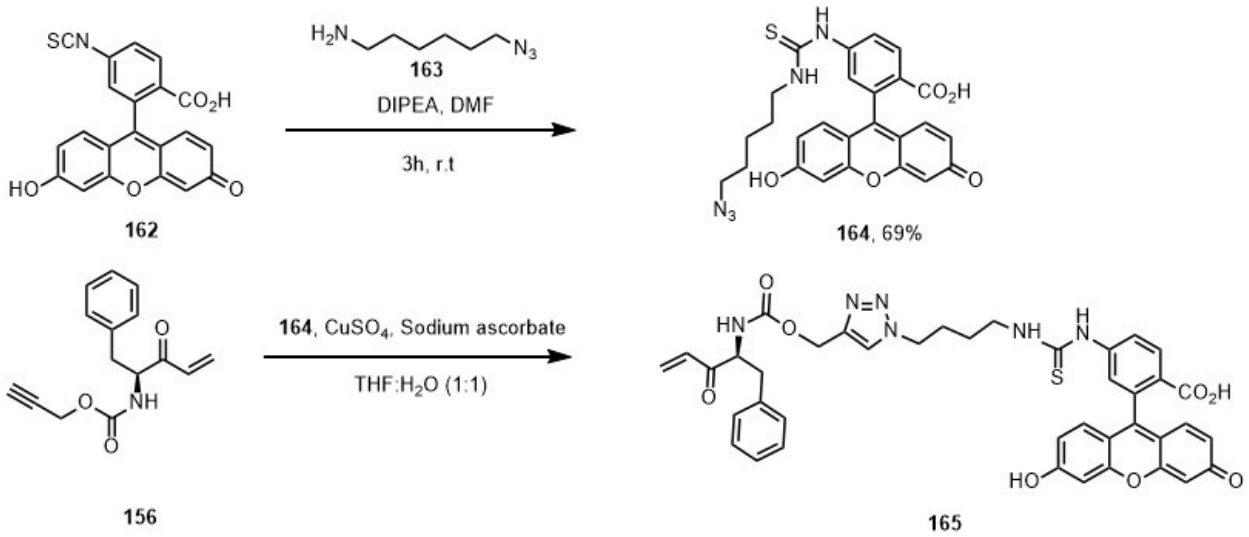

Figure 74: Synthesis of **165**

This compound was incubated with AKT1, followed by gel electrophoresis and confirmation of labeling by in-gel fluorescence scanning (**Figure 75**). Once the AKT1 band was confirmed to be labeled by **165**, it was excised and subjected to trypsin digestion. The mass-spectrum was obtained on a LTQ Orbitrap Velos instrument and an

average 93% coverage was obtained. **165** was shown to modify the AKT fragment Cys310 (**Table 9**). Modification of other cysteines was not observed.

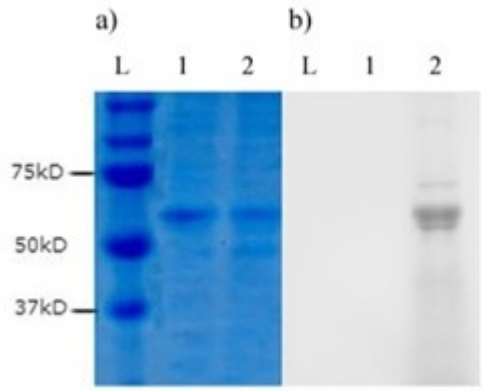

Figure 75: Labeling of AKT1 with **165**. **a**) Coomassie Blue Staining **b**) Fluorescence image at 488/526 nm (Lane 1: AKT1 only, Lane 2: AKT1 incubated with **165**)

Table 9: Mass Spectrometry Data for AKT1 Fragment Modified by **165**

	^{308}TFCGTPEYLAPEVLEDNDYGR^{328}	
	Mass Found	Mass Calculated
Unmodified	2389.04	2389.06
Modified with 165	3177.33	3177.32

To determine the selectivity of **165** in a cellular context, we incubated the compound with cell lysates from the HCT-116 cell line. HCT-116 carries two mutations that constitutively

activate the PI3K/AKT signaling pathway (one in the large subunit of PI3K and the other that constitutively activates Ras). The cell lysates were treated with increasing concentrations of **165** (0 – 100 μM final concentration) and incubated at room temperature for 1 hour. Following this, the labeling reactions were separated by gel electrophoresis on a 10% SDS-PAGE gel (**Figure 76**, **A**). Labeled proteins were visualized on an in-gel fluorescence scanner. AKT alone was detected by Western Blot with biotin-conjugated AKT (pan) antibody and streptavidin horseradish peroxidase (**Figure 76**, **B**). All proteins in the cell lysates were visualized using Coomassie stain (**Figure 76**, **C**)

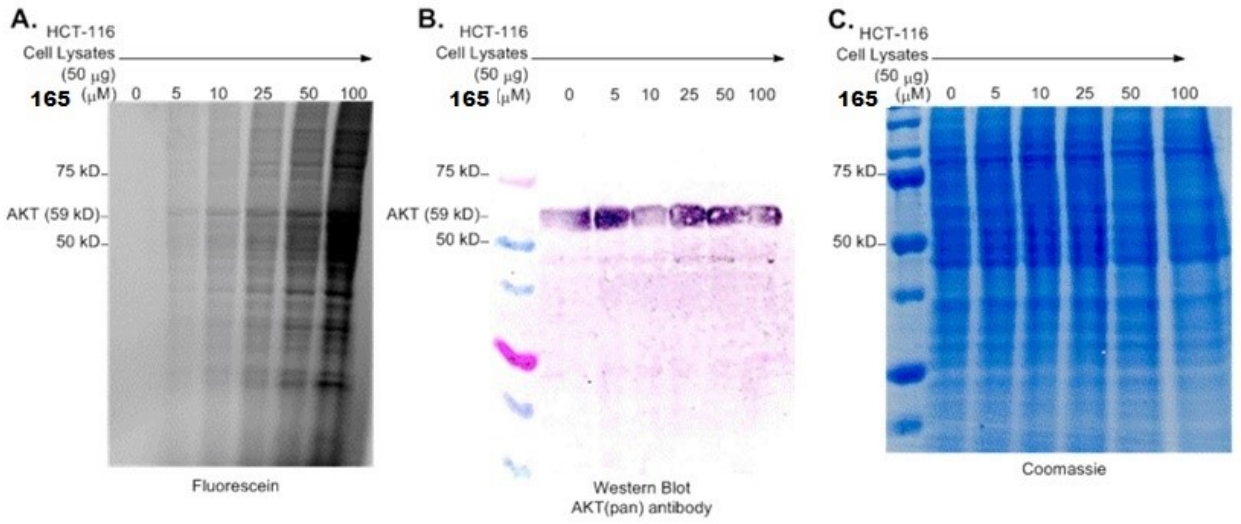

Figure 76: Labeling of AKT in HCT-116 cell lysates by compound **165**

Figure 76 shows that the major band labeled by the probe **165** corresponds to the molecular weight of AKT, as is shown by the western Blot (**Figure 76**, **B**). This shows that additional bands are labeled, especially at higher concentrations and that non-specific labeling occurs. The compound **148** displays non-specific labeling in cells lysates, hence, despite the vinyl ketone electrophile being highly potent and selective for AKT over PKAα, it cannot be used for further elaboration because of its non-selective binding to proteins.

3.4: Synthesis and Biological Activity of the second set of compounds

Our approach to develop covalent inhibitors for AKT till now was to focus on identification of an appropriate electrophile by structural elements from the C-terminal end of the Hamilton compound **121**. This led us to identify the vinyl ketones **148** and **151**, which were potent inhibitors of AKT and were highly selective for AKT against PKAα. However, in a cellular context, we found that these compounds displayed non selective labeling of other proteins in the cell. To address this issue of improving selectivity for AKT over other proteins we chose to shift our focus from the electrophile and examine rest of the substrate binding site. Our new approach was:

- Dial down the reactivity of the electrophile so that it would not react indiscriminately with other proteins in the cell.
- Include additional binding elements from reported inhibitors, so that the non-covalent interactions from the inhibitor provide more selectivity for AKT.

We envisioned that using an electrophile that had moderate to low reactivity towards Cys310 in AKT would make it less susceptible for indiscriminate labelling. Compound **133** has an IC_{50} of 1.11 μM towards AKT. Hence, we decided to use the α-iodoacetamide electrophile and also prepare and screen the α-bromo and α-chloro electrophiles. **TPCK** has been used traditionally as an active site label for serine proteases (**Figure 77**). It has been shown by mass spectrometry to label Cys310 in AKT1 and no inhibition of AKT was seen *in vitro* in concentrations up to 500 μM[184, 185]. Thus, we decided to use the phenylalanine chloromethyl ketone core as an electrophile.

For additional binding elements, we included the N-terminal fragment of the Hamilton inhibitor **121**. We did not include the 3-naphthyl group from the *p*-amino benzoic acid fragment in the α-haloacetamide compounds for the ease of synthesis, rationalizing that this fragment can be included for later analogues if the compounds were active. For the α-chloromethyl ketone analogues, we used a phenyl group at that position instead (**Figure 77**).

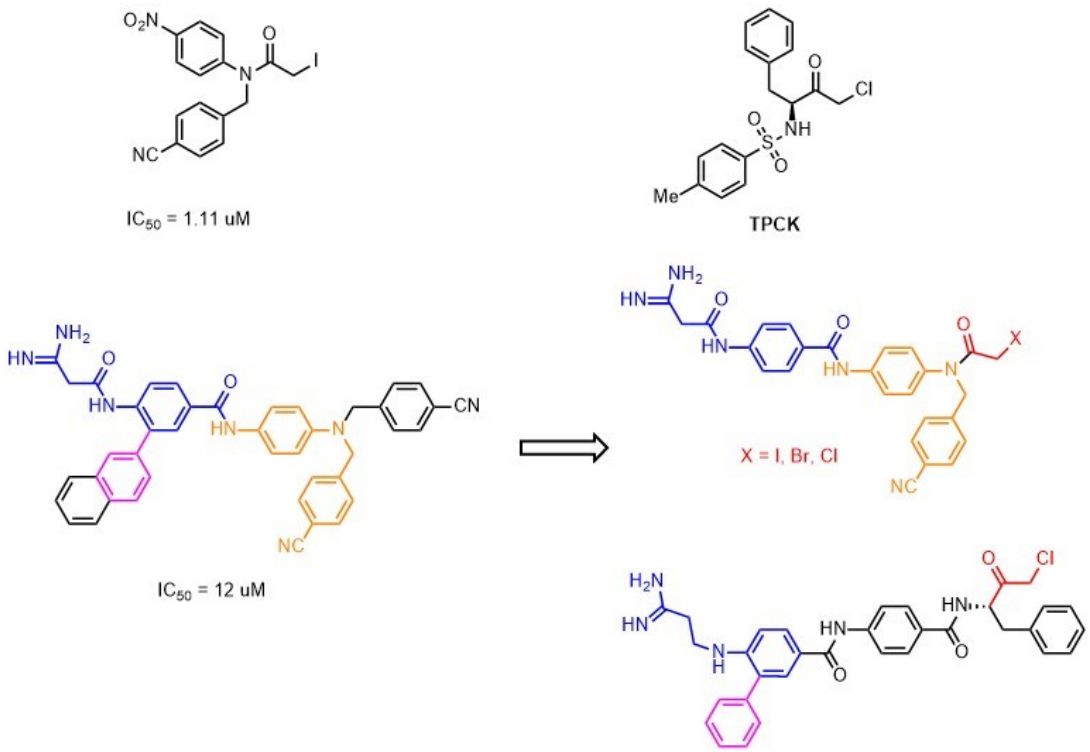

Figure 77: Rationale for second set of compounds

As a control analog, we decided to prepare the compounds **198** and **203** (**Figure 78**). Compound **198** would give us a qualitative estimate of electrophilicity of the α-chloromethyl ketone against AKT. Compound **203** would give clues about the non-covalent interactions with AKT. It was designed as a hybrid, based on the GSK3β peptide and Hamiltons peptidomimetic **121**.

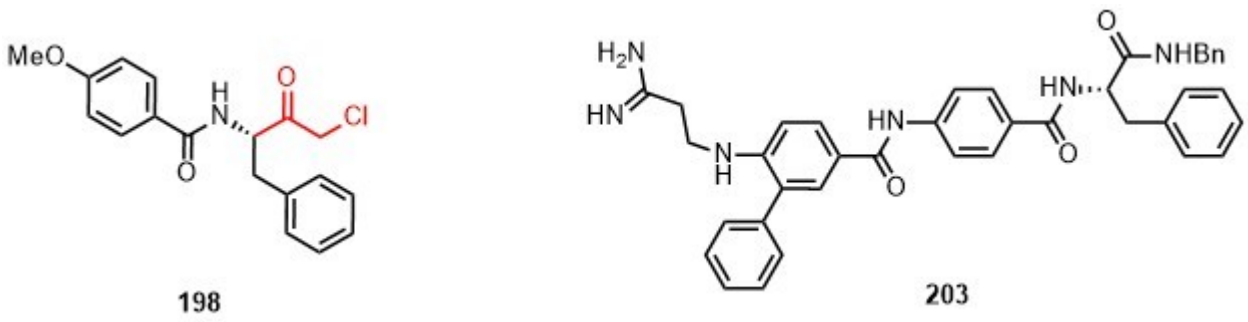

Figure 78: Control compounds

3.4.1: Synthesis of the α-haloacetamide compounds

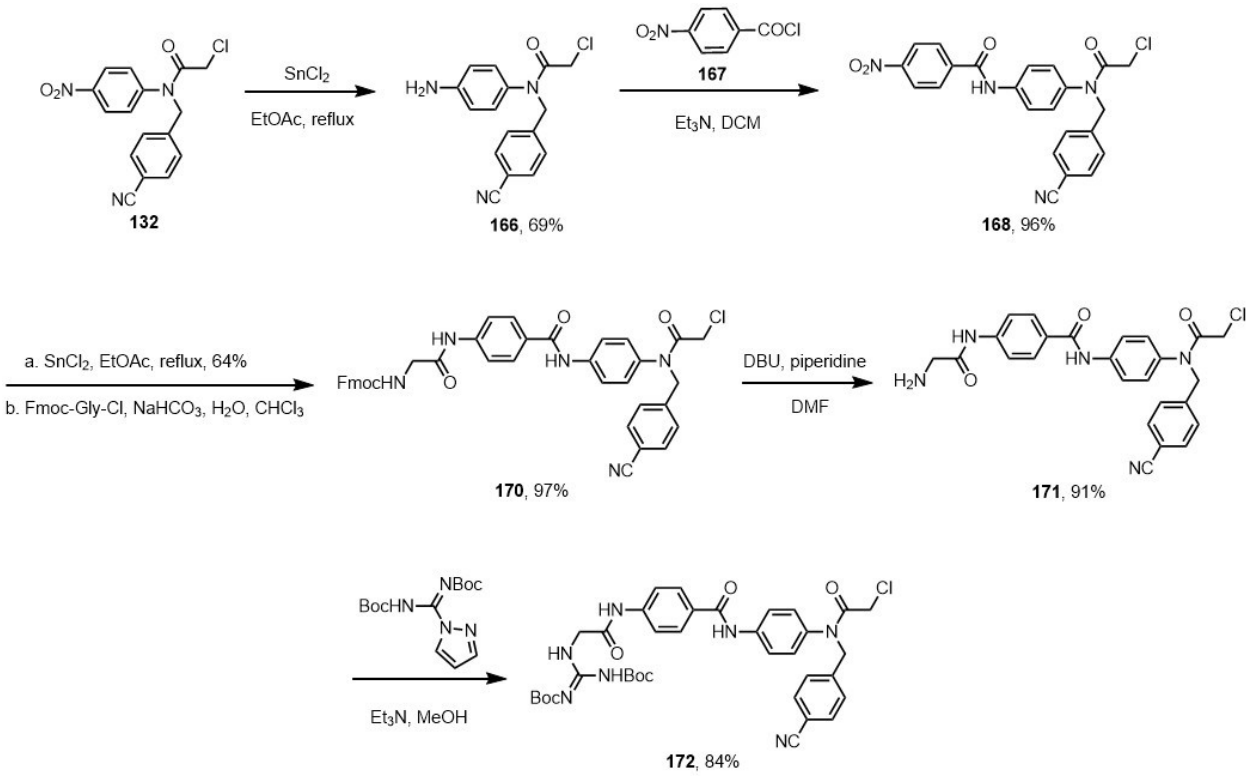

Figure 79: Synthesis of intermediate **172**

Our synthetic routes to these compounds was designed such that the steps were linear and more fragments were added from the C-terminal to the N-terminal end. This route would be successful only if the electrophile that would be installed in the beginning would

survive all the synthetic conditions leading to the product. Gratifyingly, the α-chloro acetamide was stable enough to be installed from the start of the synthetic route and be carried till the end. The more reactive α-bromo and α-iodo could be synthesized under Finkelstein conditions at the penultimate step in the route. We started the synthesis of the α-haloacetamides from the intermediate **132** that was previously prepared (**Figure 79**). The para-nitro group was reduced in refluxing tin chloride to give the aniline **166**, which was coupled with 4-nitrobenzoic acid by acid-chloride **167**, coupling to give compound **168**. The newly introduced para-nitro group was reduced with tin chloride in refluxing ethyl acetate to give the aniline **169**. The aniline was coupled with Fmoc-Gly-Cl using sodium bi-carbonate as the base in a mixture of water and chloroform to give the Fmoc-protected compound **170**. The protecting group Fmoc was removed using base and the primary amine was coupled to the Diboc protected amidine reagent: *N,N'*-Di-Boc-1H-pyrazole-1-carboxamidine in methanol, with triethylamine as the base to give the compound **172**. The Diboc-protecting group was removed under acidic conditions using TFA to give the α-chloro acetamidate **173** (**Figure 80**). The α-chloro group was exchanged either to a bromo or iodo under Finkelstein conditions by refluxing it with sodium bromide or sodium iodide in acetone to give compounds **174** and **176**. The Diboc-protecting group was removed under acidic conditions to give the final compounds **175** and **177.**

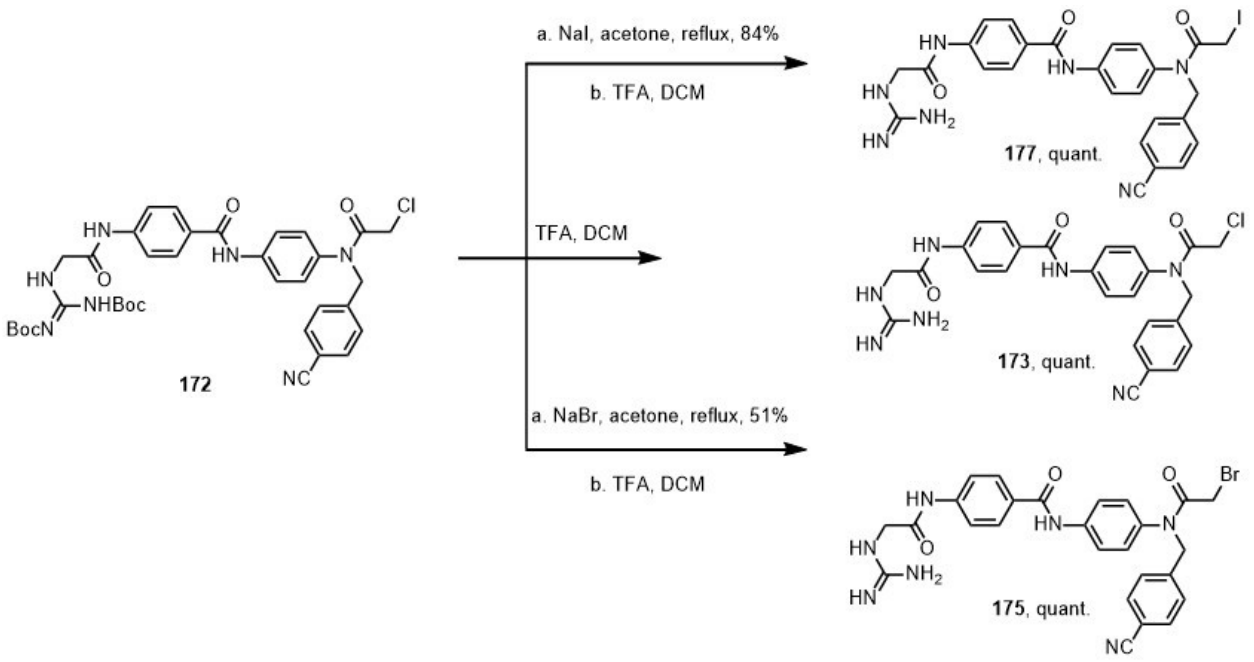

Figure 80: Synthesis of the α-haloacetamides **173**, **175** and **177**

3.4.2: Synthesis of the α-chloromethyl ketone compounds and control compounds

To synthesize the chloromethyl ketone compounds, we had to synthesize the N-terminal fragment of the Hamilton's compound **187** separately and then couple it with the C-terminal chloromethyl ketone fragment. We tried to prepare these compounds in an analogous manner as that of the α-haloacetamides, but the α-chloromethyl ketone electrophile was too reactive and did not survive the reaction conditions.

Our synthetic route starts with the preparation of the N-terminal binding fragment **187** (**Figure 81**). Starting from 3-bromo-4-nitrobenzoic acid **178**, the carboxylic acid was protected as a *tert*-butyl ester using *tert*-Butyl 2,2,2-trichloroacetamidate and the Lewis acid boron trifluoride diethyl etherate to give compound **179**. Other common reaction conditions like *tert*-butanol and EDCI or *tert*-butyl bromide did not give any product. Suzuki reaction with phenylboronic acid catalyzed by palladium-

tetrakistriphenylphosphine was carried out to give compound **180**. The *tert*-butyl protecting group was removed with acid to give compound **181**. Using standard acid chloride coupling the fragment benzyl 4-amino benzoate was coupled to the acid **181** to give the amide **182**. The nitro group was reduced with tin chloride in refluxing ethyl acetate to give the aniline **183**. To this intermediate *N*-Boc-2-aminoacetaldehyde was coupled by reductive amination using sodium cyanoborohydride as the reductant to give compound **184**. The *N*-Boc group was removed using acid and the amidine fragment was coupled using the reagent *N,N'*-Di-Boc-1H-pyrazole-1-carboxamidine with triethylamine as the base to give compound **186**. The benzyl protecting group was removed using catalytic hydrogenation using palladium on carbon to get the fragment **187**.

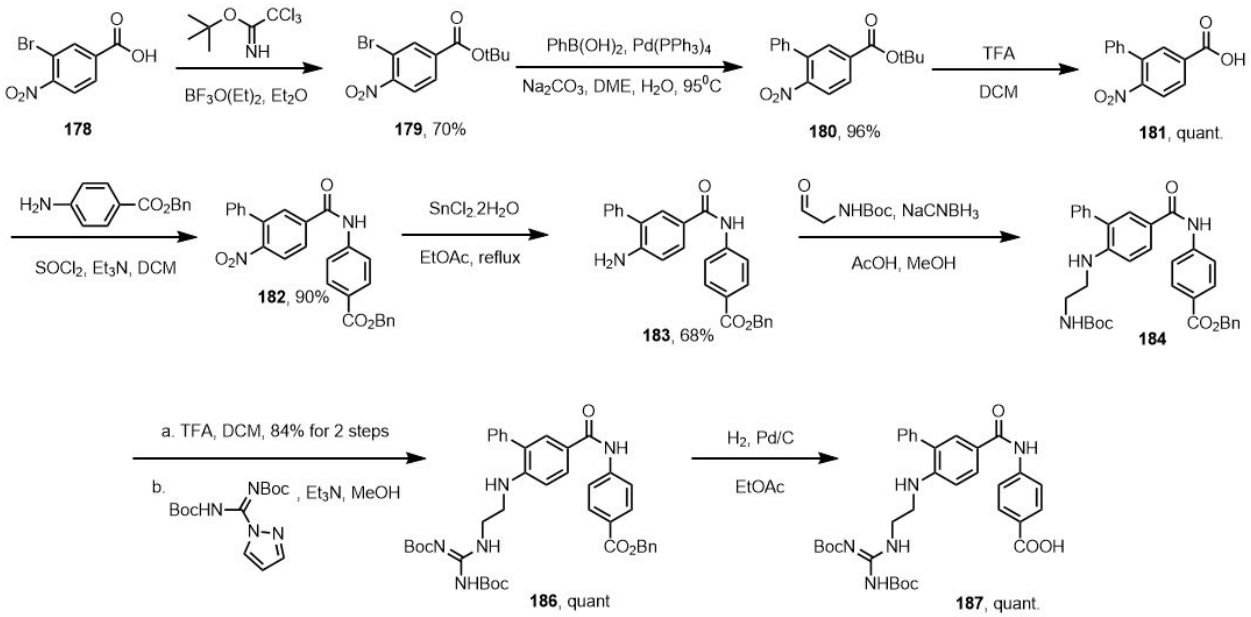

Figure 81: Synthesis of the fragment **187**.

We prepared the phenylalanine chloromethylketone **189** as described in **Figure 82**. Starting from Boc-Phe-OH **146** was converted into the α-diazoketone **188** with diazomethane. The intermediate mixed anhydride is initially formed with isobutyl

chloroformate, which forms the α-diazoketone **188** in 95% on treatment with a diazomethane solution in ether. Compound **188** is hydrolyzed by hydrochloric acid in dioxane to give compound **189** in quantitative yield.

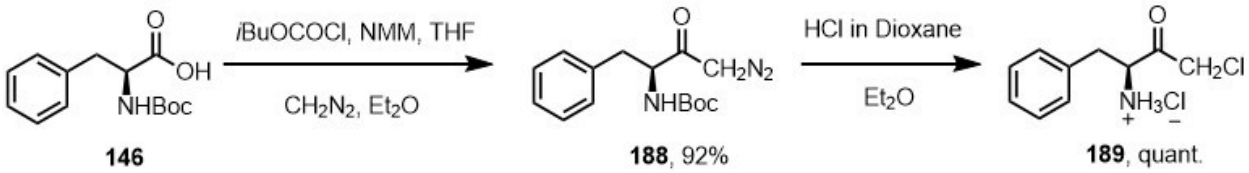

Figure 82: Preparation of the α-diazoketone **189**

Much to our consternation, subsequent attempts to couple α-chloromethyl ketone **189** with the Hamilton fragment **187** under standard peptide coupling conditions led to exhaustive degradation and no isolable product was detected on TLC. We tried various peptide coupling reagents like carbodiimides, mixed anhydrides and phosphonium/uronium based salts, but no reaction condition tried gave product (**Figure 83**).

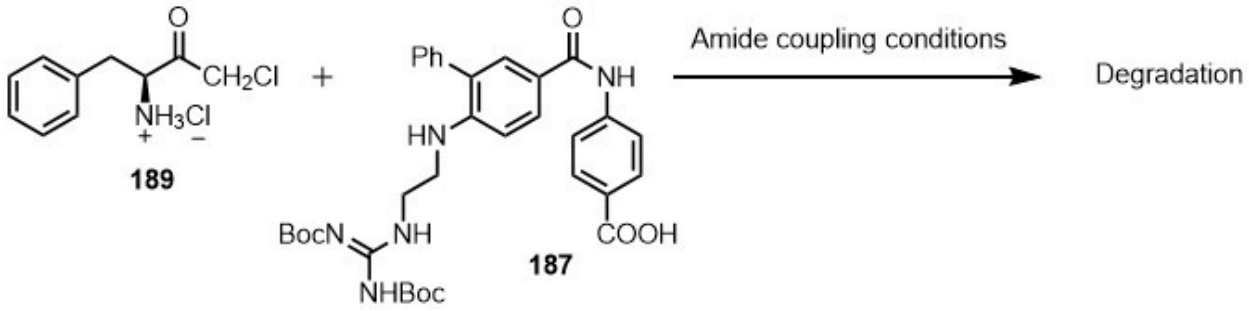

Figure 83: Attempted amide coupling of the α-chloromethyl ketone

We reasoned that peptide coupling reactions were not progressing because that the compound **189** is not stable to base due of the presence of the electrophilic α-chloromethyl ketone moiety. Also, we did not find any reports in literature where the

phenylalanine chloromethylketone **189** was coupled to any small molecule carboxylic acid substrates except in solid phase peptide coupling procedures where 6-10 equivalents of **189** was used. Therefore, we decided to reduce the ketone to the halohydrin, making the primary alkyl chloride much less reactive, and then carrying out the oxidation of the secondary alcohol to the ketone in the end stage to reveal the electrophile.

As described in **Figure 84**, we selectively hydrolyzed the α-diazoketone to α-chloromethyl ketone in presence of the *N*-Boc group by addition of 1.5 equiv of HCl in dioxane at -20^{0}C, giving compound **190** in quantitative yield. The secondary alcohol was reduced using sodium borohydride in methanol and the *N*-Boc group was deprotected using trifluoroacetic acid to give the halohydrin **192**.

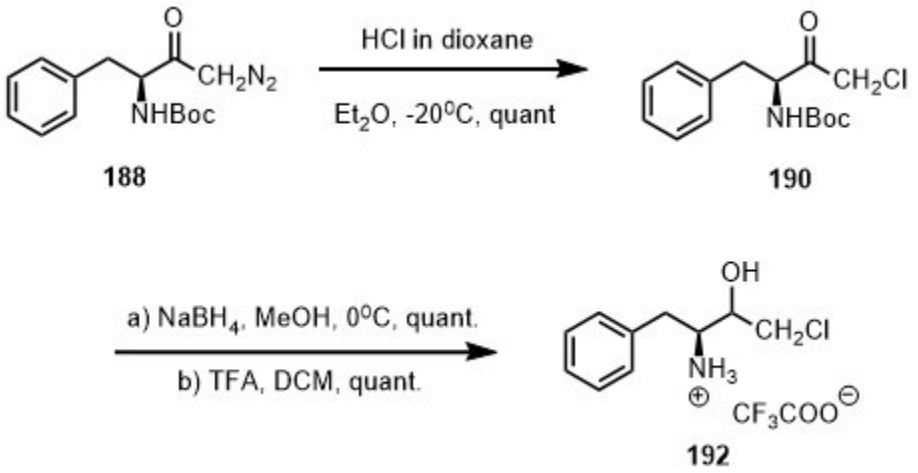

Figure 84: Synthesis of compound **192**

In the next step, this compound was reacted with the Hamilton fragment **187** using the peptide coupling reagent PyBOP and Hunigs base in dichloromethane overnight (**Figure 85**). Much to our surprise, the amide **193** was obtained as a diastereomeric mixture epimeric at the secondary alcohol in 90% yield. The secondary alcohol was oxidized to

the ketone using Dess-Martin periodane and the *N*-Boc protecting groups on the guanidine were removed under acidic conditions to give **195** in quantitative yield.

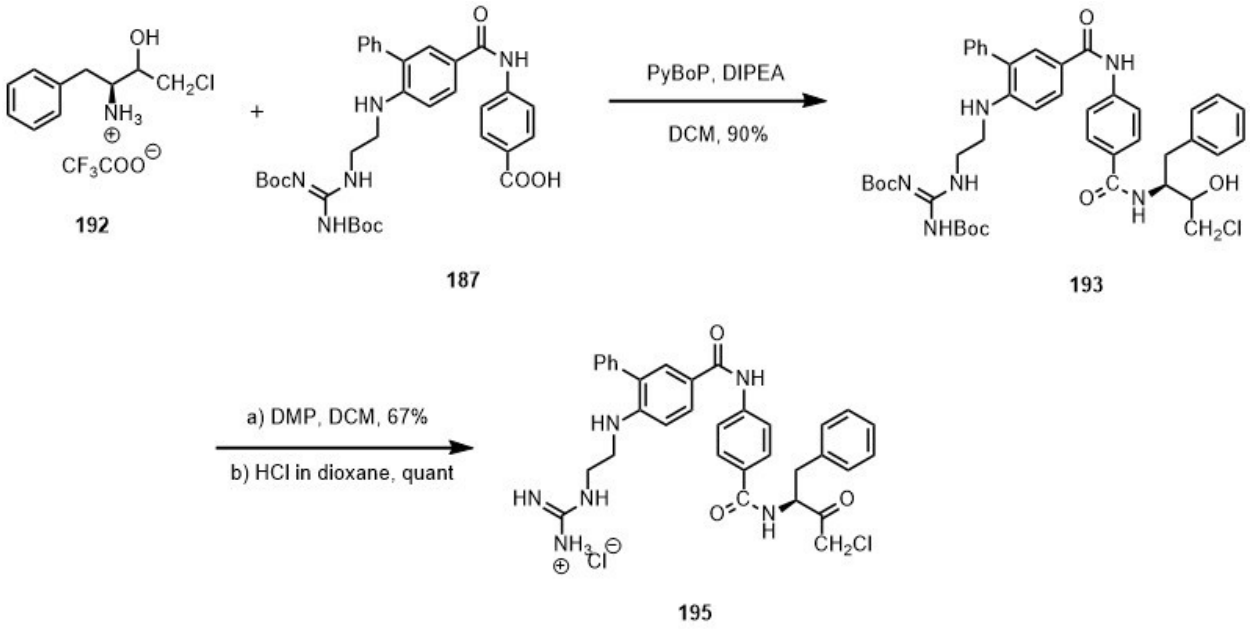

Figure 85: Synthesis of the α-chloromethyl ketone **195**

Bolstered by our above mentioned success in coupling the α-chloromethyl ketone, we prepared the control compound **198** in a similar fashion (**Figure 86**). 4-methoxybenzoic acid **196** was coupled to the halohydrin **192** using the peptide coupling reagent PyBOP and Hunigs base to give the compound **197** in 91% yield. This secondary alcohol was oxidized to the ketone using Dess-Martin periodane in dichloromethane to give **198** in 50% yield.

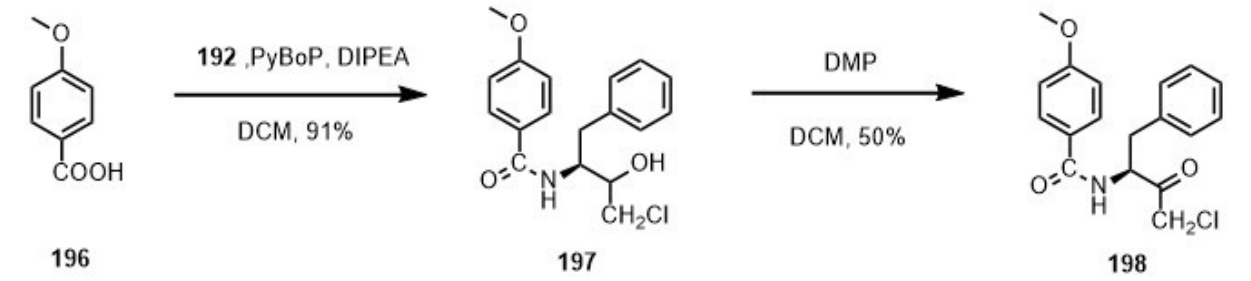

Figure 86: Synthesis of the control compound **198**

Next, we prepared the control analog **203**, which is a hybrid between GSK3β and the Hamilton's compound **121** as described in **Figure 87**. Compound **200** was prepared by a standard EDCI coupling between benzylamine **199** and Boc-Phe-OH **146** to give the product in 75% yield. The *N*-Boc group was removed under acidic conditions and was coupled to Hamilton's fragment **187** using the peptide coupling reagent PyBOP and Hunig's base to give the amide **202** in 80% yield, following which the *N*-Boc protecting groups on the guanidine were removed under acidic conditions to give **203** in quantitative yield.

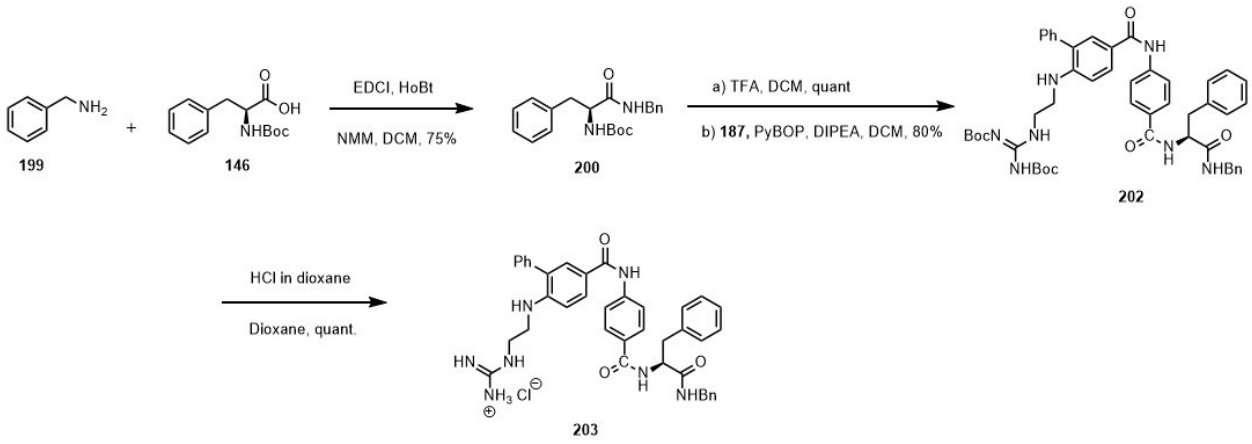

Figure 87: Synthesis of the control analog **203**

3.4.3: Biochemical evaluation of full-length compounds and controls

We evaluated this second set of compounds by the Z-LYTE assay for AKT inhibition as described earlier and the results are shown in **Table 10**.

Table 10: IC_{50} of second set of compounds

Compound	AKT1 IC_{50} (μM)
173	>100
175	>100
177	>100
195	0.578
198	>25
203	>25

3.5: Results and discussion

Based on the second set of compounds that were prepared and evaluated, the most active compound turned out to be **195** with an IC_{50} of 0.578 μM. This compound is derived from the GSK3β peptide sequence (Phe10 from ^{3}GRPRTTSFAE^{12}) with the N-terminal portion of the Hamilton non-covalent analog **121** and the chloromethyl ketone electrophile appended to the C-terminal phenylalanine. The compound **198**, which has the phenylalanine chloromethyl ketone electrophile coupled with a *p*-methoxybenzoic acid has an IC_{50} > 25 μM. This indicates that the phenylalanine chloromethyl ketone by itself is not a potent inhibitor of AKT and our results are in line with the activity reported for **TPCK** for inhibition of AKT[184, 185]. The non-covalent control analog **203** also has an IC_{50} > 25 μM, indicating that the chloromethyl ketone electrophile is necessary for inhibition. The α-haloacetamides **173**, **175**, **177** were not active with IC_{50}s > 100 μM. This indicates that the 3-position phenyl substituent in the N-terminal portion is important for guiding the compound into the substrate binding pocket of AKT or the sequence that we used to attach the electrophile was not optimal.

Our design and selection within the first set of compounds involved utilizing only the C-terminal portion of the Hamilton compound **121** and screening various electrophiles. This led to the selection of the most potent electrophile that had only minimal fragments of the Hamilton compound **121** to guide selectivity. The major downfall of this approach was, that by including minimal binding elements of the Hamilton compound, we focused our identification of compounds solely based on the reactivity of the electrophile, leading to a compound that was potent for AKT but not selective in a cellular context. Our design concept for the second set of compounds synthesized involved dialing down the reactivity of the electrophile so that it would not display non-selective binding and including either most of the binding elements of the Hamilton compound **121** or a hybrid between the GSK3β peptide and the Hamilton compound **121**. For this purpose, we used the α-haloacetamides and the α-chloromethyl ketone as electrophiles, which are much milder in comparison with the vinyl-ketone, and inclusion of the whole N-terminal binding fragment of Hamilton's compound **121**. This led to the identification of **195** as a potent sub-micromolar inhibitor of AKT. Further experiments have to be done to discern the selectivity of this compound for AKT, but we expect **195** to be selective towards AKT in a cellular context because of the relatively milder reactivity of the chloromethyl ketone electrophile in comparison to the vinyl-ketone and inclusion of additional binding elements from Hamilton compound **121** and GSK3β peptide.

3.6: Future work

1. Compound **195** was identified as a potent sub-micromolar inhibitor of AKT. Before we move on to optimizing the structure and analyzing reactivity and selectivity patterns, we plan to confirm the mechanism of action of the compound. The IC_{50}

of the inactivated electrophile (**204**, **Figure 88**), where the methyl-ketone is used instead, will confirm a covalent mechanism of action. Mass spectrometry with labeled AKT will indicate the residue that is covalently modified by **195**. We expect Cys310 to be labeled based on the labeling of Cys310 by **TPCK**.

2. To test the selectivity of the compound among other kinases especially within the AGC kinase family, **195** must be tested in a kinase selectivity screen assay. The data from this kinase panel will determine whether **195** is selective as an AKT inhibitor. To evaluate the cellular selectivity of **195** among other kinases we propose to do a protein profiling experiment. Compound **205**, which has an alkyne functional handle substituted on the 3/4-position of the phenyl will be prepared. Selection of this 3-position is based on the observation that a naphthyl group in compound **121** increases affinity. We will incubate this compound with cell lysates and subject the lysates to copper-promoted click conditions using a fluorescent azide tag. Visualizing these lysates on a SDS-page gel will determine other proteins labeled by compound **205**.
3. Finally, optimizing the potency and selectivity of the compound towards AKT can be done by further chemical manipulation. The reactivity of the electrophile can be further dialed down if needed by using a fluoromethyl ketone. The affinity of the compound can be increased by using further binding elements from Hamilton's compound **121,** i.e., substituting the phenylalanine to 4-cyanophenylalanine, phenyl for a naphthyl, and or changing the ethylamine linker to a glycine linker. These optimizations are shown as compound **206**, and are expected to yield a compound that will be more potent/selective for AKT.

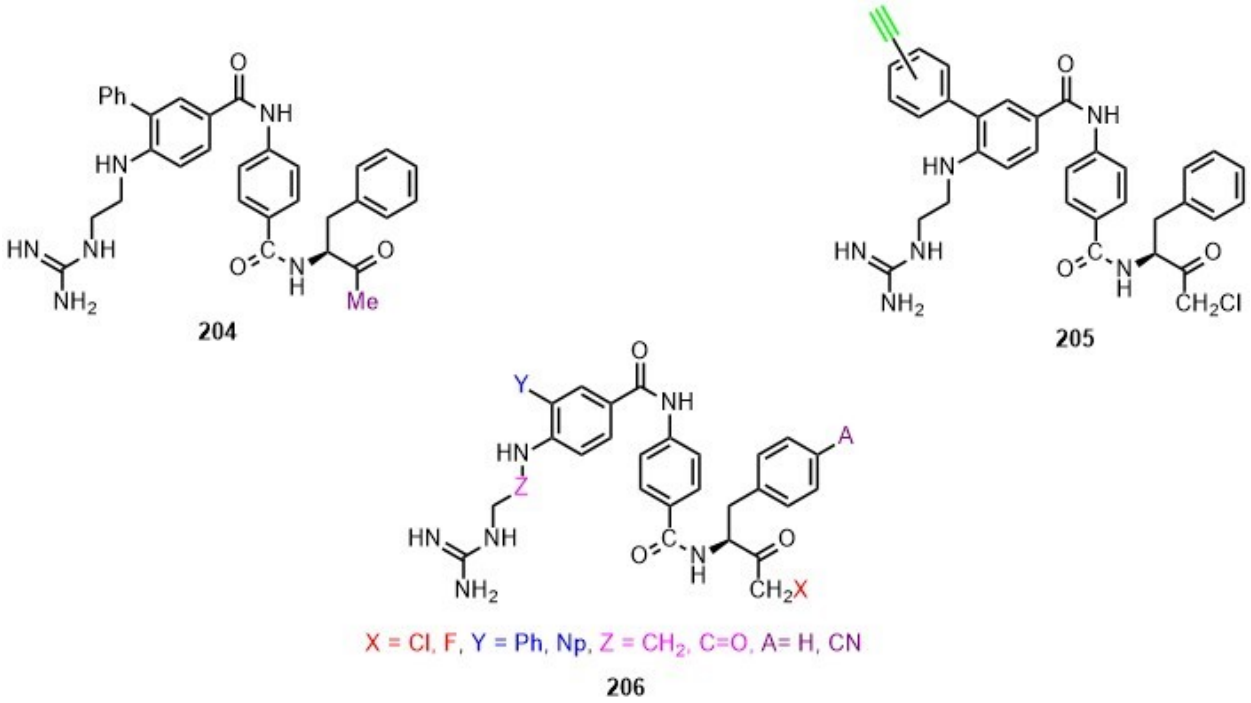

Figure 88: Future analogues of Compound **195** to be prepared.

CHAPTER 4: EXPERIMENTALS

4.1 Experimental for Flavone-based analogues inspired by the natural product simocyclinone D8 as DNA gyrase inhibitors.

4.1.1 Chemistry Experimentals

Chemical reagents and solvents were purchased from Sigma-Aldrich (MO, USA), Alfa-Aesar (MA, USA), Fisher Scientific (PA, USA). Analytical Thin Layer Chromatography (TLC) was performed using silica gel GHLF plates (Analtech Inc., DE, USA). Flash chromatography was performed on TELEDYNE ISCO CombiFlash® Rf instrument using RediSep Rf Normal-phase Flash Columns (4-gm, 12-gm, 24-gm or 40-gm). ^{1}H NMR and ^{13}C NMR spectra were recorded on a Bruker TopSpin 400 MHz using deuterated chloroform ($CDCl_3$) or methanol (CD_3OD). All chemical shifts are reported as δ in units of parts per million (ppm) relative to chloroform and methanol residual peaks at 7.26 and 3.31 respectively (^{1}H NMR spectra); 77.16 and 49.00 respectively (^{13}C NMR spectra). The data is reported as: chemical shifts (ppm), multiplicity (s = singlet, d = doublet, dd = doublet of doublets, t = triplet, q = quartet, m = multiplet), coupling constant(s) (Hz) and integral values. Electrospray ionization (ESI) mass spectra were obtained from Perkin Elmer Flexar UPLC/AxION2 TOF Mass Spectrometer.

General procedures

A. Procedure for N-phthalylglycine acid chloride couplings with anilines and deprotection

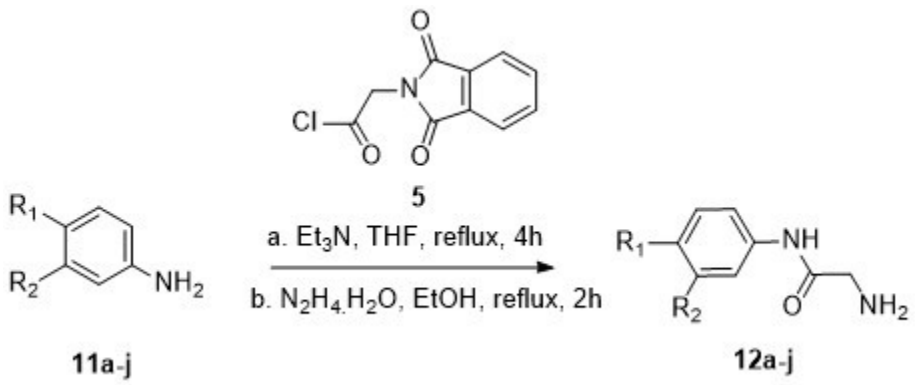

a. To a suspension of N-phthaloylglycine **5** (1.0 equiv) in chloroform (0.2 M) was added thionyl chloride (1.5 equiv). The reaction mixture was refluxed for 4 hours, after which the solution was concentrated *in vacuo*. The mixture was then taken in THF (0.4 M) and cooled down to 0 °C in an ice bath. To this was added a solution of the suitably functionalized aniline **11a-j** (1.2 equiv) and triethylamine (2.0 M) in THF (0.4 M). The reaction mixture was then refluxed overnight, following which it was diluted with ethyl acetate and washed subsequently with 1 N HCl and saturated $NaHCO_3$. The ethyl acetate layer was concentrated *in vacuo* and the crude was used in the next step without purification.

b. To a solution of the crude from the previous step in ethanol (0.2 M) was added hydrazine hydrate (2.0 equiv). The reaction mixture was refluxed for 2 hours and the resulting thick suspension was filtered over celite and washed with ethyl acetate. The filtrate was concentrated and was purified by column chromatography (silica gel, methanol/dichloromethane, 10% v/v) to give the desired amine **12a-j**.

B. Procedure for amide couplings

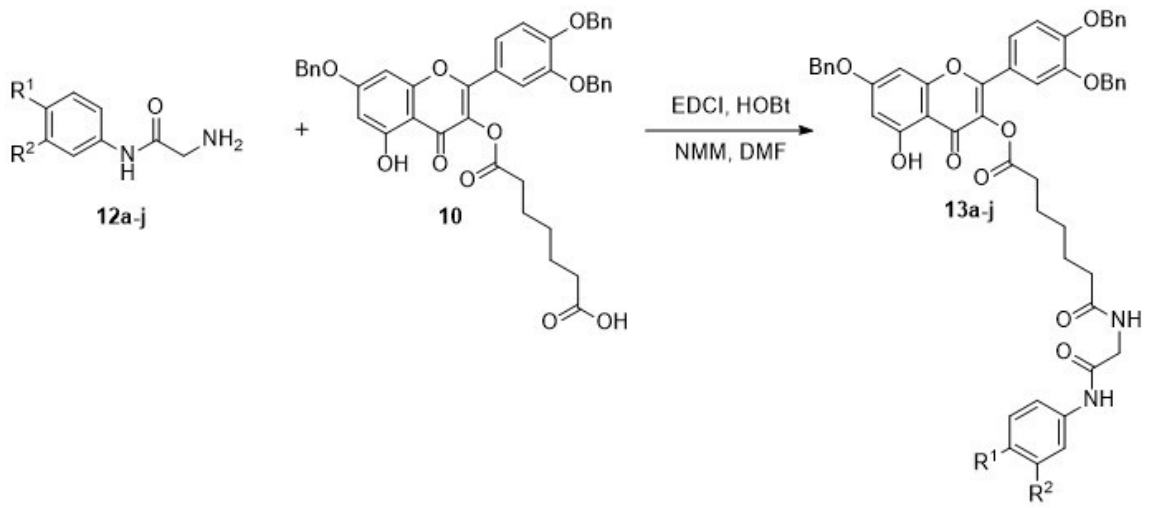

To a solution of the acid **10** (1.0 equiv) in DMF (0.4 M) was added EDCI (1.3 equiv), HOBt (1.1 equiv) and NMM (2.0 equiv). The reaction mixture was stirred for 30 minutes, followed by addition of the amine **12a-j** (1.0 equiv) in DMF (0.4 M). The mixture was stirred overnight, after which it was diluted with ethyl acetate and washed with excess 1 N HCl solution. The ethyl acetate layer was dried over sodium sulfate and concentrated *in vacuo* and was purified by column chromatography (silica gel, methanol/dichloromethane, 5% v/v) to give the desired amide **13a-j**.

C. Procedure for removal of silyl protecting groups

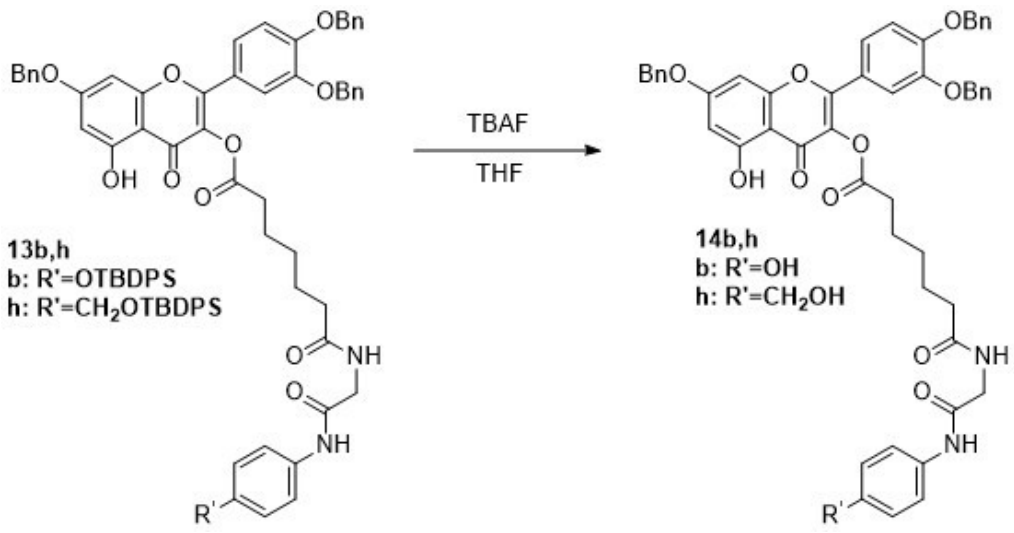

To a solution of the amide **13b, h** in THF (0.1 M) was added a 1 M solution of TBAF in THF (3.0 equiv). The reaction mixture was stirred at room temperature overnight and was diluted with ethyl acetate and washed with saturated ammonium chloride solution. The ethyl acetate layer was concentrated *in vacuo* and was purified by column chromatography (silica gel, methanol/dichloromethane, 10% v/v) to give the desired alcohol **14b** and **14h**.

D. Procedure for the removal of benzyl protecting groups

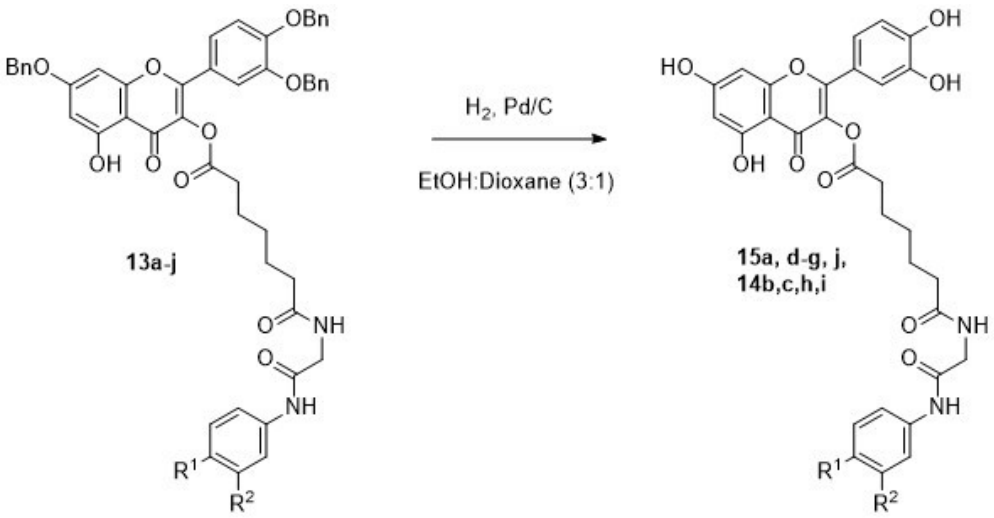

To a solution of the amide **13a-j** in ethanol:dioxane (3:1), was added 5% Pd/C (25% w/w). The reaction mixture was stirred overnight in an atmosphere of hydrogen (balloon pressure). The mixture was then filtered over celite and was purified by column chromatography (silica gel, methanol/dichloromethane, 10% v/v) to give the desired phenol **15a, 15d-g, 15j, 14b-c, 14h-i** .

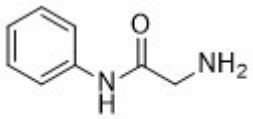

12a

2-Amino-N-phenylacetamide (12a): Compound **12a** was prepared according to general procedure **A** and was obtained in 75% overall yield (0.113 g, 0.73 mmol). ^{1}H NMR (400 MHz, CD_3OD) δ 7.56 (d, J=7.8, 2H) 7.63 (t, 2H), 7.42 (t, 1H), 3.42 (s, 2H).

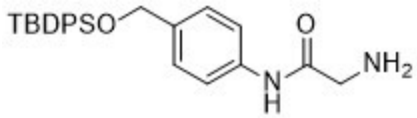

12b

2-Amino-N-(4-((tert-butyldiphenylsilyloxy)methyl)phenyl)acetamide (12b): Compound **12b** was prepared according to general procedure A and was obtained in 67% yield (0.42 g, 1.0 mmol). ^{1}H NMR (400 MHz, CD_3OD) *δ* 7.53 (d, *J=8*, 2H), 7.45-7.36 (m, 10H), 7.27 (d, *J=8*, 2H), 4.72 (s, 2H), 3.46 (s, 2H), 1.07 (s, 9H).

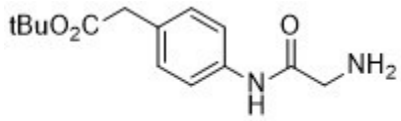

12c

***t*ert-butyl 2-(4-(2-aminoacetamido)phenyl)acetate (12c):** Compound **12c** was prepared according to general procedure A and was obtained in 72% yield (0.319 g, 1.2 mmol). ^{1}H NMR (400 MHz, CD_3OD) *δ* 7.53 (d, *J=9*, 1H), 7.38 (d, *J=8*, 1H), 7.19 (dd, *J1=8, J2=9,* 2H), 3.59 (s, 2H), 3.49 (s, 1H), 3.43 (s, 1H), 1.44 (d, *J=7*, 9H).

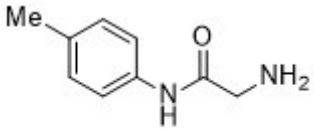

12d

2-amino-N-(p-tolyl)acetamide (12d): Compound **12d** was prepared according to general procedure A and was obtained in 64% yield (0.35 g, 2.13 mmol). ^{1}H NMR (400 MHz, $CDCl_3$) *δ* 9.31 (br. s., 1H), 7.47 (d, *J* = 8.30 Hz, 2H), 7.12 (d, *J* = 8.30 Hz, 2H), 3.43 (s, 2H), 2.31 (s, 3H).

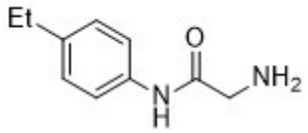

12e

2-amino-N-(4-ethylphenyl)acetamide (12e): Compound **12e** was prepared according to general procedure A and was obtained in 76 % yield (0.27 g, 1.51 mmol). ^{1}H NMR (400 MHz, $CDCl_3$) δ 6.66 (d, J = 8.53 Hz, 2H), 6.48 (d, J = 8.53 Hz, 2H), 3.06 (s, 2H), 2.08 (q, J = 7.61 Hz, 2H), 0.66 (t, J = 7.53 Hz, 3H).

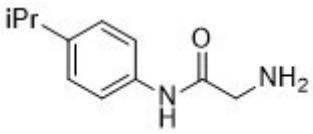

12f

2-amino-N-(4-isopropylphenyl)acetamide (12f): Compound **12f** was prepared according to general procedure A and was obtained in 69% yield (0.31 g, 1.61 mmol). ^{1}H NMR (400 MHz, $CDCl_3$) δ 7.21 (d, J = 8.30 Hz, 2H), 7.00 (d, J = 8.28 Hz, 2H), 3.58 (s, 2H), 2.86 (td, J = 6.93, 13.99 Hz, 1H), 1.18 (d, J = 7.03 Hz, 6H).

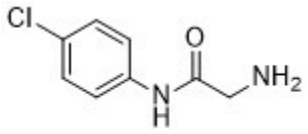

12g

2-amino-N-(4-chlorophenyl)acetamide (12g): Compound **12g** was prepared according to general procedure A and was obtained in 73% yield (0.137 g, 0.74 mmol). ^{1}H NMR

(400 MHz, $CDCl_3$) δ 9.42 (br. s., 1H), 7.53 (d, *J* = 8.78 Hz, 2H), 7.26 (d, *J* = 8.80 Hz, 2H), 3.44 (s, 2H).

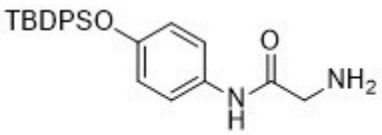

12h

2-Amino-N-(4-(tert-butyldiphenylsilyloxy)phenyl)acetamide (12h): Compound **12h** was prepared according to general procedure A and was obtained in 61% yield (0.3 g, 0.74mmol). ^{1}H NMR (400 MHz, $CDCl_3$) δ 7.43-7.34 (m, 10H), 6.87 (d, *J=9*, 2H), 6.78 (d, *J=9*, 2H), 3.6 (s, 2H), 1.1 (s, 9H).

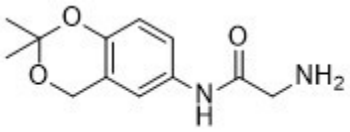

12i

2-Amino-N-(2,2-dimethyl-4H-benzo[d][1,3]dioxin-6-yl)acetamide (12i): Compound **12i** was prepared according to general procedure A and was obtained in 80% yield (0.289 g, 1.22 mmol). ^{1}H NMR (400 MHz, CD_3OD) δ 6.99 (dd, *J1=2, J2=6*, 1H), 6.89 (d, *J=2,* 1H), 6.86 (d, *J=8*, 1H), 4.87 (s, 2H), 3.57 (s, 2H), 1.52 (s, 6H).

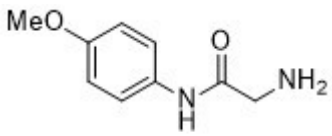

12j

2-amino-N-(4-methoxyphenyl)acetamide (12j): Compound **12j** was prepared according to general procedure A and was obtained in 79% yield (0.175 g, 0.97 mmol). ^{1}H NMR (400 MHz, $CDCl_3$) δ 9.24 (br. s., 1H), 7.52 (d, *J* = 9.00 Hz, 2H), 6.88 (d, *J* = 9.00 Hz, 2H), 3.80 (s, 3H), 3.47 (s, 2H), 1.89 (br. s., 2H).

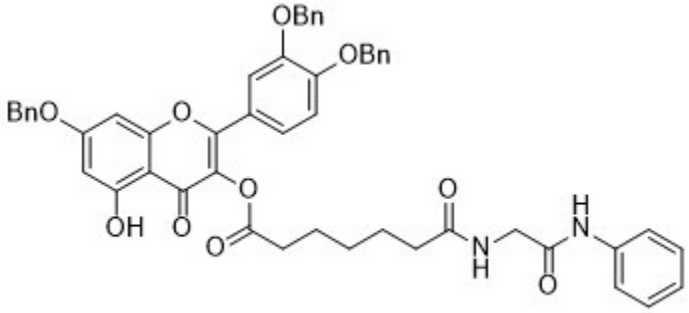

13a

7-(Benzyloxy)-2-(3,4-bis(benzyloxy)phenyl)-5-hydroxy-4-oxo-4H-chromen-3-yl 7-oxo-7-(2-oxo-2-(phenylamino)ethylamino)heptanoate (13a): Compound **13a** was prepared according to general procedure **B** and was obtained in 79% yield (0.45 g, 0.53 mmol). ^{1}H NMR (400 MHz, $CDCl_3$) δ 7.84 (dd, *J1*=2.3, *J2*=*6,* 1H), 7.81 (d, *J*=*2*, 1H), 7.64 (d, *J*=*8*, 2H), 7.42-7.24 (m, 17H), 7.1 (t, *J*=*7.78*, 1H), 7.02 (d, *J*=*9*, 1H), 6.5 (d, *J*=*2,* 1H), 6.44 (d, *J*=*2*, 1H), 5.14 (s, 2H), 5.13 (s, 2H), 5.04 (s, 2H), 4.08 (d, *J*=*5*, 2H), 2.55 (t, *J*=*7*, 2H), 2.2 (t, *J*=*7*, 2H), 1.75-1.61 (m, 4H), 1.43-1.35 (m, 2H).

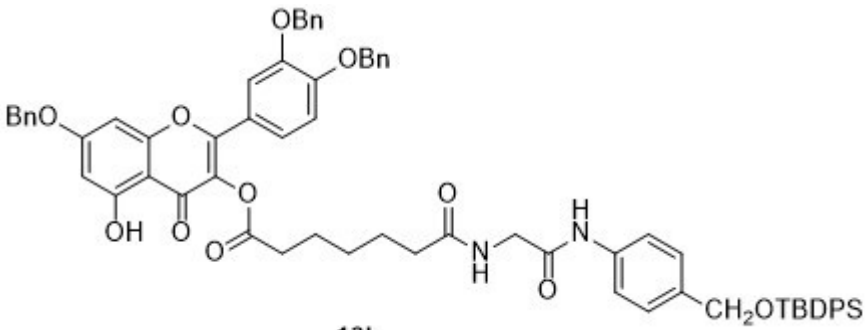

13b

7-(Benzyloxy)-2-(3,4-bis(benzyloxy)phenyl)-5-hydroxy-4-oxo-4H-chromen-3-yl 7-(2-(4-((tert-butyldiphenylsilyloxy)methyl)phenylamino)-2-oxoethylamino)-7-oxoheptanoate (13b): Compound **13b** was prepared according to general procedure **B** and was obtained in 82% yield (0.582 g, 0.53 mmol). ^{1}H NMR (400 MHz, $CDCl_3$) δ 7.68 (dd, *J1=1, J2=7*, 2H), 7.49 (d, *J=8*, 2H), 7.44-7.28 (m, 27H), 7.02 (d, *J=9*, 1H), 6.51 (d, *J=2*, 1H), 6.45 (d, *J=2*, 1H), 5.15 (s, 2H), 5.13 (s, 2H), 5.04 (s, 2H), 4.72 (s, 2H), 4.07 (d, *J=6*, 2H), 2.56 (t, *J=7*, 2H), 2.2 (t, *J=8*, 2H), 1.76-1.61 (m, 4H), 1.44-1.36 (m, 2H), 1.07 (s, 9H).

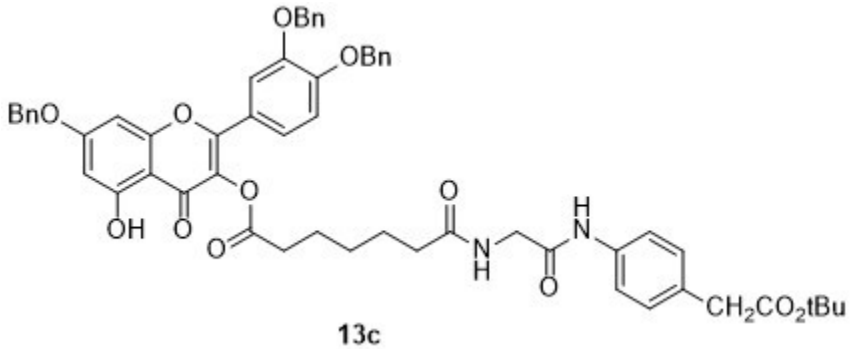

13c

7-(Benzyloxy)-2-(3,4-bis(benzyloxy)phenyl)-5-hydroxy-4-oxo-4H-chromen-3-yl 7-(2-(4-(2-tert-butoxy-2-oxoethyl)phenylamino)-2-oxoethylamino)-7-oxoheptanoate (13c): Compound **13c** was prepared according to general procedure **B** and was obtained

in 77% yield (0.48 g, 0.5 mmol). ^{1}H NMR (400 MHz, $CDCl_3$) δ 7.85 (dd, *J1=2.05, J2=6.65,* 1H), 7.8 (d, *J=2,* 1H), 7.48-7.2 (m, 19H), 7.02 (d, *J=9*, 1H), 6.5 (d, *J=2,* 1H), 6.44 (d, *J=2,* 1H), 5.15 (s, 2H), 5.13 (s, 2H), 5.06 (s, 2H), 4.07 (s, 2H), 3.47 (s, 2H), 2.54 (t, *J=8*, 2H), 2.26 (t, *J=8,* 2H), 1.7-1.61 (m, 4H), 1.42 (s, 9H), 1.33-1.21 (m, 2H).

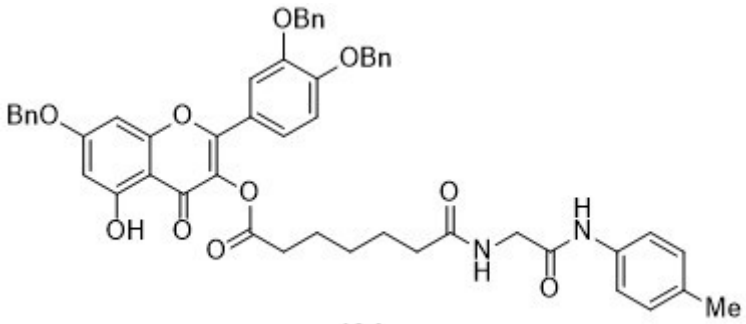

13d

7-(benzyloxy)-2-(3,4-bis(benzyloxy)phenyl)-5-hydroxy-4-oxo-4H-chromen-3-yl 7-oxo-7-((2-oxo-2-(p-tolylamino)ethyl)amino)heptanoate (13d): Compound **13d** was prepared according to general procedure **B** and was obtained in 53% yield (0.044 g, 0.051 mmol).

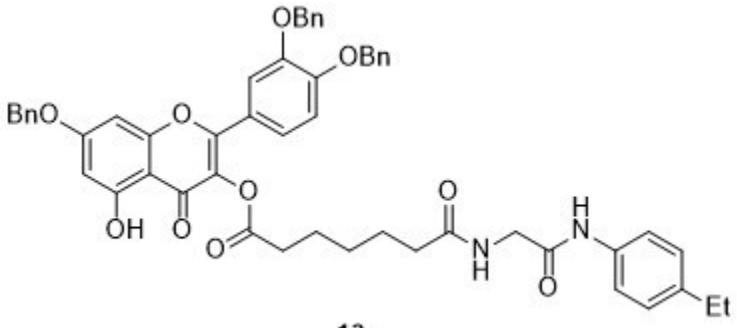

13e

7-(benzyloxy)-2-(3,4-bis(benzyloxy)phenyl)-5-hydroxy-4-oxo-4H-chromen-3-yl 7-((2-((4-ethylphenyl)amino)-2-oxoethyl)amino)-7-oxoheptanoate (13e): Compound **13e** was prepared according to general procedure **B** and was obtained in 83% yield (0.057 g, 0.058 mmol). ^{1}H NMR (400 MHz, CDCl3) δ 8.48 (br. s., 1H), 7.77 - 7.90 (m, 1H),

7.23 - 7.51 (m, 17H), 7.14 (d, *J* = 8.28 Hz, 2H), 7.03 (d, *J* = 8.78 Hz, 1H), 6.51 (d, *J* = 2.30 Hz, 1H), 6.45 (d, *J* = 2.26 Hz, 1H), 5.15 (d, *J* = 10.79 Hz, 4H), 5.07 (s, 2H), 4.10 (br. s., 2H), 2.47 - 2.68 (m, 4H), 2.28 (t, *J* = 7.50 Hz, 2H), 1.56 - 1.75 (m, 4H), 1.25 - 1.40 (m, 2H), 1.21 (t, *J* = 7.53 Hz, 3H).

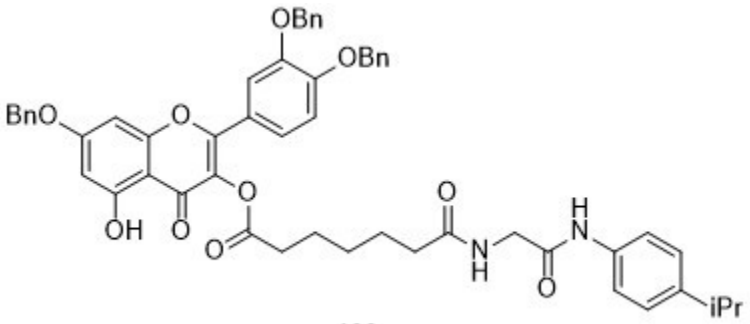

13f

7-(benzyloxy)-2-(3,4-bis(benzyloxy)phenyl)-5-hydroxy-4-oxo-4H-chromen-3-yl 7-((2-((4-isopropylphenyl)amino)-2-oxoethyl)amino)-7-oxoheptanoate (13f): Compound **13f** was prepared according to general procedure **B** and was obtained in 72% yield (0.05 g, 0.087 mmol). ^{1}H NMR (400 MHz, CDCl3) δ 8.36 (br. s., 1H), 7.76 - 7.90 (m, 1H), 7.25 - 7.49 (m, 17H), 7.15 - 7.24 (m, 2H), 6.98 - 7.11 (m, 1H), 6.48 - 6.54 (m, 1H), 6.45 (d, *J* = 2.26 Hz, 1H), 5.15 (d, *J* = 10.54 Hz, 4H), 5.07 (s, 2H), 4.08 (br. s., 2H), 2.81 - 2.95 (m, 1H), 2.55 (t, *J* = 7.53 Hz, 2H), 2.27 (t, *J* = 7.65 Hz, 2H), 1.58 - 1.79 (m, 4H), 1.26 - 1.32 (m, 2H), 1.20 - 1.25 (m, 6H).

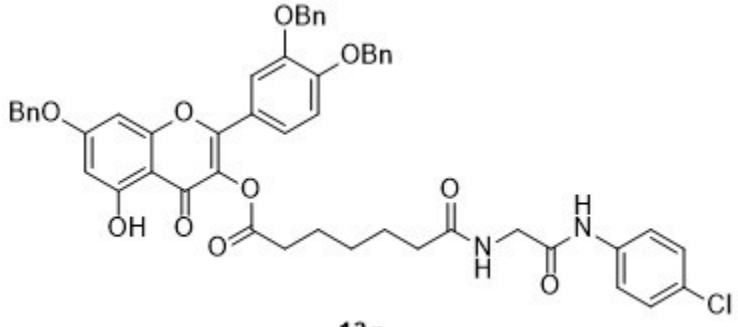

13g

7-(benzyloxy)-2-(3,4-bis(benzyloxy)phenyl)-5-hydroxy-4-oxo-4H-chromen-3-yl 7-((2-((4-chlorophenyl)amino)-2-oxoethyl)amino)-7-oxoheptanoate (13g): Compound **13g** was prepared according to general procedure **B** and was obtained in 46% yield (0.031 g, 0.035 mmol). ^{1}H NMR (400 MHz, $CDCl_3$) δ 12.61 (s, 1H), 8.69 (s, 1H), 7.76 - 7.87 (m, 2H), 7.21 - 7.51 (m, 19H), 7.03 (d, *J* = 8.80 Hz, 1H), 6.52 (d, *J* = 2.20 Hz, 1H), 6.46 (d, *J* = 2.20 Hz, 1H), 6.25 (t, *J* = 5.27 Hz, 1H), 5.06 - 5.20 (m, 4H), 5.03 (s, 2H), 4.06 (d, *J* = 5.27 Hz, 2H), 2.58 (t, *J* = 7.20 Hz, 2H), 2.20 (t, *J* = 7.40 Hz, 2H), 1.52 - 1.80 (m, 4H), 1.35 - 1.49 (m, 2H).

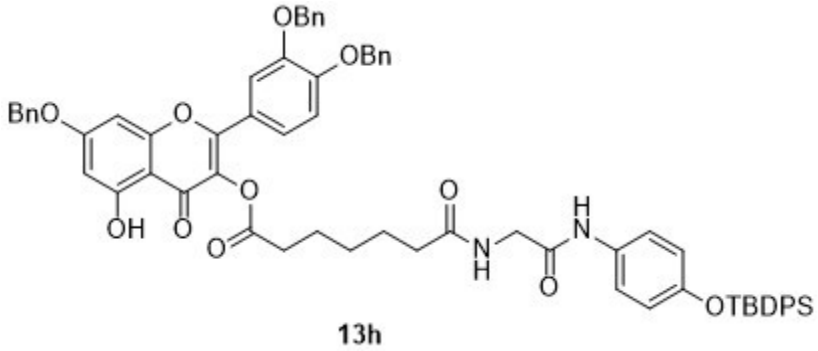

13h

7-(Benzyloxy)-2-(3,4-bis(benzyloxy)phenyl)-5-hydroxy-4-oxo-4H-chromen-3-yl 7-(2-(4-(tert-butyldiphenylsilyloxy)phenylamino)-2-oxoethylamino)-7-oxoheptanoate (13h): Compound **13h** was prepared according to general procedure **B** and was obtained in 67% yield (0.61 g, 0.55 mmol). ^{1}H NMR (400 MHz, $CDCl_3$) δ 7.7-7.68 (m, 2H), 7.42-7.21 (m, 29H), 6.7 (d, *J=8*, 1H), 6.5 (d, *J=2*, 1H), 6.44 (d, *J=2*, 1H), 5.14 (s, 2H), 5.13 (s, 2H), 5.03 (s, 2H), 3.98 (d, *J=5*, 2H), 2.54 (t, *J=7*, 2H), 2.17 (t, *J=2*, 2H), 1.73-1.58 (m, 4H), 1.39-1.35 (m, 2H), 1.08 (s, 9H).

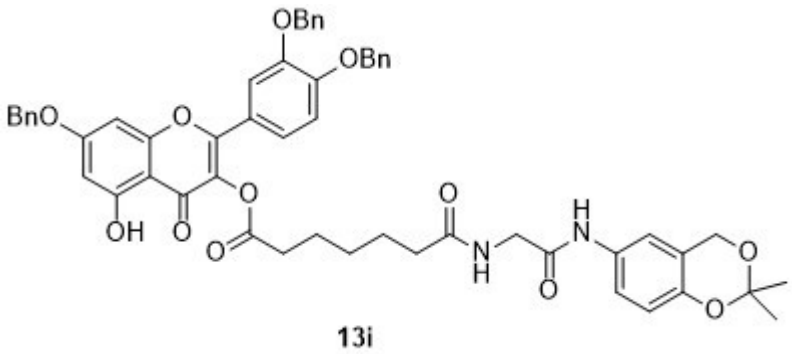

13i

7-(Benzyloxy)-2-(3,4-bis(benzyloxy)phenyl)-5-hydroxy-4-oxo-4H-chromen-3-yl 7-(2-(2,2-dimethyl-4H-benzo[d][1,3]dioxin-6-ylamino)-2-oxoethylamino)-7-oxoheptanoate (13i): Compound **13i** was prepared according to general procedure **B** and was obtained in 81% yield (0.512 g, 0.55 mmol). ^{1}H NMR (400 MHz, $CDCl_3$) δ 7.85 (dd, *J1=2, J2=7,* 1H), 7.8 (d, *J=2,* 1H), 7.42-7.3 (m, 17H), 7.12 (dd, *J1=2, J2=6,* 1H), 7.02 (d, *J=9,* 1H), 6.75 (d, *J=8,* 1H), 6.5 (d, *J=2,* 1H), 6.44 (d, *J=2,* 1H), 5.15 (s, 2H), 5.13 (s, 2H), 5.05 (s, 2H), 4.79 (s, 2H), 4.04 (d, *J=5,* 2H), 2.54 (t, *J=8,* 2H), 2.25 (t, *J=8,* 2H), 1.72-1.6 (m, 4H), 1.42-1.35 (m, 2H), 1.51 (s, 6H).

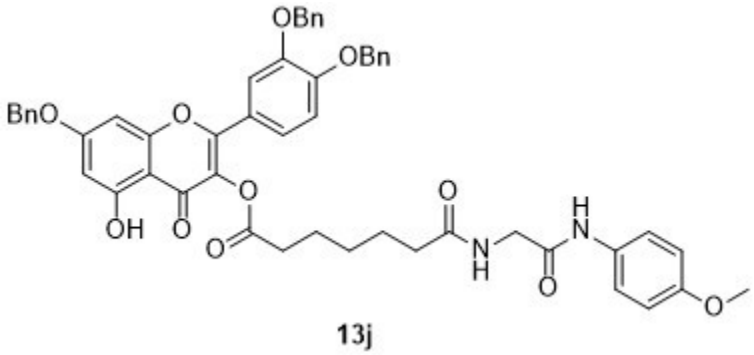

13j

7-(benzyloxy)-2-(3,4-bis(benzyloxy)phenyl)-5-hydroxy-4-oxo-4H-chromen-3-yl 7-((2-((4-methoxyphenyl)amino)-2-oxoethyl)amino)-7-oxoheptanoate (13j): Compound **13j** was prepared according to general procedure **B** and was obtained in 55%

yield (0.057 g, 0.065 mmol). ^{1}H NMR (400 MHz, CDCl3) *δ* 12.64 (s, 1H), 8.74 (s, 1H), 7.75 - 7.91 (m, 2H), 7.22 - 7.48 (m, 18H), 7.06 - 7.14 (m, 2H), 7.02 (d, *J* = 8.78 Hz, 1H), 6.51 (d, *J* = 2.01 Hz, 1H), 6.45 (d, *J* = 2.26 Hz, 1H), 5.03 - 5.17 (m, 6H), 4.10 (d, *J* = 5.02 Hz, 2H), 2.55 (t, *J* = 7.40 Hz, 2H), 2.29 (s, 3H), 2.22 (t, *J* = 7.40 Hz, 2H), 1.59 - 1.78 (m, 4H), 1.33 - 1.47 (m, 2H).

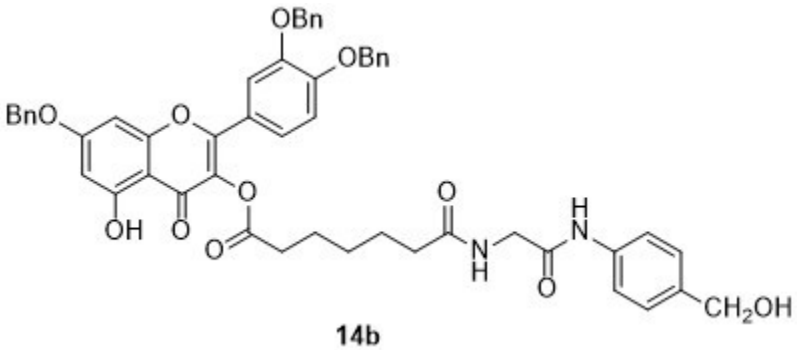

14b

7-(Benzyloxy)-2-(3,4-bis(benzyloxy)phenyl)-5-hydroxy-4-oxo-4H-chromen-3-yl 7-(2-(4-(hydroxymethyl)phenylamino)-2-oxoethylamino)-7-oxoheptanoate (14b): Compound **14b** was prepared according to general procedure **C** and was obtained in 67% yield (0.363 g, 0.41 mmol). ^{1}H NMR (400 MHz, $CDCl_3$) *δ* 7.79 (dd, *J1=2, J2=7,* 1H), 7.73 (d, *J=2,* 1H), 7.43-7.18 (m, 19H), 6.96 (d, *J=9*, 1H), 6.44(d, *J=2,* 1H), 6.38 (d, *J=2,* 1H), 5.09 (s, 2H), 5.07 (s, 2H), 4.99 (s, 2H), 4.56 (s, 2H), 4.01 (d, *J=6,* 2H), 2.47 (t, *J=7*, 2H), 2.2 (t, *J=8,* 2H), 1.65-1.54 (m, 4H), 1.44-1.36 (m, 2H).

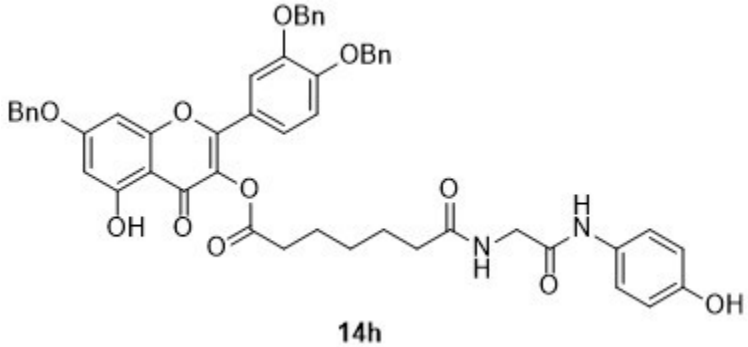

14h

7-(Benzyloxy)-2-(3,4-bis(benzyloxy)phenyl)-5-hydroxy-4-oxo-4H-chromen-3-yl 7-(2-(4-hydroxyphenylamino)-2-oxoethylamino)-7-oxoheptanoate (14h): Compound **14h** was prepared according to general procedure **C** and was obtained in 65% yield (0.317 g, 0.367 mmol). ^{1}H NMR (400 MHz, CD_3OD) *δ* 7.88 (dd, *J1=2, J2=7,* 1H), 7.79 (d, *J=2*, 1H), 7.53-7.2 (m, 20H), 6.71 (d, *J=2*, 1H), 6.43 (d, *J=2,* 1H), 3.98 (s, 2H), 2.56 (t, *J=7*, 2H), 2.27 (t, *J=7,* 2H), 1.72-1.6 (m, 4H), 1.44-1.42 (m, 2H).

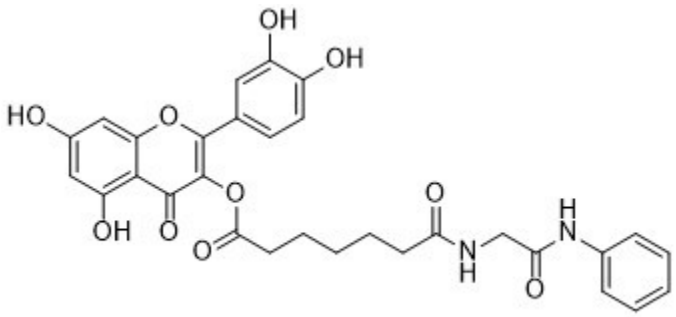

15a

2-(3,4-Dihydroxyphenyl)-5,7-dihydroxy-4-oxo-4H-chromen-3-yl7-oxo-7-(2-oxo-2-(phenylamino)ethylamino)heptanoate (15a): Compound **15a** was prepared according to general procedure **D** and was obtained in 43% yield (0.253 g, 0.44 mmol). ^{1}H NMR (400 MHz, CD_3OD) *δ* 7.99-7.96 (m, 1H), 7.89 (s, 1H), 7.52 (d, *J=8*, 2H), 7.28 (t, *J=7*, 2H), 7.1 (t, *J=7*, 1H), 7.02 (d, *J=9*, 1H), 6.39 (s, 1H), 4.0 (s, 2H), 2.66 (t, *J=7*, 2H), 2.36 (t, *J=7*, 2H), 1.82-1.71 (m, 4H) 1.57-1.51 (m, 2H). ^{13}C NMR (100 MHz, CD3OD) *δ* 177.3, 176.6, 175.9, 169.7, 165.6, 162.5, 158.2, 148.7, 148.0, 146.2, 139.5, 137.2, 129.8, 125.3, 124.1, 121.6, 121.2, 116.2, 116.0, 104.5, 99.2, 94.4, 70.6, 56.1, 44.0, 36.6, 34.6, 32.1, 30.6,

29.7, 29.5, 26.4, 25.6. HRMS (ESI) $C_{30}H_{28}N_2O_{10}$ *m/z* [M-H]$^-$ found 575.1686, expected 575.1665.

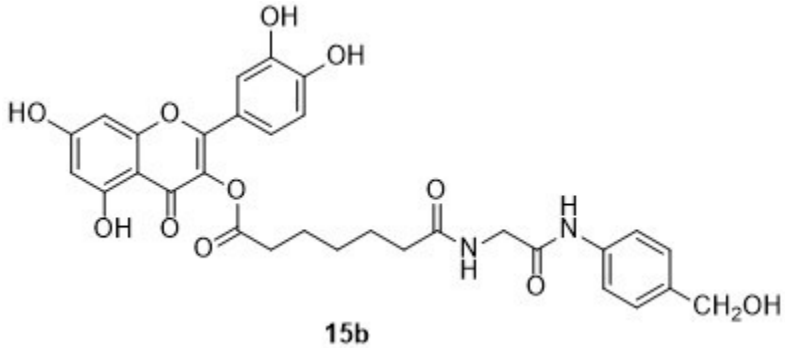

15b

2-(3,4-Dihydroxyphenyl)-5,7-dihydroxy-4-oxo-4H-chromen-3-yl7-(2-(4-(hydroxymethyl)phenylamino)-2-oxoethylamino)-7-oxoheptanoate (15b): Compound **15b** was prepared according to general procedure **D** and was obtained in 33% yield (0.241 g, 0.4 mmol). ^{1}H NMR (400 MHz, CD_3OD) *δ* 7.97 (dd, *J1=2, J2=7,* 1H), 7.88 (d, *J=2*, 1H), 7.38 (d, *J=8*, 2H), 7.07 (d, *J=8*, 2H), 7.01 (d, *J=9*, 1H), 6.37 (m, 1H), 6.17 (d, *J=2*, 1H), (3.98 (s, 2H), 2.64 (t, *J=5*, 2H), 2.35 (t, *J=7*, 2H), 1.81-1.71 (m, 4H), 1.54-1.5 (m, 2H). ^{13}C NMR (100MHz, DMSO-d6) *δ* 176.0, 172.5, 171.1, 164.0, 161.0, 167.6, 156.1, 150.8, 138.3, 138.2, 136.3, 136.2, 126.4, 122.7, 119.1, 116.8, 115.5, 98.2, 59.6, 54.8, 33.2, 33.1, 28.1, 28.0, 24.8, 24.2, 24.1, 20.3, 20.6. HRMS (ESI) $C_{31}H_{30}N_2O_{11}$ *m/z* [M-H]$^-$ found 605.1771, expected 605.1772.

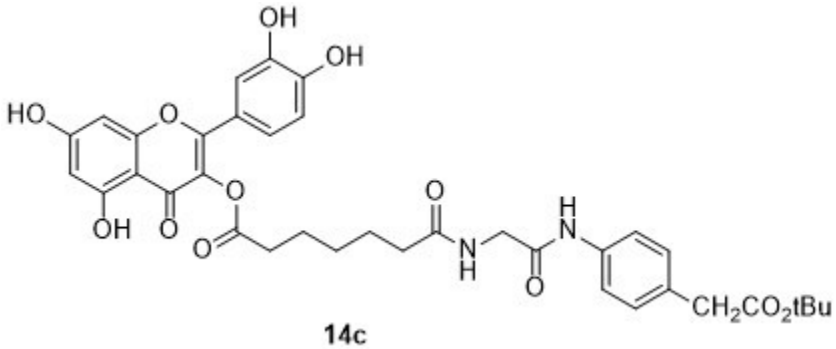

14c

2-(3,4-Dihydroxyphenyl)-5,7-dihydroxy-4-oxo-4H-chromen-3-yl7-(2-(4-(2-tert-butoxy-2-oxoethyl)phenylamino)-2-oxoethylamino)-7-oxoheptanoate (14c): Compound **14c** was prepared according to general procedure **D** and was obtained in 52% yield (0.248 g, 0.36 mmol). ^{1}H NMR (400 MHz, CD_3OD) *δ* 7.59 (d, *J=9*, 2H), 7.43 (d, *J=2*, 1H), 7.38 (dd, *J1=2, J2=6*, 1H), 7.29 (d, *J=8*, 2H), 7.01 (d, *J=8*, 1H), 6.53 (d, *J=2,* 1H), 6.339 (d, *J=2*, 1H), 4.09 (s, 2H), 3.58 (s, 2H), 2.76 (t, *J=7,* 2H), 2.4 (t, *J=8*, 2H), 1.86-1.76 (m, 4H), 1.55-1.52 (m, 2H), 1.52 (s, 9H).

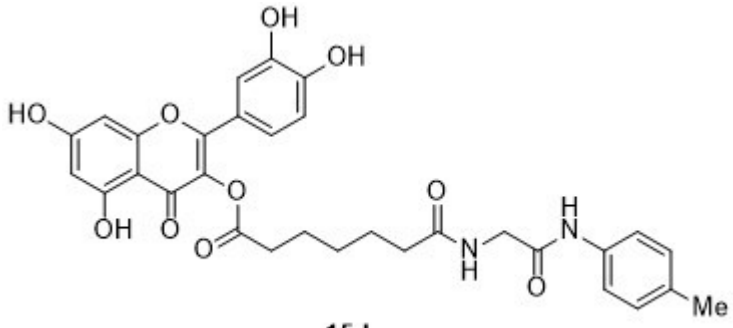

15d

2-(3,4-dihydroxyphenyl)-5,7-dihydroxy-4-oxo-4H-chromen-3-yl7-oxo-7-((2-oxo-2-(p-tolylamino)ethyl)amino)heptanoate (15d): Compound **15d** was prepared according to general procedure **D** and was obtained in 31% yield (0.043 g, 0.073 mmol). ^{1}H NMR (400 MHz, CD_3OD) *δ* 7.98 (dd, *J* = 1.63, 8.66 Hz, 1H), 7.81 - 7.91 (m, 1H), 7.32 - 7.44 (m, 2H), 6.95 - 7.15 (m, 3H), 6.39 (br. s., 1H), 6.12 - 6.22 (m, 1H), 3.99 (s, 2H), 2.66 (t, *J* = 7.30 Hz, 2H), 2.35 (t, *J* = 7.50 Hz, 2H), 2.27 (s, 3H), 1.67 - 1.85 (m, 4H), 1.47 - 1.60 (m, 2H).

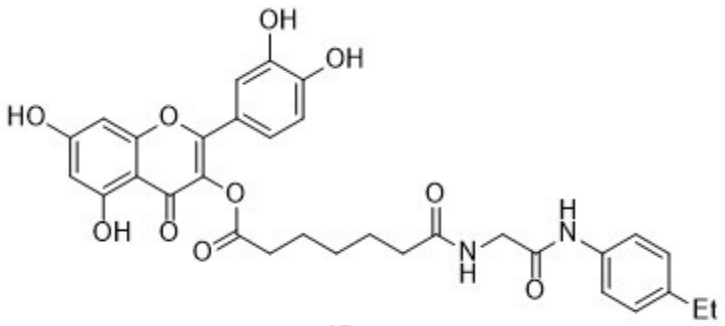

15e

2-(3,4-dihydroxyphenyl)-5,7-dihydroxy-4-oxo-4H-chromen-3-yl7-((2-((4ethylphenyl)amino)-2-oxoethyl)amino)-7-oxoheptanoate (15e): Compound **15e** was prepared according to general procedure **D** and was obtained in 41% yield (0.07 g, 0.116 mmol). ^{1}H NMR (400 MHz, DMSO-d_6) δ 12.40 (s, 1H), 9.83 (s, 1H), 8.11 (t, J = 5.65 Hz, 1H), 7.93 (dd, J = 2.26, 8.78 Hz, 1H), 7.85 (d, J = 2.26 Hz, 1H), 7.40 - 7.51 (m, 2H), 7.00 - 7.14 (m, 3H), 6.39 - 6.46 (m, 1H), 6.13 - 6.22 (m, 1H), 3.84 (d, J = 5.77 Hz, 2H), 2.50 - 2.63 (m, 4H), 2.18 (t, J = 7.40 Hz, 2H), 1.50 - 1.71 (m, 4H), 1.33 - 1.44 (m, 2H), 1.13 (t, J = 7.53 Hz, 3H). ^{13}C NMR (101 MHz, DMSO-d_6) δ 175.8, 172.6, 171.2, 167.6, 163.9, 160.5, 156.2, 150.8, 145.5, 138.6, 138.2, 136.5, 136.0, 127.9, 122.7, 122.1, 119.1, 116.8, 103.1, 98.2, 93.6, 42.5, 35.0, 30.6, 28.0, 27.6, 24.9, 24.1, 15.6, 15.1. HRMS (ESI) $C_{32}H_{32}N_2O_{10}$ *m/z* $[M+H]^+$ found 605.2038, expected 605.2135.

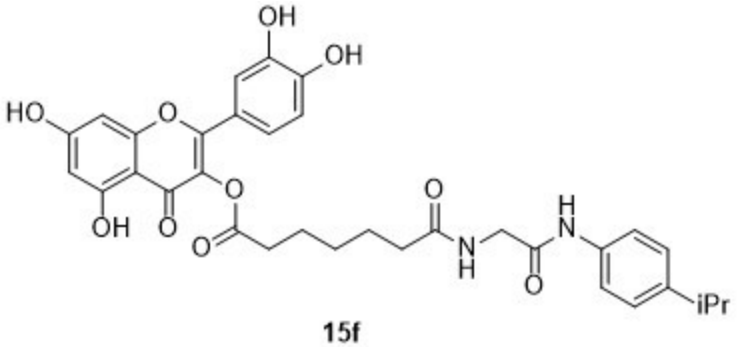

15f

2-(3,4-dihydroxyphenyl)-5,7-dihydroxy-4-oxo-4H-chromen-3-yl7-((2-((4-isopropylphenyl)amino)-2-oxoethyl)amino)-7-oxoheptanoate (15f): Compound **15f** was prepared according to general procedure **D** and was obtained in 46 % yield (0.09 g, 0.145 mmol). ^{1}H NMR (400 MHz, CD_3OD) *δ* 7.96 (dd, *J* = 2.26, 8.53 Hz, 1H), 7.80 - 7.89 (m, 1H), 7.38 - 7.45 (m, 2H), 7.07 - 7.17 (m, 2H), 7.01 (d, *J* = 8.78 Hz, 1H), 6.37 (d, *J* = 2.01 Hz, 1H), 6.12 - 6.21 (m, 1H), 3.99 (s, 2H), 2.78 - 2.89 (m, 1H), 2.65 (t, *J* = 7.30 Hz, 2H), 2.35 (t, *J* = 7.53 Hz, 2H), 1.68 - 1.85 (m, 4H), 1.46 - 1.58 (m, 2H), 1.14 - 1.24 (m, 6H). ^{13}C NMR (101 MHz, DMSO-d_6) δ 175.9, 172.5, 172.5, 172.5, 171.2, 171.0, 167.6, 164.0, 160.7, 160.7, 156.1, 150.8, 145.5, 145.2, 143.2, 138.2, 136.6, 136.0, 129.2, 126.3, 122.6, 122.0, 121.9, 119.2, 116.8, 103.0, 98.2, 93.5, 42.5, 34.9, 33.1, 33.1, 32.8, 28.0, 24.8, 24.1, 23.8. HRMS (ESI) $C_{33}H_{34}N_2O_{10}$ *m/z* $[M+H]^+$ found 619.2260, expected 619.2291.

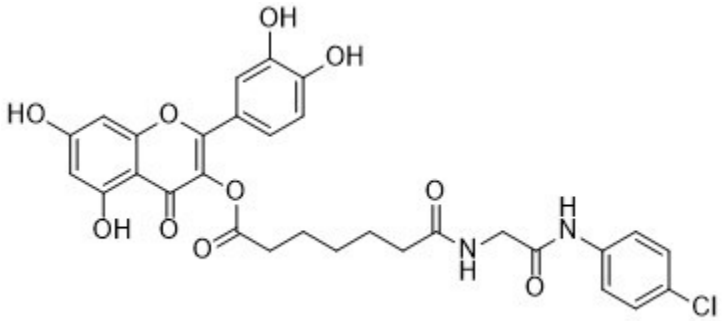

15g

2-(3,4-dihydroxyphenyl)-5,7-dihydroxy-4-oxo-4H-chromen-3-yl7-((2-((4-chlorophenyl)amino)-2-oxoethyl)amino)-7-oxoheptanoate (15g): Compound **15g** was prepared according to general procedure **D** and was obtained in 15% yield (0.02 g, 0.033 mmol). ^{1}H NMR (400 MHz, CD_3OD) *δ* 7.93 – 8.01 (m, 1H), 7.77 – 7.93 (m, 1H), 7.44 – 7.58 (m, 2H), 7.18 – 7.33 (m, 2H), 6.96 – 7.15 (m, 2H), 6.32 – 6.43 (m, 1H), 6.11 – 6.22 (m, 1H), 4.00 (d, *J* = 5.77 Hz, 2H), 2.66 (t, *J* = 7.30 Hz, 2H), 2.35 (t, *J* = 7.30 Hz,

2H), 1.64 – 1.87 (m, 4H), 1.54 (dt, *J* = 3.26, 7.53 Hz, 2H). ^{13}C NMR (101 MHz, CD3OD) δ 177.5, 176.8, 176.8, 165.7, 162.6, 158.4, 148.9, 148.2, 146.4, 138.6, 137.4, 134.1, 130.0, 129.9, 129.9, 125.4, 124.3, 122.7, 121.9, 121.4, 116.4, 116.2, 104.7, 99.4, 94.6, 44.2, 36.7, 36.7, 34.8, 29.8, 29.8, 26.5, 25.8.

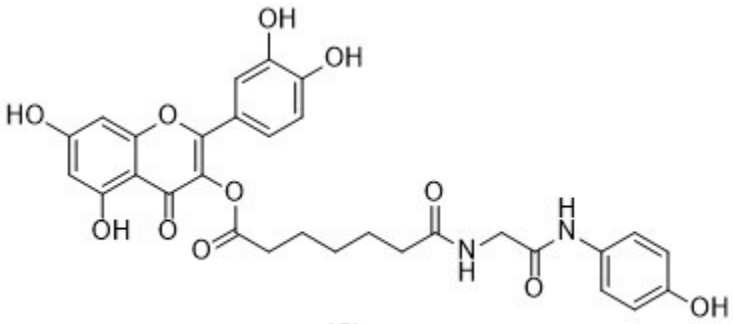

15h

2-(3,4-Dihydroxyphenyl)-5,7-dihydroxy-4-oxo-4H-chromen-3-yl7-(2-(4-hydroxyphenylamino)-2-oxoethylamino)-7-oxoheptanoate (15h): Compound **15h** was prepared according to general procedure **D** and was obtained in 34% yield (0.258 g, 0.43 mmol). ^{1}H NMR (400 MHz, CD_3OD) *δ* 7.99 (dd, *J1=2, J2=7*, 1H), 7.89 (d, *J=2*, 1H), 7.3 (d, *J=9*, 2H), 7.03 (d, *J=9,* 1H), 6.72 (d, *J=9,* 2H), 6.41 (d, *J=2*, 1H), 6.18 (d, *J=2*, 1H), 3.97 (s, 2H), 2.67 (t, *J=7*, 2H), 2.35 (t, *J=7*, 2H), 1.82-1.72 (m, 4H), 1.55-1.51 (m, 2H). ^{13}C NMR (100MHz, CD3OD) *δ* 177.1, 172.0, 165.1, 163.0, 158.7, 158.3, 153.2, 150.3, 148.1, 146.6, 130.5, 125.3, 124.7, 123.3, 122.3, 121.4, 118.6, 116.2, 104.1, 100.5, 98.3, 96.0, 94.1, 44.2, 36.7, 34.6, 26.3, 25.7, 25.5. HRMS (ESI) $C_{30}H_{28}N_2O_{11}$ *m/z* $[M-H]^-$ found 591.1591, expected 591.1615.

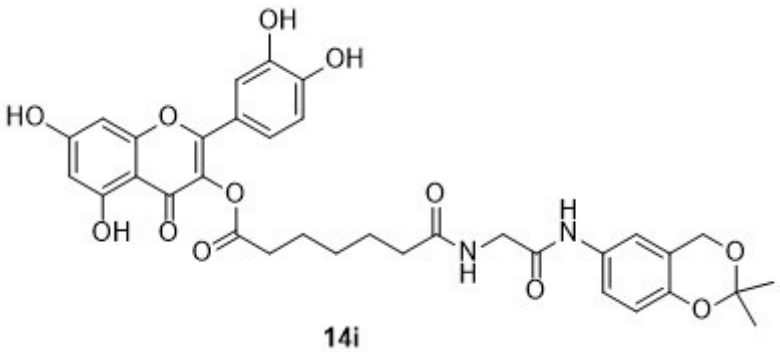

14i

2-(3,4-Dihydroxyphenyl)-5,7-dihydroxy-4-oxo-4H-chromen-3-yl7-(2-(2,2-dimethyl-4H-benzo[d][1,3]dioxin-6-ylamino)-2-oxoethylamino)-7-oxoheptanoate (14i): Compound **14i** was prepared according to general procedure **D** and was obtained in 57% yield (0.193 g, 0.29 mmol). ^{1}H NMR (400 MHz, CD_3OD) δ 7.32 (d, *J=2,* 1H), 7.28 (dd, *J1=2, J2=6*, 2H), 7.2 (dd, *J1=2, J2=6*, 1H), 6.91 (d, *J=8*, 1H), 6.7 (d, *J=9*, 1H), 6.42 (d, *J=2*, 1H), 6.23 (d, *J=2*, 1H), 4.91 (s, 2H), 3.97 (s, 2H), 2.66 (t, *J=7*, 2H), 2.3 (t, *J=8*, 2H), 1.76-1.66 (m, 4H), 1.48 (s, 6H), 1.46-1.4 (m, 2H).

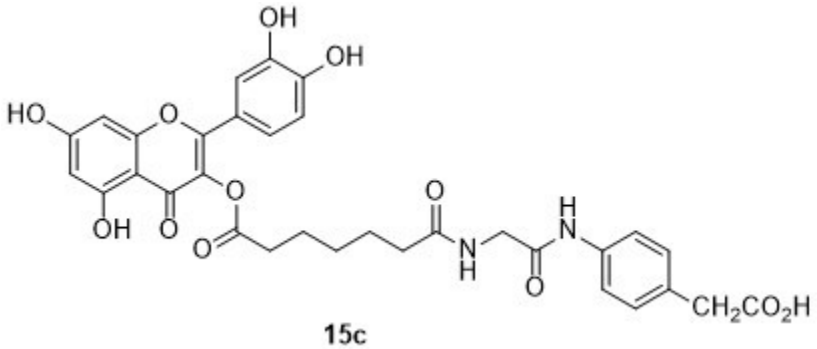

15c

2-(4-(2-(7-(2-(3,4-Dihydroxyphenyl)-5,7-dihydroxy-4-oxo-4H-chromen-3-yloxy)-7-oxoheptanamido)acetamido)phenyl)acetic acid (15c): Compound **14c** (0.1 g, 0.145 mmol, 1.0 equiv) was dissolved in a mixture of triethylsilane (0.06 mL, 0.36 mmol, 2.5 equiv) and DCM (1.45 mL, 0.1 M). To this mixture was added TFA (0.145 mL, 1.9 mmol, 13.0 equiv) and was stirred overnight at room temperature. The reaction mixture was

concentrated and dried *in vacuo* to obtain pure **15c** (0.085 g, 0.13 mmol, 92%). ^{1}H NMR (400 MHz, CD_3OD) *δ* 7.5 (d, *J=8*, 2H), 7.33 (d, *J=2*, 1H), 7.28 (dd, *J1=2, J2=6*, 1H), 7.22 (d, *J=8*, 2H), 6.9 (d, *J=8*, 1H), 6.43 (d, *J1=2,* 1H), 6.24 (d, *J=2*, 1H), 3.99 (s, 2H), 3.56 (s, 2H), 2.66 (t, *J=7*, 2H), 2.3 (t, *J=7*, 2H), 1.76-1.66 (m, 4H), 1.44-1.39 (m, 2H). ^{13}C NMR (100MHz, CD_3OD) *δ* 177.2, 176.7, 175.5, 172.5, 169.7, 166.2, 163.1, 158.7, 158.5, 150.3, 146.6, 138.3, 132.0, 131.5, 122.2, 122.1, 116.6, 116.3, 105.4, 100.2, 95.1, 44.1, 41.3, 36.6, 34.5, 29.5, 26.3, 25.5. HRMS (ESI) $C_{32}H_{30}N_2O_{12}$ *m/z* $[M+H]^+$ found 635.1866, expected 635.1877.

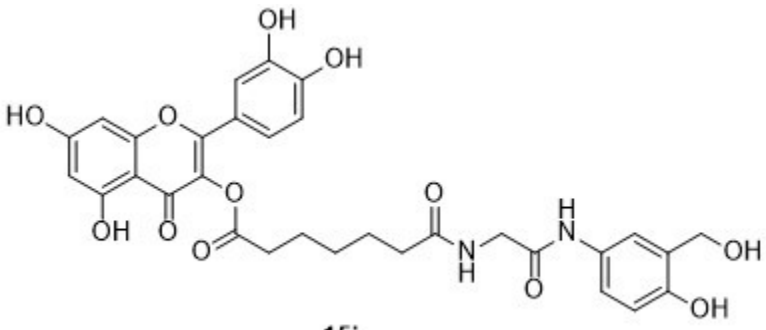

15i

2-(3,4-Dihydroxyphenyl)-5,7-dihydroxy-4-oxo-4H-chromen-3-yl7-(2-(4-hydroxy-3-(hydroxymethyl)phenylamino)-2-oxoethylamino)-7-oxoheptanoate (15i): Compound **14i (**0.074 g, 0.111 mmol, 1.0 equiv) was dissolved in a mixture of 1 N HCl:THF (1:1, 0.6 mL, 0.2 M). The mixture was stirred for 90 minutes and was concentrated *in vacuo* to obtain compound **15i** (0.025 g, 0.04 mmol, 36% yield. ^{1}H NMR (400 MHz, CD_3OD) *δ* 7.39-7.37 (m, 1H), 7.33 (d, *J=2*, 1H), 7.28 (dd, *J1=2, J2=6*, 2H), 6.91 (d, *J=8*, 1H), 6.71 (d, *J=9*, 1H), 6.44 (d, *J=2*, 1H), 6.24 (d, *J=2*, 1H), 4.61 (s, 2H), 3.97 (s, 2H), 2.66 (t, *J=7*, 2H), 2.3 (t, *J=8*, 2H), 1.76-1.64 (m, 4H), 1.15-1.41 (m, 2H). ^{13}C NMR (100MHz, CD_3OD) *δ* 177.2, 172.6, 166.2, 163.1, 158.7, 158.5, 153.6, 150.3, 148.7, 146.6, 131.5, 125.7, 124.1, 123.3, 122.2, 121.7, 116.6, 116.3, 116.1, 105.4, 100.2, 99.3, 95.1, 94.4, 70.9, 58.4, 44.0, 36.6,

34.6, 26.3, 25.7, 25.5. HRMS (ESI) $C_{31}H_{30}N_2O_{12}$ *m/z* $[M-H]^-$ found 621.1721, expected 621.1720.

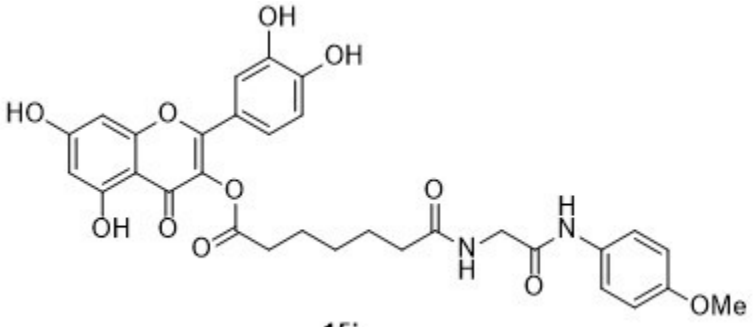

15j

2-(3,4-dihydroxyphenyl)-5,7-dihydroxy-4-oxo-4H-chromen-3-yl7-((2-((4-methoxyphenyl)amino)-2-oxoethyl)amino)-7-oxoheptanoate (15j): Compound **15j** was prepared according to general procedure **D** and was obtained in 27% yield (0.034 g, 0.056 mmol). ^{1}H NMR (400 MHz, CD_3OD) δ 7.98 (dd, *J* = 2.13, 8.66 Hz, 1H), 7.85 – 7.92 (m, 2H), 7.74 (td, *J* = 1.00, 8.28 Hz, 1H), 7.46 – 7.58 (m, 2H), 7.37 – 7.44 (m, 2H), 7.02 (d, *J* = 8.53 Hz, 1H), 6.81 – 6.86 (m, 2H), 6.37 – 6.41 (m, 1H), 6.16 – 6.21 (m, 1H), 3.98 (s, 2H), 3.75 (s, 3H), 2.59 – 2.71 (m, 2H), 2.35 (t, *J* = 7.40 Hz, 2H), 1.67 – 1.87 (m, 4H), 1.46 – 1.59 (m, 2H).

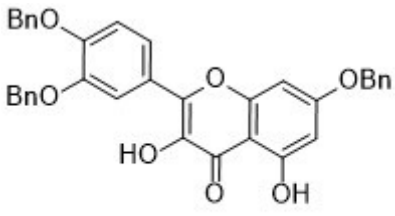

6

7-(benzyloxy)-2-(3,4-bis(benzyloxy)phenyl)-3,5-dihydroxy-4H-chromen-4-one (6): Quercetin (0.977 g, 3.23 mmol, 1.0 equiv) was dissolved in DMF (26 mL, 0.125M) and was cooled to 0 °C. To this mixture was added potassium carbonate (1.43 g, 10.34 mmol, 3.2 equiv) and benzyl bromide (1.23 mL, 3.13 mmol, 3.5 equiv). The reaction mixture was allowed to slowly warm to room temperature and stirred overnight. The reaction was diluted with ethyl acetate and washed with copious amounts of 1N HCl. The ethyl acetate layer was dried over sodium sulfate and concentrated *in vacuo.* The crude was purified by column chromatography (silica gel, acetone/hexane, 20% v/v) to give the desired compound **2** (0.925 g, 1.62 mmol, 50%). ^{1}H NMR (400 MHz, DMSO-d6) δ 7.9 (d, *J=2,* 1H), 7.84 (dd, *J1=2, J2=2,* 1H), 7.51-7.32 (m, 15H), 7.25 (d, *J=9*, 1H), 6.85 (d, *J=2*, 1H), 6.44 (d, *J=2,* 1H), 5.24 (s, 4H), 5.2 (s, 2H).

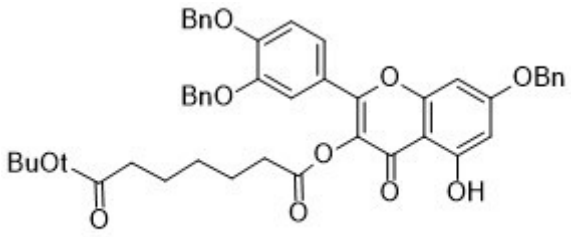

9

1-(7-(Benzyloxy)-2-(3,4-bis(benzyloxy)phenyl)-5-hydroxy-4-oxo-4H-chromen-3-yl) 7-tert-butyl heptanedioate (9): 7-tert-butoxy-7-oxoheptanoic acid (0.036 g, 0.168 mmol, 1.2 equiv) was dissolved in THF (2.8 mL, 0.05M), after which was added EDCI (0.032 g, 0.168 mmol, 1.2 equiv), Hunig's base (0.03 mL, 0.168 mmol, 1.2 equiv) and DMAP (0.0017 g, 0.014 mmol, 0.1 equiv). To this solution was added compound **6** (0.08 g, 0.14 mmol, 1.0 equiv) and the mixture was stirred overnight. The reaction mixture was washed with 1 N HCl and extracted into ethyl acetate. The ethyl acetate layer was dried over sodium sulfate and was purified by column chromatography (silica gel, ethyl

acetate/hexane, 25% v/v) to give the desired compound **9** (0.106 g, 0.13 mmol, 98%). ^{1}H NMR (400 MHz, $CDCl_3$) δ 7.54-7.29 (m, 17H), 6.36 (d, *J=2,* 1H), 6.48 (d, *J=2*, 1H), 5.6 (dd, *J1=2, J2=4*, 1H), 5.21 (s, 2H), 5.19 (s, 2H), 5.11 (s, 2H), 2.54 (t, *J=8*, 2H), 2.34 (t, *J=8*, 2H), 1.76-1.71 (m, 4H), 1.43 (s, 9H), 1.41-1.32 (m, 2H).

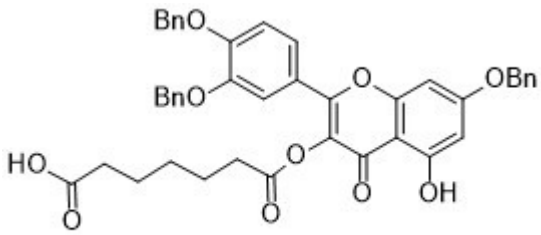

10

7-(7-(Benzyloxy)-2-(3,4-bis(benzyloxy)phenyl)-5-hydroxy-4-oxo-4H-chromen-3-yloxy)-7-oxoheptanoic acid (10): To the solution of compound **9 (**1.23 g, 1.6 mmol, 1.0 equiv) in DCM (16.0 mL, 0.1M) was added triethylsilane (0.64mL, 4.0 mmol, 2.5 equiv) and trifluoroacetic acid (1.6 mL, 20.8 mmol, 13.0 equiv). The reaction mixture was stirred overnight, concentrated *in vacuo* and purified by column chromatography (silica gel, dichloromethane/methanol, 5% v/v) to give the desired compound **10 (**0.876 g, 1.22 mmol, 76%). ^{1}H NMR (400 MHz, $CDCl_3$) δ 7.47-7.33 (m, 17H), 7.01 (d, *J=9,* 1H), 6.49 (d, *J=2,* 1H), 6.45 (d, *J=2,* 1H), 5.24 (s, 2H), 5.2 (s, 2H), 5.13 (s, 2H), 2.54 (t, *J=7*, 2H), 2.36 (t, *J=7,* 2H), 1.77-1.62 (m, 4H), 1.46-1.38 (m, 2H).

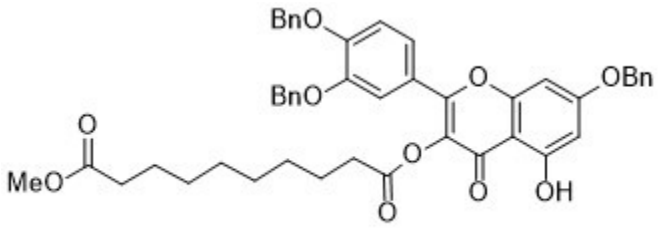

14k

1-(7-(Benzyloxy)-2-(3,4-bis(benzyloxy)phenyl)-5-hydroxy-4-oxo-4H-chromen-3-yl)10-methyl decanedioate (14k): 10-methoxy-10-oxodecanoic acid (87 mg, 0.4 mmol, 1.2 equiv) was dissolved in THF (8.0 mL 0.05M), after which was added EDCI (77 mg, 0.4 mmol, 1.2 equiv), Hunig's base (0.07 mL, 0.4 mmol, 1.2 equiv) and DMAP (5 mg, 0.04 mmol, 0.1 equiv). To this solution was added compound **6** (0.193 g, 0.34 mmol, 1.0 equiv) and the mixture was stirred overnight. The reaction mixture was washed with 1N HCl and extracted into ethyl acetate. The ethyl acetate layer was dried over sodium sulfate and was purified by column chromatography (silica gel, ethyl acetate/hexane, 25% v/v) to give the desired compound **14k** (0.152 g, 0.2 mmol, 58%). ^{1}H NMR (400MHz, $CDCl_3$) δ 7.5-7.32 (m, 17H), 6.48 (d, *J=2,* 1H), 6.44 (d, *J=2*, 1H), 5.59 (dd, *J1=2, J2=4*, 1H), 5.24 (s, 2H), 5.19 (s, 2H), 5.13 (s, 2H), 3.66 (s, 3H), 2.53 (t, *J=8*, 2H), 2.34 (t, *J=8*, 2H), 2.1-1.79 (m, 4H), 1.74-1.3 (m, 8H).

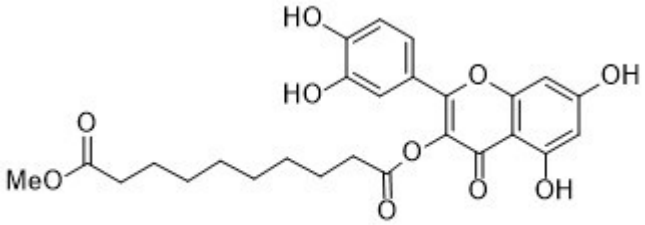

15k

1-(2-(3,4-Dihydroxyphenyl)-5,7-dihydroxy-4-oxo-4H-chromen-3-yl) 10-methyl decanedioate (15k): Compound **15k** was prepared from compound **14k** according to

general procedure **D** and was obtained in 27% yield (0.041 g, 0.08 mmol). ^{1}H NMR (400 MHz, DMSO-d6) *δ* 7.3 (d, *J=2,* 1H), 7.25 (dd, *J1=2, J2=6*, 1H), 6.9 (d, *J=9,* 1H), 6.46 (d, *J=2,* 1H), 6.24 (d, *J=2,*1H), 3.56 (s, 3H), 2.62 (t, *J=7*, 2H), 2.28 (t, *J=7,* 2H), 1.64-1.58 (m, 2H), 1.53-1.48 (m, 2H), 1.3-1.24 (m, 10H). ^{13}C NMR (100 MHz, CD_3OD) *δ* 177.2, 176.2, 172.6, 166.2, 163.1, 158.7, 158.5, 150.3, 146.6, 131.5, 122.2, 122.1, 116.5, 116.3, 105.3, 100.2, 95.1, 51.9, 34.8, 34.6, 30.1, 29.9, 25.9, 25.8. HRMS (ESI) $C_{26}H_{28}O_{10}$ *m/z* $[M-H]^-$ found 499.1593, expected 499.1604.

4.1.2: Biology Experimentals

Negatively supercoiled pBR322 DNA was purchased from New England Biolabs, (Beverly, MA). Relaxed plasmid DNA was prepared by incubating pBR322 with calf thymus Topo I (Life Technologies, Carlsbad, CA). Human Topo II and kinetoplast (kDNA) were purchased from Topogen (Fort Orange, FL).

E. coli Gyr A and Gyr B were overexpressed using the pET expression system[186] and purified by unpublished protocols similar to those described previously[187, 188]. Briefly, a soluble fraction containing GyrA was precipitated with ammonium sulfate (60% saturation), followed by chromatography on Q Sepharose FF, diethylaminoethyl cellulose DE52, and Sephacryl S-200. A soluble fraction containing GyrB was also precipitated with ammonium sulfate (60% saturation), followed by chromatography on diethylaminoethyl cellulose DE52, Q Sepharose FF, and Sephacryl S-200. The final preparations of GyrA and GyrB proteins were greater than 97% homogeneous for a single band on an SDS-polyacrylamide gel (data not shown). Purified GyrA and GyrB were mixed at a molar ratio of 1:1 to reconstitute active gyrase. All column resins were purchased from GE Healthcare (Chalfont St. Giles, UK).

Supercoiling assay

The effect of the compounds on the supercoiling activity of *E. coli* gyrase was assessed as previously described[189]. Reaction mixtures (20 µL) contained 50 mM Tris-HCl (pH 8.0 at 23°C), 10 mM $MgCl_2$, 100 mM potassium glutamate, 10 mM DTT, 50 µg/mL BSA, 1 mM ATP, 0.3 µg of relaxed plasmid pBR322, 5 µg/mL tRNA, 10 fmoles of *E. coli* gyrase, and various concentrations of the compounds (diluted in 50% DMSO from a 20 mM stock solution in 100% DMSO). After incubating reaction mixtures at 37 °C for 15 minutes, reactions were terminated by addition of EDTA to 25 mM and further incubation at 37°C for 5 min. DNA products were analyzed by electrophoresis through vertical 1.2% agarose gels at 2 V/cm for 15 hours in TAE buffer. Gels were stained with ethidium bromide prior to being photographed and quantified using an Eagle Eye system. All reactions were performed at least in duplicate.

Decatenation assays

The effect of the compounds on the catalytic activity of the α form of human Topo II was assessed by a decatenation assay using kinetoplast DNA (kDNA) as the substrate as previously described[27]. Reaction mixtures (20 µL) contained 50 mM Tris-HCl (pH 8.0 at 23°C), 10 mM $MgCl_2$, 200 mM potassium glutamate, 10 mM DTT, 50 µg/mL BSA, 1 mM ATP, 0.3 µg of kDNA, 5 µg/mL tRNA, 2 units of Topo II, and various concentrations of the compounds (diluted as described for the supercoiling assay). After incubating reaction mixtures at 37 °C for 15 min, reactions were terminated by addition of EDTA to 25 mM and further incubation at 37°C for 5 min. Reaction products were analyzed by agarose

gel electrophoresis as described for the supercoiling assay. All reactions were performed at least in duplicate.

DNA cleavage assays

DNA cleavage assays were performed as previously described[190] to determine the ability of the analogues to act as a topoisomerase poison. DNA cleavage reaction mixtures (20 µl) were as described for the supercoiling assay or decatenation assay, except that potassium glutamate was omitted, relaxed plasmid pBR322 was used as the substrate, and either 100 fmol of *E. coli* gyrase or 5 units of human Topo II was used. Reaction mixtures were incubated for 10 minutes at 37°C, and then SDS was added to 1%, and reactions were continued at 37 °C for 10 min. After addition of EDTA and proteinase K to a final concentration of 40 mM and 100 µg/mL, respectively, the reaction mixtures were further incubated at 37 °C for 15 minutes (for *E. coli* gyrase) or 50 °C for one hour (human Topo II). The DNA products were purified by extraction with phenol/chloroform/isoamyl alcohol (25:24:1, v/v/v) and analyzed by electrophoresis through vertical 1.2% agarose gels at 2 V/cm for 12 hours in TAE buffer. Ethidium bromide was present in both the agarose gels and the TAE buffer at a concentration of 0.5 µg/mL. Gels were destained in water and then photographed and quantified using an Eagle Eye system. All reactions were performed at least in duplicate.

DNA unwinding assay

A DNA unwinding assay[37] was performed as previously described[189] to determine the

ability of the compounds to intercalate into DNA. Reaction mixtures (20 µl) contained 50 mM Tris-HCl (pH 7.5 at 23°C), 1 mM $MgCl_2$, 0.5 mM DTT, 50 µg/mL BSA, 0.3 µg of relaxed pBR322, 0.8 units of calf thymus Topo I and the indicated concentrations of the compounds (diluted as described for the supercoiling assay). Ethidium bromide was used as a positive control. Reaction mixtures were incubated at 37°C for 15 minutes. DNA products were purified by extraction with phenol/chloroform/isoamyl alcohol (25:24:1, v/v/v) and analyzed by electrophoresis through vertical 1.2% agarose gels at 2 V/cm for 15 hours in TAE buffer. Gels were stained with ethidium bromide prior to being photographed and quantified using a Stratagene Eagle Eye gel documentation system (Agilent Technologies, Santa Clara, CA). All reactions were performed at least in duplicate. Quercetin was purchased from Sigma-Aldrich (St. Louis, MO).

SPR Experimental Procedure

Linear, 5' biotinylated DNA was dissolved in SPR buffer (10 mM HEPES pH 7.3, 3 mM EDTA, 0.005% surfactant P20) to give a concentration of 600 nM. The DNA was immobilized on the surface of flow cell two of a streptavidin-coated sensor chip by flowing 50 µL of the solution through at a rate of 10 µL per minute. Flow cells one and two were then capped with 100 µL of a 1 mg/mL solution of biotin in SPR buffer. The BioCore T200 instrument was then primed with SPR buffer containing 1% (v/v) DMSO, and the flow rate was increased to 50 µL/min. To test the compound's ability to inhibit the DNA-DNA gyrase binding interaction, a premixed solution of DNA gyrase (100 nM) with or without compound (100 µM) was injected over flow cells one and two for 7 minutes. After allowing four minutes for dissociation, the surface of the flow cell was regenerated using 1 M NaCl

in 50 mM NaOH for 30 seconds (**Figure 89**).

Negative Control (DNA Gyrase only)

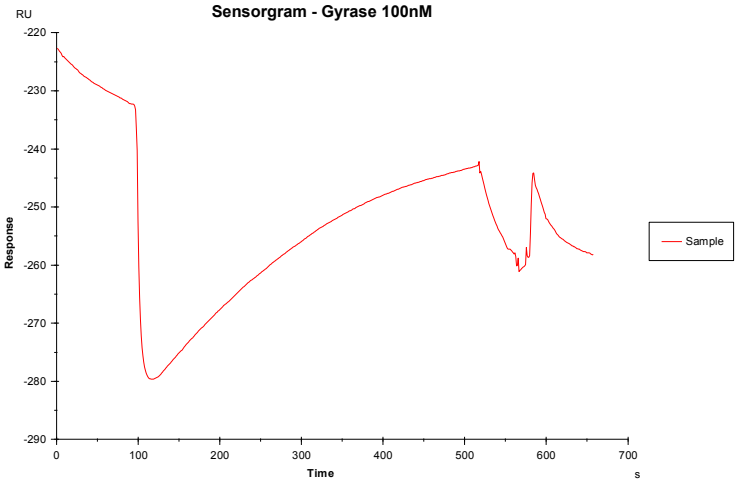

Positive Control (SD8)

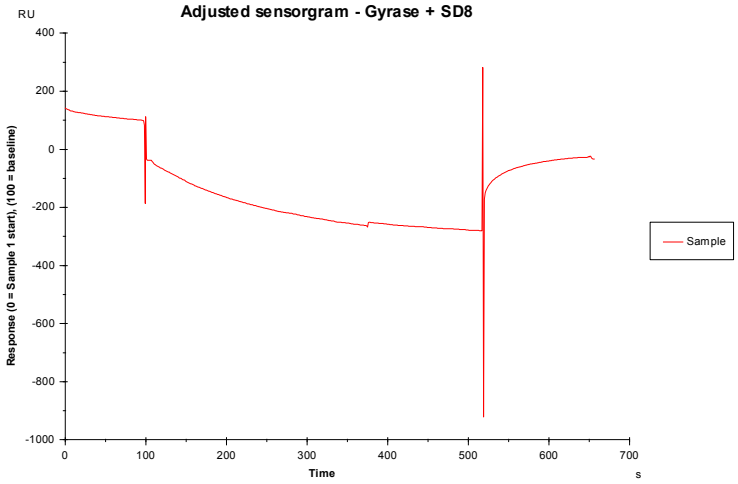

DNA gyrase with compound 15A

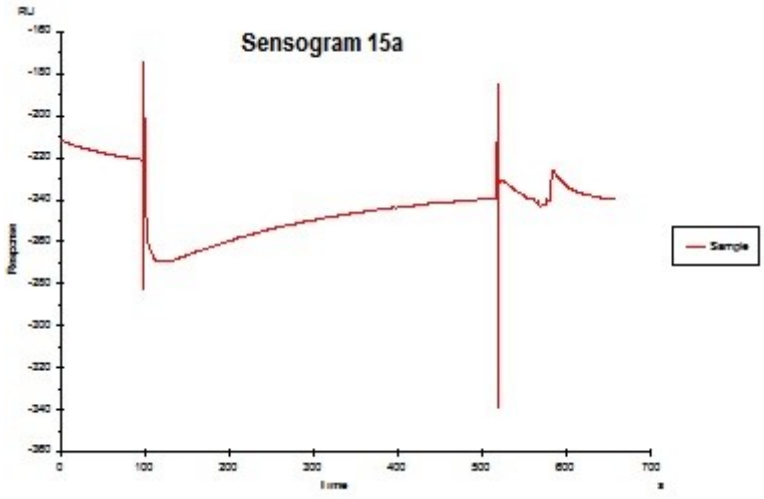

Figure 89: SPR Sensograms

4.2: Experimental for Studies toward Total Synthesis of SD8

Chemical reagents and solvents were purchased from Sigma-Aldrich (MO, USA), Alfa-Aesar (MA, USA), Fisher Scientific (PA, USA). Analytical Thin Layer Chromatography (TLC) was performed using silica gel GHLF plates (Analtech Inc., DE, USA). Flash chromatography was performed on a TELEDYNE ISCO CombiFlash® Rf instrument using RediSep Rf Normal-phase Flash Columns (4-gm, 12-gm, 24-gm or 40-gm). ^{1}H NMR spectra were recorded on a Bruker TopSpin 400 MHz using deuterated chloroform ($CDCl_3$) or methanol (CD_3OD). All chemical shifts are reported as δ in units of parts per million (ppm) relative to chloroform and methanol residual peaks at 7.26 and 3.31 respectively (^{1}H NMR spectra); 77.16 and 49.00 respectively (^{13}C NMR spectra). The data is reported as: chemical shifts (ppm), multiplicity (s = singlet, d = doublet, dd = doublet of doublets, t = triplet, q = quartet, m = multiplet), coupling constant(s) (Hz) and

integral values. Electrospray ionization (ESI) mass spectra were obtained from Perkin Elmer Flexar UPLC/AxION2 TOF Mass Spectrometer.

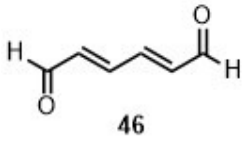

46

(2*E*,4*E*)-hexa-2,4-dienedial

A mixture of glyoxal trimer dihydrate (1.4 g, 6.7 mmol, 1.0 equiv) and (triphenylphospharanylidene) acetaldehyde (12.16 g, 40.0 mmol, 6.0 equiv) was heated to 80°C in DMF (80 mL, 0.08 M) for 12 hours. The reaction mixture was extracted into ethyl acetate and washed with water and the ethyl acetate was purified over silica gel to obtain the compound **46** (1.29 g, 11.7 mmol, 64%). ^{1}H NMR (400 MHz, $CDCl_3$) δ 9.73 (dd, J = 0.75, 7.78 Hz, 2H), 7.23 - 7.37 (m, 2H), 6.43 - 6.63 (m, 2H).

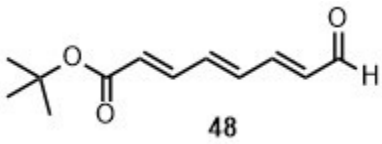

48

***tert*-butyl (2E,4E,6E)-8-oxoocta-2,4,6-trienoate**

To a solution of mucodialdehyde (0.062 g, 0.56 mmol, 1.2 equiv) in THF, cooled to 0°C was added a mixture of *tert*-Butyl diethylphosphonoacetate (0.118 g, 0.47 mmol, 1.0 equiv) and barium hydroxide (0.121 g, 0.705 mmol, 1.5 equiv) in THF:H_2O (5.6 mL, 0.1 M, 40:1) over 30 minutes, after which the reaction was warmed up to room temperature

and stirred for 90 minutes. The reaction mixture was purified over silica gel to obtain the compound **48** (0.041 g, 0.197 mmol, 42%).

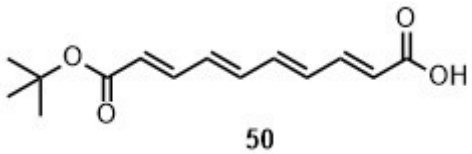

50

(2*E*,4*E*,6*E*,8*E*)-10-(tert-butoxy)-10-oxodeca-2,4,6,8-tetraenoic acid

To a solution of diethylphosphonoacetic acid (0.06 mL, 0.365 mmol, 1.1 equiv) in THF (0.8 mL, 0.4 M) cooled to -60°C was added n-BuLi (2.5 M soln in hexanes, 0.316 mL, 0.8 mmol, 2.4 equiv) and the mixture was stirred for 30 minutes. To this solution was added the aldehyde (0.069 g, 0.331 mmol, 1.0 equiv) dropwise and the solution was stirred for 30 minutes at -60°C and warmed to room temperature and stirred for 3 hours. The reaction was quenched by addition of 1 N HCl and the compound was purified over silica gel (0.075 g, 0.33 mmol, quant). ^{1}H NMR (400 MHz, $CDCl_3$) δ 7.40 (dd, J = 11.17, 15.18 Hz, 1H), 7.13 - 7.24 (m, 1H), 6.41 - 6.71 (m, 4H), 5.94 (dd, J = 15.06, 18.57 Hz, 2H), 1.51 (s, 9H).

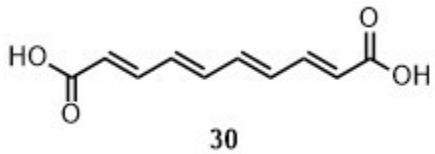

30

(2*E*,4*E*,6*E*,8*E*)-deca-2,4,6,8-tetraenedioic acid

Fumagillin B (dicyclohexyammonium salt) from MEDIVET (0.021 g / 1.0 g, 5g, 0.229 mmol) was taken up into saturated sodium bicarbonate solution and was extracted into DCM. The DCM layer was concentrated and was stirred with 1 N NaOH solution (excess)

overnight, followed by addition of 6 N HCl to precipitate out the tetraene diacid which was collected by flitration (0.04 g, 0.2 mmol, 90%). ^{1}H NMR (400 MHz, DMSO-d_6) δ 7.15 - 7.32 (m, 2H), 6.73 - 6.85 (m, 2H), 6.53 - 6.70 (m, 2H), 5.99 (d, J = 15.31 Hz, 2H).

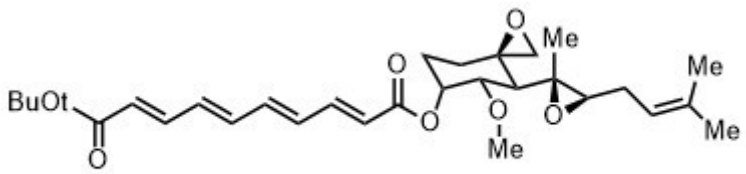

52

1-(*tert*-butyl) 10-((3R,4S,5S,6R)-5-methoxy-4-((2R,3R)-2-methyl-3-(3-methylbut-2-en-1-yl)oxiran-2-yl)-1-oxaspiro[2.5]octan-6-yl) (2E,4E,6E,8E)-deca-2,4,6,8-tetraenedioate

Fumagillin (0.14 g, 0.3 mmol, 1.0 equiv), obtained from extraction of fumagillin B (MEDIVET) with sodium bicarbonate was dissolved in DMF (3.0 mL, 0.1 M). To this solution was added cesium carbonate (2.58 g, 7.93 mmol, 26.0 equiv), benzyltriethylammonium chloride (0.069 g, 0.305 g, 1.0 equiv) and *tert*-butyl bromide (1.64 mL, 14.65 mmol, 48 equiv). The solution was heated at 60°C overnight and was diluted with DCM and washed with saturated ammonium chloride solution. The DCM layer was purified over silica gel to obtain the compound **52** (0.091 g, 0.177 mmol, 60%). ^{1}H NMR (400 MHz, $CDCl_3$) δ 7.04 - 7.29 (m, 2H), 6.47 - 6.61 (m, 2H), 6.29 - 6.47 (m, 2H), 5.93 (d, J = 15.31 Hz, 1H), 5.83 (d, J = 15.31 Hz, 1H), 5.59 - 5.69 (m, 1H), 5.16 (t, J = 7.40 Hz, 1H), 3.62 (dd, J = 2.76, 11.04 Hz, 1H), 3.34 - 3.41 (m, 3H), 3.19 - 3.30 (m, 1H), 2.88 - 2.97 (m, 2H), 2.76 - 2.83 (m, 1H), 2.46 - 2.58 (m, 2H), 2.24 - 2.37 (m, 1H), 1.89 - 2.19 (m, 6H), 1.72 - 1.87 (m, 2H), 1.64 - 1.72 (m, 4H), 1.60 (s, 4H), 1.43 (s, 9H), 1.16 (s, 3H).

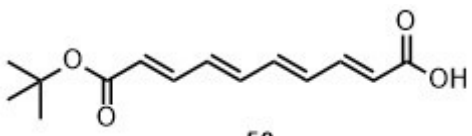

50

(2*E*,4*E*,6*E*,8*E*)-10-(tert-butoxy)-10-oxodeca-2,4,6,8-tetraenoic acid

The above obtained fumagillin *tert*-butyl ester (0.091 g, 0.176 mmol, 1.0 equiv) was dissolved in THF:EtOH (3:1, 1.76 mL, 0.1 M) and was added a solution of sodium hydroxide (1N, 1.76 mmol, 10.0 equiv) and stirred for 3 hours. The solution was stirred for 3 hours, followed by quenching with 1 N HCl and was purified over silica gel to obtain the compound **50** (0.042 g, 0.17 mmol, quant). ^{1}H NMR (400 MHz, $CDCl_3$) δ 7.40 (dd, *J* = 11.17, 15.18 Hz, 1H), 7.13 - 7.24 (m, 1H), 6.41 - 6.71 (m, 4H), 5.94 (dd, *J* = 15.06, 18.57 Hz, 2H), 1.51 (s, 9H).

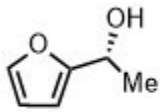

54

(*R*)-1-(furan-2-yl)ethan-1-ol

To a solution of the furan ketone **53** (0.11 mg, 1.0 mmol) in H_2O (0.5 mL), formic acid/triethylamine (1:1, 0.5 mL) and Noyori asymmetric transfer hydrogenation catalyst (*R*)-Ru(η^6-mesitylene)-(*R, R*)-TsDPEN **A** (0.0095 g, 0.5 mol%). The resulting solution was stirred at 40 °C for 8 hours. The reaction mixture was diluted with water and extracted with diethyl ether. The combined organic layers were washed with saturated $NaHCO_3$, dried over Na_2SO_4, and concentrated under reduced pressure. The crude product was

purified by silica gel to give furan alcohol **54** (0.089 g, 0.79 mmol, 79%). ^{1}H NMR (400 MHz, $CDCl_3$) δ 7.34 (dd, J = 0.88, 1.88 Hz, 1H), 6.30 (dd, J = 1.76, 3.26 Hz, 1H), 6.20 (td, J = 0.75, 3.26 Hz, 1H), 4.85 (q, J = 6.69 Hz, 1H), 1.51 (d, J = 6.53 Hz, 3H).

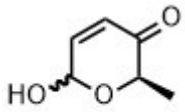

55

(2*R*)-6-hydroxy-2-methyl-2H-pyran-3(6*H*)-one

Compound furan alcohol **54** (0.5 g, 4.46 mmol), 9.9 mL of THF, and 5.0 mL of H_2O were added to a round bottom flask and cooled to 0^{o}C. Solid $NaHCO_3$ (0.75 g, 8.9 mmol, 2.0 equiv), $NaOAc•3H_2O$ (0.61 g, 4.46 mmol, 1.0 equiv), and NBS (0.53 g, 4.46 mmol, 1.0 equiv) were added to the solution and the mixture was stirred for 1 hour at 0 ^{o}C. The reaction was quenched with saturated $NaHCO_3$, extracted with Et_2O, dried (Na_2SO_4), concentrated under reduced pressure and purified by silica gel chromatography to give pyranone **55** (0.26 g, 2.01 mmol, 45%). ^{1}H NMR (400 MHz, $CDCl_3$) δ 6.73 (dd, J = 3.51, 10.04 Hz, 1H), 5.99 (d, J = 10.29 Hz, 1H), 5.18 (d, J = 3.51 Hz, 1H), 4.74 (d, J = 11.80 Hz, 1H), 4.59 (d, J = 11.80 Hz, 1H), 4.46 (q, J = 6.78 Hz, 1H), 1.27 (d, J = 6.78 Hz, 3H).

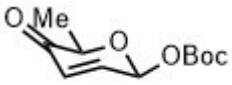

56

***tert*-butyl ((2S,6R)-6-methyl-5-oxo-5,6-dihydro-2H-pyran-2-yl) carbonate**

To a benzene solution (21 mL) of pyranone **55** (1.281 g, 10.0 mmol, 1.0 equiv) and $(Boc)_2O$ (3.5 g, 16.0 mmol) was added sodium acetate (0.985 g, 12.0 mmol). After stirring at 80 ^{o}C for 2 hours, the mixture was cooled down to room temperature and was quenched by addition of saturated $NaHCO_3$ solution, extracted with Et2O, dried (Na_2SO_4), and

concentrated under reduced pressure. The crude product was purified by silica gel flash chromatography to give two diastereomers of *tert*-butyl 5,6-dihydro-6-methyl-5-oxo-2H-pyran-2-yl carbonate; **β** (0.55 g, 2.4 mmol, 24%). ^{1}H NMR (400 MHz, $CDCl_3$) δ 6.81 - 6.95 (m, 1H), 6.36 (dd, *J* = 1.38, 2.64 Hz, 1H), 6.20 (dd, *J* = 1.25, 10.29 Hz, 1H), 4.37 (q, *J* = 7.03 Hz, 1H), 1.51 (s, 12H).

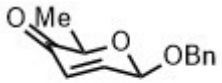

57

(2*R*,6*R*)-6-(benzyloxy)-2-methyl-2H-pyran-3(6H)-one

A DCM (2.3 mL) solution of Boc pyranone **56β** (0.52 g, 2.28 mmol, 1.0 equiv) and benzyl alcohol 0.48 mL, 4.56 mmol, 2.0 equiv) was cooled to 0˚ C. A DCM (1.4 mL) solution of $Pd_2(DBA)_3$•$CHCl_3$ (0.055 g, 0.06 mmol, 2.5 mol%) and PPh_3 (0.06 g, 0.23 mmol, 10 mol%) was added to the reaction mixture at 0°C. The reaction mixture was stirred at 0 °C for 2 hours and was quenched with saturated $NaHCO_3$ solution, extracted with diethyl ether, dried over sodium sulfate, and concentrated under reduced pressure. The crude product was purified by silica gel flash chromatography to give **57** (340 mg, 2.17 mmol, 95%). ^{1}H NMR (400 MHz, $CDCl_3$) δ 7.30 - 7.43 (m, 5H), 6.92 (dd, *J* = 2.01, 10.29 Hz, 1H), 6.15 (dd, *J* = 1.51, 10.29 Hz, 1H), 5.33 - 5.46 (m, 1H), 4.96 (d, *J* = 11.80 Hz, 1H), 4.70 (d, *J* = 11.80 Hz, 1H), 4.25 (dq, *J* = 0.75, 6.86 Hz, 1H), 1.54 (d, *J* = 6.78 Hz, 3H).

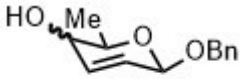

58

(2*R*,6*R*)-6-(benzyloxy)-2-methyl-3,6-dihydro-2H-pyran-3-ol

A DCM (1.5 mL) solution of enone **57** (0.3 g, 1.37 mmol, 1.0 equiv) and $CeCl_3$ in MeOH solution (1.24 mL) was cooled to -78 °C. $NaBH_4$ (0.052 g, 1.37 mmol) was added and the reaction mixture was stirred at -78 °C for 3 hours. The reaction mixture was diluted with diethyl ether and was quenched with saturated aqueous $NaHCO_3$, extracted with Et_2O and concentrated under reduced pressure. The crude product was purified by silica gel flash chromatography to give allylic alcohols **58** (0.17 g, 1.08 mmol, 79%). ^1H NMR (400 MHz, $CDCl_3$) δ 7.14 - 7.33 (m, 5H), 5.67 - 5.80 (m, 1H), 5.00 - 5.12 (m, 1H), 4.80 (dd, J = 11.80, 18.57 Hz, 1H), 4.49 - 4.62 (m, 1H), 3.58 (quin, J = 6.46 Hz, 1H), 1.79 (br. s., 1H), 1.23 - 1.33 (m, 3H).

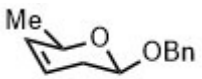

59

(2*R*,6*R*)-2-(benzyloxy)-6-methyl-3,6-dihydro-2H-pyran

To a solution of dry N-methyl morpholine (NMM) (1.9 mL, 2.04 mmol, 3.0 equiv) triphenyl phosphine (0.59 g, 2.25 mmol, 3.3 equiv) and was cooled to -30 °C under Ar atmosphere. Diisopropylazodicarboxylate (0.41 mL, 2.04 mmol, 3.0 equiv) was added and the reaction was stirred for 5 minutes, allylic alcohol **58** (0.15 g, 0.68 mmol, 1.0 equiv) was added in a 1 M solution of NMM and the reaction mixture was stirred for 10 minutes, followed by addition of *o*-nitrobenzenesulfonyl hydrazide (NBSH) (0.444 g, 2.04 mmol, 3.0 equiv). The reaction was stirred at -30 °C for 2 hours and was monitored by TLC. Upon consumption of starting material, the reaction was warmed up to room temperature and stirred for another 2 hours. The reaction mixture was diluted with diethyl ether and was quenched with saturated aqueous $NaHCO_3$, extracted with diethyl ether and concentrated under reduced pressure. The crude product was purified over silica gel to to give product

59 (0.133 g, 0.65 mmol, 97%). ^{1}H NMR (400 MHz, $CDCl_3$) δ 7.15 - 7.33 (m, 5H), 5.55 - 5.66 (m, 1H), 5.52 (tdd, *J* = 1.38, 2.67, 10.13 Hz, 1H), 4.87 (d, *J* = 12.05 Hz, 1H), 4.67 (dd, *J* = 3.51, 7.78 Hz, 1H), 4.55 (d, *J* = 12.05 Hz, 1H), 4.21 - 4.31 (m, 1H), 2.04 - 2.26 (m, 2H), 1.25 (d, *J* = 6.78 Hz, 3H).

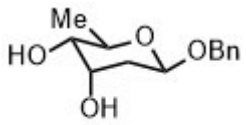

60

(2*R*,3*S*,4*S*,6*R*)-6-(benzyloxy)-2-methyltetrahydro-2H-pyran-3,4-diol

To a DCM (2.7 mL, 0.47 M) solution of olefin **17** (0.255g, 1.25 mmol, 1.0 equiv) at 0 °C was added a solution of (50% w/v) of N-methyl morpholine N-oxide / water (0.57 mL). Crystalline OsO4 (0.00318 g, 1 mol %) was added and the reaction was stirred for 3 hours. The reaction was quenched by adding EtOAc and saturated aqueous $NaHCO_3$. The organic layer was separated and concentrated and was purified over silica gel to obtain the diol **60** (0.24 g, 1.007 mmol, 80%). ^{1}H NMR (400 MHz, $CDCl_3$) δ 7.25 - 7.40 (m, 5H), 4.84 - 4.96 (m, 2H), 4.58 (d, *J* = 11.80 Hz, 1H), 4.08 - 4.17 (m, 1H), 3.76 (qd, *J* = 6.27, 9.29 Hz, 1H), 3.35 (dd, *J* = 3.26, 9.29 Hz, 1H), 2.14 (ddd, *J* = 2.26, 3.64, 13.93 Hz, 1H), 1.80 (ddd, *J* = 3.01, 9.41, 13.93 Hz, 1H), 1.35 (d, *J* = 6.27 Hz, 3H).

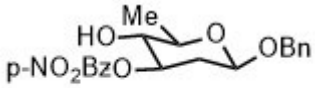

61

(2*R*,3*R*,4*R*,6*R*)-6-(benzyloxy)-4-methoxy-2-methyltetrahydro-2H-pyran-3-ol

A THF (1.37 mL, 0.67M) solution of diol **60** (7.0 g, 29.4 mmol) at 0 °C were added PPh_3 (0.495 g, 1.88 mmol, 2.05 equiv) and p-nitrobenzoic acid (0.309 g, 1.85 mmol, 2.0 equiv).

DIAD (0.36 mL, 1.85 mmol, 2.0 equiv) in THF was added dropwise and the reaction mixture was warmed up to room temperature and stirred overnight. The solution was quenched with saturated aqueous $NaHCO_3$, extracted with diethyl ether, and purified over silica gel to give compound **61**, which was used directly for the next step.

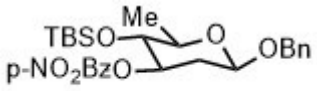

62

(((2*R*,3*R*,4*R*,6*R*)-6-(benzyloxy)-4-methoxy-2-methyltetrahydro-2H-pyran-3-yl)oxy)(tert-butyl)dimethylsilane

To the above obtained alcohol **61** (0.242 g, 0.625 mmol, 1.0 equiv) in DCM (3.9 mL, 0.16 M) was added 2,6-lutidine (0.17 mL, 0.75 mmol, 1.2 equiv) and cooled to 0 °C. To this solution was added TBSOTf (0.12 mL, 1.0 mmol, 1.6 equiv) and the reaction was allowed to warm up to room temperature and stirred for 3 hours. The reaction mixture was quenched by addition of 1N HCl and purified over silica gel to obtain the tri-protected olivose sugar **62** (0.139 g, 0.38 mmol, 30% overall for 2 steps). ^{1}H NMR (400 MHz, $CDCl_3$) *δ* 8.26 - 8.35 (m, 2H), 8.16 - 8.24 (m, 2H), 7.28 - 7.40 (m, 5H), 5.14 (ddd, *J* = 5.27, 8.60, 11.73 Hz, 1H), 4.91 (d, *J* = 12.05 Hz, 1H), 4.58 - 4.72 (m, 2H), 3.55 (t, *J* = 8.66 Hz, 1H), 3.41 (qd, *J* = 6.18, 8.82 Hz, 1H), 2.40 (ddd, *J* = 2.01, 5.27, 12.30 Hz, 1H), 1.80 (dt, *J* = 9.66, 12.11 Hz, 1H), 1.39 (d, *J* = 6.27 Hz, 3H), 0.77 (s, 9H), 0.09 (s, 3H), -0.13 (s, 3H).

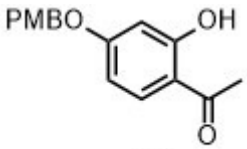

64

1-(2-hydroxy-4-((4-methoxybenzyl)oxy)phenyl)ethan-1-one

To a refluxing solution of 2',4'-dihydroxyacetophenone (3 g, 19.72 mmol, 1.0 equiv) and potassium carbonate (6 g, 43.39 mmol, 2.2 equiv) in acetonitrile (40 mL, 0.5 M) was added PMBCl (2.67 mL, 19.72 mmol, 1.0 equiv) and the solution was refluxed for 16 hours, following which it was quenched by 1N HCl, extracted into ethyl acetate and washed with 1N HCl solution. The ethyl acetate layer was dried and purified over silica gel to obtain the compound **64** (2.45 g, 9.07mmol, 46% yield). ^{1}H NMR (400 MHz, $CDCl_3$) δ 12.74 (s, 1H), 7.64 (d, *J* = 9.29 Hz, 1H), 7.35 (d, *J* = 8.80 Hz, 2H), 6.93 (d, *J* = 8.70 Hz, 2H), 6.51 (qd, *J* = 2.49, 4.83 Hz, 2H), 5.03 (s, 2H), 3.83 (s, 3H), 2.56 (s, 3H).

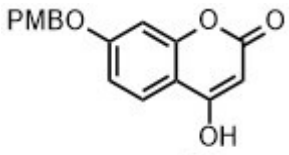

65

4-hydroxy-7-((4-methoxybenzyl)oxy)-2H-chromen-2-one

To a refluxing suspension of sodium hydride (60%, 1.09 g, 27.24 mmol, 2.0 equiv) in toluene (91 mL, 0.1 M), was added a solution of compound **64** (2.47 g, 9.08 mmol, 1.0 equiv) in toluene dropwise, followed by dimethyl carbonate (1.15 mL, 13.63 mmol, 1.5 equiv) and the reaction was allowed to stir overnight under reflux. The following day, the reaction was cooled to 0 °C and quenched with 1 N HCl and diluted with ethyl acetate. The ethyl acetate layer was washed with 1 N HCl solution and concentrated. The product was precipitated out using methanol to get the coumarin **65** (2.79 g, 9.08 mmol, quant). ^{1}H NMR (400 MHz, DMSO-d_6) δ 12.32 (br. s., 1H), 7.70 (d, *J* = 8.78 Hz, 1H), 7.40 (d, *J* =

8.80 Hz, 2H), 7.01 (d, *J* = 2.51 Hz, 1H), 6.93 - 6.99 (m, 3H), 5.45 (s, 1H), 5.11 (s, 2H), 3.75 (s, 3H).

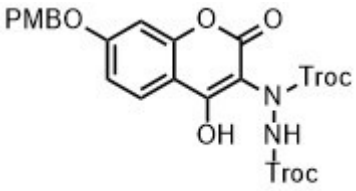

67

bis(2,2,2-trichloroethyl) 1-(4-hydroxy-7-((4-methoxybenzyl)oxy)-2-oxo-2H-chromen-3-yl)hydrazine-1,2-dicarboxylate

To a solution of the coumarin **65** (0.1 g, 0.335 mmol, 1.0 equiv) in acetonitrile (0.67 mL, 0.5 M) was added ammonium acetate (0.00516 g, 0.067 mmol, 0.2 equiv) and bis(2,2,2-trichloroethyl) azodicarboxylate (0.153 g, 0.4 mmol, 1.2 equiv). The reaction mixture was stirred for 2 hours and the product was purified over silica gel to obtain the compound **67** (0.226 g, 0.335 mmol, quant). ^{1}H NMR (400 MHz, $CDCl_3$) δ 7.95 (br. s., 1H), 7.85 (d, *J* = 8.78 Hz, 1H), 7.37 (d, *J* = 8.53 Hz, 2H), 6.86 - 7.03 (m, 4H), 5.08 (s, 2H), 4.73 - 5.04 (m, 4H), 3.84 (s, 3H).

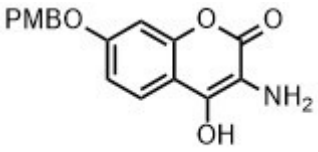

68

3-amino-4-hydroxy-7-((4-methoxybenzyl)oxy)-2H-chromen-2-one

To a solution of the coumarin **67** (0.226 g, 0.333 mmol, 1.0 equiv) in acetic acid (2.38 mL, 0.14 mL) was added acetone (238 µL) and zinc (0.68 g, 10.37 mmol, 31.0 equiv) and the

reaction was stirred overnight. The following day, the reaction was filtered through celite, basified with sodium bicarbonate solution and extracted into DCM. The DCM layer was purified over silica to obtain the aminocoumarin **68** (0.048 g, 0.15 mmol, 46%). ^{1}H NMR (400 MHz, DMSO-d_6) δ 7.75 (d, *J* = 8.53 Hz, 1H), 7.40 (d, *J* = 8.78 Hz, 2H), 6.79 - 7.00 (m, 4H), 5.08 (s, 2H), 3.76 (s, 3H).

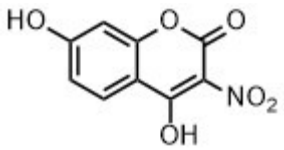

70

4,7-dihydroxy-3-nitro-2*H*-chromen-2-one

To a solution of the coumarin **68** (0.5 g, 2.108 mmol, 1.0 equiv) in DMF (10.54 mL, 0.2 M), was added 1-dodecanethiol (3.54 mL, 14.76 mmol, 7.0 equiv) and potassium tert-butoxide (0.592 g, 5.27 mmol, 2.5 equiv). The reaction mixture was heated at 120 °C overnight, followed by quenching the reaction with 1 N HCl and extracting the product into ethyl acetate, which was purified over silica gel to obtain the compound **70** (0.416 g, 1.87 mmol, 88%). ^{1}H NMR (400 MHz, DMSO-d_6) δ 10.13 (br. s., 1H), 7.67 (d, *J* = 8.53 Hz, 1H), 6.62 (dd, *J* = 2.26, 8.53 Hz, 1H), 6.45 (d, *J* = 2.26 Hz, 1H).

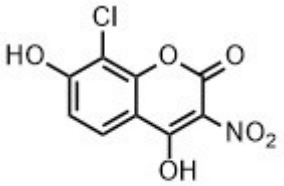

71

8-chloro-4,7-dihydroxy-3-nitro-*2H*-chromen-2-one

To a solution of the nitrocoumarin (0.055 g, 0.25 mmol, 1.0 equiv) in dioxane:water (1:1, 1.23 mL, 0.2 M) was added chloramine-T hydrate (0.07 g, 0.25 mmol, 1.0 equiv). The reaction mixture was heated at reflux overnight and was extracted into ethyl acetate and dried. Analysis of the crude mixture by ^{1}H NMR indicated a 50% conversion into product **71**. ^{1}H NMR (400 MHz, DMSO-d_6) δ 10.14 (s, 2H), 7.64 (d, *J* = 8.53 Hz, 1H), 6.83 (d, *J* = 8.53 Hz, 1H).

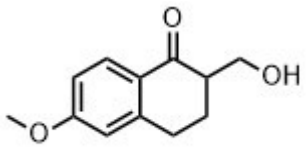

73

2-(hydroxymethyl)-6-methoxy-3,4-dihydronaphthalen-1(*2H*)-one

To a solution of n-butyllithium (0.7 mL, 1.7 mmol, 3.0 equiv) in THF (8.1 mL, 0.07M) was added 2,2,6,6-tetramethylpiperidine (0.29 mL, 1.7 mmol, 3.0 equiv) at -10 °C. The solution was stirred for 30 minutes and then cooled to -78 °C and compound **72** (0.1 g, 0.57 mmol, 1.0 equiv) was added in THF dropwise and stirred for an additional one hour. To this, 1H-benzotriazole-methanol (0.17 g, 1.134 mmol, 2.0 equiv) was added dropwise over a period of 30 minutes and kept at this temperature for 2 hours. The solution was quenched with water and extracted into ethyl acetate and purified over silica gel to get the compound **73** (0.076 g, 0.37 mmol, 65%). ^{1}H NMR (400 MHz, $CDCl_3$) δ 8.01 (d, *J* = 8.78 Hz, 1H), 6.79 - 6.87 (m, 1H), 6.71 (d, *J* = 2.51 Hz, 1H), 3.74 - 3.97 (m, 5H), 2.90 -

3.15 (m, 2H), 2.68 (tdd, *J* = 4.49, 7.65, 13.24 Hz, 1H), 2.04 - 2.15 (m, 1H), 1.84 - 2.01 (m, 1H).

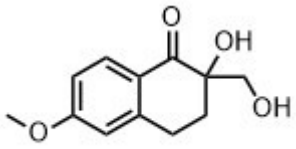

74

2-hydroxy-2-(hydroxymethyl)-6-methoxy-3,4-dihydronaphthalen-1(2*H*)-one

To a solution of the alcohol **73** (1.012 g, 4.91 mmol, 1.0 equiv) and triethylamine (1.71 mL, 12.27 mmol, 2.5 equiv) in DCM (9.82 mL, 0.5 M) was cooled to 0 °C was added TBSOTf (2.48 mL, 10.8 mmol, 2.2 equiv). The reaction was allowed to warm up to room temperature and stirred for 3 hours, following which the reaction was diluted with DCM and washed with water and concentrated and used for the next step without any further purification.

The above obtained crude was dissolved in DCE (15.0 mL, 0.2 M) and cooled to 0 °C. To this solution was added 3-chloroperbenzoic acid (2.12 g, 12.27 mmol, 2.5 equiv) and was allowed to warm up to room temperature. The reaction mixture was stirred for 2 hours and was filtered over celite and washed with DCE. The mixture was diluted with DCM and washed with half saturated sodium carbonate and the DCM layer was concentrated and was used for the next step without purification.

The crude was dissolved in THF (10.0 mL, 0.5 M) and was added TBAF (1 M in THF, 14.7 mmol, 3.0 equiv) and was allowed to stir overnight. The following day, the reaction mixture was diluted with ethyl acetate and washed with water and then brine. The ethyl

acetate layer was concentrated and purified over silica gel to obtain the diol **74** (1.087 g, 3.19 mmol, 65%). ^{1}H NMR (400 MHz, $CDCl_3$) δ 7.99 (d, *J* = 8.78 Hz, 1H), 6.87 (dd, *J* = 2.51, 8.78 Hz, 1H), 6.71 (d, *J* = 2.51 Hz, 1H), 3.88 (s, 3H), 3.60 - 3.79 (m, 2H), 3.29 - 3.43 (m, 1H), 2.95 - 3.11 (m, 2H), 2.34 - 2.50 (m, 1H), 2.11 (ddd, *J* = 6.53, 11.04, 13.30 Hz, 2H), 1.62 - 1.75 (m, 1H), 1.41 - 1.53 (m, 1H), 1.02 (t, *J* = 7.40 Hz, 2H).

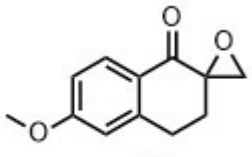

75

6-methoxy-3,4-dihydro-1*H*-spiro[naphthalene-2,2'-oxiran]-1-one

To a solution of the diol **74** (0.320 g, 1.44 mmol, 1.0 equiv) in DMF (14.4 mL, 0.1M) was added DIAD (0.57 mL, 2.88 mmol, 2.0 equiv) and tributylphosphine (0.72 mL, 2.88 mmol, 2.0 equiv). The reaction mixture was allowed to stir overnight and purified over silica gel to obtain the epoxide **75** (0.285 g, 1.39 mmol, 97%). ^{1}H NMR (700 MHz, $CDCl_3$) δ 8.07 (d, *J* = 8.80 Hz, 1H), 6.88 (dd, *J* = 2.64, 8.80 Hz, 1H), 6.76 (d, *J* = 2.64 Hz, 1H), 3.89 (s, 3H), 2.91 (d, *J* = 6.60 Hz, 1H), 2.44 - 2.59 (m, 1H), 1.95 - 2.10 (m, 2H).

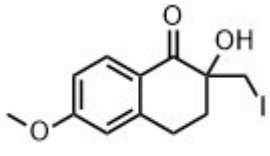

76

2-hydroxy-2-(iodomethyl)-6-methoxy-3,4-dihydronaphthalen-1(2*H*)-one

To a solution of the epoxide **75** (0.04 g, 0.196 mmol, 1.0 equiv) in THF (1.96 mL, 0.1 M) was added TBAI (0.145 g, 0.4 mmol, 2.0 equiv) and boron trifluoride etherate (0.05 mL, 0.4 mmol, 2.0 equiv). The solution was stirred for one hour and was diluted by ethyl acetate. The ethyl acetate layer was washed with water, brine and purified over silica gel to obtain the compound **76** (0.042 g, 0.125 mmol, 64%). ^{1}H NMR (700 MHz, $CDCl_3$) δ 8.00 (d, *J* = 8.80 Hz, 1H), 6.88 (dd, *J* = 2.64, 8.80 Hz, 1H), 6.62 - 6.74 (m, 1H), 3.99 (s, 1H), 3.88 (s, 3H), 3.53 (d, *J* = 11.00 Hz, 1H), 3.30 (dd, *J* = 1.32, 11.00 Hz, 1H), 2.49 (ddd, *J* = 2.42, 4.95, 13.75 Hz, 1H), 2.16 - 2.28 (m, 1H), 1.90 - 2.01 (m, 1H), 1.65 - 1.75 (m, 1H)

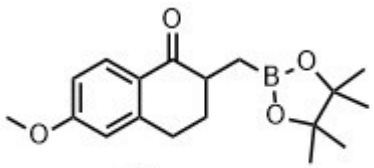

78

6-methoxy-2-((4,4,5,5-tetramethyl-1,3,2-dioxaborolan-2-yl)methyl)-3,4-dihydronaphthalen-1(*2H*)-one

Compound **72** (1.47 g, 8.34 mmol, 1.0 equiv) was dissolved in THF (42.0 mL, 0.2 M) and cooled to -78°C. A solution of LiHMDS (1 M in THF, 12.5 mL, 1.5 equiv) was added dropwise, and the solution was stirred for 30 minutes, following which iodomethylpinacol boronate (12.5 mmol, 1.5 equiv) was added and the solution was stirred at the same temperature for 30 minutes. Then the mixture was allowed to warm to room temperature and was stirred for an additional 2 hours. The reaction mixture was quenched by addition of water and extracted into ethyl acetate and purified on silica gel to get the compound **78** (1.423 g, 4.5 mmol, 55%). ^{1}H NMR (700 MHz, $CDCl_3$) δ 8.02 (d, *J* = 8.80 Hz, 1H), 6.83

(dd, *J* = 2.42, 8.58 Hz, 1H), 6.69 - 6.74 (m, 1H), 3.87 (s, 3H), 2.94 (t, *J* = 5.94 Hz, 2H), 2.57 - 2.64 (m, 2H), 2.18 (s, 1H), 2.13 (td, *J* = 6.22, 12.65 Hz, 2H), 1.24 - 1.34 (m, 9H).

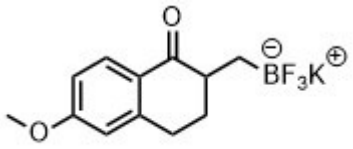

79

potassium trifluoro((6-methoxy-1-oxo-1,2,3,4-tetrahydronaphthalen-2-yl)methyl)borate

The above obtained pinacol boronate (0.925 g, 2.925 mmol, 1.0 equiv) was dissolved in acetonitrile (14.6 mL, 0.2 M) and cooled to 0 °C. To this was added saturated aqueous KHF_2 (4.5 M, 2.6 mL, 4.0 equiv) dropwise at 0 °C and the solution was stirred for 3 hours at room temprature. The resulting suspension was concentrated in vacuo and was purified by continuous Soxhlet extraction with acetone for 12 hours to provide the compound **79** (0.864 g, 2.92 mmol, quant). ^{1}H NMR (400 MHz, DMSO-d_6) δ 7.77 (d, *J* = 8.78 Hz, 1H), 6.71 - 6.87 (m, 2H), 3.80 (s, 3H), 2.64 - 2.79 (m, 1H), 2.30 (tdd, *J* = 3.73, 7.69, 11.45 Hz, 1H), 2.03 - 2.14 (m, 1H), 1.79 - 1.92 (m, 1H), 0.44 (ddd, *J* = 2.89, 6.78, 13.43 Hz, 1H), -0.01 - 0.12 (m, 1H).

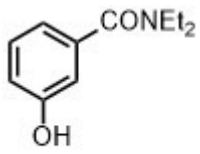

81

***N,N*-diethyl-3-hydroxybenzamide**

To a solution of 3-hydroxybenzoic acid (2.5 g, 18.1 mmol, 1.0 equiv) in DCM (30.0 mL, 0.6 M), cooled to 0 °C was added oxalyl chloride (1.84 mL, 22.0 mmol, 1.2 equiv) and DMF (0.35 mL, catalytic). The reaction was allowed to warm up to room temperature and stirred for 3 hours, followed by removal of all the solvents in vacuo. The crude was dissolved in DCM (30 mL, 0.6 M) and was cooled to 0 °C. To this was added a solution of diethylamine (2.81 mL, 26.89 mmol, 1.48 equiv) and triethylamine (5.04 mL, 36.2 equiv, 2.0 equiv) in DCM (60 mL). The reaction mixture was allowed to warm up to room temperature and stirred overnight. The solution was concentrated in vacuo and the product was purified out over silica gel (3.2 g, 16.6 mmol, 92%).

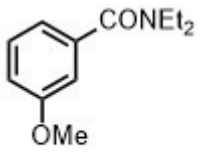

81'

***N,N*-diethyl-3-methoxybenzamide**

The above prepared phenol (3.48 g, 18.1 mmol, 1.0 equiv) was dissolved in acetone (60 mL, 0.3 M) and was added potassium carbonate (3.75 g, 27.15 mmol, 1.5 equiv) and was refluxed. To this solution was added methyl iodide (1.69 mL, 27.15 mmol, 1.5 equiv) and was allowed to react overnight. The crude mixture was allowed to cool down and quenched with 1 N HCl and extracted into ethyl acetate. The ethyl acetate layer was purified over silica gel to get compound **81'** (3.7 g, 18.0 mmol, quant).

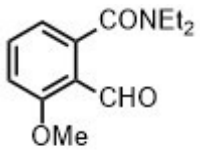

82

***N,N*-diethyl-2-formyl-3-methoxybenzamide**

To a solution of the amide **81'** (1.7 g, 8.24 mmol, 1.0 equiv) in diethyl ether (22.0 mL, 0.4 M) was cooled to -78 °C was added TMEDA (1.23 mL, 8.24 mmol, 1.0 equiv) and dropwise added s-BuLi (7.1 mL, 9.9 mmol, 1.2 equiv). The solution was allowed to stir for one hour followed by the dropwise addition of DMF (0.77 mL, 9.9 mmol, 1.2 equiv). The reaction was maintained for one hour at -78 °C followed by allowing it to warm up to room temperature overnight. The reaction was quenched by addition of 1N HCl and followed by extraction into ethyl acetate. The ethyl acetate layer was purified over silica gel to obtain compound **82** (1.22 g, 5.52 mmol, 67%). ^{1}H NMR (400 MHz, $CDCl_3$) δ 10.49 (s, 1H), 7.55 (dd, *J* = 7.53, 8.53 Hz, 1H), 7.01 (dd, *J* = 0.75, 8.53 Hz, 1H), 6.85 (td, *J* = 0.75, 7.53 Hz, 1H), 3.95 (s, 3H), 3.59 (q, *J* = 7.19 Hz, 2H), 3.07 (q, *J* = 7.03 Hz, 2H), 1.33 (t, *J* = 7.15 Hz, 3H), 1.01 (t, *J* = 7.15 Hz, 3H).

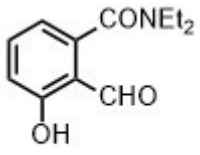

82'

***N,N*-diethyl-2-formyl-3-hydroxybenzamide**

To a solution of compound **82** (0.744 g, 3.162 mmol, 1.0 equiv) in DCM (16.0 mL, 0.2 M), cooled to -78 °C was added boron tribromide (1M in DCM, 2.5 equiv). The reaction was

allowed to warm to room temperature and kept overnight. Saturated solution of ammonium chloride was added to quench the reaction and the product was extracted into DCM and purified over silica gel to give compound **82'** (0.605 g, 2.73 mmol, 87%). ^{1}H NMR (400 MHz, $CDCl_3$) δ 11.58 (s, 1H), 9.95 (d, *J* = 0.50 Hz, 1H), 7.53 (dd, *J* = 7.40, 8.41 Hz, 1H), 7.01 (td, *J* = 0.75, 8.53 Hz, 1H), 6.84 (dd, *J* = 1.00, 7.53 Hz, 1H), 3.62 (br. s., 2H), 3.21 (q, *J* = 7.11 Hz, 2H), 1.29 (t, *J* = 7.00 Hz, 3H), 1.10 (t, *J* = 7.00 Hz, 3H).

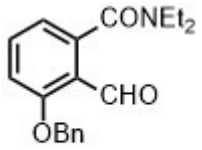

83

3-(benzyloxy)-*N,N*-diethyl-2-formylbenzamide

Benzyl bromide (0.483 mL, 4.065 mmol, 1.5 equiv) was added to a solution of the compound **81'** (0.6 g, 2.71 mmol, 1.0 equiv), sodium hydride (60%, 4.065 mmol, 1.5 equiv) in DMF (13.5 mL, 0.2 M) cooled to 0 °C. The solution was allowed to warm up to room temperature over 4 hours and cooled to 0 °C again. The reaction was quenched by addition of 1N HCl followed by extraction of the product into ethyl acetate and purification over silica gel to obtain compound **83** (0.641 g, 2.05 mmol, 76%). ^{1}H NMR (400 MHz, $CDCl_3$) δ 10.56 (d, *J* = 0.75 Hz, 1H), 7.51 (dd, *J* = 7.53, 8.28 Hz, 1H), 7.33 - 7.47 (m, 5H), 7.05 (dd, *J* = 0.88, 8.41 Hz, 1H), 6.78 - 6.90 (m, 1H), 5.21 (s, 2H), 3.59 (q, *J* = 7.11 Hz, 2H), 3.07 (q, *J* = 7.28 Hz, 2H), 1.32 (t, *J* = 7.15 Hz, 3H), 1.01 (t, *J* = 7.20 Hz, 3H).

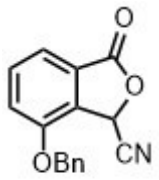

84

7-(benzyloxy)-3-oxo-1,3-dihydroisobenzofuran-1-carbonitrile

To a solution of the compound **83** (0.37 g, 1.19 mmol, 1.0 equiv) in DCM (6.0 mL, 0.2 M) was added 18-crown-6 (0.063 g, 0.24 mmol, 0.2 equiv), potassium cyanide (0.016 g, 0.24 mmol, 0.2 equiv), TMSCN (0.221 mL, 1.67 mmol, 1.4 equiv) and cooled to 0°C. To this solution, dropwise (CAUTION: EVOLUTION OF HCN GAS) was added glacial acetic acid (3.0 mL, 0.4 M). The solution was stirred at 0 °C for 3 hours, followed by stirring at room temperature overnight. The reaction was quenched by addition of 1 N HCl and extraction into DCM. The DCM layer was purified over silica gel to obtain the compound **84** (0.214 g, 0.8 mmol, 68%). ^{1}H NMR (400 MHz, $CDCl_3$) δ 7.50 - 7.64 (m, 2H), 7.32 - 7.48 (m, 5H), 7.20 - 7.29 (m, 1H), 6.00 (s, 1H), 5.18 - 5.34 (m, 2H).

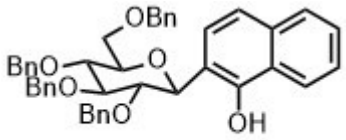

87

2-((2*S*,3*S*,4*R*,5*R*,6*R*)-3,4,5-tris(benzyloxy)-6-((benzyloxy)methyl)tetrahydro-2*H*-pyran-2-yl)naphthalen-1-ol

To a solution of 2,3,4,6-Tetra-*O*-benzyl-D-glucopyranose **86** (0.3 g, 0.55 mmol, 1.0 equiv) in DCM (12.0 mL, 0.023 M) was added trifluoroacetic anhydride (0.084 mL, 0.6 mmol, 1.09 equiv) and stirred for 1h at room temperature. The reaction was concentrated in vacuo and dissolved in DCM (12.0 mL) and added 1-naphthol **85** (0.238 g, 1.65 mmol, 2.97 equiv) and cooled to 0 °C. To this solution was added trifluoromethanesulfonic acid (0.09 mL, 1.021 mmol, 1.84 equiv) dropwise, and the solution was allowed to warm up to room temperature and stirred for 3 hours. The reaction was quenched by addition of water, extracted into DCM and purified over silica gel to obtain the product **87** (0.138 g, 0.2 mmol, 37%). ^{1}H NMR (400 MHz, $CDCl_3$) δ 7.99 - 8.26 (m, 2H), 7.87 - 7.99 (m, 1H), 7.65 - 7.87 (m, 1H), 7.38 - 7.51 (m, 3H), 7.06 - 7.36 (m, 18H), 5.15 (br. s., 1H), 5.03 - 5.12 (m, 1H), 4.28 - 4.47 (m, 2H), 4.00 - 4.23 (m, 4H), 3.86 - 4.00 (m, 1H).

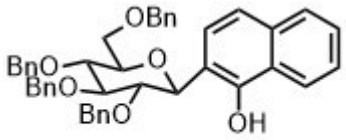

87

2-((2*S*,3*S*,4*R*,5*R*,6*R*)-3,4,5-tris(benzyloxy)-6-((benzyloxy)methyl)tetrahydro-2*H*-pyran-2-yl)naphthalen-1-ol

To a solution of 1-naphthol **85** (0.029 g, 0.2 mmol, 2.0 equiv) and 2,3,4,6-Tetra-*O*-benzyl-D-glucopyranose **86** (0.054 g, 0.1 mmol, 1.0 equiv) and silver perchlorate (0.00415 g, 0.02 mmol, 20 mol%) in DCM (1.0 mL, 0.1 M was added TMSOTf (4.0 µL, 0.02 mmol, 20 mol%) at 0 °C. The reaction mixture was stirred for 2 hours, followed by quenching the reaction with triethylamine and purification over silica gel to give the compound **87** (0.021 g, 0.032 mmol, 32% yield). ^{1}H NMR (400 MHz, $CDCl_3$) δ 7.99 - 8.26 (m, 2H), 7.87 - 7.99

(m, 1H), 7.65 - 7.87 (m, 1H), 7.38 - 7.51 (m, 3H), 7.06 - 7.36 (m, 18H), 5.15 (br. s., 1H), 5.03 - 5.12 (m, 1H), 4.28 - 4.47 (m, 2H), 4.00 - 4.23 (m, 4H), 3.86 - 4.00 (m, 1H).

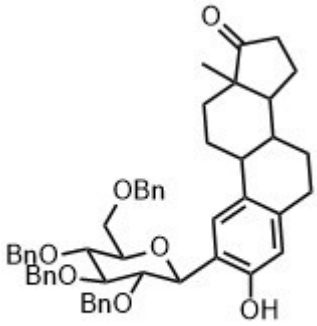

89

3-hydroxy-13-methyl-2-((2*S*,3*S*,4*R*,5*R*,6*R*)-3,4,5-tris(benzyloxy)-6-((benzyloxy)methyl)tetrahydro-2*H*-pyran-2-yl)-6,7,8,9,11,12,13,14,15,16-decahydro-17*H*-cyclopenta[*a*]phenanthren-17-one

To a solution of estrone **88** (0.029 g, 0.2 mmol, 2.0 equiv) and 2,3,4,6-Tetra-*O*-benzyl-D-glucopyranose **86** (0.054 g, 0.1 mmol, 1.0 equiv) and silver perchlorate (0.00415 g, 0.02 mmol, 20 mol%) in DCM (1.0 mL, 0.1 M was added TMSOTf (4.0 µL, 0.02 mmol, 20 mol%) at 0 °C. The reaction mixture was stirred for 2 hours, followed by quenching the reaction with triethylamine and purification over silica gel to give the compound **89** (0.029 g, 0.037 mmol, 37% yield). ^{1}H NMR (400 MHz, $CDCl_3$) δ 6.91 - 7.19 (m, 15H), 6.82 - 6.90 (m, 1H), 6.71 - 6.79 (m, 1H), 3.98 - 4.03 (m, 1H), 3.69 - 3.97 (m, 6H), 2.47 - 2.75 (m, 2H), 2.24 - 2.47 (m, 2H), 1.91 - 2.10 (m, 6H), 1.73 - 1.90 (m, 3H), 1.23 - 1.49 (m, 7H), 1.11 - 1.22 (m, 3H), 0.75 - 0.81 (m, 2H), 0.71 - 0.75 (m, 3H).

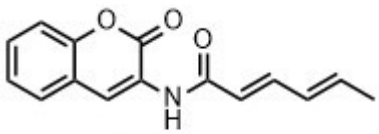

92

(2*E*,4*E*)-*N*-(2-oxo-2*H*-chromen-3-yl)hexa-2,4-dienamide

To a solution of 3-aminocoumarin **90** (0.1 g, 0.621 mmol, 1.0 equiv) in pyridine:DCM (30%, 0.06 M) was added sorbic acid **91** (0.14 g, 1.241 mmol, 2.0 equiv) and EDCI (0.298 g, 1.55 mmol, 2.5 equiv) and the solution was let stir overnight. The following day, reaction mixture was diluted with DCM, washed with copper sulfate solution, dried and purified over silica gel to obtain the amide **92** (0.094 g, 0.37 mmol, 59%). ^{1}H NMR (400 MHz, CDCl3) δ 8.71 - 8.87 (m, 1H), 8.08 (br. s., 1H), 7.53 (dd, *J* = 1.51, 7.78 Hz, 1H), 7.42 - 7.48 (m, 1H), 7.28 - 7.40 (m, 3H), 6.18 - 6.29 (m, 2H), 5.94 (d, *J* = 15.06 Hz, 1H), 1.90 (d, *J* = 5.27 Hz, 3H).

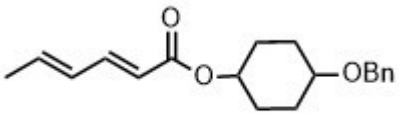

94

4-(benzyloxy)cyclohexyl (2*E*,4*E*)-hexa-2,4-dienoate

To a solution of sorbic acid **93** (0.163 g, 1.45 mmol, 1.5 equiv) in toluene (10.0 mL, 0.1 M) cooled to 0 °C was added triethylamine (0.54 mL, 3.9 mmol, 4.0 equiv) and 2,4,6-trichlorobenzoyl chloride (0.26 mL, 1.65 mmol, 1.7 equiv). The reaction was stirred for 1 hour followed by addition of the alcohol **93** (0.2 g, 0.97 mmol, 1.0 equiv) and DMAP (0.24 g, 1.94 mmol, 2.0 equiv) and was stirred overnight at room temperature. The following day, the reaction was quenched with sodium bicarbonate solution and extracted into

diethyl ether. The ether layer was purified over silica gel to give the compound **94** (0.15g, 0.5 mmol, 51%). ^{1}H NMR (400 MHz, CDCl3) δ 7.19 - 7.43 (m, 5H), 6.07 - 6.28 (m, 2H), 5.70 - 5.83 (m, 1H), 4.82 - 4.98 (m, 1H), 4.51 - 4.59 (m, 2H), 3.40 - 3.58 (m, 1H), 1.99 - 2.10 (m, 2H), 1.80 - 1.99 (m, 5H), 1.61 - 1.79 (m, 2H), 1.40 - 1.61 (m, 2H).

4.3: Experimental for Design and Synthesis of Substrate-Competitive Covalent Inhibitors of AKT

4.3.1: Chemistry Experimentals

Chemical reagents and solvents were purchased from Sigma-Aldrich (MO, USA), Alfa-Aesar (MA, USA), Fisher Scientific (PA, USA). Analytical Thin Layer Chromatography (TLC) was performed using silica gel GHLF plates (Analtech Inc., DE, USA). Flash chromatography was performed on TELEDYNE ISCO CombiFlash® Rf instrument using RediSep Rf Normal-phase Flash Columns (4-gm, 12-gm, 24-gm or 40-gm). ^{1}H NMR and ^{13}C NMR spectra were recorded on a Bruker TopSpin 400 MHz using deuterated chloroform ($CDCl_3$) or methanol (CD_3OD). All chemical shifts are reported as δ in units of parts per million (ppm) relative to chloroform and methanol residual peaks at 7.26 and 3.31 respectively (^{1}H NMR spectra); 77.16 and 49.00 respectively (^{13}C NMR spectra). The data is reported as: chemical shifts (ppm), multiplicity (s = singlet, d = doublet, dd = doublet of doublets, t = triplet, q = quartet, m = multiplet), coupling constant(s) (Hz) and integral values. Electrospray ionization (ESI) mass spectra were obtained from Perkin Elmer Flexar UPLC/AxION2 TOF Mass Spectrometer.

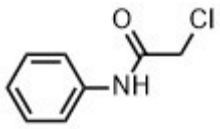

125

2-Chloro-N-phenylacetamide

To a stirred solution of aniline **123** (1.0 g, 10.74 mol, 1.0 equiv) and triethylamine (1.79 mL, 12.9 mmol, 1.2 equiv) in dichlomethane (11.0 mL, 1.0 M), cooled to 0 °C, was added chloroacetyl chloride (1.03 mL, 12.9 mmol, 1.2 equiv) dropwise and the mixture was allowed to warm up to room temperature overnight after which the mixture was washed with 1 N HCl and dried over anhydrous sodium sulfate. The DCM layer was concentrated in vacuo and purified over silica gel to get the desired compound **125** (1.821 g, 10.73 mmol, quant). ^{1}H NMR (400 MHz, $CDCl_3$) δ 8.24 (br. s., 1H), 7.56 (d, *J* = 8.53 Hz, 2H), 7.38 (t, *J* = 7.91 Hz, 2H), 7.13 - 7.23 (m, 1H), 4.21 (s, 2H). ^{13}C NMR (101 MHz, CDCl3) δ 163.9, 136.6, 129.1, 125.3, 120.2, 42.9. HRMS (ESI) C_8H_9ClNO *m/z* $[M+H]^+$ found 170.0338, expected 170.0373.

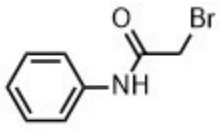

129

2-bromo-*N*-phenylacetamide

To a stirred solution of aniline **123** (0.2 g, 2.15 mmol, 1.0 equiv and triethylamine (0.36 mL, 2.6 mmol, 1.2 equiv) in dichlomethane (2.5 mL, 1.0 M), cooled to 0 °C was added bromoacetyl chloride (0.215 mL, 2.6 mmol, 1.2 equiv) dropwise and the mixture was allowed to warm up to room temperature overnight after which the mixture was washed

with 1 N HCl and dried over anhydrous sodium sulfate. The DCM layer was concentrated in vacuo and purified over silica gel to get the desired compound **129** (0.45 g, 2.13 mmol, quant). ^{1}H NMR (400 MHz, $CDCl_3$) δ 8.23 (br. s., 1H), 7.55 (t, *J* = 7.30 Hz, 2H), 7.37 (t, *J* = 8.03 Hz, 2H), 7.14 - 7.22 (m, 1H), 4.21 (s, 2H). ^{13}C NMR (101 MHz, CDCl3) δ 163.8, 136.7, 129.1, 125.2, 120.1, 29.4. HRMS (ESI) C_8H_9BrNO *m/z* $[M+H]^+$ found 213.9827, expected 213.9867.

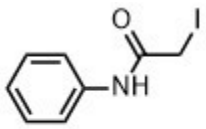

127

2-iodo-*N*-phenylacetamide

To a solution of the aniline **123** (0.5 g, 2.95 mmol, 1.0 equiv) in acetone (15.0 mL, 0.2 M) was added sodium iodide (1.76 g, 11.79 mmol, 4.0 equiv) and refluxed overnight, following which the solution was allowed to cool to room temp and the acetone was removed in vacuo. The crude was taken up in ethyl acetate and washed with sodium thiosulphate solution and was dried over anhydrous sodium sulphate and was purified over silica gel to get the compound **127** (0.645 g, 2.47 mmol, 84%). ^{1}H NMR (400 MHz, $CDCl_3$) δ 7.70 (br. s., 1H), 7.51 (d, *J* = 7.53 Hz, 2H), 7.36 (t, *J* = 8.03 Hz, 2H), 7.12 - 7.20 (m, 1H), 3.87 (s, 2H). ^{13}C NMR (101 MHz, $CDCl_3$) δ 164.9, 137.3, 129.1, 125.0, 120.0, -0.1. HRMS (ESI) C_8H_9INO *m/z* $[M+H]^+$ found 261.9692, expected 261.9728.

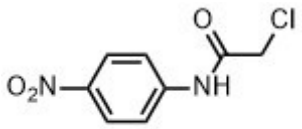

126

2-chloro-*N*-(4-nitrophenyl)acetamide

To a stirred solution of aniline **124** (1.5 g, 10.86 mmol, 1.0 equiv and triethylamine (1.81 mL, 13.03 mmol, 1.2 equiv) in dichlomethane (11.0 mL, 1.0 M), cooled to 0 ˚C was added chloroacetyl chloride (1.04 mL, 13.03 mmol, 1.2 equiv) dropwise and the mixture was allowed to warm up to room temperature overnight after which the mixture was washed with 1 N HCl and dried over anhydrous sodium sulfate. The DCM layer was concentrated in vacuo and purified over silica gel to get the desired compound **126** (0.586 g, 2.73 mmol, 25%). ^{1}H NMR (400 MHz, $CDCl_3$) δ 8.27 (d, *J* = 9.29 Hz, 2H), 8.06 (br. s., 1H), 7.78 (d, *J* = 9.03 Hz, 2H), 4.25 (s, 2H). ^{13}C NMR (101 MHz, $CDCl_3$) δ 167.5, 145.0, 143.7, 125.2, 119.6, 40.5.

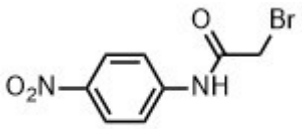

130

2-bromo-*N*-(4-nitrophenyl)acetamide

To a stirred solution of aniline **124** (1.0 g, 7.24 mmol, 1.0 equiv and triethylamine (1.2 mL, 8.7 mmol, 1.2 equiv) in dichlomethane (2.5 mL, 1.0 M), cooled to 0 ˚C was added bromoacetyl chloride (1.2 mL, 8.7 mmol, 1.2 equiv) dropwise and the mixture was allowed to warm up to room temperature overnight after which the mixture was washed with 1 N

HCl and dried over anhydrous sodium sulfate. The DCM layer was concentrated in vacuo and purified over silica gel to get the desired compound **130** (0.882 g, 3.4 mmol, 47%). ^{1}H NMR (400 MHz, $CDCl_3$) δ 8.49 (br. s., 1H), 8.27 (d, *J* = 9.00 Hz, 2H), 7.78 (d, *J* = 9.00 Hz, 2H), 4.25 (s, 2H). ^{13}C NMR (101 MHz, $CDCl_3$) δ 164.2, 144.4, 142.3, 125.1, 119.5, 29.1

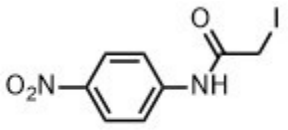

128

2-iodo-*N*-(4-nitrophenyl)acetamide

To a solution of the aniline **124** (0.586 g, 2.73 mmol, 1.0 equiv) in acetone (13.0 mL, 0.2 M) was added sodium iodide (1.64 g, 10.92 mmol, 4.0 equiv) and refluxed overnight, following which the solution was allowed to cool to room temprature and the acetone was removed in vacuo. The crude was taken up in ethyl acetate and washed with sodium thiosulphate solution and was dried over anhydrous sodium sulphate and was purified over silica gel to get the compound **128** (0.468 g, 1.53 mmol, 56%). ^{1}H NMR (400 MHz, $CDCl_3$) δ 8.25 (d, *J* = 9.03 Hz, 2H), 7.72 (d, *J* = 9.29 Hz, 2H), 3.90 (s, 2H). ^{13}C NMR (101 MHz, CD_6CO) δ 168.1, 146.0, 125.8, 120.0, 0.0. HRMS (ESI) $C_8H_6IN_2O_3$ *m/z* $[M-H]^-$ found 304.9442, expected 304.9423.

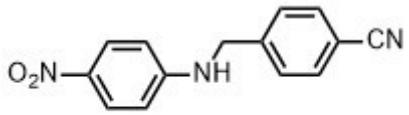

131

4-(((4-nitrophenyl)amino)methyl)benzonitrile

To a solution of the aniline **124** (0.1 g, 0.72 mmol, 1.0 equiv) and 4-formylbenzonitrile (0.095 g, 0.72 mmol, 1.0 equiv) in dichloroethane (2.42 mL, 0.3 M) was added glacial acetic acid (0.041 mL, 0.72 mmol, 1.0 equiv) and sodium triacetoxyborohydride (0.215 g, 1.01 mmol, 1.4 equiv). The mixture was stirred for 2.5 hours at room temperature, following which DCE was removed in vacuo. The crude was taken in ethyl acetate and washed with sat. sodium bicarbonate solution. The ethyl acetate layer was dried over sodium sulphate and the product was crystallized from DCM to give **131** (0.096 g, 0.38 mmol, 52%). ^{1}H NMR (400 MHz, CD_6CO) δ 8.02 (d, *J* = 9.00 Hz, 2H), 7.76 (d, *J* = 8.50 Hz, 2H), 7.62 (d, *J* = 8.50 Hz, 2H), 6.75 (d, *J* = 9.00 Hz, 2H), 4.67 (s, 2H)

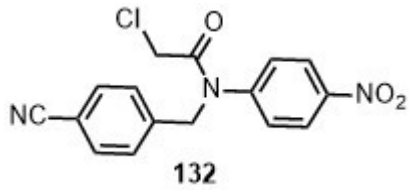

132

2-chloro-*N*-(4-cyanobenzyl)-*N*-(4-nitrophenyl)acetamide

To a stirred solution of aniline **131** (0.2 g, 0.79 mmol, 1.0 equiv and triethylamine (0.13 mL, 0.95 mmol, 1.2 equiv) in dichlomethane (4.0 mL, 0.2 M), cooled to 0 °C, was added chloroacetyl chloride (0.075 mL, 0.95 mmol, 1.2 equiv) dropwise and the mixture was allowed to warm up to room temperature overnight after which the mixture was washed

with 1 N HCl and dried over anhydrous sodium sulfate. The DCM layer was concentrated in vacuo and purified over silica gel to get the desired compound **132** (0.202 g, 0.61 mmol, 77%). ^{1}H NMR (400 MHz, $CDCl_3$) δ 8.29 (d, *J* = 9.03 Hz, 2H), 7.63 (d, *J* = 8.53 Hz, 2H), 7.34 (d, *J* = 8.53 Hz, 2H), 7.29 (d, *J* = 8.78 Hz, 2H), 5.00 (s, 2H), 3.89 (s, 2H)

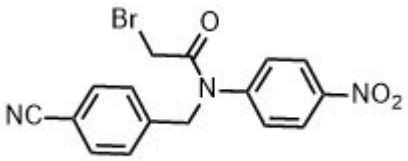

134

2-bromo-*N*-(4-cyanobenzyl)-*N*-(4-nitrophenyl)acetamide

To a stirred solution of aniline **131** (0.2 g, 0.79 mmol, 1.0 equiv and triethylamine (0.13 mL, 0.95 mmol, 1.2 equiv) in dichlomethane (4.0 mL, 0.2 M), cooled to 0 ˚C, was added bromoacetyl chloride (0.08 mL, 0.95 mmol, 1.2 equiv) dropwise and the mixture was allowed to warm up to room temperature overnight after which the mixture was washed with 1 N HCl and dried over anhydrous sodium sulfate. The DCM layer was concentrated in vacuo and purified over silica gel to get the desired compound **134** (0.216 g, 0.58 mmol, 69%). ^{1}H NMR (400 MHz, $CDCl_3$) δ 8.28 (d, *J* = 8.78 Hz, 2H), 7.62 (d, *J* = 8.28 Hz, 2H), 7.34 (d, *J* = 8.03 Hz, 2H), 7.29 (d, *J* = 9.03 Hz, 2H), 5.00 (s, 2H), 3.89 (s, 2H). ^{13}C NMR (101 MHz, $CDCl_3$) δ 166.1, 146.2, 141.0, 132.7, 129.2, 128.9, 125.5, 118.2, 112.3, 53.4, 25.9.

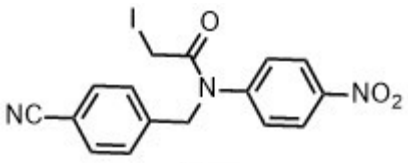

133

2-iodo-*N*-(4-cyanobenzyl)-*N*-(4-nitrophenyl)acetamide

To a solution of the aniline **132** (0.081 g, 0.246 mmol, 1.0 equiv) in acetone (13.0 mL, 0.2 M) was added sodium iodide (0.148 g, 0.989 mmol, 4.0 equiv) and refluxed overnight, following which the solution was allowed to cool to room temprature and the acetone was removed in vacuo. The crude was taken up in ethyl acetate and washed with sodium thiosulphate solution, dried over anhydrous sodium sulphate, and was purified over silica gel to get the compound **133** (0.118 g, 0.24 mmol, quant). ^{1}H NMR (400 MHz, CD_6CO) δ 8.30 (d, *J* = 9.03 Hz, 2H), 7.68 (d, *J* = 9.03 Hz, 2H), 7.73 (d, *J* = 8.53 Hz, 2H), 7.51 (d, *J* = 8.50 Hz, 2H), 5.11 (s, 2H), 3.83 (s, 2H). ^{13}C NMR (101 MHz, CD_6CO) δ 168.8, 149.2, 144.1, 133.9, 130.6, 126.5, 119.8, 112.9, 54.3, -1.1. HRMS (ESI) $C_{16}H_{13}IN_3O_3$ *m/z* $[M+H]^+$ found 421.9951, expected 422.0001.

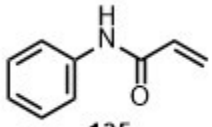

135

***N*-phenylacrylamide**

To a stirred solution of aniline **123** (1.0 g, 10.74 mmol, 1.0 equiv) and triethylamine (1.79 mL, 12.9 mmol, 1.2 equiv) in dichlomethane (11.0 mL, 1.0 M), cooled to 0 °C was added acryloyl chloride (1.05 mL, 12.88 mmol, 1.2 equiv) dropwise and the mixture was allowed to warm up to room temperature overnight after which the mixture was washed with 1N HCl and dried over anhydrous sodium sulfate. The DCM layer was concentrated in vacuo and purified over silica gel to get the desired compound **135** (1.182 g, 8.03 mmol, 75%).

^{1}H NMR (400 MHz, CDCl3) δ 7.59 (d, *J* = 7.03 Hz, 2H), 7.31 - 7.40 (m, 2H), 7.09 - 7.18 (m, 1H), 6.45 (dd, *J* = 1.25, 16.81 Hz, 1H), 6.26 (dd, *J* = 10.16, 16.94 Hz, 1H), 5.78 (dd, *J* = 1.25, 10.04 Hz, 1H). ^{13}C NMR (101 MHz, $CDCl_3$) δ 137.7, 131.2, 129.0, 127.7, 124.6, 120.0. HRMS (ESI) $C_9H_{10}NO$ *m/z* $[M+H]^+$ found 148.0741, expected 148.0762.

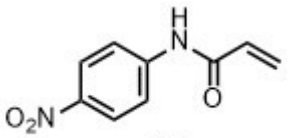

136

***N*-(4-nitrophenyl)acrylamide**

To a stirred solution of aniline **124** (1.5 g, 10.86 mmol, 1.0 equiv) and triethylamine (1.81 mL, 13.03 mmol, 1.2 equiv) in dichlomethane (11.0 mL, 1.0 M), cooled to 0° was added acryloyl chloride (1.06 mL, 13.03 mmol, 1.2 equiv) dropwise and the mixture was allowed to warm up to room temperature overnight after which the mixture was washed with 1 N HCl and dried over anhydrous sodium sulfate. The DCM layer was concentrated in vacuo and purified over silica gel to get the desired compound **136** (0.322 g, 1.68 mmol, 15%). ^{1}H NMR (400 MHz, $CDCl_3$) δ 8.25 (d, *J* = 9.00 Hz, 2H), 7.79 (d, *J* = 9.00 Hz, 2H), 6.52 (dd, *J* = 1.00, 16.81 Hz, 1H), 6.28 (dd, *J* = 10.29, 16.81 Hz, 1H), 5.90 (dd, *J* = 1.13, 10.16 Hz, 1H). ^{13}C NMR (101 MHz, $CDCl_3$) δ 143.5, 130.4, 129.6, 125.1, 119.3.

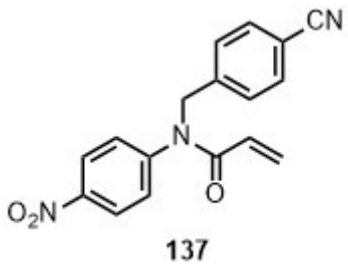

137

***N*-(4-cyanobenzyl)-*N*-(4-nitrophenyl)acrylamide**

To a stirred solution of aniline **131** (0.096 g, 0.38 mmol, 1.0 equiv) and triethylamine (0.064 mL, 0.46 mmol, 1.2 equiv) in dichlomethane (2.0 mL, 0.2 M), cooled to 0 ˚C was added acryloyl chloride (0.064 mL, 0.46 mmol, 1.2 equiv) dropwise and the mixture was allowed to warm up to room temperature overnight after which the mixture was washed with 1N HCl and dried over anhydrous sodium sulfate. The DCM layer was concentrated in vacuo and purified over silica gel to get the desired compound **137** (0.076 g, 0.25 mmol, 65%). ^{1}H NMR (400 MHz, $CDCl_3$) δ 8.25 (d, *J* = 8.53 Hz, 2H), 7.61 (d, *J* = 8.28 Hz, 2H), 7.35 (d, *J* = 8.03 Hz, 2H), 7.23 (d, *J* = 8.78 Hz, 2H), 6.53 (dd, *J* = 1.38, 16.94 Hz, 1H), 6.06 (dd, *J* = 10.29, 16.56 Hz, 1H), 5.72 (dd, *J* = 1.51, 10.54 Hz, 1H), 5.09 (s, 2H). ^{13}C NMR (101 MHz, $CDCl_3$) δ 165.3, 147.2, 141.8, 132.6, 132.4, 130.1, 128.8, 128.3, 127.6, 127.6, 127.0, 126.2, 125.9, 125.0, 118.3, 111.7, 111.4, 52.7. HRMS (ESI) $C_{17}H_{12}N_3O_3$ *m/z* $[M-H]^-$ found 306.0819, expected 306.0878.

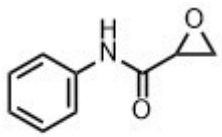

138

***N*-phenyloxirane-2-carboxamide**

To a solution of aniline **135** (0.1 g, 0.68 mmol, 1.0 equiv) in dichloromethane (4.0 mL, 0.2 M) was added m-CPBA (1.6 g, 6.8 mmol, 10.0 equiv). The mixture was refluxed overnight, followed by extracting the crude into ethylacetate and washing with sat. sodium bicarbonate solution. The ethylacetate layer was concentrated and purified on silica gel to give the desired compound **138** (0.020 g, 0.13 mmol, 18%). ^{1}H NMR (400 MHz, $CDCl_3$)

δ 7.79 (br. s., 1H), 7.49 - 7.56 (m, 2H), 7.35 (t, *J* = 8.00 Hz, 2H), 7.10 - 7.18 (m, 1H), 3.58 (dd, *J* = 2.64, 4.64 Hz, 1H), 3.11 (dd, *J* = 4.64, 5.40 Hz, 1H), 2.93 (dd, *J* = 2.60, 4.50 Hz, 1H). ^{13}C NMR (101 MHz, CD_6CO) δ 168.0, 130.1, 125.3, 125.1, 121.2, 120.9, 50.7, 47.6. HRMS (ESI) $C_9H_{10}NO_2$ *m/z* $[M+H]^+$ found 164.0684, expected 164.0711.

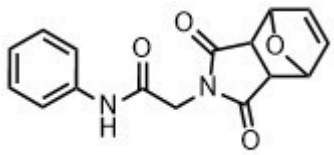

140

2-(1,3-dioxo-1,3,3a,4,7,7a-hexahydro-2H-4,7-epoxyisoindol-2-yl)-N-phenylacetamide

To a stirred solution of aniline **127** (0.24 g, 0.9 mmol, 1.2 equiv) and imide **139** [191](0.127 g, 0.77 mmol, 1.0 equiv) in acetonitrile (8.0 mL, 0.1 M) was added potassium carbonate (0.212 g, 1.54 mmol, 2.0 equiv) and refluxed overnight. The ethyl acetate solution was cooled, washed with 1N HCl, dried over sodium sulphate and purified over silica gel to obtain compound **140** (0.059 mg, 0.2 mmol, 26%). ^{1}H NMR (400 MHz, $CDCl_3$) δ 7.64 (br. s., 1H), 7.49 (d, *J* = 7.53 Hz, 2H), 7.30 (d, *J* = 7.50 Hz, 2H), 7.11 (t, *J* = 7.53 Hz, 1H), 6.60 (s, 2H), 5.41 (s, 2H), 4.34 (s, 2H), 3.03 (s, 2H)

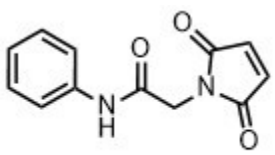

141

2-(2,5-dioxo-2,5-dihydro-1H-pyrrol-1-yl)-N-phenylacetamide

Maleimide **140** (0.059 g, 0.26 mmol) was heated in anisole (0.5 mL, 0.5 M) at 140 °C for 4 hours. The solution was purified over silica gel to obtain compound **141** (0.036 g, 0.16 mmol, 60%). ^{1}H NMR (400 MHz, $CDCl_3$) δ 7.48 (d, *J* = 7.78 Hz, 2H), 7.40 (br. s., 1H), 7.33 (t, *J* = 7.65 Hz, 2H), 7.10 - 7.18 (m, 1H), 6.83 (s, 2H), 4.35 (s, 2H). ^{13}C NMR (101 MHz, $CDCl_3$) δ 170.1, 134.6, 129.1, 124.9, 120.0, 41.3. HRMS (ESI) $C_{12}H_{11}N_2O_3$ *m/z* $[M+H]^+$ found 231.0724, expected 231.0769.

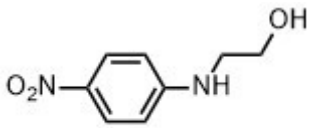

143

2-((4-nitrophenyl)amino)ethan-1-ol

To a solution of 1-fluoro-4-nitrobenzene **142** (0.2 g, 1.42 mmol, 1.0 equiv) in DMSO (3.0 mL, 0.5 M) was added ethanolamine (0.096 g, 1.56 mmol, 1.1 equiv) and potassium carbonate (294 mg, 2.13 mmol, 1.5 equiv). The mixture was warmed to 45 °C and kept overnight. The crude solution in DMSO was taken up in ethyl acetate and washed with water. The ethyl acetate layer was dried on sodium sulfate and purified over sodium sulfate to give the compound **143** (0.225 g, 1.24 mmol, 87%). ^{1}H NMR (400 MHz, CDCl3) δ 8.11 (d, *J* = 9.00 Hz, 2H), 6.59 (d, *J* = 9.00 Hz, 2H), 3.92 (t, *J* = 5.00 Hz, 2H), 3.41 (t, *J* = 5.00 Hz, 2H)

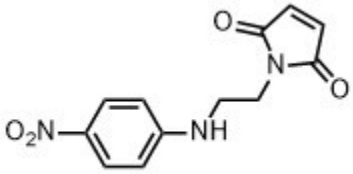

144

1-(2-((4-nitrophenyl)amino)ethyl)-1H-pyrrole-2,5-dione

To a solution of compound **143** (0.1 g, 0.549 mmol, 1.1 equiv) in THF (5.5 mL, 0.15 M) at -78 °C was added DEAD (0.087 g, 0.5 mmol, 1.0 equiv), triphenylphosphine (0.131 g, 0.5 mmol, 1.0 equiv) and tert-butanol (0.024 mL, 0.25 mmol, 0.5 equiv). The mixture was stirred for 30 minutes followed by addition of maleimide (0.049 g, 0.5 mmol, 1.0 equiv) and was raised to room temperature and stirred overnight. The crude mixture was taken up in ethyl acetate and washed with water and the ethyl acetate layer dried over sodium sulfate and purified over silica gel to obtain compound **144** (0.034 g, 0.13 mmol, 24%). ^{1}H NMR (400 MHz, CD_6CO) δ 8.03 (d, *J* = 9.29 Hz, 2H), 6.87 (s, 2H), 6.73 (d, *J* = 9.29 Hz, 2H), 3.68 - 3.78 (m, 2H), 3.53 (q, *J* = 6.44 Hz, 2H). ^{13}C NMR (101 MHz, CD_6CO) δ 172.3, 155.5, 139.0, 135.9, 127.4, 112.5, 42.4. HRMS (ESI) $C_{12}H_{12}N_3O_4$ *m/z* $[M+H]^+$ found 262.0830, expected 262.0827.

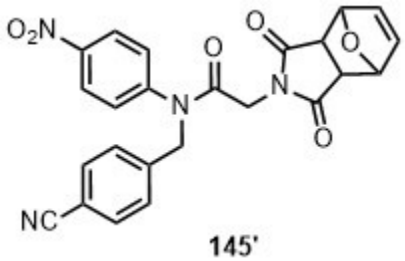

145'

***N*-(4-cyanobenzyl)-2-(1,3-dioxo-1,3,3a,4,7,7a-hexahydro-2H-4,7-epoxyisoindol-2-yl)-N-(4-nitrophenyl)acetamide**

To a solution of the compound **133** (0.036 g, 0.085 mmol, 1.0 equiv) in acetonitrile (0.85 mL, 0.1 M) was added compound **139** (0.027 g, 0.085 mmol, 1.0 equiv) and potassium carbonate (0.012 g, 0.085 mmol, 1.0 equiv). The mixture was stirred at 50 °C for 2 hours, followed by concentration of the solvent and washing the crude in ethyl acetate with 1 N

HCl to obtain the product **145'**, which was sufficiently pure to be used for the next step. ^{1}H NMR (400 MHz, $CDCl_3$) δ 8.28 (d, *J* = 8.53 Hz, 2H), 7.62 (d, *J* = 8.28 Hz, 2H), 7.30 - 7.41 (m, 4H), 6.53 (s, 4H), 5.26 (s, 2H), 4.98 (s, 2H), 4.01 (s, 2H). ^{13}C NMR (101 MHz, Acetone) δ 171.7, 167.5, 148.8, 148.2, 143.9, 136.3, 133.9, 130.9, 130.6, 126.7, 119.7, 112.9, 54.1, 40.9.

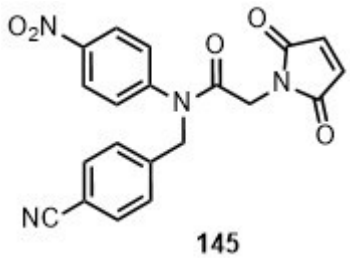

145

***N*-(4-cyanobenzyl)-2-(2,5-dioxo-2,5-dihydro-1H-pyrrol-1-yl)-N-(4-nitrophenyl)acetamide**

The compound **145'** (0.066 g, 0.144 mmol, 1.0 equiv) was stirred in anisole (0.3 mL, 0.5 M) at 140 °C overnight, after which the compound **145** was isolated by purification on silica gel (0.04 g, 0.1 mmol, 71%). ^{1}H NMR (400 MHz, $CDCl_3$) δ 8.31 (d, *J* = 8.78 Hz, 2H), 7.62 (d, *J* = 8.28 Hz, 2H), 7.38 (d, *J* = 8.78 Hz, 2H), 7.32 (d, *J* = 8.03 Hz, 2H), 6.80 (s, 2H), 4.97 (s, 2H), 4.06 (s, 2H). HRMS (ESI) $C_{20}H_{15}N_4O_5$ *m/z* $[M+H]^+$ found 391.1045, expected 391.1042.

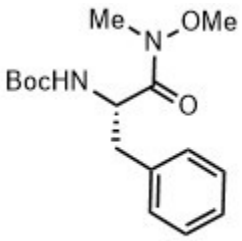

147

***tert*-Butyl(*S*)-(1-(methoxy(methyl)amino)-1-oxo-3-phenylpropan-2-yl)carbamate:** To a mixture of EDCI (0.920 g, 4.8 mmol) and HOBt (0.595 g, 4.4 mmol) in anhydrous dichloromethane (16.7 mL) was added 2-(*tert*-butoxycarbonylamino)-3-phenylpropanoic acid **146** (1.061 g, 4 mmol) and stirred at 0 °C for 30 min. *N,O*-Dimethylhydroxylamine hydrochloride (0.449 g, 4.6 mmol) and *N*-methylmorpholine (0.53 mL, 4.4 mmol) were added to the mixture and the reaction was stirred at room temperature for 16 hours. The reaction mixture was washed with 1 N HCl and then saturated $NaHCO_3$. The organic layer was dried over anhydrous sodium sulphate and concentrated *in vacuo*. The crude product was purified by column chromatography (silica gel, ethyl acetate:hexane 1:4) to give the desired product as colorless oil **147** (1.13 g, 96% yield). ^1H NMR (400 MHz, $CDCl_3$) δ 7.28 (m, 2H) 7.22 (d, *J*=7.2, 1H), 7.17 (d, *J*=7.6, 2H), 5.14 (br, 1H), 4.95 (br, 1H), 3.65 (s, 3H), 3.16 (s, 3H), 3.05 (dd, *J1*=6.2, *J2*=13.5, 1H), 2.89 (m, 1H), 1.39 (s, 9H).

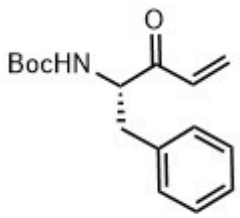

148

***tert*-Butyl 3-oxo-1-phenylpent-4-en-2-ylcarbamate**

Weinreb amide **147** (0.13 g, 0.42 mmol) was dissolved in anhydrous THF (1.3 mL). The reaction mixture was cooled to -40 °C in a dry ice/acetonitrile bath and purged with argon before 1 M vinyl magnesium bromide in THF (1.26 mL, 1.26 mmol) was added dropwise. After 3 hours stirring at -40 °C, the reaction mixture was poured into cold 3 N HCl, and

extracted three times with ethyl acetate. The combined organic layers were dried over anhydrous sodium sulphate and concentrated *in vacuo*. The crude product was purified over silica gel chromatography to obtain the desired product as white solid **148** (0.081 g, 70% yield). ^{1}H NMR (400MHz, $CDCl_3$) δ 7.25 (m, 3H) 7.10 (d, *J*=7.4, 2H), 6.41 (m, 2H), 5.83 (d, *J*=10.4, 1H), 5.22 (m, 1H), 4.86 (q, *J*=9, 1H), 3.14 (dd, *J1*=6.4, *J2*=13.8, 1H), 2.98 (dd, *J1*=8.0, *J2*=15.4, 1H), 1.42 (s, 9H). ^{13}C NMR (100MHz, $CDCl_3$) δ 197.9, 155.2, 136.0, 133.5, 130.2, 129.6, 128.6, 127.1, 79.9, 58.3, 38.2, 28.4. HRMS (ESI) $C_{16}H_{21}NO_3$ *m/z* $[M+Na]^+$ found 298.1415, expected 298.1419.

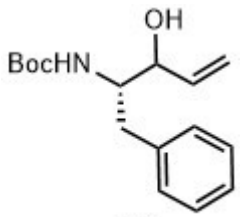

149

***t*ert-butyl ((2S)-3-hydroxy-1-phenylpent-4-en-2-yl)carbamate**

To the vinyl ketone **148** 0.265 g, 0.962 mmol, 1.0 equiv) in methanol (3.21 mL, 0.3M) cooled to 0 °C was added sodium bohydride (0.109 g, 2.9 mmol, 3.0 equiv). The mixture was stirred for 2 hours, following which it was quenched with dilute acetic acid, taken up in ethyl acetate and washed with saturated sodium bicarbonate solution. The ethyl acetate layer was dried over anhydrous sodium sulfate and concentrated to get the compound **149** (0.267 g, 0.96 mmol, quant), which was sufficiently pure to use for the next step.

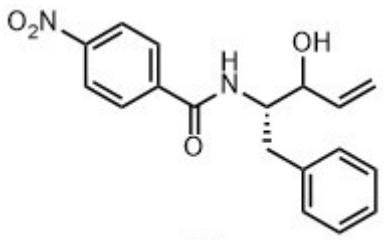

150

***N*-((2S)-3-hydroxy-1-phenylpent-4-en-2-yl)-4-nitrobenzamide**

The a solution of the alcohol **149** (0.117 g, 0.422 mmol, 1.0 equiv) in DCM (0.9 mL, 0.5 M), cooled to 0 °C was added 2,6-lutidine (0.16 mL, 1.5 M) and TMSOTf (0.163 mL, 1M). The solution was warmed to room temperature and stirred for 3 hours, following which it was concentrated in vacuo and was added into a solution of 4-nitrobenzoic acid (0.071 g, 0.422 mmol, 1.0 equiv), PyBOP (0.221 g, 0.422 mmol, 1.0 equiv), DIPEA (0.15 mL, 0.844 mmol, 2.0 equiv) in DCM (4.2 mL, 0.1 M). The mixture was stirred overnight and was diluted with DCM and washed with 1 N HCl. The DCM layer was dried on sodium sulfate and was purified over silica gel to get the alcohol **150** (0.103 g, 0.32 mmol, 75%). ^{1}H NMR (400 MHz, $CDCl_3$) δ 8.17 - 8.38 (m, 2H), 7.77 - 7.93 (m, 1H), 7.63 - 7.77 (m, 1H), 7.13 - 7.40 (m, 5H), 5.84 - 6.11 (m, 1H), 5.46 (td, *J* = 1.47, 17.13 Hz, 1H), 5.28 - 5.39 (m, 1H), 4.35 - 4.59 (m, 1H), 2.99 - 3.15 (m, 1H), 2.93 (dd, *J* = 9.41, 14.43 Hz, 1H)

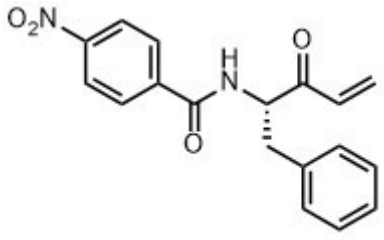

151

(*S*)-4-nitro-N-(3-oxo-1-phenylpent-4-en-2-yl)benzamide

The alcohol **150** (0.030 g, 0.092 mmol, 1.0 equiv) was dissolved in DCM (1.0 mL, 0.1 M) and Dess-Martin periodinane (0.039 g, 0.092 mmol, 1.0 equiv) was added. The mixture was stirred at room temprature overnight, followed by dilution with DCM and washing with sodium thiosulfate solution. The DCM layer was dried and purified over silica gel to get the vinyl ketone **151** (0.029 g, 0.089 mmol, 97%). ^{1}H NMR (400 MHz, $CDCl_3$) δ 8.29 (d, *J* = 9.00 Hz, 2H), 7.89 (d, *J* = 9.00 Hz, 2H), 7.20 - 7.37 (m, 5H), 7.03 - 7.18 (m, 2H), 6.94 (d, *J* = 6.27 Hz, 1H), 6.40 - 6.61 (m, 2H), 5.99 (dd, *J* = 1.63, 9.91 Hz, 1H), 5.38 (dt, *J* = 4.77, 6.90 Hz, 1H), 3.38 (dd, *J* = 6.78, 14.05 Hz, 1H), 3.14 - 3.30 (m, 1H). ^{13}C NMR (101 MHz, CD_6CO) δ 197.7, 165.7, 150.6, 140.9, 138.7, 138.4, 134.5, 130.2, 130.1, 129.7, 129.5, 129.2, 127.5, 124.4, 59.3, 36.9. HRMS (ESI) $C_{18}H_{17}N_2O_4$ *m/z* [M+H] $^{+}$ found 325.1198, expected 325.1188.

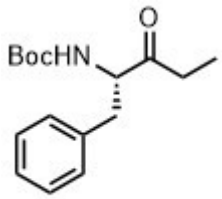

152

***t*ert-butyl (S)-(3-oxo-1-phenylpentan-2-yl)carbamate**

To a solution of the vinyl ketone **148** (0.009 g, 0.032 mmol) in ethyl acetate (1 mL) was added 5% Pd/C (20% w/w). The reaction mixture was stirred under a hydrogen balloon at room temperature overnight. The catalyst was removed by filtration, and the filtrate was concentrated *in vacuo* to afford the desired product as white solid **152** (0.009 g, quantitative yield). ^{1}H NMR (400MHz, $CDCl_3$) *δ* 7.28 (m, 3H), 7.14 (d, *J*=6.8, 2H), 5.12 (s, 1H), 4.54 (q, *J*=7.4, 1H), 3.00 (m, 2H), 2.38 (m, 2H), 1.41 (s, 9H), 1.00 (t, *J*= ,3H). ^{13}C

NMR (100MHz, $CDCl_3$) δ 209.9, 155.3, 136.4, 129.4, 128.8, 127.1, 80.0, 60.0, 38.3, 34.3, 28.5, 7.5. HRMS (ESI) $C_{16}H_{23}NO_3$ *m/z* $[M+H]^+$ found 278.1735, expected 278.1756; $[M+Na]^+$ found 300.1566, expected 300.1575.

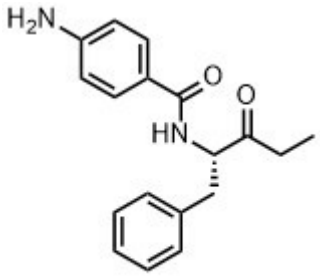

153

(*S*)-4-amino-N-(3-oxo-1-phenylpentan-2-yl)benzamide

To a solution of the vinyl ketone **151** (0.01 g, 0.03 mmol) in ethyl acetate (0.3 mL, 0.1 M) was added 5% Pd/C (20% w/w). The reaction mixture was stirred under a hydrogen balloon at room temperature overnight. The catalyst was removed by filtration, and the filtrate was concentrated *in vacuo* to afford the desired product as white solid **153** (0.008 g, 0.025 mmol, quant). ^{1}H NMR (400 MHz, $CDCl_3$) δ 7.58 (d, *J* = 8.50 Hz, 2H), 7.20 - 7.33 (m, 3H), 7.12 - 7.19 (m, 2H), 6.65 (d, *J* = 8.50 Hz, 2H), 5.04 (q, *J* = 6.78 Hz, 1H), 3.98 (br. s., 2H), 3.18 (dd, *J* = 3.26, 6.27 Hz, 2H), 2.37 - 2.55 (m, 2H), 1.04 (t, *J* = 7.28 Hz, 3H). ^{13}C NMR (101 MHz, $CDCl_3$) δ 209.6, 166.5, 149.8, 136.2, 129.3, 128.8, 128.6, 127.1, 123.5, 114.1, 58.9, 37.9, 34.3, 7.4. HRMS (ESI) $C_{18}H_{21}N_2O_2$ *m/z* $[M+H]^+$ found 297.1590, expected 297.1603.

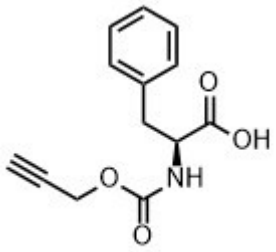

154

(Prop-2-yn-1-yloxy)carbonyl)-*L*-phenylalanine

To a solution of sodium hydroxide (0.467 g, 4 mmol) in water (8 mL) was added (*L*)-phenylalanine **146**, followed by propargyl chloroformate (0.39 mL, 4 mmol). The reaction was stirred at room temperature for 16 hours. The reaction mixture was then acidified to pH 4 with 2 N HCl, and extracted three times with ethyl acetate. The combined organic fractions were pooled, dried over anhydrous sodium sulfate, concentrated *in vacuo* to obtain compound **154** as white solid (0.438g, 44% yield).). ^{1}H NMR (400MHz, CD_3OD) δ 7.23-7.28 (m, 5H), 4.89 (m, 1H), 4.61 (s, 2H), 3.05 (dd, *J1*=5.80, *J2*=13.9, 1H), 2.86 (m, 2H).

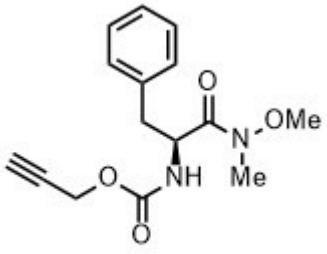

155

Prop-2-yn-1-yl (S)-(1-(methoxy(methyl)amino)-1-oxo-3-phenylpropan-2-yl)carbamate

To a solution of **154** (0.438 g, 1.8 mmol) in anhydrous DCM (9 mL) in an ice-water bath was added EDCI (0.479 g, 2.5 mmol) and HOBt (0.297 g, 2.2 mmol). After stirring at 0 ^{o}C

for 1 hour, the reaction mixture was added *N,O*-dimethylhydroxylamine hydrochloride (0.224 g, 2.3 mmol) and *N*-methylmorpholine (0.24 mL, 2.2 mmol). The reaction was warmed up to room temperate and stirred for 16 hours. The reaction mixture was washed with 1N HCl and then saturated $NaHCO_3$. The organic layer was dried over anhydrous sodium sulphate and concentrated *in vacuo*. The crude product was purified by column chromatography (silica gel, ethyl acetate:hexane 1:4) to give the desired product **155** as yellow oil (0.312 g, 61% yield). ^{1}H NMR (400 MHz, CD_3OD) *δ* 7.23-7.29 (m, 5H), 4.89 (m, 1H), 4.60 (s, 2H), 3.73 (s, 3H), 3.17 (s, 3H), 3.04 (dd, *J1*=5.9, *J2*=13.3, 1H), 2.86 (m, 2H).

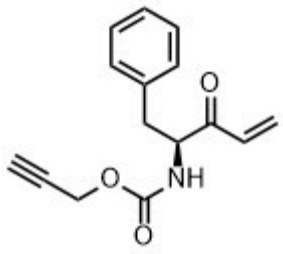

156

Prop-2-yn-1-yl (*S*)-(3-oxo-1-phenylpent-4-en-2-yl)carbamate (36). A reaction mixture containing **155** (0.312 g, 1.1 mmol) in anhydrous THF (5.5 mL) was cooled to -40 ^{o}C in a dry ice/acetonitrile bath and purged with argon before 1 M vinyl magnesium bromide in THF (3.3 mL, 3.3 mmol) was added dropwise. After 3 hours stirring at -40 ^{o}C, the reaction mixture was poured into cold 3 N HCl, and extracted three times with ethyl acetate. The combined organic layers were dried over anhydrous sodium sulphate and concentrated *in vacuo*. The crude product was purified over silica gel chromatography to obtain the desired product as white solid **156** (0.136 g, 53% yield). ^{1}H NMR (400 MHz, CD_3OD) *δ* 7.22-7.28 (m, 5H), 6.61 (dd, *J1*=10.1, *J2*=12.4, 1H), 6.36 (d, *J*=17.4, 1H), 5.87 (d, *J*=11.4, 1H), 4.72 (m, 1H), 4.60 (s, 2H), 3.24 (dd, *J1*=5.5, *J2*=13.9, H), 2.87 (m, 2H).

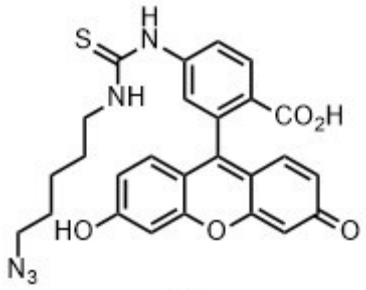

164

4-(3-(5-azidopentyl)thioureido)-2-(6-hydroxy-3-oxo-3H-xanthen-9-yl)benzoic acid

To a solution of fluorescein 5-isothiocynate **162** (0.050 g, 0.128 mmol, 1.13 equiv) and Hunigs base (0.073 mL, 0.42 mmol, 3.5 equiv) in DMF (1.2 mL, 0.1 M) was added **163** (17 mg, 0.12 mmol, 1.0 equiv). The reaction mixture was stirred for 3 hours at room temperature, followed by dilution with ethyl acetate and washing with 1N HCl solution. The ethyl acetate layer was purified over silica to obtain compound **164** (43 mg, 0.088 mmol, 69%). ^{1}H NMR (400 MHz, CD_3OD) δ 7.98 (s, 1H), 7.76 (dd, *J* = 1.63, 8.16 Hz, 1H), 7.16 (d, *J* = 8.03 Hz, 1H), 6.69 (s, 4H), 6.56 (dd, *J* = 1.63, 9.41 Hz, 2H), 1.56 - 1.74 (m, 4H), 1.39 - 1.53 (m, 4H), 1.26 - 1.33 (m, 2H)

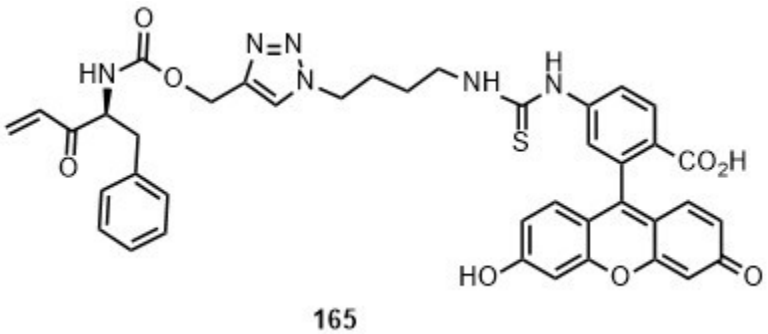

165

(*S*)-2-(6-hydroxy-3-oxo-3H-xanthen-9-yl)-4-(3-(4-(4-((((3-oxo-1-phenylpent-4-en-2-yl)carbamoyl)oxy)methyl)-1H-1,2,3-triazol-1-yl)butyl)thioureido)benzoic acid

To a solution of $CuSO_4$ (8 mg, 0.039 mmol) and sodium ascorbate (catalytic amount) in a mixture of 1:1 THF:water (1 mL) was added **156** (10 mg, 0.039 mmol) and Fluorescein Azide **145** (21 mg, 0.039 mmol). The reaction was stirred at room temperature for 1 hour. The reaction mixture then evaporated to dryness in vacuo and purified over silica gel chromatography to obtain the product as dark pink solid **165** (12 mg, 40% yield). MS (ESI) $C_{94}H_{97}N_{11}O_{21}S$ *m/z* $[M+H]^+$ 789.44.

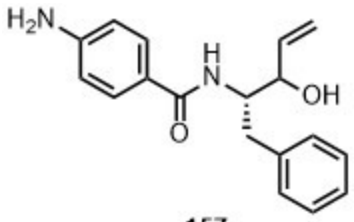

157

4-amino-N-((2S)-3-hydroxy-1-phenylpent-4-en-2-yl)benzamide

To a solution of the alcohol **150** (0.11 g, 0.34 mmol, 1.0 equiv) in ethyl acetate (2.0 mL, 0.1 M) was added tin chloride dehydrate (0.228 g, 1.0 mmol, 3.0 equiv) and was refluxed for 3 hours. The reaction mixture was diluted with ethyl acetate and was washed with saturated sodium bicarbonate solution, following which it was dried over sodium sulfate and was concentrated in vacuo. The crude was sufficiently pure to be used in the next step without purification. ^{1}H NMR (400 MHz, $CDCl_3$) δ 7.48 - 7.55 (m, 1H), 7.40 - 7.46 (m, 1H), 7.19 - 7.34 (m, 5H), 6.55 - 6.69 (m, 2H), 5.85 - 6.04 (m, 1H), 5.41 (td, *J* = 1.60, 17.13 Hz, 1H), 5.23 - 5.36 (m, 1H), 4.21 - 4.48 (m, 2H), 2.82 - 3.09 (m, 2H).

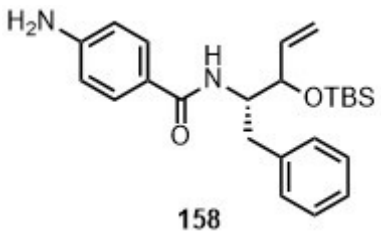

158

4-amino-N-((2S)-3-((tert-butyldimethylsilyl)oxy)-1-phenylpent-4-en-2-yl)benzamide

To the solution of the aniline from the previous step (0.1 g, 0.34 mmol, 1.0 equiv) in DCM (1.7 mL, 0.2 M) was added 2,6-lutidine (0.06 mL, 0.45 mmol, 1.5 equiv) and the solution was cooled to 0° C. To this mixture was added TBSOTf (0.086 mL, 0.37 mmol, 1.1 equiv) dropwise, the mixture was allowed to warm to room temperature and stirred overnight, following which the DCM layer was diluted and washed with 1 N HCl and purified over silica gel to get the compound **158** (0.063 g, 0.153 mmol, 45% overall yield for 2 steps). ^{1}H NMR (400 MHz, $CDCl_3$) δ 7.54 (d, *J* = 8.53 Hz, 1H), 7.45 (d, *J* = 8.78 Hz, 1H), 7.12 - 7.32 (m, 5H), 6.55 - 6.70 (m, 2H), 5.78 - 6.05 (m, 2H), 5.38 (td, *J* = 1.73, 17.13 Hz, 1H), 5.24 (td, *J* = 1.69, 10.42 Hz, 1H), 5.06 - 5.20 (m, 1H), 4.34 - 4.52 (m, 1H), 3.90 (d, *J* = 3.26 Hz, 1H), 2.79 - 3.08 (m, 2H), 1.00 (s, 3H), 0.88 - 0.96 (m, 6H), 0.15 (s, 1H), 0.08 (s, 2H), -0.02 (d, *J* = 19.32 Hz, 3H)

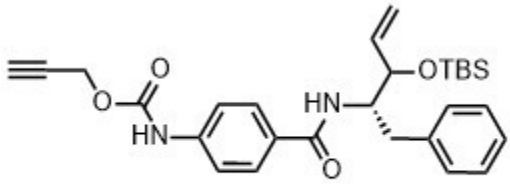

159

prop-2-yn-1-yl (4-(((2S)-3-((tert-butyldimethylsilyl)oxy)-1-phenylpent-4-en-2-yl)carbamoyl)phenyl)carbamate

To the solution of the aniline **158** (0.035 mg, 0.085 mmol, 1.0 equiv) in DCM (0.8 mL, 0.1 M) was added triethylamine (0.013 mL, 0.09 mmol, 1.1 equiv) and the solution was cooled to 0 °C. To this solution was added propargyl chloroformate (0.01 mL, 0.09 mmol, 1.1 equiv) and the mixture was allowed to warm to room temperature and kept overnight, followed which it was diluted with DCM and washed with 1 N HCl and concentrated in vacuo. The crude was sufficiently pure to be used for the next step without purification.

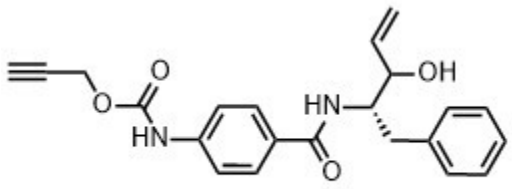

160

prop-2-yn-1-yl (4-(((2S)-3-hydroxy-1-phenylpent-4-en-2-yl)carbamoyl)phenyl)carbamate

The above reaction crude (0.085 mmol, 1.0 equiv) was dissolved in THF (0.85 mL, 0.1 M) and TBAF (1 M in THF, 1.5 equiv) was added. The mixture was stirred at room temperature overnight and was diluted with ethyl acetate and washed with 1 N HCl solution. The ethyl acetate layer was dried over sodium sulfate and purified over silica gel to obtain compound **160** (0.010 g, 0.026 mmol, 31% overall for 2 steps). ^{1}H NMR (400 MHz, CD_6CO) δ 9.01 (br. s., 1H), 7.69 - 7.82 (m, 2H), 7.51 - 7.64 (m, 2H), 7.08 - 7.37 (m, 5H), 5.88 - 6.13 (m, 1H), 5.23 - 5.41 (m, 2H), 5.03 - 5.20 (m, 1H), 4.74 - 4.82 (m, 2H), 4.49 - 4.58 (m, 1H), 4.24 - 4.43 (m, 3H), 2.77 (br. s., 1H).

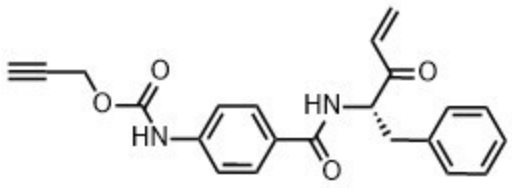

161

prop-2-yn-1-yl (S)-(4-((3-oxo-1-phenylpent-4-en-2-yl)carbamoyl)phenyl)carbamate

To a solution of the above alcohol **160** (0.01 g, 0.026 mmol, 1.0 equiv) in DCM (0.3 mL, 0.1 M) was added Dess – Martin periodinane (0.011 g, 0.026 mmol, 1.0 equiv) and the mixture was stirred at room temperature overnight, following which it was diluted with DCM and was washed with sodium thiosulfate solution. The DCM layer was dried over sodium sulfate and purified over silica gel to obtain compound **161** (0.007 g, 0.0186 mmol, 71%). ^{1}H NMR (400 MHz, $CDCl_3$) δ 7.64 (d, *J* = 8.53 Hz, 2H), 7.39 (d, *J* = 8.78 Hz, 2H), 7.11 - 7.25 (m, 3H), 6.97 - 7.05 (m, 2H), 6.89 (s, 1H), 6.75 (d, *J* = 7.03 Hz, 1H), 6.28 - 6.51 (m, 2H), 5.85 (dd, *J* = 1.51, 10.04 Hz, 1H), 5.29 (dt, *J* = 5.02, 6.90 Hz, 1H), 4.72 (d, *J* = 2.26 Hz, 2H), 3.25 (dd, *J* = 6.65, 13.93 Hz, 1H), 3.12 (dd, *J* = 4.89, 13.93 Hz, 1H), 2.45 (t, *J* = 2.38 Hz, 1H). ^{13}C NMR (101 MHz, $CDCl_3$) δ 197.3, 166.0, 152.1, 140.7, 135.6, 133.3, 130.6, 129.5, 129.2, 129.0, 128.7, 128.5, 128.3, 127.1, 118.1, 75.2, 57.4, 53.0, 37.7.

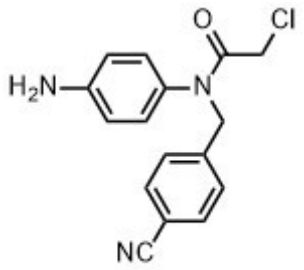

166

***N*-(4-aminophenyl)-2-chloro-N-(4-cyanobenzyl)acetamide**

A solution of the compound **132** (0.115 g, 0.348 mmol, 1.0 equiv) in ethyl acetate (4.0 mL, 0.1 M) was refluxed with tin chloride dihydrate (0.4 g, 1.745 mmol, 5.0 equiv) overnight, followed which the mixture was diluted with ethyl acetate, washed with saturated sodium bicarbonate solution and the ethyl acetate layer was purified over silica gel to obtain compound **166** (0.072 mg, 0.24 mmol, 69%). ^{1}H NMR (400 MHz, $CDCl_3$) δ 7.58 (d, *J* = 8.50 Hz, 2H), 7.34 (d, *J* = 8.50 Hz, 2H), 6.76 (d, *J* = 8.50 Hz, 2H), 6.61 (d, *J* = 8.50 Hz, 2H), 4.87 (s, 2H), 3.89 (s, 2H).

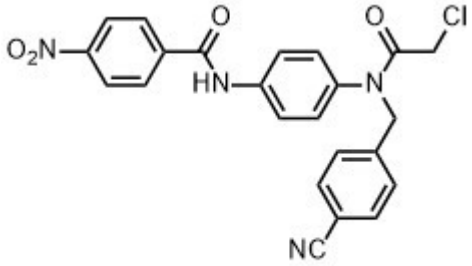

168

***N*-(4-(2-chloro-N-(4-cyanobenzyl)acetamido)phenyl)-4-nitrobenzamide**

To a solution of 4-nitrobenzoic acid (0.033 g, 0.192 mmol, 1.2 equiv) in DCM (0.2 mL, 0.1 M) was added oxalyl chloride (0.06 mL, 0.64 mmol, 4.0 equiv). To this solution was added one drop of DMF (catalytic) and was stirred for an hour. The solution was concentrated in vacuo to get a white solid **167**. The solid was dissolved in DCM (0.1 mL, 0.2 M) and was cooled to 0 °C. A solution of the aniline **166** (0.048 g, 0.16 mmol, 1.0 equiv) and

triethylamine (0.05 mL, 0.32 mmol, 2.0 equiv) in DCM (0.1 mL, 0.2 M) was slowly added to the acid chloride and the mixture was brought up to room temperature overnight. The reaction mixture was diluted with DCM and washed subsequently with 1 N HCl and 1 N NaOH solutions and dried over sodium sulfate. The DCM layer was concentrated in vacuo and purified over silica gel to obtain compound **168** (0.069 g, 0.154 mmol, 96%). ^{1}H NMR (400 MHz, $CDCl_3$) δ 8.38 (d, *J* = 8.78 Hz, 2H), 8.05 (d, *J* = 9.03 Hz, 2H), 7.71 (d, *J* = 8.80 Hz, 2H), 7.61 (d, *J* = 8.28 Hz, 2H), 7.36 (d, *J* = 8.50 Hz, 2H), 7.09 (d, *J* = 8.78 Hz, 2H), 4.95 (s, 2H), 3.90 (s, 2H).

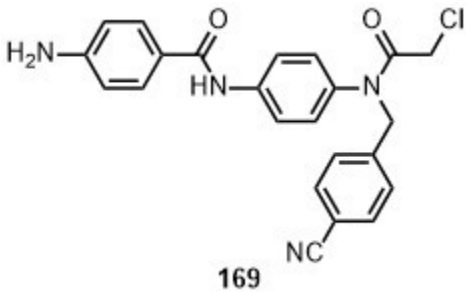

169

4-amino-N-(4-(2-chloro-N-(4-cyanobenzyl)acetamido)phenyl)benzamide

The above prepared amide **168** (0.069 mg, 0.154 mmol, 1.0 equiv) was dissolved in ethyl acetate (1.6 mL, 0.1 M) and was refluxed overnight with tin chloride dihydrate (0.174 mg, 0.77 mmol, 5.0 equiv), after which the mixture was diluted with ethyl acetate, washed with saturated sodium bicarbonate solution, dried with sodium sulfate and purified over silica gel to get compound **169** (0.041 mg, 0.094 mmol, 64%). ^{1}H NMR (400 MHz, $CDCl_3$) δ 7.71 (d, *J* = 8.50 Hz, 2H), 7.66 (d, *J* = 8.80 Hz, 2H), 7.60 (d, *J* = 8.28 Hz, 2H), 7.35 (d, *J* = 8.30 Hz, 2H), 7.02 (d, *J* = 8.80 Hz, 2H), 6.72 (d, *J* = 8.53 Hz, 2H), 4.93 (s, 2H), 4.09 (br. s., 2H), 3.89 (s, 2H).

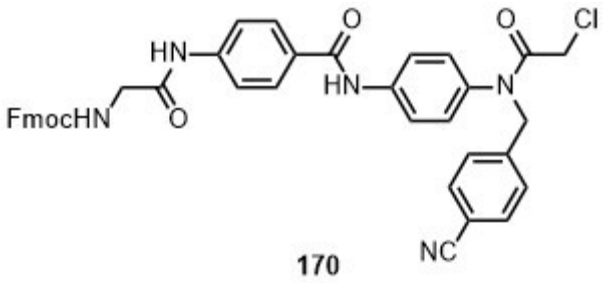

170

(9*H*-fluoren-9-yl)methyl (2-((4-((4-(2-chloro-N-(4-cyanobenzyl)acetamido)phenyl)carbamoyl)phenyl)amino)-2-oxoethyl)carbamate

To a solution of the aniline **169** (0.031 mg, 0.074 mmol, 1.0 equiv) in chloroform (0.6 mL, 0.1 M) was added Fmoc glycyl chloride (0.035 g, 0.11 mmol, 1.5 equiv) and a solution of $NaHCO_3$ in water (10%, 10.0 equiv) and the mixture was stirred vigorously for 90 minutes. The mixture was diluted with DCM and washed with 1N HCl and purified over silica gel to obtain the title compound **170** (0.05 g, 0.07 mmol, 97%). ^{1}H NMR (400 MHz, $CDCl_3$) δ 8.37 (br. s., 1H), 8.07 (s, 1H), 7.77 (d, *J* = 7.53 Hz, 2H), 7.80 (d, *J* = 8.53 Hz, 2H), 7.70 (d, *J* = 8.80 Hz, 2H), 7.51 - 7.63 (m, 6H), 7.25 - 7.44 (m, 6H), 7.03 (d, *J* = 8.50 Hz, 2H), 5.57 (br. s., 1H), 4.93 (s, 2H), 4.52 (d, *J* = 6.80 Hz, 2H), 4.24 (t, *J* = 6.78 Hz, 1H), 4.00 (d, *J* = 5.27 Hz, 2H), 3.88 (s, 2H).

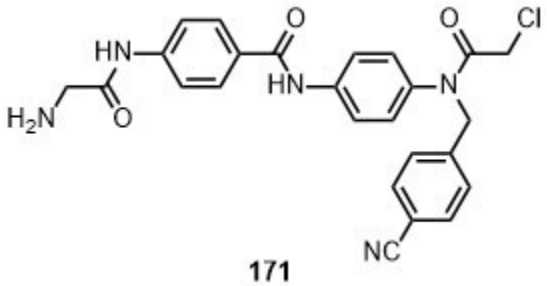

171

4-(2-aminoacetamido)-N-(4-(2-chloro-N-(4-cyanobenzyl)acetamido)phenyl)benzamide

To a solution of the above Fmoc protected amide **170** (0.05 g, 0.072 mmol, 1.0 equiv) in DMF (0.3 mL, 0.33 M) was added DBU:piperidine (0.012 mL, 1:1, 4% v/v) and the mixture was stirred for 30 minutes. The mixture was passed over a short plug of silica to obtain the compound **171** (0.034 mg, 0.07 mmol, quant) and was used for the next step without any further purification.

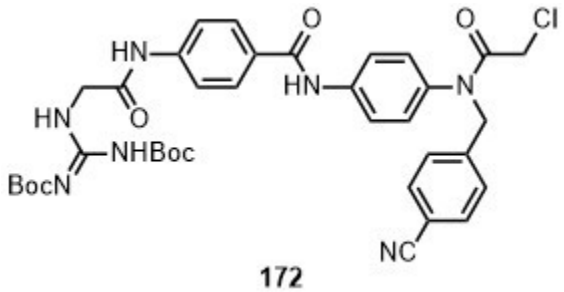

172

***N*-(4-(N-(4-cyanobenzyl)-2-chloroacetamido)phenyl)-4-(2-(N,N-Di-Boc-1H-guanidino)acetamido))benzamide**

To a solution of the primary amine **171** (0.036 g, 0.076 mmol, 1.0 equiv) and triethylamine (0.042 mL, 0.3 mmol, 4.0 equiv) in methanol (0.8 mL, 0.1 M) was added *N,N'*-Di-Boc-1H-pyrazole-1-carboxamidine (0.036 g, 0.113 mmol, 1.5 equiv). The reaction mixture was stirred at room temperature overnight and was purified over silica gel to obtain compound **172** (0.046 g, 0.064 mmol, 84%). ^{1}H NMR (400 MHz, $CDCl_3$) δ 11.38 (s, 1H), 10.34 (s, 1H), 8.99 (t, *J* = 5.90 Hz, 1H), 8.31 (s, 1H), 7.71 (d, *J* = 8.78 Hz, 2H), 7.74 (d, *J* = 8.53 Hz, 2H), 7.49 - 7.65 (m, 4H), 7.34 (d, *J* = 8.03 Hz, 2H), 6.99 (d, *J* = 8.78 Hz, 2H), 4.90 (s, 2H), 4.17 (d, *J* = 6.02 Hz, 2H), 2.92 (s, 2H), 2.38 (br. s., 2H), 1.51 (s, 18H).

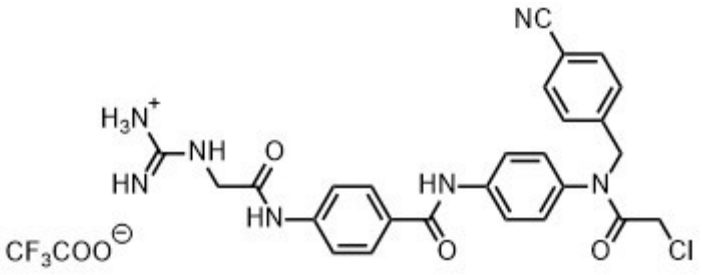

173

1-(2-((4-((4-(2-chloro-N-(4-cyanobenzyl)acetamido)phenyl)carbamoyl)phenyl)amino)-2-oxoethyl)guanidinium 2,2,2-trifluoroacetate

To a solution of the above compound **172** (0.02 g, 0.027 mmol, 1.0 equiv) in DCM (0.15 mL, 0.2 M) was added TFA (0.15 mL, 0.2 M) and stirred overnight. The reaction mixture was dried in vacuo to obtain the title compound **173**. (0.016 mg, 0.027 mmol, quant). ^{1}H NMR (400 MHz, CD_3OD) δ 7.93 (d, *J* = 8.78 Hz, 2H), 7.76 (d, *J* = 8.78 Hz, 2H), 7.80 (d, *J* = 8.78 Hz, 2H), 7.68 (d, *J* = 8.30 Hz, 2H), 7.44 (d, *J* = 8.30 Hz, 2H), 7.18 (d, *J* = 8.78 Hz, 2H), 5.04 (s, 2H), 3.87 (s, 2H), 3.51 - 3.66 (m, 3H). ^{13}C NMR (101 MHz, CD_3OD) δ 173.2, 168.3, 168.2, 165.7, 159.8, 143.4, 143.2, 141.3, 135.9, 133.7, 131.2, 131.0, 130.0, 129.9, 123.6, 120.5, 119.6, 112.9, 61.7, 21.0, 14.6.

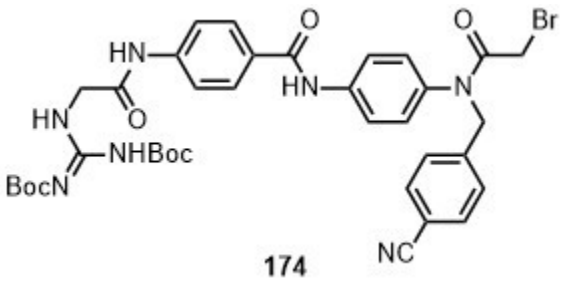

174

***N*-(4-(N-(4-cyanobenzyl)-2-bromoacetamido)phenyl)-4-(2-(N,N-Di-Boc-1H-guanidino)acetamido))benzamide**

The acetamide **172** (0.048 g, 0.0067 mmol, 1.0 equiv) was dissolved in acetone (1.0 mL, 0.1 M) and refluxed with sodium bromide (0.207 g, 2.0 mmol, 30.0 equiv) overnight. The reaction mixture was concentrated and taken up in ethyl acetate, washed with sodium thiosulfate solution and purified over silica gel to obtain the compound **174** (0.026 mg, 0.034 mmol, 51%). ^{1}H NMR (400 MHz, $CDCl_3$) δ 11.37 (s, 1H), 10.37 (br. s., 1H), 8.99 (br. s., 1H), 8.26 (br. s., 1H), 7.70 (d, *J* = 7.53 Hz, 2H), 7.75 (d, *J* = 8.03 Hz, 2H), 7.44 - 7.65 (m, 4H), 7.34 (d, *J* = 7.78 Hz, 2H), 6.99 (d, *J* = 8.03 Hz, 2H), 5.30 (s, 1H), 4.90 (br. s., 2H), 4.17 (d, *J* = 5.27 Hz, 2H), 2.92 (br. s., 2H), 2.38 (br. s., 2H), 1.51 (br. s., 18H).

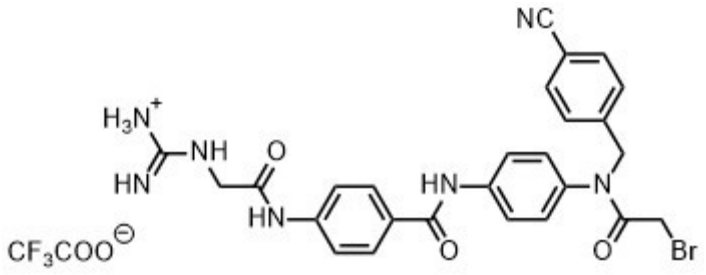

175

1-(2-((4-((4-(2-bromo-N-(4-cyanobenzyl)acetamido)phenyl)carbamoyl)phenyl)amino)-2-oxoethyl)guanidinium 2,2,2-trifluoroacetate

To a solution of the above compound **174** (0.026 g, 0.034 mmol, 1.0 equiv) in DCM (0.17 mL, 0.2 M) was added TFA (0.17 mL, 0.2 M) and stirred overnight. The reaction mixture was dried in vacuo to obtain the title compound **175**. (0.019 mg, 0.03 mmol, quant). ^{1}H NMR (700 MHz, CD_3OD) δ 7.93 (d, *J* = 8.36 Hz, 2H), 7.80 (d, *J* = 8.40 Hz, 2H), 7.76 (d, *J* = 8.80 Hz, 2H), 7.67 (d, *J* = 7.90 Hz, 2H), 7.44 (d, *J* = 7.90 Hz, 2H), 7.18 (d, *J* = 8.80 Hz, 2H), 5.03 (s, 2H), 4.14 (s, 2H), 3.87 (s, 2H), 3.57 (d, *J* = 11.88 Hz, 2H). ^{13}C NMR (101

MHz, CD_3OD) δ 168.3, 168.1, 165.7, 154.4, 153.2, 151.7, 151.3, 147.1, 143.4, 141.3, 135.9, 133.7, 130.9, 130.7, 130.0, 129.9, 123.6, 120.5, 115.5, 112.9, 92.9, 89.0, 85.9, 85.6, 63.5, 55.6, 45.5, 28.1.

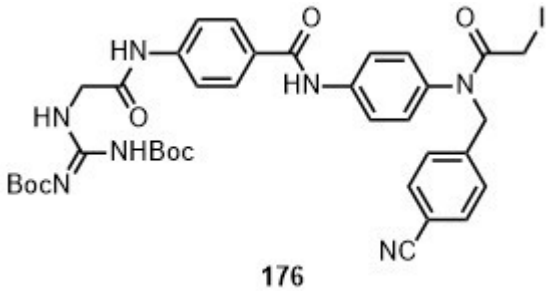

176

***N*-(4-(N-(4-cyanobenzyl)-2-iodoacetamido)phenyl)-4-(2-(N,N-Di-Boc-1H-guanidino)acetamido))benzamide**

The acetamide **172** (0.043 g, 0.006 mmol, 1.0 equiv) was dissolved in acetone (1.0 mL, 0.1 M) and refluxed with sodium iodide (0.3 g, 0.6 mmol, 30.0 equiv) overnight. The reaction mixture was concentrated and taken up in ethyl acetate, washed with sodium thiosulfate solution and purified over silica gel to obtain the compound **176** (0.041 mg, 0.05 mmol, 84%). ^{1}H NMR (400 MHz, $CDCl_3$) δ 12.30 (br. s., 1H), 9.12 (br. s., 1H), 8.59 (br. s., 1H), 8.24 (br. s., 1H), 7.79 (d, *J* = 6.78 Hz, 2H), 7.53 - 7.69 (m, 3H), 7.41 - 7.53 (m, 2H), 7.29 (br. s., 2H), 7.21 (d, *J* = 2.26 Hz, 1H), 6.92 (d, *J* = 6.78 Hz, 2H), 4.83 (br. s., 2H), 4.08 (d, *J* = 3.51 Hz, 2H), 3.61 (br. s., 2H), 3.44 (br. s., 2H), 2.88 (br. s., 2H), 2.34 (br. s., 2H), 1.19 (s, 18H).

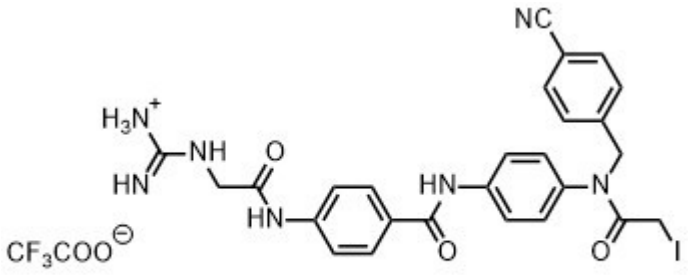

177

1-(2-((4-((4-(N-(4-cyanobenzyl)-2-iodoacetamido)phenyl)carbamoyl)phenyl)amino)-2-oxoethyl)guanidinium 2,2,2-trifluoroacetate

To a solution of the above compound **176** (0.041 g, 0.05 mmol, 1.0 equiv) in DCM (0.25 mL, 0.2 M) was added TFA (0.25 mL, 0.2 M) and stirred overnight. The reaction mixture was dried in vacuo to obtain the title compound **177**. (0.03 mg, 0.05 mmol, quant). ^{1}H NMR (700 MHz, CD_3OD) δ 7.93 (d, *J* = 8.80 Hz, 2H), 7.81 (d, *J* = 8.80 Hz, 2H), 7.76 (d, *J* = 8.80 Hz, 2H), 7.67 (d, *J* = 8.36 Hz, 2H), 7.43 (d, *J* = 8.36 Hz, 2H), 7.18 (d, *J* = 8.80 Hz, 2H), 4.29 (s, 2H), 3.88 (s, 2H), 3.57 (d, *J* = 11.88 Hz, 2H). ^{13}C NMR (101 MHz, CD3OD) δ 168.3, 165.8, 159.4, 158.9, 154.1, 143.5, 141.3, 136.0, 133.7, 130.9, 130.0, 129.9, 129.3, 127.9, 123.6, 120.6, 119.6, 117.6, 114.8, 112.9, 58.6, 55.6, 45.9, 0.1

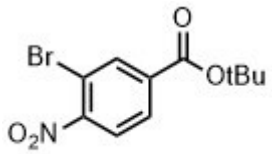

179

***tert*-butyl 3-bromo-4-nitrobenzoate**

To a solution of 3-bromo-4-nitrobenzoic acid **178** (0.435 g, 1.77 mmol, 1.0 equiv) and *tert*-butyl 2,2,2-trichloroacetamidate (0.38 mL, 2.122 mmol, 1.2 equiv) in diethyl ether (9.0 mL, 0.2 M) cooled to 0°C, was slowly added boron trifluoride diethyl etherate (0.022 mL, 0.177

mmol, 0.1 equiv). The reaction was slowly allowed to warm up to room temperature overnight, followed which it was washed with saturated sodium bicarbonate solution and the ether layer was purified over silica gel to obtain the compound **179** (0.373 g, 1.23 mmol, 70%). ^{1}H NMR (400 MHz, $CDCl_3$) δ 8.32 (d, *J* = 1.76 Hz, 1H), 8.04 (dd, *J* = 1.76, 8.28 Hz, 1H), 7.83 (d, *J* = 8.53 Hz, 1H), 1.62 (s, 9H).

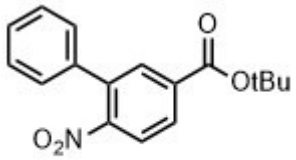

180

***tert*-butyl 6-nitro-[1,1'-biphenyl]-3-carboxylate**

A solution of the ester **179** (0.03 g, 0.1 mmol, 1.0 equiv), phenylboronic acid (0.013 g, 0.1 mmol, 1.0 equiv), tetrakis(triphenylphosphine)palladium(0) (0.006 g, 0.005 mmol, 5 mol%), sodium carbonate (0.027 g, 0.25 mmol, 2.5 equiv) in DME:H_2O (0.5 mL, 3:1, 0.2 M) was stirred vigorously overnight at 95 °C. The following day, the reaction mixture was diluted with diethyl ether and washed with 1 N HCl and purified over silica gel to get the compound **180** (0.028 g, 0.095 mmol, 96%). ^{1}H NMR (400 MHz, $CDCl_3$) δ 8.00 - 8.14 (m, 2H), 7.85 (d, *J* = 8.28 Hz, 1H), 7.40 - 7.50 (m, 3H), 7.28 - 7.40 (m, 2H), 1.62 (s, 9H)

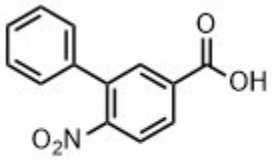

181

6-nitro-[1,1'-biphenyl]-3-carboxylic acid

The above prepared ester **180** (0.02 g, 0.067 mmol, 1.0 equiv) was dissolved in DCM (0.35 mL, 0.2 M) and was added TFA (0.35 mL, 0.2 M). The reaction mixture was stirred for 4 hours followed by removal of the excess TFA by vacuum to yield the compound **181** (0.016 mg, 0.066 mmol, quant). ^{1}H NMR (400 MHz, CD_3OD) δ 8.17 (dd, *J* = 1.88, 8.41 Hz, 1H), 8.09 (d, *J* = 1.51 Hz, 1H), 7.93 (d, *J* = 8.28 Hz, 1H), 7.40 - 7.49 (m, 3H), 7.30 - 7.37 (m, 2H)

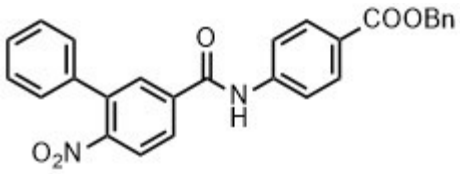

182

benzyl 4-(6-nitro-[1,1'-biphenyl]-3-carboxamido)benzoate

To a solution of the acid **181** (0.07 g, 0.29 mmol, 1.0 equiv) in DCM (3.0 mL, 0.2 M) was added thionyl chloride (0.21 mL, 2.9 mmol, 10.0 equiv) and was refluxed for 4 hours, after which the excess thionyl chloride was removed under vacuum to obtain the acid chloride .The acyl chloride was taken in DCM (1.5 mL, 0.4 M) and cooled to 0 °C. To this solution was added a solution of benzyl 4-amino benzoate (0.066 g, 0.288 mmol, 1.0 equiv), triethylamine (0.06 mL, 0.432 mL, 1.5 equiv) in DCM (1.5 mL, 0.4 M). The reaction mixture was allowed to warm up to room temperature and stirred overnight, after which the reaction was diluted by DCM, washed subsequently with 1 N HCl and 1 N NaOH and purified on silica gel to obtain the compound **182**. (0.118 g, 0.26 mmol, 90%). ^{1}H NMR (400 MHz, $CDCl_3$) δ 8.27 (s, 1H), 8.10 (d, *J* = 8.80 Hz, 2H), 7.85 - 8.02 (m, 3H), 7.75 (d, *J* = 8.80 Hz, 2H), 7.28 - 7.51 (m, 10H), 5.37 (s, 2H).

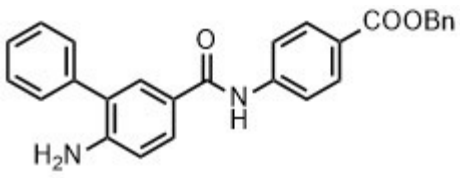

183

benzyl 4-(6-amino-[1,1'-biphenyl]-3-carboxamido)benzoate

To a solution of the benzyl ester **182** (0.182 g, 0.4 mmol, 1.0 equiv) in ethyl acetate (4.0 mL, 0.1 M) was added tin chloride dehydrate (0.273 g, 1.21 mmol, 3.0 equiv) and refluxed for 90 minutes. The reaction mixture was diluted with ethyl acetate and washed with saturated sodium bicarbonate solution and the ethyl acetate layer was purified over silica gel to obtain the compound **183** (0.119 g, 0.281 mmol, 69%). ^{1}H NMR (400 MHz, $CDCl_3$) δ 8.07 (d, *J* = 8.70 Hz, 2H), 7.96 (s, 1H), 7.68 - 7.77 (m, 3H), 7.66 (d, *J* = 2.26 Hz, 1H), 7.31 - 7.51 (m, 10H), 6.79 (d, *J* = 8.53 Hz, 1H), 5.36 (s, 2H), 4.18 (s, 2H).

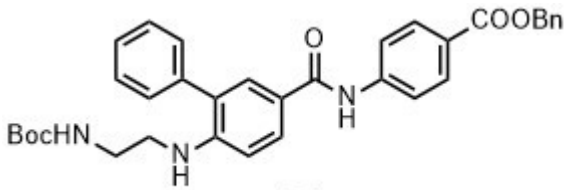

184

benzyl 4-(6-((2-((tert-butoxycarbonyl)amino)ethyl)amino)-[1,1'-biphenyl]-3-carboxamido)benzoate

To the solution of the above prepared aniline **183** (0.086 g, 0.203 mmol, 1.0 equiv) in methanol (2.0 mL, 0.1 M) with molecular seives was added *N*-Boc-2-aminoacetaldehyde (0.012 mg, 0.203 mmol, 1.0 equiv), glacial acetic acid (0.21 mL, 0.203 mmol, 1.0 equiv) and was stirred for one hour. To this solution was added sodium cyanoborohydride (0.013 g, 0.203 mmol, 1.0 equiv) and the mixture was stirred overnight. The reaction mixture was

concentrated under vacuum and was taken into DCM and washed with saturated sodium bicarbonate solution. The DCM layer was concentrated and used for the next step without purification. ^{1}H NMR (400 MHz, $CDCl_3$) δ 8.03 - 8.12 (m, 2H), 7.89 (s, 1H), 7.82 (dd, *J* = 2.26, 8.53 Hz, 1H), 7.72 (d, *J* = 8.78 Hz, 2H), 7.57 - 7.68 (m, 1H), 7.30 - 7.54 (m, 10H), 6.79 (dd, *J* = 8.41, 19.20 Hz, 1H), 5.36 (s, 2H), 3.72 (t, *J* = 5.02 Hz, 1H), 3.32 (s, 3H), 1.47 (d, *J* = 6.02 Hz, 9H).

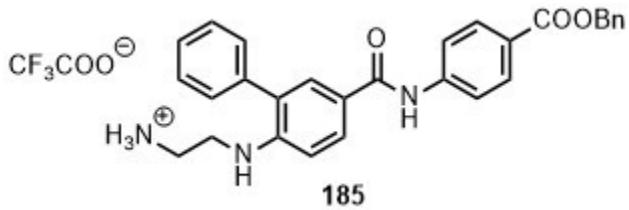

185

2-((5-((4-((benzyloxy)carbonyl)phenyl)carbamoyl)-[1,1'-biphenyl]-2-yl)amino)ethan-1-aminium

The compound from the above step (0.108 g, 0.191 mmol, 1.0 equiv) was dissolved in DCM (1.0 mL, 0.2 M) and TFA (1.0 mL, 0.2 M) was added and the mixture was stirred for 3 hours, followed by purification of the compound on silica gel to obtain compound **185** (0.099 g, 0.171 mmol, 84% for 2 steps). ^{1}H NMR (400 MHz, CD_6CO) δ 7.93 - 8.05 (m, 5H), 7.75 (d, *J* = 2.26 Hz, 1H), 7.31 - 7.54 (m, 10H), 7.04 (d, *J* = 8.78 Hz, 1H), 5.36 (s, 2H), 4.02 (t, *J* = 5.90 Hz, 2H), 3.81 (t, *J* = 5.90 Hz, 2H).

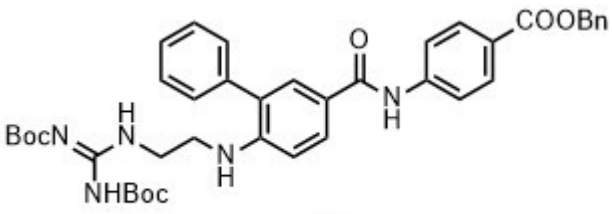

186

benzyl (Z)-4-(6-((2-(2,3-bis(tert-butoxycarbonyl)guanidino)ethyl)amino)-[1,1'-biphenyl]-3-carboxamido)benzoate

To a solution of the primary amine TFA salt **185** (0.099 g, 0.071 mmol, 1.0 equiv) and triethylamine (0.1 mL, 0.684 mmol, 4.0 equiv) in methanol (2.0 mL, 0.1 M) was added *N,N'*-Di-Boc-1H-pyrazole-1-carboxamidine (0.08 g, 0.26 mmol, 1.5 equiv). The reaction mixture was stirred at room temperature overnight and was purified over silica gel to obtain compound **186** (0.051 g, 0.071 mmol, quant). ^{1}H NMR (400 MHz, CD_6CO) δ 11.61 (s, 1H), 9.58 (s, 1H), 8.46 (d, *J* = 5.52 Hz, 1H), 7.84 - 8.07 (m, 5H), 7.72 (d, *J* = 2.51 Hz, 1H), 7.27 - 7.55 (m, 10H), 7.17 (d, *J* = 8.78 Hz, 1H), 5.36 (s, 2H), 3.60 - 3.71 (m, 2H), 3.45 - 3.57 (m, 2H), 2.78 (br. s., 1H), 1.53 (s, 9H), 1.47 (s, 9H).

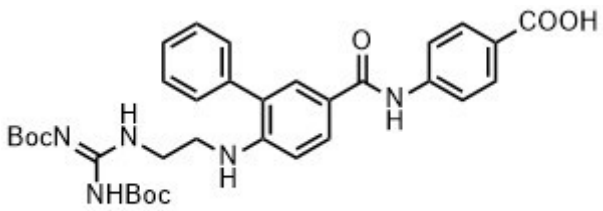

187

(Z)-4-(6-((2-(2,3-bis(tert-butoxycarbonyl)guanidino)ethyl)amino)-[1,1'-biphenyl]-3-carboxamido)benzoic acid

To the solution of the above prepared guanidine **186** (0.051 g, 0.072 mmol, 1.0 equiv) in ethyl acetate (1.0 mL, 0.1 M) was added 5% Pd/C (25% w/w). The reaction mixture was stirred under a hydrogen balloon at room temperature overnight. The product was eluted by filtration using copious amounts of acetone, and the filtrate was concentrated *in vacuo* to afford the desired product as white solid **187** (0.045 g, 0.072 mmol, quant). ^{1}H NMR (400 MHz, CD_6CO) δ 11.61 (br. s., 1H), 9.55 (br. s., 1H), 8.47 (br. s., 1H), 7.81 - 8.07 (m,

5H), 7.73 (s, 1H), 7.43 - 7.52 (m, 3H), 7.27 - 7.43 (m, 2H), 7.16 (d, *J* = 6.78 Hz, 1H), 5.19 (t, *J* = 4.89 Hz, 1H), 3.58 - 3.70 (m, 2H), 3.52 (d, *J* = 6.02 Hz, 2H), 1.53 (s, 9H), 1.47 (s, 9H).

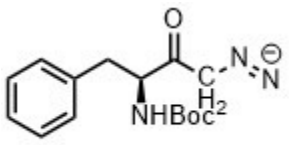

188

(*S*)-(3-((tert-butoxycarbonyl)amino)-2-oxo-4-phenylbutyl)diazen-1-ide

To a solution of Boc-Phe-OH **146** (1.326 g, 5.0 mmol, 1.0 equiv) and 4-methyl morpholine (0.58 mL, 5.25 mmol, 1.05 equiv) in THF (7.14 mL, 0.7 M) cooled to 0 °C was slowly added isobutyl chloroformate (0.68 mL, 5.25 mmol, 1.05 equiv). The reaction was stirred for one hour followed by the addition of a solution of diazomethane in diethyl ether. The reaction was allowed to warm to room temperature and stirred overnight, followed by purification of the product over silica gel to obtain brown crystals of **188**. (1.378 g, 4.74 mmol, 95%). ^{1}H NMR (400 MHz, $CDCl_3$) δ 7.15 - 7.35 (m, 5H), 5.22 (br. s., 1H), 5.09 (br. s., 1H), 4.42 (br. s., 1H), 3.03 (d, *J* = 6.78 Hz, 2H), 1.42 (s, 9H).

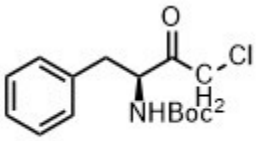

190

tert-butyl (S)-(4-chloro-3-oxo-1-phenylbutan-2-yl)carbamate

The above prepared diazo ketone **188** (0.1 g. 0.35 mmol, 1.0 equiv) was dissolved in diethyl ether (4.0 mL, 0.1 M) and cooled to -20 °C. To this solution was added HCl in

dioxane (4 N, 0.13 mL, 1.5 equiv) slowly and the reaction was allowed to stir for 4 hours, after which the pH of the solution was adjusted to 7.0 using triethyl amine and the reaction was diluted with ether. The ether layer was washed with 1 N HCl, dried and purified over silica gel to obtain the product **190**. (0.102 mg, 0.34 mmol, quant). ^{1}H NMR (400 MHz, $CDCl_3$) δ 7.24 - 7.38 (m, 3H), 7.13 - 7.21 (m, 2H), 5.02 (br. s., 1H), 4.68 (d, *J* = 7.28 Hz, 1H), 4.17 (d, *J* = 16.31 Hz, 1H), 3.99 (d, *J* = 16.31 Hz, 1H), 2.95 - 3.16 (m, 2H), 1.42 (s, 9H).

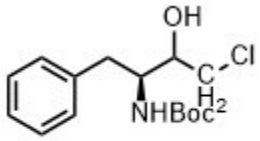

191

***tert*-butyl ((2S)-4-chloro-3-hydroxy-1-phenylbutan-2-yl)carbamate**

To a solution of the α-chloro ketone **190** (0.043 g, 0.144 mmol, 1.0 equiv) in methanol (0.8 mL, 0.2 M) cooled to 0 °C, was added sodium borohydride (0.011 g, 0.29 mmol, 2.0 equiv). The reaction mixture was stirred for 2 hours at 0 °C, followed by quenching the mixture with dilute acetic acid. The reaction was taken up in ethyl acetate, washed with 1 N HCl and dried in vacuo to obtain the product **191** (0.043 g, 0.14 mmol, quant).

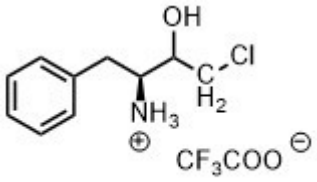

192

(2*S*)-4-chloro-3-hydroxy-1-phenylbutan-2-aminium 2,2,2-trifluoroacetate

To the solution of the above compound **191** (0.043 g, 0.14 mmol, 1.0 equiv) in DCM (0.7 mL, 0.2 M) was added TFA (0.7 mL, 0.2 M). The reaction was stirred at room temperature for 3 hours, after which the solvents were removed vacuo to obtain the compound **192**. (0.044 g, 0.14 mmol, quant). ^{1}H NMR (400 MHz, CD_6CO) δ 7.83 (br. s., 2H), 7.11 - 7.39 (m, 5H), 4.22 - 4.41 (m, 1H), 4.01 - 4.17 (m, 1H), 3.60 - 3.87 (m, 2H), 2.99 - 3.28 (m, 2H).

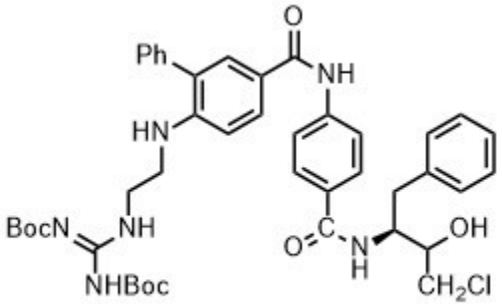

193

To a solution of the acid **187** (0.053 g, 0.86 mmol, 1.0 equiv) in DCM (1.0 mL, 0.1 M) was added PyBOP (0.045 g, 0.86 mmol, 1.0 equiv), DIPEA (0.03 mL, 0.17 mmol, 2.0 equiv) and stirred for 30 minutes, followed by the addition of the amine **192** (0.034 g, 0.086 mmol, 1.0 equiv). The reaction was stirred overnight, after which it was washed with 1 N HCl and the DCM layer was purified over silica gel to get the compound **193** (0.062 g, 0.078 mmol, 90%). ^{1}H NMR (400 MHz, $CDCl_3$) δ 11.47 (br. s., 1H), 8.50 (t, *J* = 5.40 Hz, 1H), 8.25 (s, 1H), 7.77 - 7.85 (m, 1H), 7.61 - 7.73 (m, 6H), 7.51 - 7.60 (m, 3H), 7.33 - 7.50 (m, 8H), 7.15 - 7.33 (m, 7H), 6.78 (d, *J* = 8.53 Hz, 1H), 6.37 (d, *J* = 8.03 Hz, 1H), 4.32 - 4.53 (m, 2H), 3.93 - 4.18 (m, 2H), 3.49 - 3.69 (m, 4H), 3.37 (t, *J* = 6.53 Hz, 2H), 3.01 - 3.16 (m, 2H), 1.49 (s, 9H), 1.52 (s, 9H)

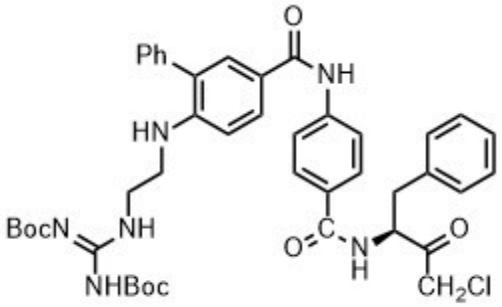

194

To the above prepared alcohol **193** (0.062 g, 0.078 mmol, 1.0 equiv) in DCM (1.0 mL, 0.1 M) was added Dess Martin periodinane (0.04 g, 0.093 mmol, 1.2 equiv). The reaction mixture was stirred for one hour at room temperature, followed by dilution of the reaction with DCM, washing with sodium thiosulfate solution and purification of the DCM layer over silica gel to obtain the α-chloro ketone **194** (0.022 g, 0.028 mmol, 67%). ^{1}H NMR (400 MHz, $CDCl_3$) δ 8.50 (t, *J* = 5.40 Hz, 1H), 8.18 (s, 1H), 7.81 (dd, *J* = 2.26, 8.53 Hz, 1H), 7.59 - 7.76 (m, 5H), 7.25 - 7.48 (m, 10H), 7.15 - 7.23 (m, 3H), 6.80 (d, *J* = 8.53 Hz, 1H), 6.70 (d, *J* = 7.03 Hz, 1H), 5.12 (q, *J* = 7.03 Hz, 1H), 4.24 (d, *J* = 16.06 Hz, 1H), 4.05 (d, *J* = 16.06 Hz, 1H), 3.60 (q, *J* = 6.11 Hz, 2H), 3.38 (t, *J* = 6.30 Hz, 2H), 3.21 (tt, *J* = 6.93, 14.40 Hz, 2H), 1.49 (s, 9H), 1.52 (s, 9H).

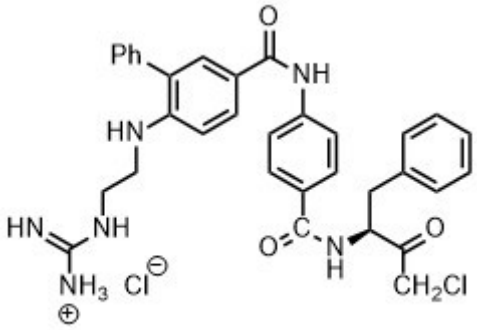

195

To a solution of the α-chloro ketone **194** (0.022 g, 0.028 mmol, 1.0 equiv) in dioxane (0.3 mL, 0.1M) was added HCl in dioxane (4 N, 0.07 mL, 10.0 equiv). The solution was stirred

overnight and the solvents were removed in vacuo to obtain the compound **195** (0.017 g, 0.026 mmol, 95%). ^{1}H NMR (400 MHz, CD_3OD) δ 7.88 (d, *J* = 6.78 Hz, 1H), 7.65 - 7.80 (m, 5H), 7.30 - 7.53 (m, 7H), 7.23 (s, 4H), 7.17 (br. s., 2H), 6.87 (d, *J* = 7.78 Hz, 1H), 4.45 (d, *J* = 16.31 Hz, 1H), 4.23 (d, *J* = 16.31 Hz, 1H), 3.58 - 3.77 (m, 2H), 3.34 - 3.57 (m, 6H), 2.97 - 3.11 (m, 1H). ^{13}C NMR (101 MHz, CD_3OD) δ 170.2, 168.7, 159.0, 149.2, 144.1, 139.8, 138.5, 131.6, 130.6, 130.4, 130.4, 130.4, 129.8, 129.5, 129.5, 129.3, 129.2, 129.1, 128.0, 123.9, 121.4, 111.2, 60.3, 43.4, 41.8, 37.0. HRMS (ESI) $C_{33}H_{35}ClN_6O_3$ *m/z* [M+H]$^{+}$ found 598.2388, expected 598.2459.

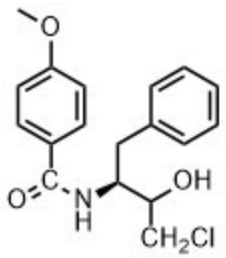

197

***N*-((2S)-4-chloro-3-hydroxy-1-phenylbutan-2-yl)-4-methoxybenzamide**

To a solution of the acid **196** (0.048 g, 0.154 mmol, 1.0 equiv) in DCM (1.0 mL, 0.1 M) was added PyBOP (0.08 g, 0.154 mmol, 1.0 equiv), DIPEA (0.06 mL, 0.154 mmol, 2.0 equiv) and stirred for 30 minutes, followed by the addition of the amine **192** (0.024 g, 0.154 mmol, 1.0 equiv). The reaction was stirred overnight, after which it was washed with 1 N HCl and the DCM layer was purified over silica gel to get the compound **197** (0.047 g, 0.14 mmol, 91%). ^{1}H NMR (400 MHz, $CDCl_3$) δ 7.56 (d, *J* = 8.78 Hz, 2H), 7.18 - 7.38 (m, 5H), 6.89 (d, *J* = 8.80 Hz, 2H), 6.12 (d, *J* = 7.78 Hz, 1H), 4.34 - 4.47 (m, 1H), 3.98 - 4.06 (m, 1H), 3.79 - 3.91 (m, 5H), 3.61 - 3.69 (m, 2H), 3.01 - 3.22 (m, 3H).

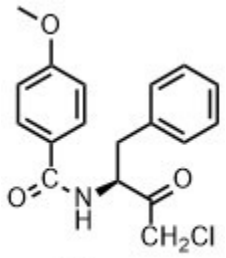

198

(*S*)-N-(4-chloro-3-oxo-1-phenylbutan-2-yl)-4-methoxybenzamide

To the above prepared alcohol **197** (0.020 g, 0.06 mmol, 1.0 equiv) in DCM (1.0 mL, 0.1 M) was added Dess Martin periodinane (0.031 g, 0.072 mmol, 1.2 equiv). The reaction mixture was stirred for one hour at room temperature, followed by dilution of the reaction with DCM, washing with sodium thiosulfate solution and purification of the DCM layer over silica gel to obtain the α-chloro ketone **198** (0.01 g, 0.03 mmol, 50%). ^{1}H NMR (400 MHz, $CDCl_3$) δ 7.68 (d, *J* = 9.00 Hz, 2H), 7.25 - 7.39 (m, 3H), 7.18 - 7.25 (m, 2H), 6.92 (d, *J* = 9.00 Hz, 2H), 6.55 (d, *J* = 6.02 Hz, 1H), 5.14 (q, *J* = 7.03 Hz, 1H), 4.24 (d, *J* = 16.06 Hz, 1H), 4.06 (d, *J* = 16.06 Hz, 1H), 3.86 (s, 3H), 3.14 - 3.28 (m, 2H). ^{13}C NMR (101 MHz, CD_6CO) δ 200.9, 167.4, 163.4, 142.1, 138.5, 133.5, 132.5, 131.6, 130.1, 130.1, 129.3, 127.5, 114.4, 59.4, 55.8, 48.6, 36.5. HRMS (ESI) $C_{18}H_{19}ClNO_3$ *m/z* [M+H] $^{+}$ found 332.1063, expected 332.1053.

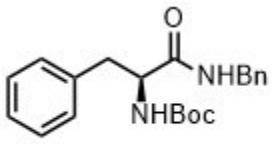

200

***tert*-butyl (S)-(1-(benzylamino)-1-oxo-3-phenylpropan-2-yl)carbamate**

To a solution of Boc-Phe-OH **146** (0.5g, 1.9 mmol, 1.0 equiv) in DCM (9.0 mL, 0.2 M) was added 1-hydroxybenzotriazole hydrate (0.306 g, 2.26 mmol, 1.2 equiv), EDCI (0.362 g, 1.89 mmol, 1.0 equiv) and NMM (0.25 mL, 2.26 mmol, 1.2 equiv). The solution was stirred for 30 minutes, followed by addition of benzylamine **199** (0.2 mL, 1.89 mmol, 1.0 equiv) and the reaction was allowed to stir overnight. The following day, the solution was diluted with DCM and washed with 1 N HCl. The DCM layer was purified over silica gel to obtain the compound **200** (0.502 g, 1.42 mmol, 75%). ^{1}H NMR (400 MHz, $CDCl_3$) δ 7.17 - 7.34 (m, 7H), 7.11 (d, *J* = 6.27 Hz, 2H), 6.05 (br. s., 1H), 5.04 (br. s., 1H), 4.37 (d, *J* = 6.00 Hz, 2H), 2.98 - 3.18 (m, 3H), 1.40 (s, 9H).

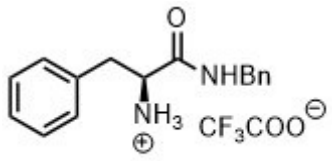

201

(*S*)-1-(benzylamino)-1-oxo-3-phenylpropan-2-aminium

To the solution of the amide **200** (0.1 g, 0.282 mmol, 1.0 equiv) in DCM (0.7 mL, 0.4 M) was added TFA (0.7 mL, 0.4 M) and the solution was stirred overnight. The following day, solvents were removed in vacuo to obtain compound **201** that was sufficiently pure to use for the next step.

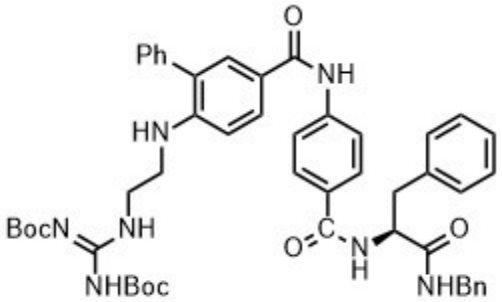

202

To the solution of the acid **187** (0.027 g, 0.044 mmol, 1.0 equiv) in DCM (1.0 mL, 0.1 M) was added PyBOP (0.023 g, 0.044 mmol, 1.0 equiv) and DIPEA (0.015 mL, 0.084 mmol, 2.0 equiv). The mixture was stirred for 30 minutes, followed by addition of the amine **201** (0.023 g, 0.044 mmol, 1.0 equiv). The solution was stirred overnight, followed by dilution with DCM, washing with 1 N HCl and purification over silica gel to obtain compound **202** (0.035 g, 0.041 mmol, 80%). ^{1}H NMR (400 MHz, $CDCl_3$) δ 11.47 (s, 1H), 8.50 (t, *J* = 5.52 Hz, 1H), 8.20 (s, 1H), 7.83 (dd, *J* = 2.13, 8.66 Hz, 1H), 7.62 - 7.74 (m, 5H), 7.35 - 7.50 (m, 5H), 7.16 - 7.32 (m, 10H), 7.02 - 7.12 (m, 2H), 6.92 (d, *J* = 7.78 Hz, 1H), 6.81 (d, *J* = 8.53 Hz, 1H), 6.34 (t, *J* = 5.65 Hz, 1H), 4.81 - 4.92 (m, 1H), 4.47 (br. s., 1H), 4.39 (dd, *J* = 6.15, 14.93 Hz, 1H), 4.28 (dd, *J* = 5.52, 14.81 Hz, 1H), 3.60 (q, *J* = 6.11 Hz, 2H), 3.34 - 3.44 (m, 2H), 3.26 (dd, *J* = 6.02, 13.55 Hz, 1H), 3.14 (dd, *J* = 8.03, 13.55 Hz, 1H), 1.51 (d, *J* = 8.78 Hz, 18H).

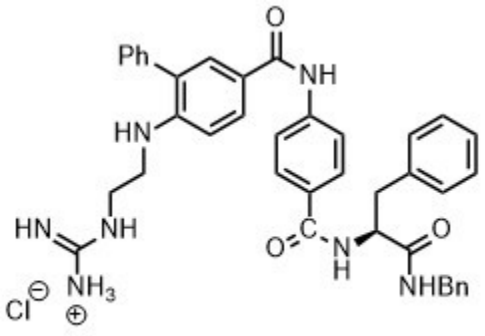

203

(*S*)-1-(2-((5-((4-((1-(benzylamino)-1-oxo-3-phenylpropan-2-yl)carbamoyl)phenyl)carbamoyl)-[1,1'-biphenyl]-2-yl)amino)ethyl)guanidinium chloride

To a solution of the above prepared amide **202** (0.035 g, 0.041 mmol, 1.0 equiv) in dioxane (0.4 mL, 0.1 M) was added HCl in dioxane (4 N, 0.1 mL, 10.0 equiv). The solution was stirred overnight and the solvents were removed in vacuo to obtain the compound **203** (0.026 g, 0.04 mmol, quant). ^{1}H NMR (400 MHz, CD_3OD) δ 7.92 (br. s., 1H), 7.65 - 7.85 (m, 5H), 7.34 - 7.55 (m, 6H), 7.07 - 7.33 (m, 12H), 6.95 (br. s., 1H), 4.74 - 4.88 (m, 2H), 4.25 - 4.43 (m, 2H), 3.69 - 3.76 (m, 1H), 3.59 (s, 2H), 3.37 - 3.48 (m, 4H), 3.23 (dd, *J* = 6.15, 13.43 Hz, 1H), 3.03 - 3.14 (m, 1H). ^{13}C NMR (101 MHz, CD_3OD) δ 169.4, 168.3, 158.7, 148.2, 143.6, 139.3, 138.3, 131.4, 130.3, 130.3, 130.2, 130.1, 129.9, 129.5, 129.4, 129.3, 129.1, 128.9, 128.4, 128.0, 127.7, 124.5, 121.1, 111.8, 56.8, 44.1, 41.6, 38.9. HRMS (ESI) $C_{39}H_{41}N_7O_3$ *m/z* $[M+H]^+$ found 655.3187, expected 655.3270.

4.3.2: Biological Experimentals

Assays of AKT1 were performed using Z'-LYTE Kinase Assay Kit – Ser/Thr 6 peptide (Invitrogen, NY, USA) in non-binding low-volume 384-well plates (Cat. No 3676, Corning, NY, USA). All the reagents were diluted in kinase buffer (50 mM HEPES pH 7.5, 0.01% BRIJ-35, 10 mM $MgCl_2$, 1 mM EDTA). All compounds were prepared as 10 mM soulutions in DMSO and diluted to 0.8% final DMSO concentrations in the assay. A typical 10 µL assay contained 6 ng of AKT1, 75 µM ATP and 2 µM peptide substrate in kinase buffer in the presence/absence of tested compounds. The assays were incubated at room

temperature for 1 h, following by the addition of 5 µL of development reagent and further incubation at room temperature for another hour. The kinase reaction was terminated by the addition of 5 µL of stop reagent. The FRET signal was measured using Flexstation 3 microplate reader (molecular Devices, CA, USA) with an excitation wavelength of 410 nm and emission wavelengths of 458 nm and 522 nm. The percent inhibition was calculated according to the kit guidelines. Staurosporine (CalBiochem) was used as the control compound. Data analysis, curve fitting and calculation of error was performed using Prism software from GraphPad. The IC_{50}s (**Table 11**) were calculated from the graphs obtained below (**Figure 90**);

Table 11: IC_{50s} (µM) of compounds

Compound	IC_{50} (µM)	95% Confidence Interval
125	>100	
129	10.59	7.53 – 14.89
127	3.25	2.32 – 4.55
141	1.55	1.35 – 1.79
135	>100	
138	>100	
128	2.33	1.84 – 2.96
133	1.11	1.00 – 1.24
144	1.79	1.53 – 2.09
145	1.97	1.44 – 4.11

151	0.32	0.26 – 0.40
152	>100	
156	2.44	1.23 – 2.76
153	> 100	
161	0.82	0.68 – 0.98
173	> 100	
175	> 100	
177	> 100	
198	>25	
195	0.578	0.314 – 1.065
203	>25	

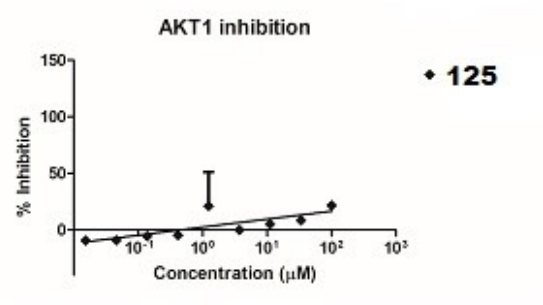

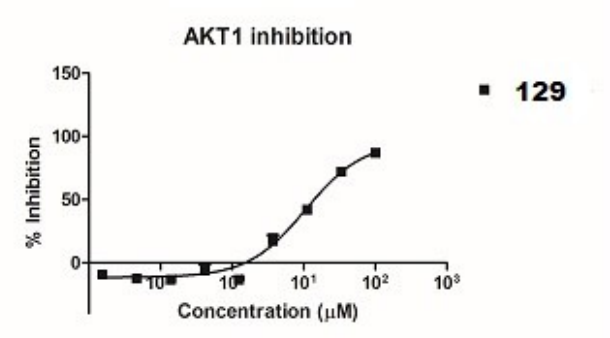

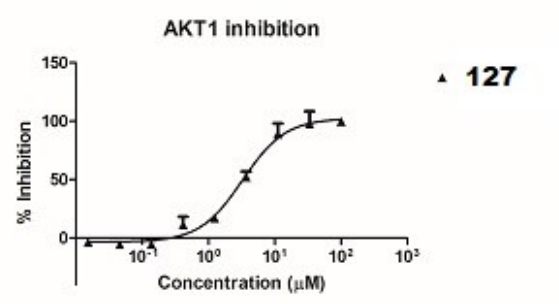

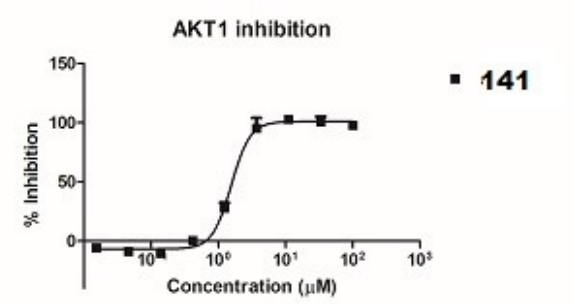

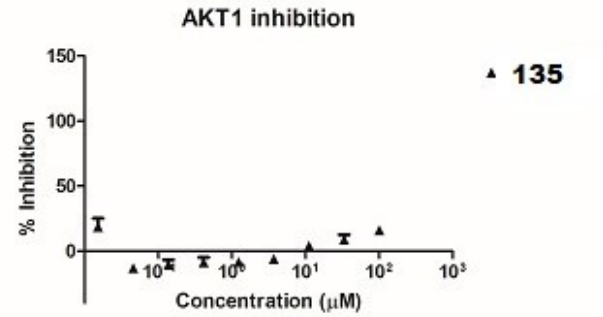

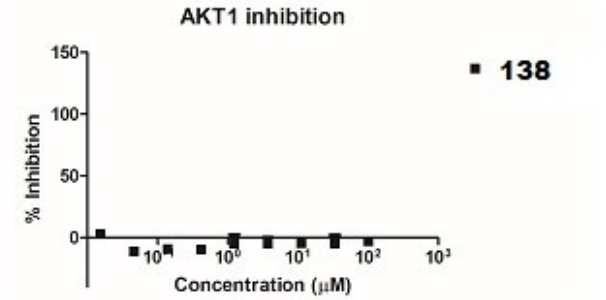

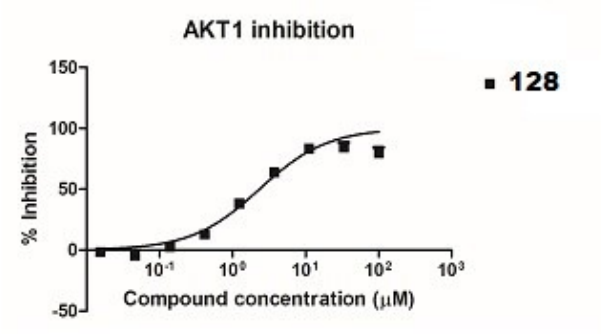

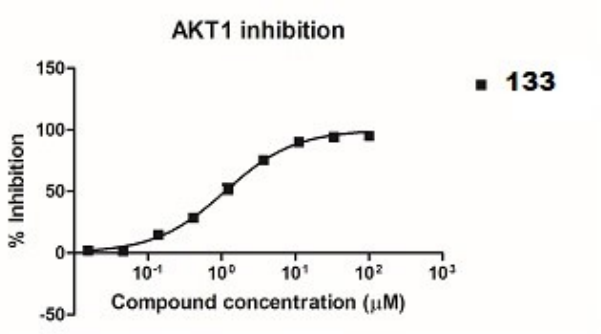

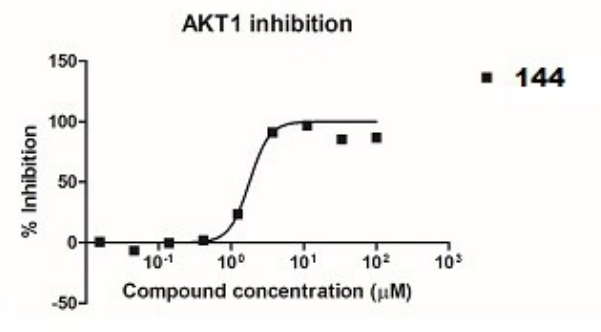

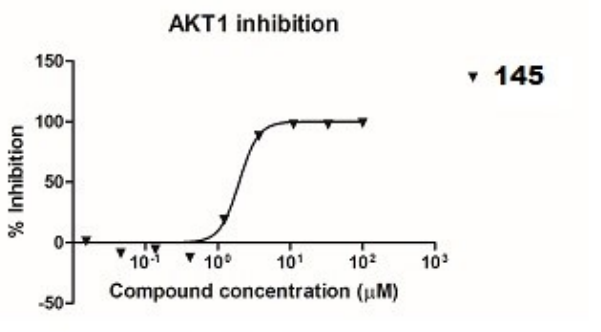

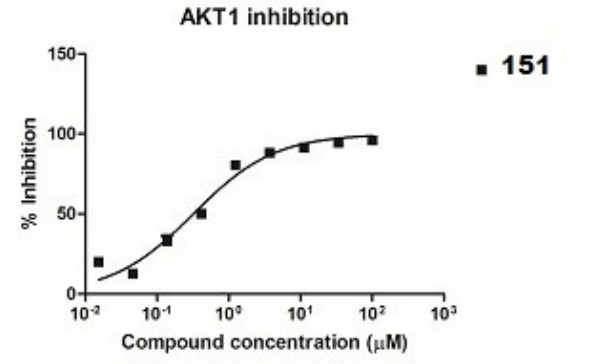

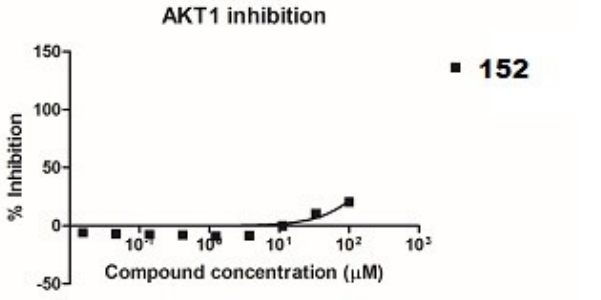

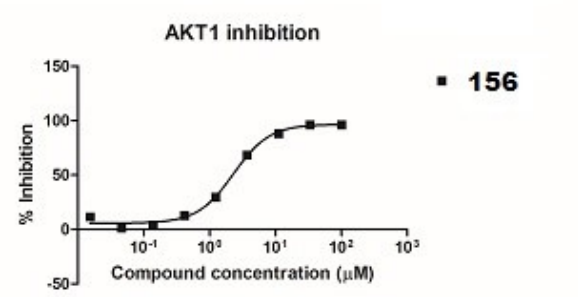

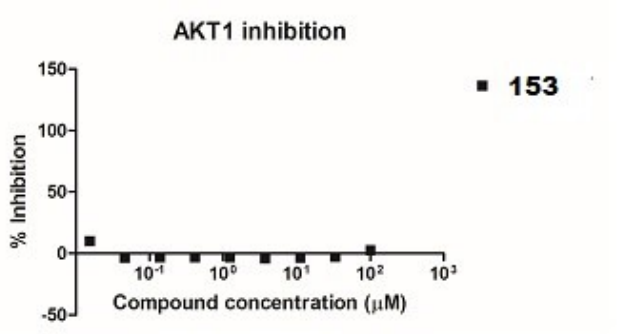

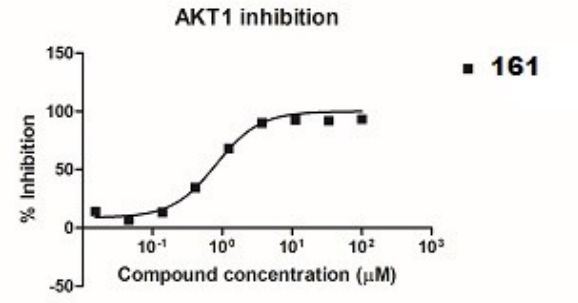

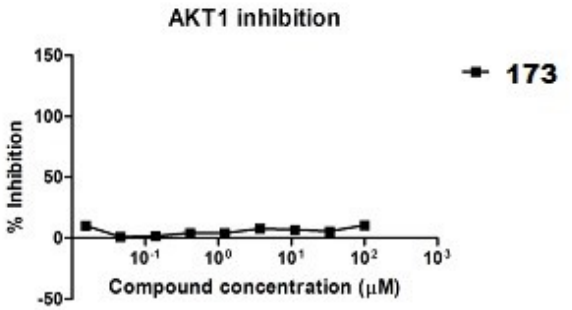

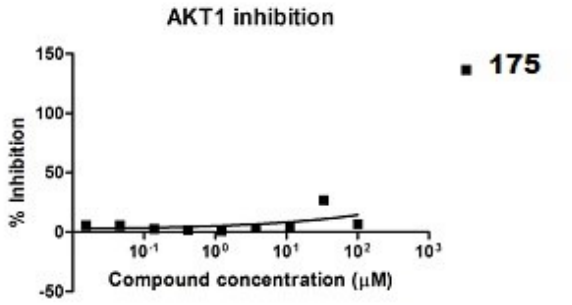

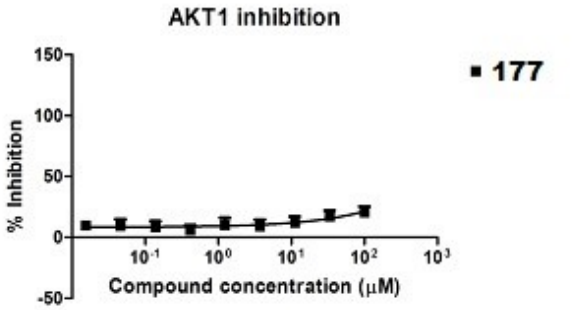

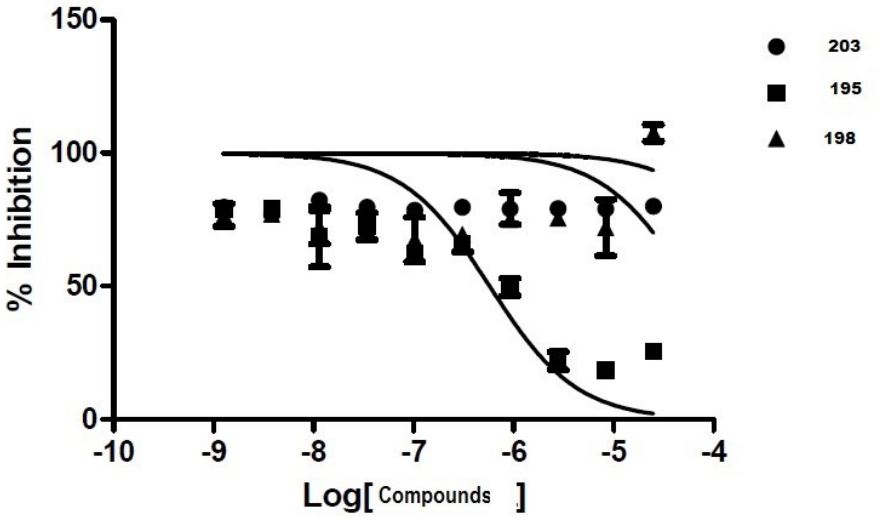

Figure 90: Graphs used to calculate IC_{50}s for compounds

The assays of PKAα were performed using Z′-LYTE Kinase Assay Kit – Ser/Thr 1 Peptide (Invitrogen, NY, USA) in non-binding low-volume 384-well plates (Cat. No 3676, Corning, NY,USA). All the reagents were diluted in kinase buffer (50 mM HEPES pH 7.5, 0.01% BRIJ-35, 10mM MgCl2, 1 mM EDTA). The compounds were prepared as 10 mM solutions in DMSO and diluted to 0.8% final DMSO concentration in the assay. A typical 10 µL assay contained 0.3 ng of PKAα, 4 µM ATP and 2 µM peptide substrate in kinase buffer in the presence/absence of tested compounds. The assays were incubated at room temperature for 1 h. 5 µL of development reagent was then added and the assay mixture was incubated at room temperature for further 1 h. The kinase reaction was terminated by the addition of 5 µL of stop reagent. The FRET signal was measured using a Flexstation 3 microplate reader (Molecular Devices, CA, USA) using an excitation wavelength of 410 nm and emission wavelengths of 458 nm and 522 nm. The percent inhibition was calculated according to the kit guidelines. Staurosporine (CalBiochem) was

used as a control compound. The IC_{50}s (**Table 12**) were calculated from the graphs obtained below (**Figure 91**)

Table 12: IC_{50} of compounds against PKAα

Compound	IC_{50} (μM)	Confidence interval
151	>100	
161	13.47	11.75 – 15.43

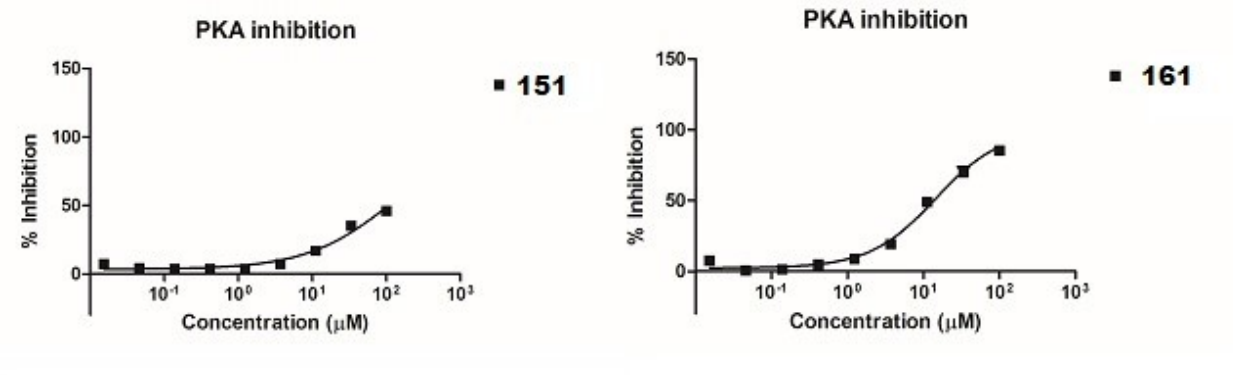

Figure 91: Graphs used to calculate IC_{50}s for PKAα

Literature Cited

1. Freire-Moran, L.; Aronsson, B.; Manz, C.; Gyssens, I. C.; So, A. D.; Monnet, D. L.; Cars, O. Critical shortage of new antibiotics in development against multidrug-resistant bacteria—time to react is now. *Drug Resist. Updates* **2011,** *14*, 118-124.
2. Zaffiri, L.; Gardner, J.; Toledo-Pereyra, L. H. History of antibiotics. From salvarsan to cephalosporins. *J. Invest. Surg.* **2012,** *25*, 67-77.
3. Wright, G. D. Antibiotics: a new hope. *Chem. Biol.* **2012,** *19*, 3-10.
4. Boucher, H. W.; Talbot, G. H.; Bradley, J. S.; Edwards, J. E.; Gilbert, D.; Rice, L. B.; Scheld, M.; Spellberg, B.; Bartlett, J. Bad bugs, no drugs: no ESKAPE! An update from the Infectious Diseases Society of America. *Clin. Infect. Dis.* **2009,** *48*, 1-12.
5. Payne, D. J.; Gwynn, M. N.; Holmes, D. J.; Pompliano, D. L. Drugs for bad bugs: confronting the challenges of antibacterial discovery. *Nat. Rev. Drug Discovery* **2007,** *6*, 29-40.
6. Collin, F.; Karkare, S.; Maxwell, A. Exploiting bacterial DNA gyrase as a drug target: current state and perspectives. *Appl. Microbiol. Biotechnol.* **2011,** *92*, 479-497.
7. Roca, J.; Berger, J. M.; Harrison, S. C.; Wang, J. C. DNA transport by a type II topoisomerase: direct evidence for a two-gate mechanism. *Proc. Nat. Acad, Sci. USA.* **1996,** *93*, 4057-4062.
8. Roca, J.; Wang, J. C. DNA transport by a type II DNA topoisomerase: evidence in favor of a two-gate mechanism. *Cell* **1994,** 77, 609-616.

9. Berger, J. M.; Gamblin, S. J.; Harrison, S. C.; Wang, J. C. Structure and mechanism of DNA topoisomerase II. *Nature* **1996**, *379*, 225-232.

10. Drlica, K.; Zhao, X. DNA gyrase, topoisomerase IV, and the 4-quinolones. *Microbiol. Mol. Biol. Rev.* **1997,** *61*, 377-392.

11. Shen, L. L.; Mitscher, L. A.; Sharma, P. N.; o'Donnell, T.; Chu, D. W.; Cooper, C. S.; Rosen, T.; Pernet, A. G. Mechanism of inhibition of DNA gyrase by quinolone antibacterials: a cooperative drug-DNA binding model. *Biochemistry* **1989,** *28*, 3886-3894.

12. Heide, L. The aminocoumarins: biosynthesis and biology. *Nat. Prod. Rep.* **2009,** *26*, 1241-1250.

13. Flatman, R. H.; Eustaquio, A.; Li, S.-M.; Heide, L.; Maxwell, A. Structure-activity relationships of aminocoumarin-type gyrase and topoisomerase IV inhibitors obtained by combinatorial biosynthesis. *Antimicrob. Agents Chemother.* **2006,** *50*, 1136-1142.

14. Widdowson, K.; Hennessy, A. Advances in structure-based drug design of novel bacterial topoisomerase inhibitors. *Future Med. Chem.* **2010,** *2*, 1619-1622.

15. Black, M. T.; Stachyra, T.; Platel, D.; Girard, A.-M.; Claudon, M.; Bruneau, J.-M.; Miossec, C. Mechanism of action of the antibiotic NXL101, a novel nonfluoroquinolone inhibitor of bacterial type II topoisomerases. *Antimicrob. Agents Chemother.* **2008,** *52*, 3339-3349.

16. Bax, B. D.; Chan, P. F.; Eggleston, D. S.; Fosberry, A.; Gentry, D. R.; Gorrec, F.; Giordano, I.; Hann, M. M.; Hennessy, A.; Hibbs, M. Type IIA topoisomerase inhibition by a new class of antibacterial agents. *Nature* **2010,** *466*, 935-940.

17. Schimana, J.; Fiedler, H.-P.; Groth, I.; Süssmuth, R.; Beil, W.; Walker, M.; Zeeck, A. Simocyclinones, novel cytostatic angucyclinone antibiotics produced by Streptomyces antibioticus Tu 6040. I. Taxonomy, fermentation, isolation and biological activities. *J. Antibiot.* **2000,** *53*, 779-787.

18. Schimana, J.; Walker, M.; Zeeck, A.; Fiedler, H. Simocyclinones: diversity of metabolites is dependent on fermentation conditions3. *J. Ind. Microbiol. Biotechnol.* **2001,** *27*, 144-148.

19. Flatman, R. H.; Howells, A. J.; Heide, L.; Fiedler, H.-P.; Maxwell, A. Simocyclinone D8, an inhibitor of DNA gyrase with a novel mode of action. *Antimicrob. Agents Chemother.* **2005,** *49*, 1093-1100.

20. Trefzer, A.; Pelzer, S.; Schimana, J.; Stockert, S.; Bihlmaier, C.; Fiedler, H.-P.; Welzel, K.; Vente, A.; Bechthold, A. Biosynthetic gene cluster of simocyclinone, a natural multihybrid antibiotic. *Antimicrob. Agents Chemother.* **2002,** *46*, 1174-1182.

21. Galm, U.; Schimana, J.; Fiedler, H.-P.; Schmidt, J.; Li, S.-M.; Heide, L. Cloning and analysis of the simocyclinone biosynthetic gene cluster of Streptomyces antibioticus Tü 6040. *Arch. Microbiol.* **2002,** *178*, 102-114.

22. Edwards, M. J.; Flatman, R. H.; Mitchenall, L. A.; Stevenson, C. E.; Le, T. B.; Clarke, T. A.; McKay, A. R.; Fiedler, H.-P.; Buttner, M. J.; Lawson, D. M. A crystal structure of the bifunctional antibiotic simocyclinone D8, bound to DNA gyrase. *Science* **2009,** *326*, 1415-1418.

23. Edwards, M. J.; Williams, M. A.; Maxwell, A.; McKay, A. R. Mass spectrometry reveals that the antibiotic simocyclinone D8 binds to DNA gyrase in a “bent-over”

conformation: evidence of positive cooperativity in binding. *Biochemistry* **2011,** *50*, 3432-3440.

24. Sissi, C.; Vazquez, E.; Chemello, A.; Mitchenall, L.; Maxwell, A.; Palumbo, M. Mapping simocyclinone D8 interaction with DNA gyrase: evidence for a new binding site on GyrB. *Antimicrob. Agents Chemother.* **2010,** *54*, 213-220.

25. Hearnshaw, S. J.; Edwards, M. J.; Stevenson, C. E.; Lawson, D. M.; Maxwell, A. A New Crystal Structure of the Bifunctional Antibiotic Simocyclinone D8 Bound to DNA Gyrase Gives Fresh Insight into the Mechanism of Inhibition. *J. Mol. Biol.* **2014**, *426*, 2023-2033.

26. Oppegard, L. M.; Hamann, B. L.; Streck, K. R.; Ellis, K. C.; Fiedler, H.-P.; Khodursky, A. B.; Hiasa, H. In vivo and in vitro patterns of the activity of simocyclinone D8, an angucyclinone antibiotic from Streptomyces antibioticus. *Antimicrob. Agents Chemother.* **2009,** *53*, 2110-2119.

27. Sadiq, A. A.; Patel, M. R.; Jacobson, B. A.; Escobedo, M.; Ellis, K.; Oppegard, L. M.; Hiasa, H.; Kratzke, R. A. Anti-proliferative effects of simocyclinone D8 (SD8), a novel catalytic inhibitor of topoisomerase II. *Invest. New Drugs* **2010,** *28*, 20-25.

28. Oppegard, L. M.; Nguyen, T.; Ellis, K. C.; Hiasa, H. Inhibition of Human Topoisomerases I and II by Simocyclinone D8. *J. Nat. Prod.* **2012,** *75*, 1485-1489.

29. Richter, S. N.; Frasson, I.; Palumbo, M.; Sissi, C.; Palù, G. Simocyclinone D8 turns on against Gram-negative bacteria in a clinical setting. *Bioorg. Med. Chem. Lett.* **2010,** *20*, 1202-1204.

30. Brown, S. D.; Farrell, D. J.; Morrissey, I. Prevalence and molecular analysis of macrolide and fluoroquinolone resistance among isolates of Streptococcus

pneumoniae collected during the 2000-2001 PROTEKT US Study. *J. Clin. Microbiol.* **2004,** *42*, 4980-4987.

31. Elliott, E.; Oosthuizen, D.; Johnson, M. M.; Piddock, L. J. Fluoroquinolone resistance in Haemophilus influenzae. *J. Antimicrob. Chemother.* **2003**, *52*, 734-735.

32. Hooper, D. C. Emerging mechanisms of fluoroquinolone resistance. *Emerging Infect. Dis.* **2001,** *7*, 337.

33. Reinhardt, A.; Köhler, T.; Wood, P.; Rohner, P.; Dumas, J.-L.; Ricou, B.; van Delden, C. Development and persistence of antimicrobial resistance in Pseudomonas aeruginosa: a longitudinal observation in mechanically ventilated patients. *Antimicrob. Agents Chemother.* **2007,** *51*, 1341-1350.

34. Mays, J. R.; Hill, S. A.; Moyers, J. T.; Blagg, B. S. The synthesis and evaluation of flavone and isoflavone chimeras of novobiocin and derrubone. *Biorg. Med. Chem.* **2010,** *18*, 249-266.

35. Webb, M.; Ebeler, S. Comparative analysis of topoisomerase IB inhibition and DNA intercalation by flavonoids and similar compounds: structural determinates of activity. *Biochem. J.* **2004,** *384*, 527-541.

36. Constantinou, A.; Mehta, R.; Runyan, C.; Rao, K.; Vaughan, A.; Moon, R. Flavonoids as DNA topoisomerase antagonists and poisons: structure-activity relationships. *J. Nat. Prod.* **1995,** *58*, 217-225.

37. Fortune, J. M.; Osheroff, N. Merbarone inhibits the catalytic activity of human topoisomerase IIα by blocking DNA cleavage. *J. Biol. Chem.* **1998,** *273*, 17643-17650.

38. Noble, C. G.; Barnard, F. M.; Maxwell, A. Quinolone-DNA interaction: sequence-dependent binding to single-stranded DNA reflects the interaction within the gyrase-DNA complex. *Antimicrob. Agents Chemother.* **2003,** *47*, 854-862.

39. Newman, D. J.; Cragg, G. M.; Snader, K. M. Natural products as sources of new drugs over the period 1981-2002. *J. Nat. Prod.* **2003,** *66*, 1022-1037.

40. O'Shea, R.; Moser, H. E. Physicochemical properties of antibacterial compounds: implications for drug discovery. *J. Med. Chem.* **2008,** *51*, 2871-2878.

41. Carreno, M. C.; Urbano, A. Recent advances in the synthesis of angucyclines. *Synlett* **2005,** *2005*, 1-25.

42. Krohn, K.; Rohr, J. Angucyclines: total syntheses, new structures, and biosynthetic studies of an emerging new class of antibiotics. In *Bioorganic Chemistry Deoxysugars, Polyketides and Related Classes: Synthesis, Biosynthesis, Enzymes*, Springer: 1997; pp 127-195.

43. Rohr, J.; Thiericke, R. Angucycline group antibiotics. *Nat. Prod. Rep.* **1992,** *9*, 103-137.

44. Matsumoto, T.; Yamaguchi, H.; Tanabe, M.; Yasui, Y.; Suzuki, K. Synthetic study of aquayamycin. Part 3: First total synthesis. *Tetrahedron Lett.* **2000,** *41*, 8393-8396.

45. Matsumoto, T.; Yamaguchi, H.; Hamura, T.; Tanabe, M.; Kuriyama, Y.; Suzuki, K. Synthetic study of aquayamycin. Part 1: Synthesis of 3-(phenylsulfonyl) phthalides possessing a β- C-olivoside. *Tetrahedron Lett.* **2000,** *41*, 8383-8387.

46. Yamaguchi, H.; Konegawa, T.; Tanabe, M.; Nakamura, T.; Matsumoto, T.; Suzuki, K. Synthetic study of aquayamycin. Part 2: Synthesis of the AB ring fragment. *Tetrahedron Lett.* **2000,** *41*, 8389-8392.

47. Kim, K.; Guo, Y.; Sulikowski, G. A. Synthetic Studies of the Angucycline Antibiotics. Stereocontrolled Assembly of the SF 2315B Ring System. *J. Org. Chem.* **1995,** *60*, 6866-6871.

48. Matsumoto, T.; Sohma, T.; Yamaguchi, H.; Kurata, S.; Suzuki, K. Benzyne-Furan Cycloaddition Approach to the Angucyclines: First Total Synthesis of Antibiotic C104. *Synlett* **1995,** *1995*, 263-266.

49. Matsumoto, T.; Sohma, T.; Yamaguchi, H.; Kurata, S.; Suzuki, K. Total synthesis of antibiotic C104: Benzyne-Furan cycloaddition approach to the angucyclines. *Tetrahedron* **1995,** *51*, 7347-7360.

50. Toshima, K.; Matsuo, G.; Ishizuka, T.; Ushiki, Y.; Nakata, M.; Matsumura, S. Aryl and allyl C-glycosidation methods using unprotected sugars. *J. Org. Chem.* **1998,** *63*, 2307-2313.

51. Allevi, P.; Anastasia, M.; Ciuffreda, P.; Sanvito, A. M.; Scala, A. A simple one pot synthesis of aromatic steroidal and non-steroidal C-glucosides via O-glucosides. *Chem. Phys. Lipids* **1992,** 63, 179-189.

52. Audia, J. E.; Boisvert, L.; Patten, A. D.; Villalobos, A.; Danishefsky, S. J. Synthesis of two useful, enantiomerically pure derivatives of (S)-4-hydroxy-2-cyclohexenone. *J. Org. Chem.* **1989,** *54*, 3738-3740.

53. Bickley, J. F.; Evans, P.; Meek, A.; Morgan, B. S.; Roberts, S. M. Novel preparation of (−)-4-hydroxycyclohex-2-enone: reaction of 4-hydroxycyclohex-2-enone and 4-

hydroxycyclopent-2-enone with some thiols. *Tetrahedron: Asymmetry* **2006,** *17*, 355-362.

54. Demir, A. S.; Sesenoglu, O. A new and efficient chemoenzymatic route to both enantiomers of 4-hydroxycyclohex-2-en-1-one. *Org. Lett.* **2002,** *4*, 2021-2023.

55. Marchand, A. P.; Xing, D.; Wang, Y.; Bott, S. G. Improved synthesis of racemic and optically active 4-hydroxycyclohex-2-en-1-one. *Tetrahedron: Asymmetry* **1995,** *6*, 2709-2714.

56. Zhu, Y.; Tu, Y.; Yu, H.; Shi, Y. Highly enantioselective epoxidation of enol silyl ethers and esters. *Tetrahedron Lett.* **1998,** *39*, 7819-7822.

57. Davis, F. A.; Sheppard, A. C. Oxidation of silyl enol ethers using 2-sulfonyloxaziridines. Synthesis of. alpha.-siloxy epoxides and. alpha.-hydroxy carbonyl compounds. *J. Org. Chem.* **1987,** *52*, 954-955.

58. Adam, W.; Fell, R. T.; Saha-Möller, C. R.; Zhao, C.-G. Synthesis of optically active α-hydroxy ketones by enantioselective oxidation of silyl enol ethers with a fructose-derived dioxirane. *Tetrahedron: Asymmetry* **1998,** *9*, 397-401.

59. Adam, W.; Fell, R. T.; Stegmann, V. R.; Saha-Möller, C. R. Synthesis of optically active α-hydroxy carbonyl compounds by the catalytic, enantioselective oxidation of silyl enol ethers and ketene acetals with (salen) manganese (III) complexes. *J. Am. Chem. Soc.* **1998,** *120*, 708-714.

60. Lopp, M.; Paju, A.; Kanger, T.; Pehk, T. Direct asymmetric α-hydroxylation of β-hydroxyketones. *Tetrahedron Lett.* **1997,** *38*, 5051-5054.

61. Paju, A.; Kanger, T.; Pehk, T.; Lopp, M. Direct asymmetric α-hydroxylation of 2-hydroxymethyl ketones. *Tetrahedron* **2002,** *58*, 7321-7326.

62. Rubottom, G.; Gruber, J. m-Chloroperbenzoic acid oxidation of 2-trimethylsilyloxy-1, 3-dienes. Synthesis of. alpha.-hydroxy and. alpha.-acetoxy enones. *J. Org. Chem.* **1978,** *43*, 1599-1602.

63. Hauser, F. M.; Dorsch, W. A.; Mal, D. Total Synthesis of (±)-O-Methyl PD 116740. *Org. Lett.* **2002,** *4*, 2237-2239.

64. Gaveby, B. M. G.; Huffman, J. C.; Magnus, P. 11a-Chlorination of the Shemyakin tricyclic ketone. *J. Org. Chem.* **1982,** *47*, 3779-3780.

65. Mehta, G.; Pan, S. C. First total synthesis of yanuthones: novel farnesylated epoxycyclohexenoid marine natural products. *Tetrahedron Lett.* **2005,** *46*, 5219-5223.

66. Yu, B.; Jiang, T.; Quan, W.; Li, J.; Pan, X.; She, X. An Efficient Method for Construction of the Angularly Fused 6, 3, 5-Tricyclic Skeleton of Mycorrhizin A and Its Analogues. *Org. Lett.* **2009,** *11*, 629-632.

67. Horiguchi, Y.; Toeda, A.; Tomoda, K.; Suzuki, H.; Sano, T. A synthesis of 1-azaanthraquinones via Diels-Alder reaction of 4-hydroxy-and 4-methoxy-2-phenylquinolinequinones with 3-trimethylsilyloxy-1, 3-butadienes: Observation of inverse regioselectivity. *Chem. Pharm. Bull.* **1998,** *46*, 1356-1363.

68. Rozek, T.; Tiekink, E. R. T.; Taylor, D. K.; Bowie, J. H. Syntheses of angucyclinones related to ochromycinone. II. Regio-and stereo-selective reduction of a tetrahydroangucyclinone. *Aust. J. Chem.* **1998,** *51*, 1057-1060.

69. Zhou, J.; Fu, G. C. Suzuki cross-couplings of unactivated secondary alkyl bromides and iodides. *J. Am. Chem. Soc.* **2004,** *126*, 1340-1341.

70. Deloux, L.; Srebnik, M.; Sabat, M. Stereospecific Synthesis of Temarotene, Its Structural Isomers, and Mixed Triaryl Alkenes from gem-Borazirconocene Alkenes. *J. Org. Chem.* **1995,** *60*, 3276-3277.

71. Molander, G. A.; Jean-Gérard, L. Scope of the Suzuki− Miyaura Cross-Coupling Reaction of Potassium Trifluoroboratoketohomoenolates. *J. Org. Chem.* **2009,** *74*, 1297-1303.

72. Molander, G. A.; Petrillo, D. E. Suzuki− Miyaura Cross-Coupling of Potassium Trifluoroboratohomoenolates. *Org. Lett.* **2008,** *10*, 1795-1798.

73. Paquette, L. A.; Hormuth, S.; Lovely, C. J. Studies Directed toward the Total Synthesis of Cerorubenic Acid-III. 4. Exploration of an Organometallic Approach to Construction of the Eastern Sector. *J. Org. Chem.* **1995,** *60*, 4813-4821.

74. Konradi, A. W.; Pedersen, S. F. Pinacol homocoupling of (S)-2-[N-(benzyloxycarbonyl) amino] aldehydes by [V2Cl3 (THF) 6] 2 [Zn2Cl6]. Synthesis of C2-symmetric (1S, 2R, 3R, 4S)-1, 4-diamino 2, 3-diols. *J. Org. Chem.* **1992,** *57*, 28-32.

75. Donnelly, A. C.; Mays, J. R.; Burlison, J. A.; Nelson, J. T.; Vielhauer, G.; Holzbeierlein, J.; Blagg, B. S. The design, synthesis, and evaluation of coumarin ring derivatives of the novobiocin scaffold that exhibit antiproliferative activity. *J. Org. Chem.* **2008,** *73*, 8901-8920.

76. Vosburg, D. A.; Weiler, S.; Sorensen, E. J. Concise stereocontrolled routes to fumagillol, fumagillin, and TNP-470. *Chirality* **2003,** *15*, 156-166.

77. Pacholec, M.; Freel Meyers, C. L.; Oberthür, M.; Kahne, D.; Walsh, C. T. Characterization of the aminocoumarin ligase SimL from the simocyclinone

pathway and tandem incubation with NovM, P, N from the novobiocin pathway. *Biochemistry* **2005,** *44*, 4949-4956.

78. Hou, D.; Lowary, T. L. Recent advances in the synthesis of 2-deoxy-glycosides. *Carbohydr. Res.* **2009,** *344*, 1911-1940.

79. Guo, H.; O'Doherty, G. A. De novo asymmetric synthesis of daumone via a palladium-catalyzed glycosylation. *Org. Lett.* **2005,** *7*, 3921-3924.

80. Zhou, M.; O'Doherty, G. A. De novo synthesis of the trisaccharide subunit of landomycins A and E. *Org. Lett.* **2008,** *10*, 2283-2286.

81. Zhou, M.; O'Doherty, G. A. De Novo Approach to 2-Deoxy-β-glycosides: Asymmetric Syntheses of Digoxose and Digitoxin1. *J. Org. Chem.* **2007,** *72*, 2485-2493.

82. Myers, A. G.; Movassaghi, M.; Zheng, B. Single-step process for the reductive deoxygenation of unhindered alcohols. *J. Am. Chem. Soc.* **1997,** *119*, 8572-8573.

83. Leblanc, Y.; Fitzsimmons, B. J. [4+ 2] Cycloaddition reaction of bis (trichloroethyl) azodicarboxylate and glycals: preparation of a C1-C1 2-amino disaccharide. *Tetrahedron Lett.* **1989,** *30*, 2889-2892.

84. Gammon, D. W.; Hunter, R.; Wilson, S. A. An efficient synthesis of 7-hydroxy-2, 6-dimethylchromeno [3, 4-] oxazol-4-one—a protected fragment of novenamine. *Tetrahedron* **2005,** *61*, 10683-10688.

85. Deguest, G.; Bischoff, L.; Fruit, C.; Marsais, F. Anionic, in Situ Generation of Formaldehyde: A Very Useful and Versatile Tool in Synthesis. *Org. Lett.* **2007,** *9*, 1165-1167.

86. Chen, B. C.; Zhou, P.; Davis, F. A.; Ciganek, E. α-Hydroxylation of Enolates and Silyl Enol Ethers. *Organic Reactions* **2003**.

87. Thoret, S.; Guéritte, F.; Guénard, D.; Dubois, J. Semisynthesis and Biological Evaluation of a Novel D-Seco Docetaxel Analogue. *Org. Lett.* **2006,** *8*, 2301-2304.

88. Hunter, T. Protein kinases and phosphatases: the yin and yang of protein phosphorylation and signaling. *Cell* **1995,** *80*, 225-236.

89. Manning, G.; Whyte, D. B.; Martinez, R.; Hunter, T.; Sudarsanam, S. The protein kinase complement of the human genome. *Science* **2002,** *298*, 1912-1934.

90. Pearce, L. R.; Komander, D.; Alessi, D. R. The nuts and bolts of AGC protein kinases. *Nat. Rev. Mol. Cell Biol.* **2010,** *11*, 9-22.

91. Staal, S. P. Molecular cloning of the akt oncogene and its human homologues AKT1 and AKT2: amplification of AKT1 in a primary human gastric adenocarcinoma. *Proc. Nat. Acad. Sci. USA.* **1987,** *84*, 5034-5037.

92. Jones, P. F.; Jakubowicz, T.; Pitossi, F. J.; Maurer, F.; Hemmings, B. A. Molecular cloning and identification of a serine/threonine protein kinase of the second-messenger subfamily. *Proc. Nat. Acad. Sci. USA.* **1991,** *88*, 4171-4175.

93. Bellacosa, A.; Staal, S.; Tsichlis, P. A retroviral oncogene, akt, encoding a serine-threonine kinase containing an SH2-like region. *Science* **1991,** *254*, 274-277.

94. COFFER, P. J.; WOODGETT, J. R. Molecular cloning and characterisation of a novel putative protein-serine kinase related to the cAMP-dependent and protein kinase C families. *Eur. J. Biochem.* **1991,** *201*, 475-481.

95. Brazil, D. P.; Hemmings, B. A. Ten years of protein kinase B signalling: a hard Akt to follow. *Trends Biochem. Sci.* **2001,** *26*, 657-664.

96. Kumar, C. C.; Madison, V. AKT crystal structure and AKT-specific inhibitors. *Oncogene* **2005,** *24*, 7493-501.

97. Franke, T. F. PI3K/Akt: getting it right matters. *Oncogene* **2008,** *27*, 6473-88.

98. Sarbassov, D. D.; Guertin, D. A.; Ali, S. M.; Sabatini, D. M. Phosphorylation and regulation of Akt/PKB by the rictor-mTOR complex. *Science* **2005,** *307*, 1098-1101.

99. Dimmeler, S.; Assmus, B.; Hermann, C.; Haendeler, J.; Zeiher, A. M. Fluid shear stress stimulates phosphorylation of Akt in human endothelial cells involvement in suppression of apoptosis. *Circ. Res.* **1998,** *83*, 334-341.

100. Skorski, T.; Bellacosa, A.; Nieborowska-Skorska, M.; Majewski, M.; Martinez, R.; Choi, J. K.; Trotta, R.; Wlodarski, P.; Perrotti, D.; Chan, T. O. Transformation of hematopoietic cells by BCR/ABL requires activation of a PI-3k/Akt-dependent pathway. *The EMBO journal* **1997,** *16*, 6151-6161.

101. Vivanco, I.; Sawyers, C. L. The phosphatidylinositol 3-Kinase AKT pathway in human cancer. *Nat. Rev. Cancer* **2002,** *2*, 489-501.

102. Padmanabhan, S.; Mukhopadhyay, A.; Narasimhan, S. D.; Tesz, G.; Czech, M. P.; Tissenbaum, H. A. A PP2A Regulatory Subunit Regulates C. elegans Insulin/IGF-1 Signaling by Modulating AKT-1 Phosphorylation. *Cell* **2009,** *136*, 939-951.

103. Bayascas, J. R.; Alessi, D. R. Regulation of Akt/PKB Ser473 phosphorylation. *Mol. Cell* **2005,** 18, 143-145.

104. Paez, J.; Sellers, W. R. PI3K/PTEN/Akt Pathway. In *Signal transduction in cancer*, Springer: 2003; pp 145-167.

105. Aman, M. J.; Lamkin, T. D.; Okada, H.; Kurosaki, T.; Ravichandran, K. S. The inositol phosphatase SHIP inhibits Akt/PKB activation in B cells. *J. Biol. Chem.* **1998,** *273*, 33922-33928.

106. Liu, Q.; Sasaki, T.; Kozieradzki, I.; Wakeham, A.; Itie, A.; Dumont, D. J.; Penninger, J. M. SHIP is a negative regulator of growth factor receptor-mediated PKB/Akt activation and myeloid cell survival. *Genes Dev.* **1999,** *13*, 786-791.

107. Choi, Y.; Zhang, J.; Murga, C.; Yu, H.; Koller, E.; Monia, B. P.; Gutkind, J. S.; Li, W. PTEN, but not SHIP and SHIP2, suppresses the PI3K/Akt pathway and induces growth inhibition and apoptosis of myeloma cells. *Oncogene* **2002,** *21*, 5289-5300.

108. Blanco-Aparicio, C.; Renner, O.; Leal, J. F.; Carnero, A. PTEN, more than the AKT pathway. *Carcinogenesis* **2007,** *28*, 1379-1386.

109. Murata, H.; Ihara, Y.; Nakamura, H.; Yodoi, J.; Sumikawa, K.; Kondo, T. Glutaredoxin exerts an antiapoptotic effect by regulating the redox state of Akt. *J. Biol. Chem.* **2003,** *278*, 50226-33.

110. Alessi, D. R.; Barry Caudwell, F.; Andjelkovic, M.; Hemmings, B. A.; Cohen, P. Molecular basis for the substrate specificity of protein kinase B; comparison with MAPKAP kinase-1 and p70 S6 kinase. *FEBS Lett.* **1996,** *399*, 333-338.

111. Manning, B. D.; Cantley, L. C. AKT/PKB signaling: navigating downstream. *Cell* **2007,** *129*, 1261-74.

112. Datta, S. R.; Dudek, H.; Tao, X.; Masters, S.; Fu, H.; Gotoh, Y.; Greenberg, M. E. Akt phosphorylation of BAD couples survival signals to the cell-intrinsic death machinery. *Cell* **1997,** *91*, 231-241.

113. Brunet, A.; Bonni, A.; Zigmond, M. J.; Lin, M. Z.; Juo, P.; Hu, L. S.; Anderson, M. J.; Arden, K. C.; Blenis, J.; Greenberg, M. E. Akt promotes cell survival by phosphorylating and inhibiting a Forkhead transcription factor. *Cell* **1999,** *96*, 857-868.

114. Ogawara, Y.; Kishishita, S.; Obata, T.; Isazawa, Y.; Suzuki, T.; Tanaka, K.; Masuyama, N.; Gotoh, Y. Akt enhances Mdm2-mediated ubiquitination and degradation of p53. *J. Biol. Chem.* **2002,** *277*, 21843-21850.

115. Mayo, L. D.; Donner, D. B. A phosphatidylinositol 3-kinase/Akt pathway promotes translocation of Mdm2 from the cytoplasm to the nucleus. *Proc. Nat. Acad. Sci. USA.* **2001,** *98*, 11598-11603.

116. Cardone, M. H.; Roy, N.; Stennicke, H. R.; Salvesen, G. S.; Franke, T. F.; Stanbridge, E.; Frisch, S.; Reed, J. C. Regulation of cell death protease caspase-9 by phosphorylation. *Science* **1998,** *282*, 1318-1321.

117. Hay, N. The Akt-mTOR tango and its relevance to cancer. *Cancer Cell* **2005,** *8*, 179-183.

118. Vander Haar, E.; Lee, S.-i.; Bandhakavi, S.; Griffin, T. J.; Kim, D.-H. Insulin signalling to mTOR mediated by the Akt/PKB substrate PRAS40. *Nat. Cell Biol.* **2007,** *9*, 316-323.

119. Liang, J.; Zubovitz, J.; Petrocelli, T.; Kotchetkov, R.; Connor, M. K.; Han, K.; Lee, J.-H.; Ciarallo, S.; Catzavelos, C.; Beniston, R. PKB/Akt phosphorylates p27, impairs nuclear import of p27 and opposes p27-mediated G1 arrest. *Nat. Med.* **2002,** *8*, 1153-1160.

120. Zhou, B. P.; Liao, Y.; Xia, W.; Spohn, B.; Lee, M.-H.; Hung, M.-C. Cytoplasmic localization of p21Cip1/WAF1 by Akt-induced phosphorylation in HER-2/neu-overexpressing cells. *Nat. Cell Biol.* **2001,** *3*, 245-252.

121. Morales-Ruiz, M.; Fulton, D.; Sowa, G.; Languino, L. R.; Fujio, Y.; Walsh, K.; Sessa, W. C. Vascular endothelial growth factor–stimulated actin reorganization and migration of endothelial cells is regulated via the serine/threonine kinase Akt. *Circ. Res.* **2000,** *86*, 892-896.

122. Michell, B.; Griffiths, J.; Mitchelhill, K.; Rodriguez-Crespo, I.; Tiganis, T.; Bozinovski, S.; De Montellano, P.; Kemp, B.; Pearson, R. The Akt kinase signals directly to endothelial nitric oxide synthase. *Curr. Biol.* **1999,** *9*, 845-S1.

123. Jiao, M.; Nan, K.-J. Activation of PI3 kinase/Akt/HIF-1α pathway contributes to hypoxia-induced epithelial-mesenchymal transition and chemoresistance in hepatocellular carcinoma. *Int. J. Oncol.* **2012,** *40*, 461.

124. Shiojima, I.; Walsh, K. Role of Akt signaling in vascular homeostasis and angiogenesis. *Circ. Res.* **2002,** *90*, 1243-1250.

125. Lawlor, M. A.; Alessi, D. R. PKB/Akt a key mediator of cell proliferation, survival and insulin responses? *J. Cell Sci.* **2001,** *114*, 2903-2910.

126. Miinea, C.; Peranen, J.; Sano, H.; Kane, S.; Sano, E.; Fukuda, M.; Lane, W. x. a. s.; Lienhard, G. x. a. e. AS160, the Akt substrate regulating GLUT4 translocation, has a functional Rab GTPase-activating protein domain. *Biochem. J* **2005,** *391*, 87-93.

127. Hajduch, E.; Litherland, G. J.; Hundal, H. S. Protein kinase B (PKB/Akt)–a key regulator of glucose transport? *FEBS Lett.* **2001,** *492*, 199-203.

128. Krycer, J. R.; Sharpe, L. J.; Luu, W.; Brown, A. J. The Akt–SREBP nexus: cell signaling meets lipid metabolism. *Trends Endocrinol. Metab.* **2010,** *21*, 268-276.

129. Altomare, D. A.; Testa, J. R. Perturbations of the AKT signaling pathway in human cancer. *Oncogene* **2005,** *24*, 7455-64.

130. Li, J.; Simpson, L.; Takahashi, M.; Miliaresis, C.; Myers, M. P.; Tonks, N.; Parsons, R. The PTEN/MMAC1 tumor suppressor induces cell death that is rescued by the AKT/protein kinase B oncogene. *Cancer Res.* **1998,** *58*, 5667-5672.

131. Di Cristofano, A.; Pandolfi, P. P. The multiple roles of PTEN in tumor suppression. *Cell* **2000,** *100*, 387-390.

132. Saito, Y.; Swanson, X.; Mhashilkar, A.; Oida, Y.; Schrock, R.; Branch, C.; Chada, S.; Zumstein, L.; Ramesh, R. Adenovirus-mediated transfer of the PTEN gene inhibits human colorectal cancer growth in vitro and in vivo. *Gene Ther.* **2003,** *10*, 1961-1969.

133. Cheng, J. Q.; Ruggeri, B.; Klein, W. M.; Sonoda, G.; Altomare, D. A.; Watson, D. K.; Testa, J. R. Amplification of AKT2 in human pancreatic cells and inhibition of AKT2 expression and tumorigenicity by antisense RNA. *Proc. Nat. Acad. Sci. USA.* **1996,** *93*, 3636-3641.

134. Jetzt, A.; Howe, J. A.; Horn, M. T.; Maxwell, E.; Yin, Z.; Johnson, D.; Kumar, C. C. Adenoviral-mediated expression of a kinase-dead mutant of Akt induces apoptosis selectively in tumor cells and suppresses tumor growth in mice. *Cancer Res.* **2003,** *63*, 6697-6706.

135. Dudek, H.; Datta, S. R.; Franke, T. F.; Birnbaum, M. J.; Yao, R.; Cooper, G. M.; Segal, R. A.; Kaplan, D. R.; Greenberg, M. E. Regulation of neuronal survival by the serine-threonine protein kinase Akt. *Science* **1997,** *275*, 661-665.

136. Shin, I.; Edl, J.; Biswas, S.; Lin, P. C.; Mernaugh, R.; Arteaga, C. L. Proapoptotic activity of cell-permeable anti-Akt single-chain antibodies. *Cancer Res.* **2005,** *65*, 2815-2824.

137. Hiromura, M.; Okada, F.; Obata, T.; Auguin, D.; Shibata, T.; Roumestand, C.; Noguchi, M. Inhibition of Akt kinase activity by a peptide spanning the βA strand of the proto-oncogene TCL1. *J. Biol. Chem.* **2004,** *279*, 53407-53418.

138. Gao, T.; Furnari, F.; Newton, A. C. PHLPP: a phosphatase that directly dephosphorylates Akt, promotes apoptosis, and suppresses tumor growth. *Molecular Cell* **2005,** *18*, 13-24.

139. Brognard, J.; Clark, A. S.; Ni, Y.; Dennis, P. A. Akt/protein kinase B is constitutively active in non-small cell lung cancer cells and promotes cellular survival and resistance to chemotherapy and radiation. *Cancer Res.* **2001,** *61*, 3986-3997.

140. Clark, A. S.; West, K.; Streicher, S.; Dennis, P. A. Constitutive and inducible Akt activity promotes resistance to chemotherapy, trastuzumab, or tamoxifen in breast cancer cells. *Molecular cancer therapeutics* **2002,** 1, 707-717.

141. Frolov, A.; Chahwan, S.; Ochs, M.; Arnoletti, J. P.; Pan, Z.-Z.; Favorova, O.; Fletcher, J.; von Mehren, M.; Eisenberg, B.; Godwin, A. K. Response Markers and the Molecular Mechanisms of Action of Gleevec in Gastrointestinal Stromal Tumors1. *Molecular. Cancer Ther.* **2003,** *2*, 699-709.

142. Bacus, S. S.; Altomare, D. A.; Lyass, L.; Chin, D. M.; Farrell, M. P.; Gurova, K.; Gudkov, A.; Testa, J. R. AKT2 is frequently upregulated in HER-2/neu-positive breast cancers and may contribute to tumor aggressiveness by enhancing cell survival. *Oncogene* **2002,** *21*, 3532-3540.

143. Hennessy, B. T.; Smith, D. L.; Ram, P. T.; Lu, Y.; Mills, G. B. Exploiting the PI3K/AKT pathway for cancer drug discovery. *Nat. Rev. Drug Discov.* **2005,** *4*, 988-1004.

144. Testa, J. R.; Tsichlis, P. N. AKT signaling in normal and malignant cells. *Oncogene* **2005,** *24*, 7391-3.

145. Pal, S. K.; Reckamp, K.; Yu, H.; Figlin, R. A. Akt inhibitors in clinical development for the treatment of cancer. *Expert Opin. Investig. Drugs* **2010,** *19*, 1355-66.

146. Kozikowski, A. P.; Kiddle, J. J.; Frew, T.; Berggren, M.; Powis, G. Synthesis and biology of 1D-3-deoxyphosphatidylinositol: a putative antimetabolite of phosphatidylinositol-3-phosphate and an inhibitor of cancer cell colony formation. *J. Med. Chem.* **1995,** *38*, 1053-1056.

147. Qiao, L.; Nan, F.; Kunkel, M.; Gallegos, A.; Powis, G.; Kozikowski, A. P. 3-Deoxy-d-m yo-inositol 1-Phosphate, 1-Phosphonate, and Ether Lipid Analogues as Inhibitors of Phosphatidylinositol-3-kinase Signaling and Cancer Cell Growth. *J. Med. Chem.* **1998,** *41*, 3303-3306.

148. Castillo, S. S.; Brognard, J.; Petukhov, P. A.; Zhang, C.; Tsurutani, J.; Granville, C. A.; Li, M.; Jung, M.; West, K. A.; Gills, J. G. Preferential inhibition of Akt and killing of Akt-dependent cancer cells by rationally designed phosphatidylinositol ether lipid analogues. *Cancer Res.* **2004,** *64*, 2782-2792.

149. Kondapaka, S. B.; Singh, S. S.; Dasmahapatra, G. P.; Sausville, E. A.; Roy, K. K. Perifosine, a novel alkylphospholipid, inhibits protein kinase B activation. *Mol. Cancer Ther.* **2003,** *2*, 1093-1103.

150. Van Ummersen, L.; Binger, K.; Volkman, J.; Marnocha, R.; Tutsch, K.; Kolesar, J.; Arzoomanian, R.; Alberti, D.; Wilding, G. A phase I trial of perifosine (NSC 639966) on a loading dose/maintenance dose schedule in patients with advanced cancer. *Clin. Cancer Res.* **2004,** *10*, 7450-7456.

151. Li, Q.; Li, T.; Zhu, G.-D.; Gong, J.; Claibone, A.; Dalton, C.; Luo, Y.; Johnson, E. F.; Shi, Y.; Liu, X. Discovery of trans-3, 4′-bispyridinylethylenes as potent and novel inhibitors of protein kinase B (PKB/Akt) for the treatment of cancer: Synthesis and biological evaluation. *Bioorg. Med. Chem. Lett.* **2006,** *16*, 1679-1685.

152. Woods, K. W.; Fischer, J. P.; Claiborne, A.; Li, T.; Thomas, S. A.; Zhu, G.-D.; Diebold, R. B.; Liu, X.; Shi, Y.; Klinghofer, V. Synthesis and SAR of indazole-pyridine based protein kinase B/Akt inhibitors. *Biorg. Med. Chem.* **2006,** *14*, 6832-6846.

153. Zhu, G.-D.; Gandhi, V. B.; Gong, J.; Thomas, S.; Woods, K. W.; Song, X.; Li, T.; Diebold, R. B.; Luo, Y.; Liu, X. Syntheses of potent, selective, and orally bioavailable indazole-pyridine series of protein kinase B/Akt inhibitors with reduced hypotension. *J. Med. Chem.* **2007,** *50*, 2990-3003.

154. Heerding, D. A.; Rhodes, N.; Leber, J. D.; Clark, T. J.; Keenan, R. M.; Lafrance, L. V.; Li, M.; Safonov, I. G.; Takata, D. T.; Venslavsky, J. W. Identification of 4-(2-(4-amino-1, 2, 5-oxadiazol-3-yl)-1-ethyl-7-{[(3 S)-3-piperidinylmethyl] oxy}-1 H-

imidazo [4, 5-c] pyridin-4-yl)-2-methyl-3-butyn-2-ol (GSK690693), a novel inhibitor of AKT kinase. *J. Med. Chem.* **2008,** *51*, 5663-5679.

155. Rouse, M. B.; Seefeld, M. A.; Leber, J. D.; McNulty, K. C.; Sun, L.; Miller, W. H.; Zhang, S.; Minthorn, E. A.; Concha, N. O.; Choudhry, A. E. Aminofurazans as potent inhibitors of AKT kinase. *Bioorg. Med. Chem. Lett.* **2009,** *19*, 1508-1511.

156. Barnett, S.; Defeo-Jones, D.; Fu, S.; Hancock, P.; Haskell, K.; Jones, R.; Kahana, J.; Kral, A.; Leander, K.; Lee, L. Identification and characterization of pleckstrin-homology-domain-dependent and isoenzyme-specific Akt inhibitors. *Biochem. J* **2005,** *385*, 399-408.

157. Calleja, V.; Laguerre, M.; Parker, P. J.; Larijani, B. Role of a novel PH-kinase domain interface in PKB/Akt regulation: structural mechanism for allosteric inhibition. *PLoS biology* **2009,** *7*, e1000017.

158. Lindsley, C. W.; Zhao, Z.; Leister, W. H.; Robinson, R. G.; Barnett, S. F.; Defeo-Jones, D.; Jones, R. E.; Hartman, G. D.; Huff, J. R.; Huber, H. E. Allosteric Akt (PKB) inhibitors: discovery and SAR of isozyme selective inhibitors. *Bioorg. Med. Chem. Lett.* **2005,** *15*, 761-764.

159. Zhao, Z.; Leister, W. H.; Robinson, R. G.; Barnett, S. F.; Defeo-Jones, D.; Jones, R. E.; Hartman, G. D.; Huff, J. R.; Huber, H. E.; Duggan, M. E. Discovery of 2, 3, 5-trisubstituted pyridine derivatives as potent Akt1 and Akt2 dual inhibitors. *Bioorg. Med. Chem. Lett.* **2005,** *15*, 905-909.

160. Li, Y.; Liang, J.; Siu, T.; Hu, E.; Rossi, M. A.; Barnett, S. F.; Defeo-Jones, D.; Jones, R. E.; Robinson, R. G.; Leander, K. Allosteric inhibitors of Akt1 and Akt2: discovery

of [1, 2, 4] triazolo [3, 4-f][1, 6] naphthyridines with potent and balanced activity. *Bioorg. Med. Chem. Lett.* **2009,** *19*, 834-836.

161. Hirai, H.; Sootome, H.; Nakatsuru, Y.; Miyama, K.; Taguchi, S.; Tsujioka, K.; Ueno, Y.; Hatch, H.; Majumder, P. K.; Pan, B.-S. MK-2206, an allosteric Akt inhibitor, enhances antitumor efficacy by standard chemotherapeutic agents or molecular targeted drugs in vitro and in vivo. *Mol. Cancer Ther.* **2010,** *9*, 1956-1967.

162. Toral-Barza, L.; Zhang, W.-G.; Huang, X.; McDonald, L. A.; Salaski, E. J.; Barbieri, L. R.; Ding, W.-D.; Krishnamurthy, G.; Hu, Y. B.; Lucas, J. Discovery of lactoquinomycin and related pyranonaphthoquinones as potent and allosteric inhibitors of AKT/PKB: mechanistic involvement of AKT catalytic activation loop cysteines. *Mol. Cancer Ther.* **2007,** *6*, 3028-3038.

163. Salaski, E. J.; Krishnamurthy, G.; Ding, W.-D.; Yu, K.; Insaf, S. S.; Eid, C.; Shim, J.; Levin, J. I.; Tabei, K.; Toral-Barza, L. Pyranonaphthoquinone lactones: a new class of AKT selective kinase inhibitors alkylate a regulatory loop cysteine. *J. Med. Chem.* **2009,** *52*, 2181-2184.

164. Yang, J.; Cron, P.; Good, V. M.; Thompson, V.; Hemmings, B. A.; Barford, D. Crystal structure of an activated Akt/protein kinase B ternary complex with GSK3-peptide and AMP-PNP. *Nat. Struct. Biol.* **2002,** *9*, 940-4.

165. Kayser, K. J.; Glenn, M. P.; Sebti, S. M.; Cheng, J. Q.; Hamilton, A. D. Modifications of the GSK3beta substrate sequence to produce substrate-mimetic inhibitors of Akt as potential anti-cancer therapeutics. *Bioorg. Med. Chem. Lett.* **2007,** *17*, 2068-73.

166. Litman, P.; Ohne, O.; Ben-Yaakov, S.; Shemesh-Darvish, L.; Yechezkel, T.; Salitra, Y.; Rubnov, S.; Cohen, I.; Senderowitz, H.; Kidron, D. A novel substrate mimetic inhibitor of PKB/Akt inhibits prostate cancer tumor growth in mice by blocking the PKB pathway. *Biochemistry* **2007,** *46*, 4716-4724.

167. Kayser-Bricker, K. J.; Glenn, M. P.; Lee, S. H.; Sebti, S. M.; Cheng, J. Q.; Hamilton, A. D. Non-peptidic substrate-mimetic inhibitors of Akt as potential anti-cancer agents. *Bioorg. Med. Chem.* **2009,** *17*, 1764-71.

168. Ranatunga, S.; Del Valle, J. R. Synthesis of GSK3beta mimetic inhibitors of Akt featuring a novel extended dipeptide surrogate. *Bioorg. Med. Chem. Lett.* **2011,** *21*, 7166-9.

169. Lindsley, C. W. The Akt/PKB family of protein kinases: a review of small molecule inhibitors and progress towards target validation: a 2009 update. *Curr. Top. Med. Chem.* **2010,** *10*, 458-477.

170. Bogoyevitch, M. A.; Fairlie, D. P. A new paradigm for protein kinase inhibition: blocking phosphorylation without directly targeting ATP binding. *Drug Discovery Today* **2007,** *12*, 622-33.

171. Gumireddy, K.; Reddy, M. V.; Cosenza, S. C.; Boominathan, R.; Baker, S. J.; Papathi, N.; Jiang, J.; Holland, J.; Reddy, E. P. ON01910, a non-ATP-competitive small molecule inhibitor of Plk1, is a potent anticancer agent. *Cancer Cell* **2005,** *7*, 275-86.

172. Zhang, J.; Yang, P. L.; Gray, N. S. Targeting cancer with small molecule kinase inhibitors. *Nat. Rev. Cancer* **2009,** *9*, 28-39.

173. Obata, T.; Yaffe, M. B.; Leparc, G. G.; Piro, E. T.; Maegawa, H.; Kashiwagi, A.; Kikkawa, R.; Cantley, L. C. Peptide and protein library screening defines optimal substrate motifs for AKT/PKB. *J. Biol. Chem.* **2000,** *275*, 36108-36115.

174. Luo, Y.; Smith, R. A.; Guan, R.; Liu, X.; Klinghofer, V.; Shen, J.; Hutchins, C.; Richardson, P.; Holzman, T.; Rosenberg, S. H. Pseudosubstrate peptides inhibit Akt and induce cell growth inhibition. *Biochemistry* **2004,** *43*, 1254-1263.

175. Parang, K.; Cole, P. A. Designing bisubstrate analog inhibitors for protein kinases. *Pharmacol. Ther.* **2002,** *93*, 145-157.

176. Johnson, D. S.; Weerapana, E.; Cravatt, B. F. Strategies for discovering and derisking covalent, irreversible enzyme inhibitors. *Future Med. Chem.* **2010,** *2*, 949-964.

177. Mah, R.; Thomas, J. R.; Shafer, C. M. Drug discovery considerations in the development of covalent inhibitors. *Bioorg. Med. Chem. Lett.* **2014,** *24*, 33-9.

178. Singh, J.; Petter, R. C.; Baillie, T. A.; Whitty, A. The resurgence of covalent drugs. *Nat. Rev. Drug Discovery* **2011,** *10*, 307-317.

179. Yellaturu, C. R.; Bhanoori, M.; Neeli, I.; Rao, G. N. N-Ethylmaleimide inhibits platelet-derived growth factor BB-stimulated Akt phosphorylation via activation of protein phosphatase 2A. *J. Biol. Chem.* **2002,** *277*, 40148-40155.

180. Elstrom, R. L.; Bauer, D. E.; Buzzai, M.; Karnauskas, R.; Harris, M. H.; Plas, D. R.; Zhuang, H.; Cinalli, R. M.; Alavi, A.; Rudin, C. M. Akt stimulates aerobic glycolysis in cancer cells. *Cancer Res.* **2004,** *64*, 3892-3899.

181. Shearn, C.; Fritz, K.; Reigan, P.; Petersen, D. R. Modification of Akt2 by 4-hydroxynonenal inhibits insulin-dependent Akt signaling in HepG2 cells. *Biochemistry* **2011,** *50*, 3984-3996.

182. Weerapana, E.; Speers, A. E.; Cravatt, B. F. Tandem orthogonal proteolysis-activity-based protein profiling (TOP-ABPP)—a general method for mapping sites of probe modification in proteomes. *Nat. Protoc.* **2007,** *2*, 1414-1425.

183. Huang, X.; Begley, M.; Morgenstern, K. A.; Gu, Y.; Rose, P.; Zhao, H.; Zhu, X. Crystal structure of an inactive Akt2 kinase domain. *Structure* **2003,** 11, 21-30.

184. Anjum, R.; Pae, E.; Blenis, J.; Ballif, B. A. TPCK inhibits AGC kinases by direct activation loop adduction at phenylalanine-directed cysteine residues. *FEBS Lett.* **2012,** *586*, 3471-6.

185. Ballif, B. A.; Shimamura, A.; Pae, E.; Blenis, J. Disruption of 3-phosphoinositide-dependent kinase 1 (PDK1) signaling by the anti-tumorigenic and anti-proliferative agent n-alpha-tosyl-l-phenylalanyl chloromethyl ketone. *J. Biol. Chem.* **2001,** *276*, 12466-75.

186. Studier, F. W.; Rosenberg, A. H.; Dunn, J. J.; Dubendorff, J. W. Use of T7 RNA polymerase to direct expression of cloned genes. *Methods Enzymol.* **1990,** *185*, 60-89.

187. Peng, H.; Marians, K. J. Escherichia coli topoisomerase IV. Purification, characterization, subunit structure, and subunit interactions. *J. Biol. Chem.* **1993,** *268*, 24481-24490.

188. Hiasa, H.; Shea, M. E. DNA gyrase-mediated wrapping of the DNA strand is required for the replication fork arrest by the DNA gyrase-quinolone-DNA ternary complex. *J. Biol. Chem.* **2000,** *275*, 34780-34786.

189. Oppegard, L. M.; Ougolkov, A. V.; Luchini, D. N.; Schoon, R. A.; Goodell, J. R.; Kaur, H.; Billadeau, D. D.; Ferguson, D. M.; Hiasa, H. Novel acridine-based compounds that exhibit an anti-pancreatic cancer activity are catalytic inhibitors of human topoisomerase II. *Eur. J. Pharmacol.* **2009,** *602*, 223-229.

190. Pfeiffer, E. S.; Hiasa, H. Determination of the primary target of a quinolone drug and the effect of quinolone resistance-conferring mutations by measuring quinolone sensitivity based on its mode of action. *Antimicrob. Agents Chemother.* **2007,** *51*, 3410-3412.

191. Stolz, R. M.; Northrop, B. H. Experimental and Theoretical Studies of Selective Thiol–Ene and Thiol–Yne Click Reactions Involving N-Substituted Maleimides. *J. Org. Chem.* **2013,** *78*, 8105-8116.

VITA

Jenson Verghese was born on 10 April, 1985 in Thiruvalla, India and is an Indian citizen. He obtained his Bachelor's in Pharmacy from the Tamil Nadu Dr. M.G.R Medical University in Chennai, India in 2006 and his Master's in Science from Virginia Commonwealth University, Richmond, Virginia in 2009. He began his doctoral studies in the Department of Medicinal Chemistry at Virginia Commonwealth University, Richmond in the fall of 2009.